

**A Thesis Submitted for the Degree of PhD at the University of Warwick**

**Permanent WRAP URL:**

<http://wrap.warwick.ac.uk/180942>

**Copyright and reuse:**

This thesis is made available online and is protected by original copyright.

Please scroll down to view the document itself.

Please refer to the repository record for this item for information to help you to cite it.

Our policy information is available from the repository home page.

For more information, please contact the WRAP Team at: [wrap@warwick.ac.uk](mailto:wrap@warwick.ac.uk)

# Overcoming Uncertainties in Sour Natural Gas Dispersion Modelling

SreeRaj Rajappan Nair

A thesis submitted in partial fulfilment of the requirements for the degree  
of

Doctor of Philosophy in Engineering

University of Warwick, School of Engineering

December 2022

## Table of Contents

List of Tables .....	6
List of Figures .....	9
Acknowledgements.....	13
Declaration and Inclusion of Material from a Prior Thesis .....	14
Executive summary .....	15
1. Introduction .....	17
1.1. Background and motivation.....	17
1.2. Natural gas production and delivery.....	18
1.3. Sourness – the concern.....	19
1.4. Role of consequence assessment in risk management.....	21
1.5. The opportunity .....	23
1.6. Study methodology and thesis outline.....	24
2. Literature review – sour natural gas dispersion modelling .....	26
2.1. Natural gas and sourness.....	26
2.2. Hydrogen sulphide – properties and toxicity concern .....	27
2.3. The hazard and incidents .....	31
2.4. Consequence modelling approaches and tools .....	34
2.5. Thermodynamic input and assumption .....	41
2.6. Meteorological factors.....	44
2.6.1. Stability class.....	45
2.6.2. Wind speed .....	46
2.6.3. Intensity of turbulence and atmospheric stability: .....	47
2.7. Topography – terrain and obstacles .....	47
2.8. Tool and relevant studies.....	49
2.9. Numerical model validation .....	53
2.10. Experiments and field trails.....	56
2.10.1. Prairie Grass field trial project.....	58
2.10.2. Prairie Grass field trial set up. ....	59
2.11. Incidents, investigation, and analysis.....	60
2.12. Uncertainties and sensitivity analysis.....	63
2.13. Literature review summary.....	63
3. Scenario definition, input parameters, and software tools.....	65
3.1. Release scenario and the physics.....	65
3.1.1. Discharge .....	66

3.1.2.	Expansion .....	66
3.1.3.	Dispersion .....	67
3.2.	Natural gas composition .....	68
3.3.	Natural gas release - Source term.....	69
3.3.1.	Discharge estimation .....	70
3.3.2.	Expansion estimation.....	72
3.4.	Atmospheric conditions and parameters.....	74
3.5.	Dispersion modelling end points.....	75
3.5.1.	Hydrogen sulphide – specified end point values.....	75
3.5.2.	Hydrogen sulphide – toxic load end point values .....	77
4.	Consequence modelling input and parameter sensitivity.....	79
4.1.	Modelling tools .....	79
4.1.1.	Tool: Aspen HYSYS by AspenTech .....	79
4.1.2.	Tool: ALOHA by US EPA.....	80
4.1.3.	Tool: Canary by Quest.....	82
4.2.	Model selection based on buoyancy.....	83
4.3.	Composition screening using HYSYS .....	87
4.3.1.	HYSYS Simulations: CH <sub>4</sub> and H <sub>2</sub> S.....	90
4.3.2.	HYSYS Simulations: multi-component sour natural gas .....	91
4.4.	Impact of water vapour in natural gas .....	94
4.5.	Parameter screening using ALOHA .....	95
4.6.	Parameter screening using Canary .....	102
4.6.1.	Source term parameters and sensitivity .....	103
4.6.2.	Environmental parameters and sensitivity.....	111
4.6.3.	Discussion .....	114
4.7.	Application of the consequence modelling results in risk assessment: .....	116
5.	OpenFOAM model set-up and validation.....	119
5.1.	Computational fluid dynamics – methodology and model development .....	119
5.1.1.	Fluid flow fundamentals and Governing equations .....	119
5.1.2.	Conservation principles and governing equations .....	122
5.1.3.	Turbulence models .....	124
5.1.4.	CFD Turbulence models.....	126
5.1.5.	Numerical modelling for fluid dynamics .....	129
5.1.6.	High Performance Computing (HPC).....	135
5.2.	OpenFOAM fundamentals .....	135
5.2.1.	Introduction .....	136
5.2.2.	Pre-processing .....	137

5.2.3.	Post-processing.....	138
5.2.4.	Solving.....	138
5.2.5.	Models and physical properties .....	141
5.3.	CFD model and validation .....	147
5.3.1.	Prairie Grass field trial project.....	148
5.3.2.	Simplified tunnel model for input and boundary conditions .....	149
5.3.3.	Full domain OpenFOAM model for Prairie Grass Field trial .....	158
5.3.4.	Results along the monitoring points and comparison with field trial.....	166
5.3.5.	Sensitivity: Mesh independence .....	167
5.3.6.	Sensitivity: Transient Turbulence Eddy simulation.....	174
5.3.7.	Sensitivity: Transient Turbulence Models .....	178
5.3.8.	Validation modelling summary .....	180
6.	Sour Natural Gas dispersion modelling results and analysis .....	182
6.1.	Case Study.....	182
6.2.	Toxicity and flammability concentrations of interest.....	183
6.3.	Case 1: Natural gas with 5% H <sub>2</sub> S.....	184
6.4.	Case 2: Natural gas with 15% H <sub>2</sub> S.....	187
6.5.	Case 3: Natural gas with 20% H <sub>2</sub> S.....	191
6.6.	Analysis of the results – sensitivity to natural gas composition .....	194
6.6.1.	Toxicity – Hydrogen sulphide .....	194
6.6.2.	Flammability – Methane .....	197
6.7.	Discussion .....	198
7.	Conclusion.....	199
7.1.	Release, dispersion and modelling.....	200
7.2.	Modelling tools and methodology .....	200
7.3.	Parameter screening and model selection.....	201
7.4.	Sourness screening and parametric sensitivity .....	202
7.5.	CFD simulations and analysis .....	203
7.6.	Discussion and future work.....	204
	Reference.....	206
	Abbreviations.....	227
	Definitions.....	229
	Appendix A: OpenFOAM solver selection and set up.....	231
	Appendix B: <i>blockMesh</i> , <i>snappyHexMesh</i> – OpenFOAM system files.....	252
	Appendix C: Turbulence at inlet using <i>fluctuationScale</i> .....	260
	Appendix D: OpenFOAM Velocity at the Probes .....	272
	Appendix E: Canary results for source term sensitivity.....	277

Appendix F: Field trial wind data (for model Boundary condition) ..... 289  
Appendix G: OpenFOAM fundamentals..... 292

## List of Tables

Table 1: Sour natural gas mixtures.....	26
Table 2: Chemical and Physical Data for Hydrogen sulphide .....	27
Table 3: Effects from acute Hydrogen sulphide exposure .....	29
Table 4: Sour gas Incidents .....	32
Table 5: Pipeline failure data analysis (Bariha et. al. 2016).....	33
Table 6: Consequence Modelling Software.....	35
Table 7: Comparison of gas diffusion modelling approach .....	38
Table 8: Comparison - Integral (2D) vs CFD (3D).....	40
Table 9: Atmospheric stability classifications.....	46
Table 10: Surface roughness length associated with terrain description.....	48
Table 11: Status of theoretical and numerical models and tools for H <sub>2</sub> S rich gas releases:...	49
Table 12: Gases (species) used in field trials and their properties .....	58
Table 13: Studies on accidental H <sub>2</sub> S rich gas releases:.....	60
Table 14: Properties of the main constituents of sour natural gas .....	68
Table 15: Constant values for effective release rate estimation (Bariha et.al. 2016). .....	71
Table 16: Mass release rates of natural gas – medium hole diameters (0.03 to 0.5 m) .....	71
Table 17: Mass release rates of methane and propane – rupture and large hole (diameter 1 m) .....	71
Table 18: ERPG values for Hydrogen Sulphide.....	75
Table 19: AEGL values for Hydrogen Sulphide .....	76
Table 20: Prairie Grass field trial case data for ALOHA model selection .....	84
Table 21: Comparison on the observed values vs estimated concentration.....	84
Table 22: Comparison on the observed vs estimated concentration / release rate .....	85
Table 23: Natural gas phase equilibrium.....	90
Table 24: Multi-component compositions for release and dispersion modelling (mol %).....	92
Table 25: Wet (saturated) and Dry base – natural gas (S6) compositions (mol%) .....	94
Table 26: ALOHA Simulation: Model input for base case and sensitivities .....	96
Table 27: Hazardous levels of pipeline release of sour natural gas.....	96
Table 28: Base case and sensitivity results – CH <sub>4</sub> .....	97
Table 29: Base case and sensitivity results – H <sub>2</sub> S .....	98
Table 30: Hazardous level distance – ALOHA validation .....	101
Table 31: Canary - Hazardous levels of pipeline release of natural gas .....	103
Table 32: Canary - Comparison of release rate (kg/s) for hole size, pressure, and temperature .....	104
Table 33: Comparison of downwind distance to flammable and toxicity hazard levels.....	106
Table 34: Natural gas (S4) compositions (mol%) and downwind distance to 100ppm H <sub>2</sub> S..	116

Table 35: Natural gas impact zone – parameter sensitivity and risk management considerations .....	118
Table 36: Two equation turbulence models .....	127
Table 37: Meshing terminology .....	131
Table 38: Capability matrix: Flow characteristics vs Solvers.....	143
Table 39: OpenFOAM solver and description .....	144
Table 40: Prairie Grass Field Trail – Temperature profile.....	148
Table 41: Prairie Grass Field Trail Case 09 – Vertical wind profile .....	148
Table 42: Prairie Grass Field Trail Case 09 diffusion results – maximum concentration along the sampling arcs .....	149
Table 43: Mesh attributes.....	167
Table 44: Meshing – Quality criteria evaluation attributes.....	168
Table 45: Summary of the grid sensitivity in percentage difference.....	168
Table 46: Turbulence model sensitivity concentration (SO <sub>2</sub> ) Observed vs Estimated for DDES <b>k<math>\omega</math></b> -SST.....	174
Table 47: Turbulence model sensitivity concentration (SO <sub>2</sub> ) Observed vs Estimated for DFSEM <b>k<math>\omega</math></b> -SST.....	174
Table 48: Turbulence model sensitivity concentration (SO <sub>2</sub> ) Observed vs Estimated for realizable <b>k<math>\epsilon</math></b> .....	178
Table 49: Concentration (SO <sub>2</sub> ) at 50 m Observed vs Estimated for sensitivity comparison summary .....	179
Table 50: Averaged concentration (SO <sub>2</sub> ) along the downwind arc of monitoring points (across all 13 probes).....	180
Table 51: OpenFOAM Natural Gas dispersion – Simulation parameters .....	183
Table 52: Case 1 OpenFOAM Natural Gas dispersion with 5% H <sub>2</sub> S – CH <sub>4</sub> and H <sub>2</sub> S concentration estimation .....	184
Table 53: Case 1 OpenFOAM Natural Gas dispersion with 5% H <sub>2</sub> S – CH <sub>4</sub> concentration at the probes.....	186
Table 54: Case 1 OpenFOAM Natural Gas dispersion with 5% H <sub>2</sub> S – H <sub>2</sub> S concentration at the probes.....	187
Table 55: Case 2 OpenFOAM Natural Gas dispersion with 15% H <sub>2</sub> S – CH <sub>4</sub> and H <sub>2</sub> S concentration estimation.....	188
Table 56: Case 2 OpenFOAM Natural Gas dispersion with 15% H <sub>2</sub> S – CH <sub>4</sub> concentration along monitoring points .....	189
Table 57: Case 2 OpenFOAM Natural Gas dispersion with 15% H <sub>2</sub> S – H <sub>2</sub> S concentration at the probes.....	190
Table 58: Case 3 OpenFOAM Natural Gas dispersion with 20% H <sub>2</sub> S – CH <sub>4</sub> and H <sub>2</sub> S concentration estimation.....	191



Table 59: Case 3 OpenFOAM Natural Gas dispersion with 20% H <sub>2</sub> S – CH <sub>4</sub> concentration along monitoring points .....	192
Table 60: Case 3 OpenFOAM Natural Gas dispersion with 20% H <sub>2</sub> S – H <sub>2</sub> S concentration along monitoring points .....	193
Table 61: OpenFOAM Natural Gas dispersion – maximum H <sub>2</sub> S concentration at downwind monitoring arcs.....	195
Table 62: Toxicity impact comparison for natural gas compositions .....	196
Table 63: OpenFOAM Natural Gas dispersion – maximum CH <sub>4</sub> concentration at downwind monitoring arcs.....	197
Table 64: fireFoam model set up folders and files .....	233
Table 65: Initial and boundary conditions.....	234
Table 66: <i>resolveFeatureAngle</i> sensitivity comparison .....	239
Table 67: <i>nCellsBetweenLevels</i> sensitivity comparison .....	242
Table 68: Meshing sensitivity for level of refinement.....	245
Table 69: Meshing sensitivity - refinementSurfaces .....	247
Table 70: Meshing sensitivity – species concentration comparison .....	250
Table 71: <i>fluctuationScale</i> and <i>alpha</i> values used .....	262
Table 72: Vertical velocity profile comparison .....	263
Table 73: <i>fluctuationScale</i> values.....	269

## List of Figures

Figure 1: Natural gas flow from reservoir to consumer .....	18
Figure 2: Research study steps.....	25
Figure 3: Hydrogen sulphide NFPA 704.....	28
Figure 4: Hydrogen sulphide warning sign .....	29
Figure 5: Hydrogen sulphide Quick card, OSHA .....	30
Figure 6: Corrosion on pipeline handling sour gas .....	31
Figure 7: Consequence modelling steps .....	34
Figure 8: Distribution (left) and spread (right) in a Gaussian model .....	37
Figure 9: Toxic cloud release display in EFFECTS software.....	39
Figure 10: Toxic cloud release display in FLACS software .....	39
Figure 11: Methane phase diagram .....	42
Figure 12: Hydrogen sulphide phase diagram.....	42
Figure 13: Prairie Grass topography of field site and the release point.....	59
Figure 14: Release point and the monitoring points at radial distances.....	59
Figure 15: Scenario development – Discharge, Expansion, Dispersion.....	65
Figure 16: Buoyancy and Dispersion .....	67
Figure 17: Input and parameter sensitivity analysis steps .....	79
Figure 18: ALOHA output – graph for bell shaped dispersion and output on map using MARPLOT .....	82
Figure 19: Hydrogen sulphide momentum jet cloud - dispersion isopleths (a) Overhead view (b) Side view .....	83
Figure 20: ALOHA verification – Heavy gas model results vs Prairie Grass field trial .....	86
Figure 21: ALOHA verification – Gaussian model results vs Prairie Grass field trial.....	86
Figure 22: Multi-component Phase Diagrams.....	88
Figure 23: Phase equilibrium curves for methane (blue), Methane-ethane-Hydrogen sulphide (green), and S4 sample (yellow).....	90
Figure 24: Phase equilibrium – impact of H <sub>2</sub> S concentration in natural gas (CH <sub>4</sub> ) .....	91
Figure 25: Phase equilibrium curve – toxic natural gas compositions .....	93
Figure 26: Sensitivity – natural gas saturation: Downwind distance to H <sub>2</sub> S concentration....	95
Figure 27: ALOHA estimated Methane (flammable) Hazard zones.....	97
Figure 28: ALOHA estimated Hydrogen sulphide (toxic) Hazard zones.....	98
Figure 29: ALOHA: Methane dispersion - sensitivity.....	100
Figure 30: ALOHA: Hydrogen sulphide dispersion – sensitivity.....	100
Figure 31: Canary - Sensitivity composition: Comparison of downwind distance to flammable and toxicity hazard levels.....	106
Figure 32: Canary - Sensitivity of downwind distance (H <sub>2</sub> S Concentration) to Release hole size .....	107

Figure 33: Canary - Sensitivity of downwind distance (H <sub>2</sub> S Concentration) to Operating pressure .....	108
Figure 34: Canary - Sensitivity of downwind distance (H <sub>2</sub> S Concentration) to Operating temperature.....	109
Figure 35: Canary - Sensitivity of downwind distance (H <sub>2</sub> S Concentration) to Release orientation .....	110
Figure 36: Canary - Sensitivity of downwind distance (H <sub>2</sub> S concentration) to Atmospheric stability and wind speed .....	111
Figure 37: Canary - Sensitivity of downwind distance (H <sub>2</sub> S Concentration) to Terrain .....	113
Figure 38: Canary - Sensitivity of downwind distance (H <sub>2</sub> S Concentration) to Humidity .....	114
Figure 39: Parameter sensitivity application example - H <sub>2</sub> S downwind distances and potential impacts .....	117
Figure 40: CFD - Control volume .....	122
Figure 41: CFD methodology - Sequence of steps .....	130
Figure 42: OpenFOAM workflow steps .....	137
Figure 43: OpenFOAM collaboration diagram for Finite volume numerical schemes .....	139
Figure 44: OpenFOAM model set up and validation steps.....	147
Figure 45: Simplified tunnel – Geometry .....	149
Figure 46: Simplified tunnel – monitoring points.....	150
Figure 47: Simplified tunnel – Mesh .....	150
Figure 48: Vertical velocity profile comparison between realizable k-ε and k-ω SST.....	151
Figure 49: Simple tunnel velocity profile along symmetry plane .....	151
Figure 50: Simplified model - Steady state Velocity profile comparison.....	152
Figure 51: Simplified model - Steady state Temperature profile comparison.....	152
Figure 52: Simplified model - Steady state Kinetic energy comparison .....	153
Figure 53: Simplified model - Steady state Epsilon comparison.....	153
Figure 54: Schematic of the Prairie Grass Experiment setup along with an illustration of the computational domain.....	159
Figure 55: Computational domain geometry for PG case simulation .....	160
Figure 56: Mesh refinement – representative set .....	161
Figure 57: Meshed domain – full model .....	162
Figure 58: The meshed domain with location of the release source compared with the field trial set up .....	162
Figure 59: Release orientation with respect to the wind direction (horizontal cross section at 0.46m).....	163
Figure 60: Species release with respect to the wind direction (horizontal cross section at 0.46m) .....	164
Figure 61: Dispersion of SO <sub>2</sub> representation from OpenFoam at time steps.....	165
Figure 62: Concentration (SO <sub>2</sub> ) estimated (OpenFOAM) at probes along 100m arc .....	166

Figure 63: Comparison between the observed (field trial) and estimated (Mesh##) SO<sub>2</sub> concentration averaged over radial distances (arcs) from the release point..... 169

Figure 64: Grid Sensitivity, estimated (Mesh#0) vs observed concentrations within the Fac2 and Fac5..... 170

Figure 65: Grid Sensitivity, estimated (Mesh#1) vs observed concentrations within the Fac2 and Fac5..... 170

Figure 66: Grid Sensitivity, estimated (Mesh#3) vs observed concentrations within the Fac2 and Fac5..... 171

Figure 67: Grid Sensitivity, estimated (Mesh#3) vs observed concentrations within the Fac2 and Fac5..... 171

Figure 68: Grid Sensitivity, percent of the estimated vs observed concentrations within the Fac2 and Fac5..... 171

Figure 69: Grid Sensitivity - Crosswind profile of the plume dispersion at 50m ..... 172

Figure 70: Grid Sensitivity - Crosswind profile of the plume dispersion at 100m ..... 172

Figure 71: Turbulence model sensitivity, Concentration (SO<sub>2</sub>) scatter plot - observed vs estimated comparison for DDES **k $\omega$** -SST ..... 175

Figure 72: Turbulence model sensitivity, Concentration (SO<sub>2</sub>) scatter plot - observed vs estimated comparison for DFSEM **k $\omega$** -SST ..... 176

Figure 73: Wind velocity along x direction for rRBF DDES **k $\omega$** -SST ..... 177

Figure 74: Wind velocity along x direction for rRBF DFSEM **k $\omega$** -SST..... 177

Figure 75: Wind velocity along y direction for rRBF DDES **k $\omega$** -SST ..... 177

Figure 76: Wind velocity along y direction for rRBF DFSEM **k $\omega$** -SST..... 177

Figure 77: Wind velocity along z direction for rRBF DDES **k $\omega$** -SST..... 178

Figure 78: Wind velocity along z direction for rRBF DFSEM **k $\omega$** -SST..... 178

Figure 79: Turbulence model sensitivity, Concentration (SO<sub>2</sub>) scatter plot - observed vs estimated comparison for kEpsilon (**k $\epsilon$** ) ..... 179

Figure 80: Case 1 OpenFOAM Natural Gas dispersion with 5% H<sub>2</sub>S - downwind dispersion of CH<sub>4</sub> concentration..... 186

Figure 81: Case 1 OpenFOAM Natural Gas dispersion with 5% H<sub>2</sub>S - downwind distribution of H<sub>2</sub>S concentration ..... 187

Figure 82: Case 2 OpenFOAM Natural Gas dispersion with 15% H<sub>2</sub>S - downwind dispersion of CH<sub>4</sub> concentration..... 189

Figure 83: Case 2 OpenFOAM Natural Gas dispersion with 15% H<sub>2</sub>S - downwind distribution of H<sub>2</sub>S concentration ..... 190

Figure 84: Case 3 OpenFOAM Natural Gas dispersion with 20% H<sub>2</sub>S - downwind dispersion of CH<sub>4</sub> concentration..... 193

Figure 85: Case 3 OpenFOAM Natural Gas dispersion with 20% H<sub>2</sub>S - downwind distribution of H<sub>2</sub>S concentration ..... 194

Figure 86: H<sub>2</sub>S concentration comparison along probes at 50 m..... 195

Figure 87: H <sub>2</sub> S concentration comparison along probes at 100m.....	195
Figure 88: H <sub>2</sub> S concentration comparison along probes at 200m.....	195
Figure 89: H <sub>2</sub> S concentration comparison along probes at 400m.....	195
Figure 90: H <sub>2</sub> S concentration comparison along probes at 800m.....	195
Figure 91: CH <sub>4</sub> concentration comparison along probes at 50m .....	197
Figure 92: CH <sub>4</sub> concentration comparison along probes at 100m .....	197
Figure 93: CH <sub>4</sub> concentration comparison along probes at 200m .....	197
Figure 94: CH <sub>4</sub> concentration comparison along probes at 400m .....	197
Figure 95: CH <sub>4</sub> concentration comparison along probes at 800m .....	198
Figure 96: fireFOAM Geometry with obstructions 75 m box.....	234
Figure 97: fireFOAM geometry and meshing.....	236
Figure 98: Meshing quality - non-orthogonality.....	237
Figure 99: Geometry and with meshing details (base case).....	238
Figure 100: Meshing sensitivity - <i>resolveFeatureAngle</i> .....	241
Figure 101: Meshing sensitivity – <i>nCellsBetweenLevels</i> – Temperature and Velocity.....	244
Figure 102: Meshing sensitivity – <i>featureLevel</i> .....	246
Figure 103: refinementSurface sensitivity – velocity profile (U) at 43 seconds .....	248
Figure 104: Meshing sensitivity – coarse, medium and fine mesh .....	249
Figure 105: Nitrogen concentration at 3 probe locations for Medium mesh .....	250
Figure 106: Nitrogen concentration at 3 probe locations for Coarse mesh.....	251

## Acknowledgements

I would like to acknowledge my family for their enduring support during my doctoral work. I could not have undertaken this seven-year journey without my spouse Lekshmi Thampi and our little sons Mahadev and Narayan (who grew a lot older). I am deeply indebted to my parents Vijaya and Rajappan, who constantly affirmed that they are proud of what I am doing. I appreciate all the prayers, understanding and the relentless support I received from the rest of my family.

I thank my esteemed supervisor – Prof. Jennifer Wen, for invaluable supervision, support, and guidance during the course of my PhD degree. My gratitude extends to part-time co. supervisor Dr. Madhav R C Vendra for his guidance on the HPC interfaces and motivating me to keep the progress. Additionally, I would like to express appreciation to Ms. Kerrie Hatton and team, School of Engineering for their treasured support enabling me steer through the distance learning (remote) and other part-time researcher challenges. I also thank Prof. Robert Critoph and Dr. Zacharie Tamainot-Telto for their mentorship and timely guidance.

I am extremely grateful to Mr. Noma Ogbeifun, colleague, and co-author of one of the research publications for the continuous support. I express my gratitude to ESI-India for OpenFOAM training and their guidance in overcoming OpenFOAM modelling challenges. I also would like to thank the leadership and colleagues at Chevron Corporation (Aberdeen - UK, Houston & Midland - USA) and at Angola LNG. I would like to express my deepest gratitude to all dear friends for their encouragement and support.

## Declaration and Inclusion of Material from a Prior Thesis

This thesis is submitted to the University of Warwick in support of my application for the degree of Doctor of Philosophy. It has been composed by me and has not been submitted in any previous application for any degree.

I hereby state that this thesis is my own work, and this thesis has not been submitted for a degree at another university.

I have authored and published papers in peer reviewed journals. I have included the information from those papers and referenced where applicable.

I have utilised my work experience from multiple projects that I have carried out for my employers. But the data and information used for this research is gathered and analysed for the sole purpose of this study and is independent from my employer (no confidential data used).

List of papers published as part of the research.

- Nair, Sreeraj & Ogbeifun, Noma O. & Wen, Jennifer (2022) 'Consequence assessment considerations for toxic natural gas dispersion modeling.' *Journal of Loss Prevention in the Process Industries*. 78:104792.
  - 2022, This paper was republished in Fire and Blast Information Group - FABIG Newsletter #85.
- Nair, Sreeraj R. & Wen, Jennifer (2019) 'Uncertainties in Sour Natural Gas Dispersion Modelling.' *Chemical Engineering Transactions*. 77:355-360. DOI: 10.3303/CET1977060

Publications, closely related to this research used as reference and motivation.

- Fearnley, Jo & Nair, SreeRaj (2009) 'Using Predictive Risk Assessment to develop user friendly tools for on and off-site emergency planning.' *ICHEME Symposium Series NO. 155, Hazards XXI*. Paper 73 [link \(icheme.org\)](http://icheme.org)
- Nair, SreeRaj & Salter, Jim (2019), Layout - A Cost Effective and Powerful Design Step in Risk Management, *Chemical Engineering Transactions*. 77: 13-18. DOI: 10.3303/CET1977003

## Executive summary

The general area of the research lies in identifying the important source term characteristics of an accidental release of hydrogen sulphide containing natural gas (sour natural gas) and the key defining parameters in the sour gas dispersion modelling. This research study led to the development of a methodology for the selection of the consequence modelling for natural gas leaks from pipelines and the key modelling parameters to be subjected to the sensitivity analysis.

The research has evaluated the modelling tools and approaches for the three phases (i) discharge, (ii) expansion and (iii) dispersion following an accidental release. Release and dispersion of sour natural gas with a range of Methane and Hydrogen Sulphide compositions is evaluated in this study. A continuous high pressure dense natural gas leak from a transfer pipeline is the scenario of concern considered. Consequence modelling of this release scenario is carried out using different tools and approaches to estimate the downwind distance for the hazardous region of concern.

The first part of the research established that the depending on the gaseous mixture properties, and ambient conditions, the sour natural gas cloud from a release could be (i) dense (gravity slump), (ii) buoyant (rises over time), or (iii) neutrally buoyant (neither rises nor drops but disperses over time). The second part of the research determined the compositions of natural gas with shifts in buoyancy behaviours and identified the list of modelling parameters to be subjected to sensitivity analysis. The third part of the research developed a higher order Computational Fluid Dynamics (CFD) model for sour natural gas dispersion modelling and determined the appropriate solver and the modifications required on the model to take account of the effect of turbulence and the compositions. The first part used US EPA software ALOHA (CAMEO Suite by US EPA), the second part used commercially available and validated software packages commonly used in the Oil & Gas Industry – HYSYS and CANARY. The third part of the research used higher fidelity model OpenFOAM, an open-source CFD software.

The research findings concluded that the dispersion of the sour natural gas:

- Is sensitive to the release source terms hole size, release rate, and orientation of release.
- Is seriously affected by the terrain, obstructions and other the turbulence related parameters, stability class, wind speed and direction.
- Not significantly sensitive to the changes in humidity and ambient temperature.



The study also determined that the mass in a sour natural gas vapour cloud can increase or decrease depending on the buoyancy, turbulence, and the terrain. The Gaussian based modelling tools are quite suitable for emissions of pollutants whose density remains similar to that of air provided that the cloud does not move too far away from the ground, that there is no obstacle, no extreme meteorological conditions prevail, and there is a certain horizontal homogeneity. If parameters move away from these conditions, sophisticated models should be used.

The findings in this research (i) enables the risk analysts, project specialists, and local planners on hazardous substance transfer route selection, (ii) minimises the inconsistency in risk assessments and (iii) overcome the uncertainty in dispersion modelling whereby the right sized risk management can be deployed.

## 1. Introduction

The general area of the research lies in minimising the uncertainty in the sour natural gas dispersion modelling for the management of process risk. The study identifies the important source term characteristics and the key defining parameters in the release and dispersion modelling of hydrogen sulphide containing natural gas.

Accidental release of sour natural gas with a range of Methane and Hydrogen Sulphide compositions is evaluated in this study. A continuous high pressure dense natural gas leak from a transfer pipeline (flow line) is the scenario of concern considered for evaluation. Consequence modelling is carried out for release and dispersion using different tools and approaches to estimate the downwind distance for the hazardous region of concern. This research study led to the development of a methodology for the selection of the consequence modelling for natural gas leaks from pipelines and the key modelling parameters to be subjected to the sensitivity analysis.

### 1.1. Background and motivation

Natural gas is a fossil energy source that formed deep beneath the earth's surface. Natural gas contains many different compounds; the largest component of natural gas is methane ( $\text{CH}_4$ ) and contains smaller amounts of other hydrocarbons and nonhydrocarbon gases, such as hydrogen sulphide ( $\text{H}_2\text{S}$ ), carbon dioxide ( $\text{CO}_2$ ), nitrogen and water vapour. We use natural gas as a fuel and to make materials and chemicals. With the demand for energy on increase, unconventional gas resources including sour natural gas is explored (Guo & Ghalambar, 2005).

Natural gas containing significant amounts of  $\text{H}_2\text{S}$  and/or  $\text{CO}_2$  is known as 'Sour natural gas.'  $\text{H}_2\text{S}$  is highly toxic (fatal effects at low concentration), extremely flammable and corrosive (AIHA 2011, UK HSE 1993). Any significant unplanned and uncontrolled sour gas releases (like loss of containment of vessels, leaks from pipeline, etc.) could result in major casualties and environment impact (Kelly et. al. 2011, Nair & Wen 2019). For example, major incidents like 2003 Kaixian blowout (the '12.23 disaster') and 2007 Kab 121 loss of containment which resulted in multiple fatalities, injuries, environmental damages, and huge economic. Such disasters signify the need to better understand the risk from sour gas handling and have risk reduction measures in place (Danielson et. al. 2009, Elsharkwy 2002).

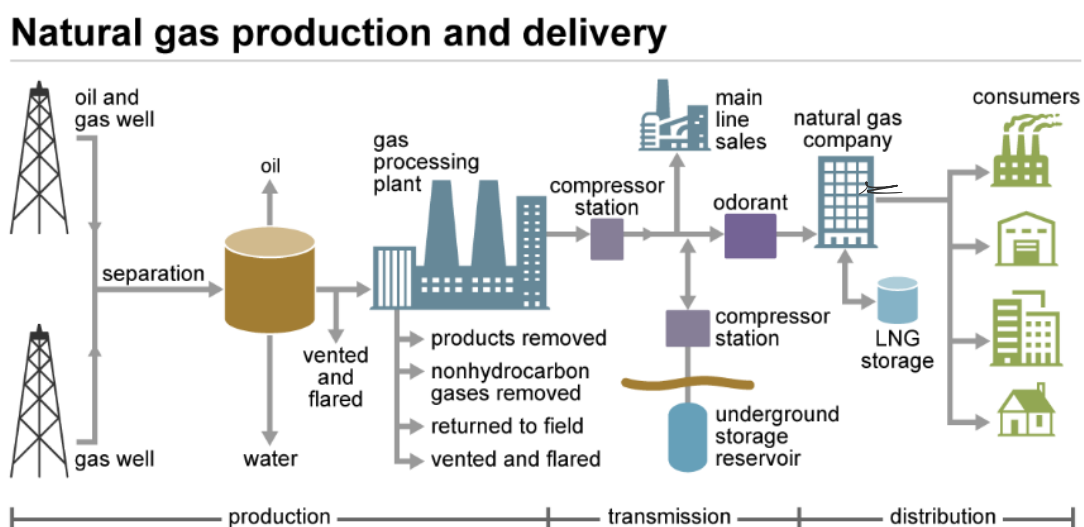
In natural gas exploration and production industry, the risk management efforts including release event prevention and consequence mitigation are prioritized using the process risk assessment outputs which is based on the scenario-based consequence modelling and its likelihood. Facility

siting and layout is a cost effective and powerful design step in process risk management (Nair & Salter, 2019). The potential impact zone (hazardous distances) from facilities, pipelines and units forms key information in site selection and layout optimization in multi-million projects. Incorrect selection of the consequence modelling approach, the software and any uncertainty in the input could lead to an inaccurate impact zone estimation which could result in disproportionate risk management efforts (Khan & Abbasi 1998b).

In addition to Oil and Gas (Energy) industrial sector, the risk from exposure to toxic H<sub>2</sub>S risk is also seen in several other industrial sectors including, animal fat and processing, breweries and fermentation processes, coal gasification plants, geo-thermal power plants, pulp & paper production, and waste treatment operations (AIHA 2011, Nilsen et.al. 2014, Danielson et.al 2009, US CSB 2003).

## 1.2. Natural gas production and delivery

Natural gas from wells is flown up to the surface and put into gathering pipelines and sent to natural gas processing plants. The gathering pipelines are small-diameter relatively low-pressure pipes. A complex gathering system can consists of thousands of miles of pipes, interconnecting the processing plant to hundreds of well in an area or a gas filed (Guo & Ghalambar, 2005). An illustration of natural gas production, treatment and consumption is given in Figure 1.



 Source: U.S. Energy Information Administration

Figure 1: Natural gas flow from reservoir to consumer

Natural gas is treated to remove impurities like H<sub>2</sub>S, CO<sub>2</sub>, water vapor before it is transported for commercial or domestic consumption. In places, where commercial consumption of natural gas as energy is not practical, it can be vented or flared or treated in capture processes for production

of sulphur or it can be re-injected for storage or increased oil recovery (Danielson et. al. 2009, GAO 2012, Speight 2007). Sour natural gas treatment to remove impurities is done at gas treatment and processing plants. Removal of H<sub>2</sub>S from sour gas is called 'sweetening'; the common processes include amine treatment unit, physical absorption unit, glycol dehydration units and sulphur recovery units.

The gas plant (usually common for several gas fields) could be at a distance from the wellheads such that the pipeline has to be routed through populated areas and through areas without continuous monitoring for any leaks. The review on incidents involving sour gas has pointed that lack of adequate knowledge of the hazards (that H<sub>2</sub>S releases could occur and the consequences of exposure) appeared to be a prime reason for the extent of the damage (Derundi et.al. 2014). The other common challenge that design engineer, project planners, plant operator and emergency responder face to design out, safely operate, plan, and mitigate the effects of toxic exposure in the event of accidental releases is the lack of information on the realistic estimate of the H<sub>2</sub>S toxic exposure zone (extent of the dispersion of the toxic cloud with potentially fatal effects) (Danielson et. al. 2009, IOGP 2010, Jiawen et.al. 2011).

This inadequacy or the gap in industry which led to major incidents and has the potential to result in disasters motivated this research. An unintended release from a pipeline transporting sour natural gas from reservoirs (gas fields) to gas processing plants is evaluated further as part of this research.

### 1.3. Sourness – the concern

H<sub>2</sub>S accompanies the release of any oil or gas from a well system where H<sub>2</sub>S exists. H<sub>2</sub>S gas causes a wide range of health effects depending on how much H<sub>2</sub>S is inhaled, and for how long. Exposure to high concentrations can quickly lead to incapacitation and death. H<sub>2</sub>S credentials as a killer are as lengthy as the history of the oil industry. The Immediately Dangerous to Life and Health (IDLH) limit set by The National Institute of Occupational Safety and Health (NIOSH), USA is only 100 parts per million (ppm). H<sub>2</sub>S has three lethal properties which make it frighteningly efficient:

- it acts rapidly
- it paralyses the respiratory centre
- it works (to fatal impacts) in concentration as small as 500 ppm

At very low concentrations H<sub>2</sub>S smells like rotten egg and hence commonly called as 'sour gas'. Exposure to greater than 700 ppm produce immediate unconsciousness and death within minutes. The only escape for a person endangered by H<sub>2</sub>S is to hold breath and try to get out of the deadly invisible cloud. It is like an invisible pool of water, if one is trapped in it, very less

chance of escaping. The sure remedy for H<sub>2</sub>S inhalation is to stay away. A real-life narrative of a survivor of sour gas exposure is given herewith.

#### **Oil field worker – Saskatchewan 2014**

Former Saskatchewan oilfield worker Jeff Crawford nearly died in a February 2014 accident.

On the eventful day in February 2014, Jeff was a 46-year-old hockey-playing oilfield worker was connecting a hose to a valve at a rural Saskatchewan production facility. The next, his face was sprayed with a mixture of oil, water, and gas. He inhaled and swallowed it, an exposure that changed rest of his life.

His medical records show that soup was laced with hydrogen sulphide (H<sub>2</sub>S), a toxic gas that carries risks to the human body ranging from burning vocal cords and olfactory senses to causing instant death.

Even after many years, Jeff's body struggles to complete its most basic tasks: chew food, swallow, taste, smell, speak properly, breathe clearly, and sleep soundly.

He says,

“I eat everything through a mashed-up liquid diet,” he says.

“I haven't smelled or tasted or eaten since the accident.

“With the medications, treatments, doctors, I relive that day every day.”

Sour gas exposure led to loss of his health, his career, his home, his independence and, eventually, his marriage.

It is alarming to note that 2014 oil field worker incident is not unique or one-off; as recently as in 2019 release of H<sub>2</sub>S hydrogen sulphide at Aghorn operating water-flood station, West Texas led to the death of one worker and spouse (US CSB 2021). This incident which happened during this research study and near the work location of the researcher highlights the significance and motivation on H<sub>2</sub>S risk management. Several similar incidents resulting in multiple fatalities and economic loss is listed in Table 4 highlights the magnitude of the sour natural gas concern.

H<sub>2</sub>S deactivates catalysts, is corrosive to metal piping and hence is eliminated from industrial processes or removed from gas before it is transported. However, removing large quantities of

H<sub>2</sub>S from natural gas is costly. Impact of H<sub>2</sub>S corrosion on the pipeline handling sour gas is given in Figure 6. Based on the historical pipeline failure rate data gathered by U.S. Department of Transportation (Muhlbauer 2003), it was estimated that 50% of moderate sized releases of sour natural gas from the pipeline do not ignite and a further 40% ignite after some delay, which implies that 90% of releases could result in toxic cloud leading to fatalities. Dispersion following accidental release of sour gas during pipeline transfer is the accident type covered by the research.

#### 1.4. Role of consequence assessment in risk management

Facilities handling chemicals and hazardous materials evaluate risk in order to address the potential major accident hazard challenges. Even with the best controls and practices (management system) in place, the potential for a major accident will never be eliminated. As a minimum, Industry Standard and Good Engineering practices shall be followed to prevent major incidents and limit the consequences to people and the environment. Predictive risk assessments are carried out to identify the range of potential consequences from hazardous scenarios, to determine the potential severity effects and how frequently such events can happen (Fearney & Nair 2009). These assessments and detailed studies help us in determining the adequacy of the safety barriers or layers of protection to effectively manage the risk by prevention, control and/or mitigation.

Risk management is the term generally used to cover the whole process of identifying and assessing risk and setting goals and creating and operating systems for their control (Mannan 2014). Among these, risk assessment aims to answer the following questions:

- Hazard – What can go wrong?
- Consequences – How bad could it be?
- Likelihood – How often might it happen?

There are several approaches and tools available for quantitative modelling or the estimation of consequences. It ranges from indexing, modelling and to experiments. Consequence assessment is a part of the overall risk assessment, which consists of the assumptions and calculations used to predict the potential impacts of an accidental release of hazardous material; this includes the estimation of release/discharge rate (source term), initial mixing, dispersion, and phase changes (Mannan 2014, Wells 1994). In general, consequence assessing approaches can be clustered into:

1. Correlations or formulae and phenomenological models: These models relate one quantity to another empirically e.g., Gaussian-type models, if probabilistic approximation is enough.
2. General purpose integral-type models: one tool composed of a few, partly phenomenological, equations to describe overall properties (the integral properties) of a flow. E.g., for dense gas release, tool model initial conditions as jet like dispersion followed by neutral Gaussian at medium and long range.
3. Computational Fluid Dynamics (CFD), Computational Three dimensional (3D); e.g., Reynolds Averaged Navier Stokes (RANS), Large Eddy Simulation (LES) or deterministic answers, detailed engineering, and modelling.
4. Experiments, wind tunnel and field testing.

Dispersion of dense gas (sour gas at certain composition could behave as dense) is significantly different from the widely recognised trace gas releases (ongoing/continuous emissions) in the atmosphere (Mohsen-Nia et.al. 1993, Mohan et. al. 1995). For high pressure, high release rate and dispersion of accidental releases of sour gas, decision maker requires more convincing results that take account of the multicomponent thermodynamics, terrain effect and the phase transitions in the releases; simple correlation like Gaussian model alone is not considered as suitable and appropriate. Conducting large scale field trials using toxic gas may not be a viable option either.

The integral models can simulate the transitions between different stages of dense-gas dispersion, including slumping, creeping, phase transition and passive dispersion. Most integral models have a pseudo-component model, and some have multi-component model (but with limited features). Pseudo-component model estimates the properties of the mixture as one component representing for a range of multiple component properties. In typical integral models, terrain effect is still not considered in the integrated models, but partially addressed by introducing surface roughness. When it comes to simulation involving complex geometry, options are limited to the likes of CFD modelling tools because the influence of surface roughness, terrain effects and obstacles is significant and cannot be neglected (Enger & Koracin, 1995, Fontaine et.al. 1991, Johnson & Marx, 2003). However, CFD approach is limited by the ability to model sub grid scale turbulence; some tools overcome this by distributed porosity concept (Porosity, Distributed Resistance - PDR model) to account for the objects which cannot be represented by the grid. Physical modelling involving the use of wind tunnel or fluid modelling facilities is useful for complex flow situations, such as releases near buildings, complex terrains,

and potential diffusion near release (IOGP 2010, Qingchin and Laibin 2011). The results of risk assessments will always be associated with some uncertainty, which may be linked to the relevance of the data basis, the models used in the estimation, the assumptions, simplifications, or expert judgements that are made (NORSOK 2001).

### 1.5. The opportunity

It is unlikely that a consequence modelling analyst will ever be able to resolve the question “Just how reliable are the results?” in the absence of concise and definite answers to the gas dispersion modelling. An incorrect estimation can lead to disproportionate risk management. Which means, multi-billion-dollar decisions taken based on these modelling results may not be leading to adequate risk reduction or on the other side could lead to spending more time and resources without significant risk reduction benefits.

A number of mathematical codes and user-friendly tools are available in the market for passive gas dispersion and for dense gas dispersion; some of the tools are simple which can be used with minimum training whereas there are complex resource intensive tools that require specialist competence and skill. Most of the tools and codes are developed for certain specific requirement/application and only validated for an array of materials, terrain, duration, dimension, and dispersion range. It is noted that in the absence of experimental data, methodology and results are extrapolated from available database and modelling parameters. This often is recognised as a constraint to the effectiveness of the consequence assessment. Some of the main limitations noted for the commonly used dispersion modelling tools and methodologies are:

- Modelling the release and dispersion of multi-component material with a range of density and properties (including toxic component H<sub>2</sub>S).
- Modelling gas dispersion without (or not adequately) taking account of the meteorology, terrain and topography effects in near field and far field.
- Dispersion modelling taking account of the meteorological effects (wind, atmospheric stability, weather, extreme conditions) for long duration releases and dispersion (active dispersion of passive clouds).
- Determining dispersion end point (criteria) for H<sub>2</sub>S containing natural gas.

This research identifies the key parameters that could influence the gas dispersion modelling and determine appropriate methodology to address the limitations, this includes:

- Source terms to be defined appropriately to reflect the release scenario.



- Meteorological inputs and atmospheric conditions that need to be subjected for sensitivity analysis for continuous release and dispersion with far field impact.
- Cloud behaviour of sour natural gas (buoyant, neutrally buoyant, and dense gas) for a range of H<sub>2</sub>S concentration which helps in the selection of appropriate dispersion model.
- Guidance for selection and deployment of time and resource intensive methodologies like Computational Fluid Dynamics.

### 1.6. Study methodology and thesis outline

Dispersion and consequence modelling is a key part of the process risk estimation and risk management in the high hazardous Oil & Gas industry. An incorrect estimation can lead to disproportionate risk management. This research addresses this challenge and provide guidance for the risk management professionals for making appropriate decisions in multi-billion-dollar capital projects and safe operation of major hazard facilities.

The overall aim of this research is to address the modelling limitations and uncertainties, specifically related to the releases from the pipeline transfer of Hydrogen sulphide bearing natural gas. Uncertainties in consequence modelling can be due to the lack of availability of suitable tools, selection of methodology, adequate input or due to the associated assumptions made. The objective of this study is to find ways to minimise the reducible error in the sour natural gas dispersion modelling and methods to overcome the uncertainties. A step-by-step research methodology was developed based on the technical guidance for the vulnerability (hazard impact) analysis of extremely hazardous substances by United States Environmental Protection Agency (US EPA) and the safety report assessment guidance by the United Kingdom Health and Safety Executive (UK HSE). The specific area of study focuses on the dispersion of sour natural gas following a release from high pressure pipeline. The phased approach initially identified the list of inputs, assumptions and modelling parameters that could have an impact on the release and gas dispersion modelling. Initial parameter screening is carried out using a general-purpose integrated tool. Following that, phase equilibrium simulation was carried out to determine the H<sub>2</sub>S composition where the sour natural gas cloud buoyancy deviates from positively buoyant to passive or dense. Detailed analysis using CFD simulations was then carried out for the selected sour natural gas compositions. Through this phased approach, the study determines the key parameters to be used for sour natural gas dispersion modelling. The overall methodology followed for this research study is summarised in Figure 2.

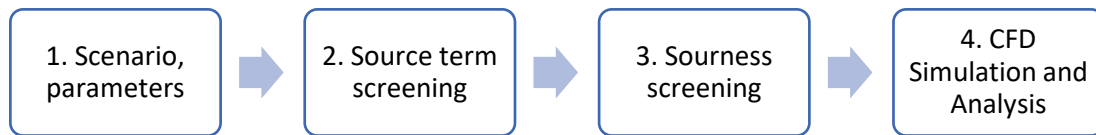


Figure 2: Research study steps

The study methodology captured in the structure of this thesis is given below:

- Identification and evaluation of the currently available software tools and the experiments to validate using literature review is discussed in Chapter 2.
- The scenario description, source term and the dispersion modelling parameter listing is given in Chapter 3.
- Parameter screening, phase equilibrium-based composition evaluation and guidance on the parameters to be subjected to sensitivity assessment is explained in Chapter 4. Application of consequence modelling in an actual application is also discussed here.
- CFD fundamentals and OpenFOAM modelling with validation is explained in Chapter 5.
- The CFD simulation results and the sensitivity to compositions is further analysed in Chapter 6.
- Chapter 7 summarises the study findings and the role of sensitivity assessment in dispersion modelling. It also lists the scope for further research.

## 2. Literature review – sour natural gas dispersion modelling

A literature review was conducted to gather information on sour natural gas characteristics and available research on the impact and related consequence assessments. Existing dispersion modelling studies, guidance, and experiments on release and dispersion behaviour and incident investigations provide a foundation for the current research. Information was gathered and reviewed to establish and streamline the research focus.

### 2.1. Natural gas and sourness

Natural gas, also called fossil gas is a naturally occurring hydrocarbon gas mixture primarily of methane, varying amounts of higher alkanes and small percentage of non-hydrocarbons. Natural gas doesn't have a standard composition. North Sea gas will differ from Russian gas, which will differ from Shale gas. For this reason, the fluid properties are given as a range, for example the density of natural gas is usually given as 0.7 - 0.9 kg/m<sup>3</sup>.

Natural gas is usually considered *sour* if there are more than 5.7 milligrams of hydrogen sulphide per cubic meter of natural gas, which is equivalent to approximately 4 ppm by volume (0.0004 vol% of H<sub>2</sub>S) under standard temperature and pressure (Speight 2007). The tubing, pipes and pumps for sour gas must be made of special metal, since H<sub>2</sub>S is corrosive (Total 2016).

In the Oil & Gas industry, with the deepening of oil & gas reservoirs exploration and development, an increasing number of sour gas reservoirs especially those with high content of H<sub>2</sub>S are developed in the world. One-fifth to one-third of all-natural gas resources in the world could fall under the sour gas classification (Kelly et.al. 2011, Total 2016). Sour natural gas reservoirs are distributed all over the world, particularly large, filed reservoirs in the Caspian Sea, Middle East, Canada, Asia Pacific and smaller more distributed in the US and other fields with excess developments. A representative range of natural gas composition is given in Table 1.

Table 1: Sour natural gas mixtures

Component (Vol %)	Alberta, Canada	Kansa, USA	McElroy, USA	Tunisia	Kazhgan, Kazakhstan	Tieshamnpo, China	Biogas
Methane (CH <sub>4</sub> )	77	73	66	97	58.8	78	63
H <sub>2</sub> S	< 4	0	< 30	<1	7.7 to 30	15	< 3
CO <sub>2</sub> , Nitrogen (N <sub>2</sub> )	<6	<15	25	2	<1	6	37
Hydrocarbon C <sub>3</sub> +	15	< 10		< 2	15 to 20	1	<1

Natural gas reserves with hydrogen sulphide concentration ranging 20% to 40% are not uncommon and some concentrations could be as high as 70% to 90%. Such sour natural gas fields

are found in Europe, Africa, North and South America, and the Far East, but the Middle East and Central Asia hold the largest volumes (Total 2016, Wen et.al. 2013). About 17% of gas reserves exploited in the US have very high levels of hydrogen sulphide and about 40% of the natural gas field in Alberta, Canada is considered sour (Kelly et.al. 2011).

## 2.2. Hydrogen sulphide – properties and toxicity concern

Hydrogen sulphide, a chemical component with formula  $H_2S$ , is a highly toxic and flammable gas; it is colourless with a characteristic odour of rotten eggs, very poisonous and corrosive. Hydrogen sulphide is a flammable gas at ambient temperature and pressure (NIOSH 1977). The National Fire Protection Association (NFPA 1974) placed hydrogen sulphide in the highest flammability classification. Chemical and physical data for Hydrogen sulphide are summarised in Table 2 (ATSDR 2006, AIHA 2011).


Table 2: Chemical and Physical Data for Hydrogen sulphide

Parameter	Data
Common name	Hydrogen sulphide
Synonyms	Dihydrogen monosulphide, Hydrosulphuric acid, Sulphuretted hydrogen, Sewer gas, stink damp, rotten-egg gas
CAS registry number	7783-06-4
Chemical formula	$H_2S$
Physical state	Colourless gas
Molecular weight	34.08
<b>Properties</b>	
Liquid density (1.013 bar at boiling point)	949.2 kg/m <sup>3</sup> (8.3 lb/gal)
Melting point	-85.49 °C
Boiling point (1.013 bar)	-60.3 °C
Flash point	26 °C
Vapour pressure (at 21 °C)	18.266 bar
Specific gravity (gas at 15°C, 1 atm.)	1.1895 (Air = 1)
Gas density (1.013 bar and 15 °C)	1.4534 kg/m <sup>3</sup>
Critical temperature	99.95 °C
Critical pressure	90 bar
Critical density	347.28 kg/m <sup>3</sup>

Parameter	Data
Conversion for various measure of H <sub>2</sub> S content in natural gas	1 ppm = 1.4 mg/m <sup>3</sup> (1mg/m <sup>3</sup> = 0.7 ppm), in air 1.0 % = 628 grains per 100 scf 1.0 % = 10,000 ppm 0.25 grains per 100 scf = 4.0 ppm by volume 0.25 grains per 100 scf = 0.0004 % by volume
<b>Property related to flammability</b>	
Flammability limits in air	4.3 – 45.5 vol%
Auto ignition temperature	260 °C
Minimum ignition energy	0.068 mJ
NFPA flammability	4 (rapid vaporization in air and burn readily)
<b>Toxicity data/ exposure guidelines</b>	
Time – Weighted average (TLV-TWA)	5 ppm (8-hour TWA concentration that may not be exceeded)
Short – Term exposure limit (TLV-STEL)	15 ppm
The OSHA permissible exposure limit (PEL) to H <sub>2</sub> S for general industry (see 29 CFR 1910.1000, Table Z-2).	20 ppm, not to be exceeded at any time during an 8-hours 50 ppm allowed for up to 10 minutes per 8-hour period
Immediately Dangerous to Life and Health (IDLH)	100 ppm

DOT hazard label classified hydrogen sulphide as poison gas and flammable gas (US DOT, 2018). The NFPA (Figure 3) classifies H<sub>2</sub>S with a hazard value '4' for both health and flammability (NFPA 2010). The explosive and flammable range of H<sub>2</sub>S is much higher than permissible exposure level to prevent toxicological effects.

#### NFPA 704

Diamond	Hazard	Value	Description
	Health	4	Can be lethal.
	Flammability	4	Burns readily. Rapidly or completely vaporizes at atmospheric pressure and normal ambient temperature.
	Instability	0	Normally stable, even under fire conditions.
	Special		

(NFPA, 2010)

Figure 3: Hydrogen sulphide NFPA 704

Toxicity of H<sub>2</sub>S is comparable to cyanide, a broad-spectrum poison, which affects multiple parts of the body. It can block oxygen, in mitochondria and stop cellular respiration. Health effects begin with prolonged exposures as low as 2 to 5 ppm, potentially resulting in nausea, tearing of the eyes, headaches, and loss of sleep. Generally, industry practice uses 10 ppm as an alarm set point to warn workers of the hazard, and to evacuate the area. Effects on human from acute exposure is given in Table 3 (Nilsen et.al. 2014, CCOHS 2016, NOAA 2022, NIOSH 2016).

H<sub>2</sub>S sometimes can be detectable by its characteristic odour; however, the sense of smell cannot be relied upon to provide a warning of higher concentrations of the gas (i.e., greater than 100 ppm) because H<sub>2</sub>S rapidly eliminates the sense of smell (due to paralysis of the olfactory nerve above 50 ppm). H<sub>2</sub>S remains in the atmosphere for approximately 1–42 days, depending on the season. It can change into sulphur dioxide and sulphates in the air. A typical warning sign to be displayed at sites with potential H<sub>2</sub>S exposure is given in Figure 4.

**Table 3: Effects from acute Hydrogen sulphide exposure**

Concentration	Effect on body
10 ppm	eye and respiratory tract irritation
100 ppm	coughing, headache, dizziness, nausea, eye irritation, loss of sense of smell in minutes
200- 250 ppm	potential for pulmonary edema (lung damage) after 20 minutes
400 ppm	loss of consciousness after short exposures, potential for respiratory arrest
500 – 700 ppm	staggering, collapse in 5 minutes, serious damage to the eyes in 30 minutes, death after 30-60 minutes
700- 1000 ppm	Immediate loss of consciousness may lead rapidly to death; prompt cardiopulmonary resuscitation may be required
1000 – 2000 ppm	nearly instant death



**Figure 4: Hydrogen sulphide warning sign**

Source: iStockphoto

It is possible for H<sub>2</sub>S gas to accumulate in any low area or in enclosed areas, such as gas venting systems, mud systems, cellars, pits, and tanks. A condition referred to as "knockdown," or swift unconsciousness, can occur in such locations, with collapse occurring with 1 to 2 breaths. Breathing then stops and death occurs within minutes if H<sub>2</sub>S exposure continues (API RP 49, 2001). Simply opening a hatch can lead to knockdown if a worker breathes in gases coming out

of the hatch. An H<sub>2</sub>S meter will not provide fast enough warning in this situation, as knockdown is almost immediate when H<sub>2</sub>S is at or above 700 ppm. A copy of the US Occupational Safety and Health Administration's (OSHA) quick card on H<sub>2</sub>S is given in Figure 5. Such information cards, warning signs and messages are used for improving awareness and maintaining the sense of vulnerability.

H<sub>2</sub>S can readily dissolve in water and dissociate to release H<sup>+</sup> which can accelerate corrosion, and this causes deterioration of the metal containment like pipeline, vessel or equipment (Shi et.al. 2015). H<sub>2</sub>S at high temperature or in the presence of catalyst reacts with SO<sub>2</sub> to form water and elemental sulphur, therefore thermodynamic properties and especially phase equilibria of gaseous systems are detrimental in release and dispersion modelling (Mohsen-Nia et al. 1993).

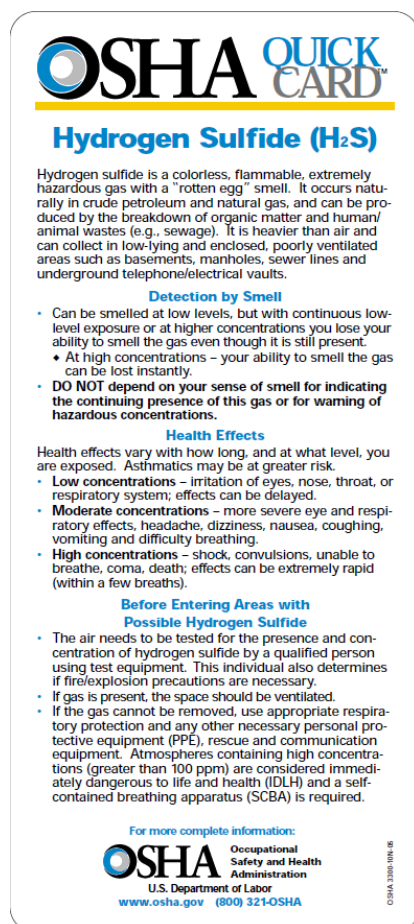


Figure 5: Hydrogen sulphide Quick card, OSHA

H<sub>2</sub>S is highly corrosive and causes metals to thin or to become brittle. Metal fatigue, including hydrogen embrittlement, or sulphide stress cracking, can result in equipment failure, which can release H<sub>2</sub>S gas, and lead to H<sub>2</sub>S exposure and injury. Therefore, employers need to take special precautions when choosing equipment when they may reasonably expect to encounter H<sub>2</sub>S.

National Association of Corrosion Engineers (NACE) standard MR 0175 includes recommendations for selection of specific materials when H<sub>2</sub>S is present. Some photographs representing the pipeline corrosion due to H<sub>2</sub>S is given in Figure 6.

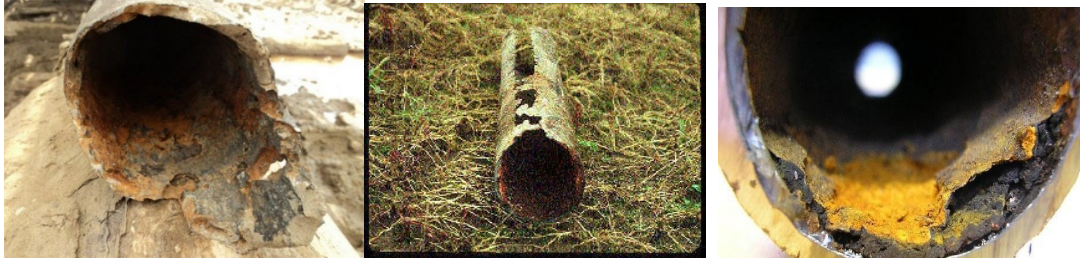


Figure 6: Corrosion on pipeline handling sour gas

Sources:

[eTool : Oil and Gas Well Drilling and Servicing | Occupational Safety and Health Administration \(osha.gov\)](#) link accessed on April 2019

[Corrosive gases CO<sub>2</sub> and H<sub>2</sub>S in the stream of produced oil and gas condensate \(himipex.com\)](#) link accessed on April 2019

[Hydrogen Sulfide Corrosion | ReStream Solutions](#) link accessed on April 2019

### 2.3. The hazard and incidents

Natural gas is commonly transported using a pipeline (Deng et. al. 2018) and loss of containment from the gas pipeline occurs due to integrity degradation and external factors like earthquakes, human activities. From 1994 through 2013, 1796 serious incidents with gas distribution, transmission and other handling resulting in 682 fatalities, 2646 injuries and about \$1.5 billion property damage. According to U.S. Occupational Safety and Health Administration records, there were 80 fatalities in 57 H<sub>2</sub>S incidents from 1984 to 1994 (Fuller & Suruda 2000). Nineteen deaths and 36 H<sub>2</sub>S-induced injuries occurred among people attempting to rescue victims overcome by the gas (US EPA 2010).

United States Department of Labor (US DoT) has H<sub>2</sub>S in the list of highly hazardous chemicals, toxics and reactive (mandatory) under the Occupational Safety and Health Administration (OSHA) Standard 29 CFR 1910 Subpart H, 1910.119 App A, Process Safety Management of highly hazardous chemicals, with a Threshold quantity 1500 pounds (US DoL 2022). Vapor concentrations on the order of 500 to 1,000 ppm or more are usually fatal within minutes (Chou 2003, UK HSE 2022, US DoL 2019). It is noted that many of the reported fatalities occurred in confined spaces (sewers, animal processing plants, manure tanks) and result from respiratory failure, initially presenting with respiratory insufficiency, non-cardiogenic pulmonary edema, coma, or cyanosis (US DoL 2022).



A number of sour natural gas release incidents (BSEE 2014, Zhang J. et.al. 2011) have happened in the recent past is given in Table 4, some of them resulted in catastrophic consequences (hundreds of fatalities).

**Table 4: Sour gas Incidents**

Incident	Date	Consequence and description
<b>Poza Rica, Mexico</b> low altitude temperature inversion	1950	Twenty-two persons died and 320 were hospitalized as a result of exposure to hydrogen sulphide which was released into the atmosphere within a 20-minute period. The source of the gas appeared to be a malfunctioning flare intended to burn off excess gas from a sulphur recovery plant. The gas piped to the flare contained 81% carbon dioxide, 16% hydrogen sulphide and 3% hydrocarbons and water
<b>Sour gas gathering line rupture, USA</b> (EPA records)	1974-1991	11 incidents, Multiple fatalities, Unspecified number of wildlife died
<b>H<sub>2</sub>S tragedy, Texas</b>	1975	Oil field pipeline, 9 fatalities
<b>Gezi, The Zhao 48# well;</b> pure H <sub>2</sub> S gas well blowout in the oil testing process	1992	6 fatalities and 24 poisoning; 20 <sup>th</sup> team of under pit operation corporation, Petroleum administration, Bureau of North China
<b>Kaixian blowout</b> (Chongqing “12.23” disaster), high sulphur gas well blowout	2003	240+ fatalities, 2000+ hospitalization, 65000 evacuated, the distance to which death was recorded extended to 1200m from the wellhead; direct economic loss of 6400 million Yuan (~900 million USD). The distance to which death was recorded extended to 1200 m from the wellhead.
<b>Sichuan (The Luo 2# well)</b>	2006	About 10000 people evacuated
<b>Kab-121 Platform;</b> well blowout, Gulf of Mexico, Oil and gas with H <sub>2</sub> S,	2007	Release from Usumacinta Jack-up at wellhead in Kab field, has resulted in 22 fatalities and damage to environment

Incident	Date	Consequence and description
<b>Southeast Saskatchewan, Canada</b>	2010-2014	43 sour gas leaking facilities “with average H <sub>2</sub> S concentrations at 30,000 ppm.” That's 30 times higher than the level that is fatal to humans. In one case, a well emitted 150,000 ppm: fatality
<b>Kashgha field, Kazakhstan</b>	2013	200 km of leaking pipeline, \$3.6billion to replace
<b>Pacific OCS, US Dept. of Interior, BSEE Safety Alert</b> 22, Feb 2014	2012-2013	H <sub>2</sub> S (40000 ppm) release from piping corrosion (due to elemental sulphur <sup>1</sup> )

Note 1: The elemental sulphur in the scale was the result of oxygen contamination in the wet, sour gas stream. Oxygen reacts with hydrogen sulphide in liquid water to form elemental sulphur.

Major sour natural gas release events like 1992 Gezi, Zhao 48# well and 2003 Kaixian blowout, the “12.23” disaster, illustrates the serious threat from handling and transporting sour gas. 90% of sour natural gas releases could result in toxic cloud dispersion with potential impacts (Muhlbauer 2004).

In their paper, Bariha et.al reported that out of 185 accidents involving natural gas, the pipeline accidents accounted for 127 and the most frequent accident were caused by mechanical failure (fatigue, creep, brittle fracture, and corrosion) of the pipelines or due to significant changes to the surrounding environment (Bariha et. al. 2016). Further analysis was carried out on the pipeline incidents using the statistics from European gas pipeline database of information on natural gas pipelines approximately 1.5 million km in length (EGIG). The failure frequency and the relative hole size comparison with the failure causes is given in Table 5. The hole sizes are defined as follows: small hole, hole size is lower than 2 cm; medium hole, hole size ranges from 2 cm up to the pipe diameter; great hole, full bore rupture or hole size is greater than the pipe diameter.

**Table 5: Pipeline failure data analysis (Bariha et. al. 2016)**

Failure causes	Failure frequency (per km)	Percentage of total failure rate (%)	Percentage of different hole size (%)		
			Small	Medium	Great
<b>External interference</b>	$3 \times 10^{-4}$	51	25	56	19
<b>Construction defects</b>	$1 \times 10^{-4}$	19	69	25	6
<b>Corrosion</b>	$8.1 \times 10^{-5}$	14	95	3	<1

Failure causes	Failure frequency (per km)	Percentage of total failure rate (%)	Percentage of different hole size (%)		
			Small	Medium	Great
Ground movement	$3.6 \times 10^{-5}$	6	29	31	40
Others/unknown	$5.4 \times 10^{-4}$	10	48	39	13

The analysis reflects that even for well designed, constructed, and maintained pipeline network, incidents happen due to various factors resulting in loss of containment.

## 2.4. Consequence modelling approaches and tools

Predictive risk assessments are carried out to determine the extent of hazardous level distances (impact zone) and how frequently such events can happen (Nair & Wen 2019). When estimating risk along the pipeline routes transferring hydrogen sulphide containing natural gas pipelines, researchers begin by determining dispersion behaviours according to key gas dispersion models. Consequence modelling tools help to evaluate the consequences from dispersion of toxic gases, smoke, fire, explosions, and other impacts. A vast array of models is available for carrying out consequence assessment and these range from simple one-dimensional phenomenological models to sophisticated three-dimensional Computational Fluid Dynamics (CFD) simulations (Coldrick 2017). Such models for predicting the behaviours of hazardous gas have been heavily researched (since the early 80s) to estimate the extent to which an affected region could be impacted by the dispersion following an accidental release. Dispersion is a term used by modellers (process risk analysts) to include advection (moving) and diffusion (spreading) of pollutant in air. A step-by-step approach for consequence modelling generally followed (Aloquaily 2018) is given in Figure 7.

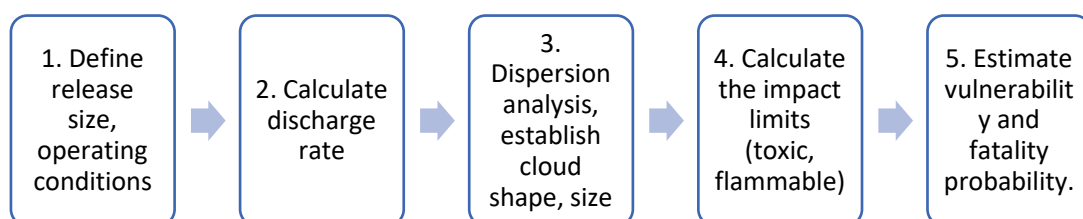


Figure 7: Consequence modelling steps

When a gas leaks from a process there is a boundary between when the gas is influenced by its process characteristics or thermodynamics (i.e., pressure, temperature, etc.) and the point where it becomes influenced by the ambient conditions (i.e. wind speed, terrain, temperature, etc.). It is extremely complicated to model a gas release due to the number of variables acting upon the released gas. It is not accurate to base a gas dispersion model on gas densities alone.

Even on a calm day with some low wind, it is enough to displace gases even though the wind cannot be felt.

For determining the right approach for consequence modelling, it is necessary to decide:

- (i) What is the scope of the study?
- (ii) What is the required depth of the study?
- (iii) How many release scenarios will be modelled?
- (iv) Who will carry out the study?
- (v) Will the analysis need to be updated in the future, or the results interrogated? If so, who will do this?

In some cases, the modelling need to be carried out in steps where the output from one step of the analysis will become the input to the next step. Several models are currently available for simulating the hazardous gas discharge, dispersion and for evaluating the extent of impact on the surrounding environment. In some cases, different tools will be required to estimate sections of the modelling based on the tool capability and the modelling phenomenon. A popular list of general-purpose software tools and widely used CFD packages which can be used for sour natural gas modelling is given in Table 6.

**Table 6: Consequence Modelling Software**

Tool and Provider	Source of further information
<i>General purpose software (Integral)</i>	
ALOHA, CAMEO by US EPA	<a href="https://www.epa.gov/cameo/aloha-software">https://www.epa.gov/cameo/aloha-software</a>
CANARY, by Quest	<a href="http://www.questconsult.com/software/canary/">http://www.questconsult.com/software/canary/</a>
CALPUFF from ESC	<a href="http://www.src.com/">http://www.src.com/</a>
EFFECTS by TNO through Gexcon	<a href="https://www.gexcon.com/products-services/EFFECTS/31/en">https://www.gexcon.com/products-services/EFFECTS/31/en</a> <a href="https://www.tno.nl/en/focus-area/urbanisation/environment-sustainability/public-safety/effects-software-for-safety-and-hazard-analysis/">https://www.tno.nl/en/focus-area/urbanisation/environment-sustainability/public-safety/effects-software-for-safety-and-hazard-analysis/</a>
ERCBH2S	<a href="https://www.aer.ca/documents/directives/ERCBH2S_Overview.pdf">https://www.aer.ca/documents/directives/ERCBH2S_Overview.pdf</a>
FRED by Shell through Gexcon	<a href="https://www.gexcon.com/products-services/FRED-Software/26/en">https://www.gexcon.com/products-services/FRED-Software/26/en</a> <a href="http://docslide.us/documents/fred-51-technical-guide.html#">http://docslide.us/documents/fred-51-technical-guide.html#</a>
HAMS-GPS from HAMSAGARS	<a href="https://www.hams-gps.net/">https://www.hams-gps.net/</a>
Phast and Safeti, from DNV-GL	<a href="https://www.dnvgl.com/software/products/phast-safeti-products.html">https://www.dnvgl.com/software/products/phast-safeti-products.html</a>
PERSEE by GDF SUEZ <sup>1</sup>	<a href="http://www.persee.fr/">http://www.persee.fr/</a>

Tool and Provider	Source of further information
TRACE, Safer Systems	<a href="https://www.safer-system.com/">https://www.safer-system.com/</a>
<i>Computational Fluid Dynamics Software</i>	
ANSYS FLUENT	<a href="http://www.ansys.com/Products/Fluids/ANSYS-Fluent">http://www.ansys.com/Products/Fluids/ANSYS-Fluent</a>
Fluidyn PANACHE	<a href="http://www.fluidyn.com/fluidyn/panache">http://www.fluidyn.com/fluidyn/panache</a>
GexCon FLACS	<a href="http://www.gexcon.com/flacs-software">http://www.gexcon.com/flacs-software</a>
Kameleon Fire Ex (KFX)	<a href="http://www.computit.no/?module=Articles;action=Article.publicShow;ID=347">http://www.computit.no/?module=Articles;action=Article.publicShow;ID=347</a>
OpenFOAM	<a href="http://openfoam.com/">http://openfoam.com/</a> - by ESI (OpenCFD Ltd) <a href="http://openfoam.org/">http://openfoam.org/</a> - The openFoam foundation

Note 1: Corporate company In-house codes with limited/no access in public domain.

The model types range from simple equations that can be solved by hand calculations to complex models that require massive amount of input data and powerful computers (US EPA 2018). Dispersion modelling tools generally depends on variables such as wind speed and direction, air temperature, rainfall, the topography of the area and the presence of obstacles. The types of models commonly used (Beggs 2002, Zhang J. et.al, 2011) are:

- (i) Gaussian models, which are described by diffusion equations,
- (ii) CFD models using fluid dynamics to model the dispersion, and
- (iii) Reduced scale models (based on wind tunnel experiments).

The Lagrangian models, which are particle tracking and the Eulerian models using the atmospheric transport equation numerically in a fixed coordinate frame (Zhang & Chen 2007).

The dispersion models used for hazard assessment predict concentrations at points distant from a source of gas (though there are differences of detail in the ability to model aerosols, obstacles, terrain etc.). The fundamental process of turbulent mixing in a stratified gas cloud in the atmosphere is incompletely understood at a fundamental level (Nilsen et. Al. 2014).

**Passive (neutrally buoyant) gas:** The Gaussian plume model is the most widely used dispersion model, which is suitable for neutral gas (Zhang J. et.al. 2011). Gaussian models are often functions of distance from the release point or time since release and describe a 3-D emission cone field generated by a point source. Gaussian based models depend on a system of differential equations called the diffusion equations (Mannan 2012, EPSC 1999). The model considers wind and atmospheric turbulence forces that move the molecules of a released gas through the air. As a cloud is transported downwind, "turbulent mixing" causes it to disperse,

thereby expanding and spreading in the crosswind (horizontal) and vertical directions. This plume model is a steady state model and therewith based around the central line. A graph of the gas concentration within any crosswind slice of a moving pollutant cloud looks like a bell-shaped curve, highest in the center and lower on the sides (Figure 8).

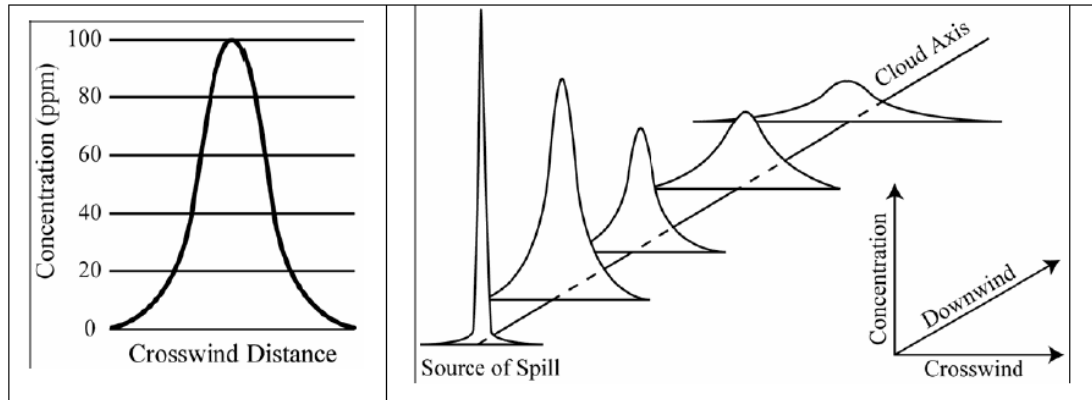


Figure 8: Distribution (left) and spread (right) in a Gaussian model

For Gaussian modelling, typically, the concentration of natural gas releases from a continuous elevated point source is estimated using Equation 1 (Ravi et. al. 2016).

$$c(x, y, z, H) = \frac{Q}{2\pi v \sigma_y \sigma_z} \exp\left(-\frac{y^2}{2\sigma_y^2}\right) \left\{ \exp\left[-\frac{(z-H)^2}{2\sigma_z^2}\right] + \exp\left[-\frac{(z+H)^2}{2\sigma_z^2}\right] \right\}$$

Equation 1

where:

$c(x, y, z, H)$  = hourly concentration at downwind distance  $c$ ,  $\mu\text{g m}^{-3}$

$v$  = mean wind speed at pollutant release height,  $\text{m s}^{-1}$

$Q$  = pollutant emission rate,  $\mu\text{g s}^{-1}$

$\sigma_y$  = standard deviation of lateral concentration distribution

$\sigma_z$  = standard deviation of vertical concentration distribution

$H$  = pollutant release height (stack height),  $\text{m}$

$y$  = crosswind distance from source to receptor,  $\text{m}$

Gaussian models have proven to be accurate within 20% at ground level at distances less than 1 km, and accurate within 40% for elevated emissions (Ravi et. al. 2016).

**Heavy gas:** A gas that has a molecular weight greater than that of air (approximately 29 kilograms per kilomole, on average) will form a “heavy” gas cloud if sufficient gas is released. When a gas that is heavier than air is released, it will initially “slump,” or sink, and as the gas cloud moves downwind, gravity affects the spread and can result in some of the vapour moving upwind of its release point (Ermark 1991, Aloqaily 2018, Mannan 2014). Farther downwind, as the cloud becomes more dispersed and its density approaches that of air, it begins to behave like a

neutrally buoyant gas. Study by Jiea et. al. compared the different gas diffusion modelling approaches with engineering applicability and accuracy for heavy gas instantaneous or continuous diffusion (Jiea et.al. 2014), a summary is given in

Table 7.

**Table 7: Comparison of gas diffusion modelling approach**

<b>Modelling approach</b>	<b>Scope of application</b>	<b>Simulation accuracy</b>	<b>Computational accuracy</b>	<b>Calculated quantity</b>	<b>Engineering applicability</b>
<b>Box model</b>	Heavy gas instantaneous or continuous diffusion	General	Better	Smaller	Good
<b>Similarity model</b>	Heavy gas instantaneous or continuous diffusion	Better	Better	Smaller	Good
<b>Shallow model</b>	Heavy gas instantaneous or continuous diffusion	Better	Better	Bigger	General
<b>Gaussian model</b>	Light gas continuous diffusion	Better	Better	Smaller	General
<b>CFD model</b>	Heavy gas instantaneous or continuous diffusion	Good	Good	Bigger	General

The integrated models can simulate the transitions between different stages of dense-gas dispersion, including slumping, creeping, phase transition and passive dispersion. A representative image of the output from integral model is given in Figure 9. As per the illustration, the impact zone is direction and obstruction independent. Each colour in the figure corresponds to a concentration of interest, typically based on assessment criteria, the receptors of concern and the purpose of modelling.

For CFD modelling, the dispersion of released gas is predicted by solving the three-dimensional conservation equations of mass, momentum, energy and species concentration. A computational domain is created to represent the terrain effects and the atmospheric boundary layer. Often this approach is used to simulate and study complex pollutant / species dispersion. A representative image of the output from FLACS, a Three-dimensional CFD model is given in Figure 10. As per the figure, the impact zone is dependent on the wind field and obstructions (different distance of impact depending on wind direction).

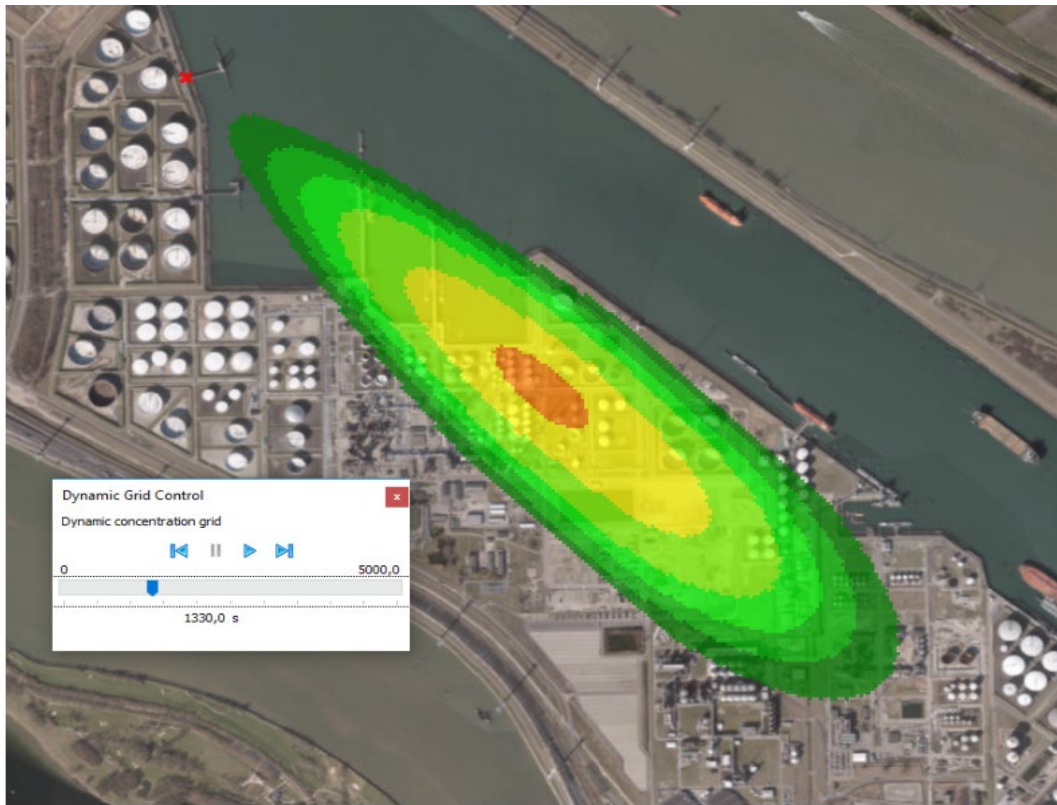


Figure 9: Toxic cloud release display in EFFECTS software

Source: <https://www.gexcon.com/products-services/EFFECTS/31/en>

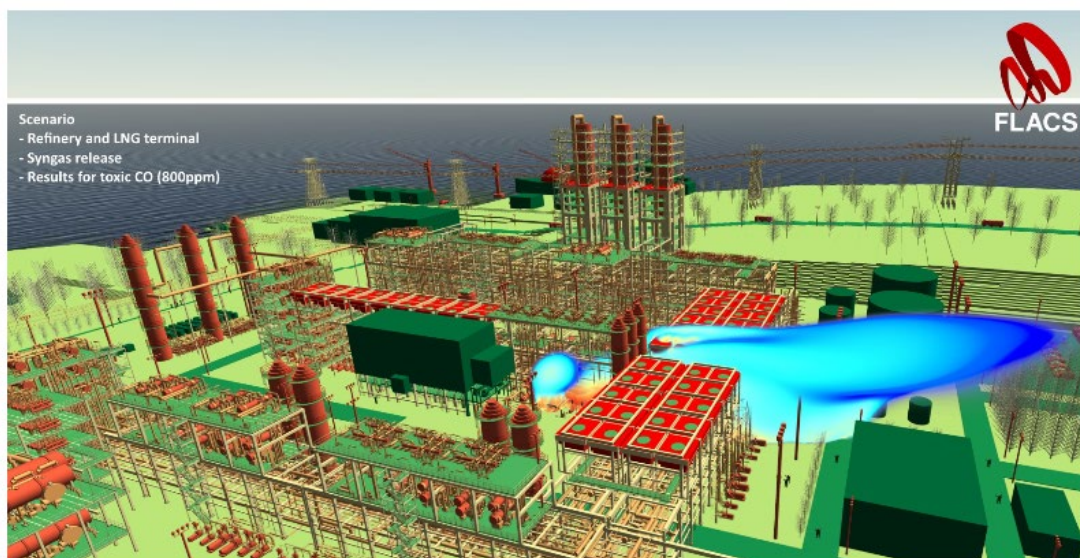


Figure 10: Toxic cloud release display in FLACS software

Source: <https://www.gexcon.com/products-services/FLACS-Software/22/en>



The turbulent flows in CFD models are often described by the continuum and momentum equations named after Navier and Stokes. For solving these equations directly (without any turbulence model), a very fine grid is necessary, requiring high computational demand, this approach is known as Direct numerical Simulation (DNS). To reduce computational resources and duration, Large Eddy Simulation (LES) and Reynolds Averaged Navier Stokes (RANS) methods are developed. For CFD modelling, the choice of numerical solution method is very important in terms of the speed of obtaining the results and their precision.

Multiple independent studies have compared integral/Gaussian models against 3-D modelling approaches (Fiorucci et.al. 2008, Libre et.al. 2010, US EPA 2005). A summary of the comparison is given in Table 8.

**Table 8: Comparison - Integral (2D) vs CFD (3D)**

Criteria	2D Model (Integral)	3D Model (CFD)
<b>Discharge, expansion and dispersion source</b>	Point sources, fixed near profiled. Air pollutant dispersion is assumed to have a normal probability distribution	Sources: point / surface / volume, 2 Phase Fluid properties variation, turbulence modelling, chemical reactions
<b>Obstacles, turbulence</b>	Simple flat terrain, no obstacles; influence captured by surface roughness parameter	Complex geometry / terrain (with obstructions like buildings, contours), trees, hills, water bodies
<b>Fluid dynamics</b>	No buoyancy for varying density, gas, particles, droplets Statistical correlation with experiments for some products	Most tools can solve for buoyancy effects by accounting for density, space & time variable variation; temperature, complex wind patterns, combustion.
<b>Thermodynamics</b>	Difficult transition between phases of correlated data; some can simulate the transitions between different stages of dense-gas dispersion	Eulerian mode to calculate all 3D wind field patterns and Lagrangian model is used more appropriately for the calculation of dispersion of species.
<b>Meteorology, diffusion</b>	Wind velocity is a single value or a function of height. Invalid / perform poorly in low winds. Approximations by generic wind velocity profile, for turbulence in BL & closure for diffusion coefficient	Wind profile considering flow field. Natural convection solved, Puff model for quick simulation. Monin-Obukov similarity theory profiles across the integration domain.
<b>Effort</b>	Simplified and simulation results within minutes	Level of details is resource intensive (specialist modeler and computing) Suitable for micro-scale (<1 km) and for short periods (<1 minute)
<b>Results</b>	Time averaged, direction independent, 2D concentrations	Detailed time-dependent, 3D concentration profiles

From the comparison, it reveals that both approaches have its advantages and disadvantages, the key is determining the appropriate methodology, understanding the limitations and use the results with caution. As pointed out by US EPA and IOGP, the inadequate information from the consequence assessments (release and dispersion modelling) of accidental sour natural gas releases is one of the key challenges in managing the risk (US EPA 2005, IOGP 2010). Whichever approach is adopted, it should be used with an understanding of its range of validity, its limitations, the input data required, the valid results that can be obtained, the results' sensitivity to the different input data, and how the results can be verified.

## 2.5. Thermodynamic input and assumption

The choices and assumptions used to describe the thermodynamic parameters of a fluid with temperature, pressure and volume may lead to significant variations in the results. Literature review (Nilsen 2014, US EPA 2017) of simple analytical/ empirical software tools with integration of the models for the discharge thermodynamics reveals that:

- (a) The models perform well for the estimations for stagnant to orifice conditions when coupled with Equation of State (EoS), phase changes are normally excluded, and critical flow is assumed (for maximum flow velocity) with geometric simplifications.
- (b) For the expansion from the orifice condition to atmospheric conditions most approaches assume:
  - a. a one-dimensional flow along the expansion zone,
  - b. no air entrainment in the expansion region prior to reaching atmospheric pressure and
  - c. the post-expansion pressure equals the ambient pressure.
- (c) The models consider the jet mixing with air for the transition between discharge phase and the earliest momentum jet phase. The unknown variables in the post-expansion region are usually solved by a combination of conservation equations, thermodynamic behaviour assumptions and EoS.

A comparative study by INERIS which evaluated DNV PHAST, ANSYS-CFX and FLACS for the impact on the phase changes following dense phase CO<sub>2</sub> concluded that these tools were in reasonable agreement with the measurements, but generally in poorer agreement than has been reported

previously for similar dispersion models in other dense-phase CO<sub>2</sub> release experiments (Gant et. al. 2014).

The expansion of pressurized fluid to atmospheric conditions can be modelled as an isenthalpic or an isentropic process or one may prefer to postulate conservation of momentum. The discharge can also be formulated as a choked jet. The initial temperature of an expanding fluid is decided by the highly transient thermodynamical processes taking place during expansion and is a key factor for dispersion modelling. The phase diagram chart showing the thermodynamic conditions of methane and hydrogen sulphide at different pressures and temperatures is given in Figure 11 (Engineering ToolBox 2020b) and Figure 12 (Engineering ToolBox 2020a).

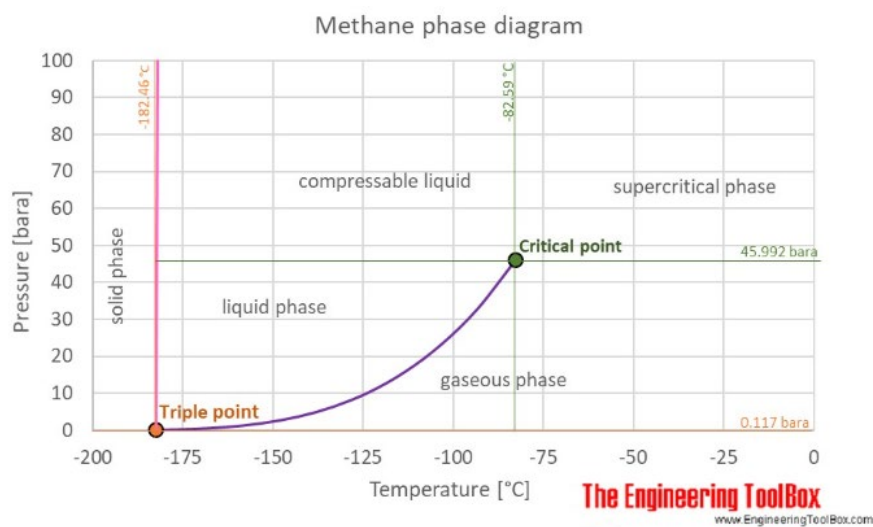


Figure 11: Methane phase diagram

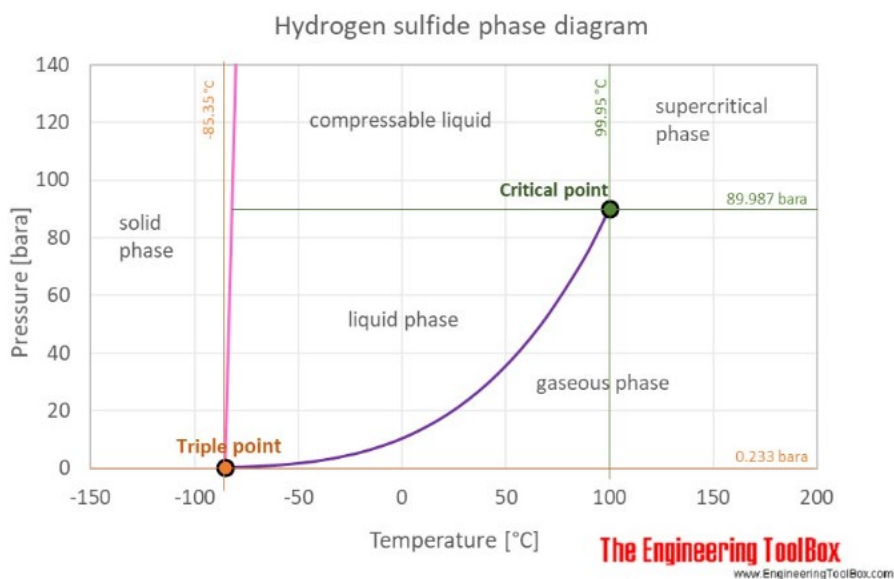


Figure 12: Hydrogen sulphide phase diagram

The methods for calculation of natural gas properties into three groups (Elsharkawy, 2002):

- (a) Pseudo-critical properties of gases using gas composition or gas gravity and estimates the gas properties from empirical correlations. Often, gas density is used to predict viscosity.
- (b) Gas composition to estimate gas properties via the method of corresponding states.
- (c) Based on Equations of State (EoS) approach.

Components in a natural gas mixture behave differently than in pure state. The accuracy of an EoS in predicting pure component properties significantly effect on the accuracy of the EoS in predicting natural gas properties. It should be noted that the accuracy of EoS in engineering is based on the adequacy of the critical point for predicting the subcritical and supercritical properties.  $H_2S$  is polar gas and hence, if the fraction of  $H_2S$  in sour natural gas is larger than few percent, the Peng-Robinson (PR) or Soave-Redlich-Kwong (SRK) equations should not be used. Calculation results for different sour gas compositions concludes that there could be significant differences in the discharge and dispersion for the combinations of EoS and expansion methods (Nilsen et. al. 2014).

Some computer codes allow the user to specify the gas mixtures as multi-component whereas in some proprietary tools a pseudo component approach is adopted. An extensive literature review was carried out to determine the equations of state of sour gases concluded that there is no simple and accurate EoS available for predicting thermodynamic properties of sour hydrocarbon gases (Mohsen-Nia et al. 1993). A comparison of various equations of state, PR, SRK and Patel-Teja (PT) EoS and corresponding state methods and correlations to predict the volumetric and transport properties of sour gases point out (Elsharkawy 2002):

- (a) Experimental and modelling studies by Li and Gu revealed that PR EoS was not accurate for phase equilibria calculations; and a 33-constant super EoS was introduced. Such a lengthy equation not considered suitable for engineering calculations.
- (b) Huron et al and Evelein and Moore used SRK-EoS to study sour hydrocarbon properties and reported phase equilibria calculations; thermodynamic and transport property calculations were not reported.
- (c) Mohsen-Nia et. al. produced a simple two-constant cubic equation of state for calculating thermodynamic properties and phase behaviour of sour natural gases. However, the literature does not explain how to calculate the constants for the plus

fraction and the validation experiments did not consider any binary interactions (Mohsen-Nia et al. 1993).

- (d) Elsharkawy investigated the effect of various schemes of Binary Interaction Numbers (BIN) on the accuracy of EoS (Elsharkawy 2002).
- (i) SRK-EoS shows better accuracy at different pressures and temperatures for various sour gas compositions.
  - (ii) PT-EoS considering the effect of non-hydrocarbon components (by incorporating the BIN proposed by William and Teja) predicted best results for compressibility and density.
  - (iii) Accuracy of EoS in predicting the volumetric properties of sour gases and gas condensates is independent on the amount of the heavier hydrocarbon content (heptane plus) and the non-hydrocarbon components (CO<sub>2</sub>, N<sub>2</sub> etc.).

## 2.6. Meteorological factors

Typical meteorological factors that govern the dispersion of pollutant species include wind speed and direction, the amount of atmospheric turbulence (as characterised by what is called the “stability class”), the ambient air temperature, the height to the bottom of any inversion aloft that may be present, cloud cover and solar radiation. Location specific meteorological data have significant impact on the dispersion modelling which is often a challenge at frontier locations (NOAA 2018). But expensive experimental setups and long-term experimental procedures are required for gathering meteorological statics (Dincer and Erdemir 2021). When atmospheric pressure is reached the modelling tools assume that mixing with air will start and depending on the phase compositions, temperature and velocity this mixing might lead to even lower temperatures. Most CFD tools estimates the atmospheric temperature profile based on Monin-Obukov similarity theory and often simulated by micro meteorological model. An unstable atmosphere enhances mechanical turbulence, whereas a stable atmosphere inhibits turbulence and neutral atmosphere neither enhances nor inhibits turbulence. The turbulence of the atmosphere is by far the most important parameter affecting dilution of a gas (Ricou and Spalding 1961). Analytical/empirical models are available for quantification of air entrainment (Morton et. al. 1993).

The NORSOK standard recommends at least eight wind directions need to be considered for the ventilation simulations for releases in confined areas like offshore installations or with obstructions closer to the release source (NORSOK 2001).

### 2.6.1. Stability class

Stability class is tendency of the atmosphere to resist or enhance vertical motion of the pollutant or the hazardous cloud of interest (Woodward 1998). It is related to both the change in temperature with elevation which is driven by wind speed and surface characteristics (roughness). Unstable enhances mechanical turbulence, stable inhibits turbulence and neutral neither enhances nor inhibits turbulence (Chambers and Johnson 2009). Atmospheric stability affects the vertical movement of air and has influence on the transportation of species. Though the strength of the horizontal wind is far greater than the vertical movement of air, the turbulence from the atmospheric stability impacts the cloud shape and size (Huertas et al 2021).

Atmospheric stability can be classified into three, unstable, stable and neutral.

- Unstable atmosphere enhances or encourage the vertical movement of air. It is the set of conditions with average or strong winds, the wind and temperature conditions help the species to disperse. These conditions are very rare both at night and during the day.
- Neutral atmosphere neither suppresses nor enhances vertical motion. It is the set of conditions with generally less strong wind; they are more frequent during day and night.
- Stable atmosphere suppresses or resists vertical motion. It is the set of conditions associated particularly with low or calm winds. In addition, a very stable atmosphere are the conditions associated with very low or most often calm winds.

There are two different sets of formulations for the stability classification, Pasquill method and Doury method. Pasquill method expresses the standard deviations as a function of the distance from the source whereas Doury classifies into two types. In general, stability is categorised into six, each designated by a letter:

- Very unstable (A)
- Unstable (B)
- Slightly unstable (C)
- Neutral (D)
- Stable (E)
- Very stable (F)

The Pasquill-Guifford-Turner classification of the atmospheric stability is given in Table 9 (NOAA 2016, Pasquill 1961).

Table 9: Atmospheric stability classifications

Surface wind speed (m/s)	Day solar insolation			Night cloudiness	
	Strong	Moderate	Slight	Cloud	Clear
<2	A	A-B	B	E	F
2-3	A-B	B	C	E	F
3-5	B	B-C	C	D	E
5-6	C	C-D	D	D	D
>6	C	D	D	D	D

As per Doury's correlation, for Pasquill classes A to D, normal diffusion conditions during daytime and for higher wind speed (> 3m/s) during night. However, during night (Pasquill class F) and low wind speed (< 3m/s) diffusion will be weak (EPSC 1999).

### 2.6.2. Wind speed

The speed of the wind varies as a function of the altitude because the ground breaks the air. The wind measurements are usually made 10 m from the ground (as per French national meteorological standard). Two types of correlation are used to estimate the speed of wind along vertical axis (EPSC 1999) (i) Logarithmic law and (ii) power law.

(i) Logarithmic law, derived from the laws of aerodynamics at low altitude for the cases of an adiabatic atmosphere (Equation 2).

$$U = \frac{U_f}{k} \ln \frac{Z}{Z_0}$$

Equation 2

Where,

- U      wind speed at altitude z
- U<sub>f</sub>    friction speed
- k      von Karman constant (typical value = 0.41)
- Z<sub>0</sub>    surface roughness

The surface roughness values is a function of the site environment, particularly in the area upwind of the emission, which is a result of compilation of different sources.

(ii) Power law method, used by the US EPA models employ a simple 'power law' function (Equation 3). The wind speed at any elevation is estimated as a function of the height of the actual (reference) wind speed measurement, atmospheric stability, and a wind profile exponent (coefficient). This law, irrespective of the surface roughness, has been established for emissions

at an altitude (e.g., stack) and does not apply to small altitudes, particularly below the altitude for the measurements of the wind speed.

$$\frac{V_1}{V_2} = \left[ \frac{z_1}{z_2} \right]^P$$

Equation 3

Where,

- $V_1$  wind speed at altitude  $z_1$
- $V_2$  wind speed at altitude  $z_2$  (actual measure at a reference height)
- $P$  coefficient dependent on atmospheric stability class (ranges from 0.1 to 0.3 for Urban and from 0.07 to 0.55 for Rural for atmospheric stability ranging from A to G)

### 2.6.3. Intensity of turbulence and atmospheric stability:

Turbulence theory divides the instantaneous wind vector  $U$  at coordinates  $(u,v,w)$  in reference to axes  $O$  into two vectors (Tapia 2009).

- One representing the mean measured speed
- One representing the instantaneous fluctuations in speed

$$\vec{U}(\text{instantaneous speed}) = \vec{U}(\text{meanspeed}) + \vec{U}'(\text{fluctuating speed})$$

Equation 4

The range of the fluctuations may be characterized by the intensity of the turbulence or the standard deviation of distribution of the directions throughout the measurement. The turbulence intensity is defined by:

$$i_x = \left[ \frac{w'^2}{\bar{u}^2} \right]^{\frac{1}{2}} \text{ for x direction}$$

Equation 5

### 2.7. Topography – terrain and obstacles

The presence of obstacles over the trajectory of the gaseous cloud may significantly affect the dispersion conditions of the cloud. A passive obstacle like a building or wall, could result in accumulation upwind and reduction in concentration in area downwind. On the other hand, multiple obstacles such as hills, valleys, industrial sites, may increase the concentrations in certain directions through the funnel or tunnel effects (EPSC 1999).

Surface roughness length (height),  $z_0$ , in the vertical wind speed profiles used as parameter to affect entrainment rates. It is applied where the obstacle height is relatively small to the height of the cloud (Woodward 1998). Higher values of  $z_0$  typically produce higher turbulence and consequently higher dispersion which usually widens the clouds and decreases the along-wind



concentration. Surface roughness length associated with terrain is given in Table 10 (Pasquill 1961, EPSC 1999).

Table 10: Surface roughness length associated with terrain description.

z <sub>0</sub> (m)	Typical terrain	Description
0.0001 to 0.002	Calm open sea or snow-covered flat ground	Large expanse of water or desert
0.005 to 0.01	Cut grass, few trees (or as in winter)	Fairly level grassy plains
0.05 to 0.03	Few trees (as in summer), many hedges	Typical farmland
0.4 to 0.5	Outskirts of town, centres of small towns	Fairly level wooded country
1 to 3	Centres of large towns, cities with tall buildings	Very hilly mountains

Terrain effects: The flow of heavy gas clouds follows the terrain much like water runoff from rain. A large-scale natural carbon dioxide release from a volcano at Lake Nyos in Cameroon in August 1986 has filled the valley with gas to a certain height. Those living above this height survived, while some 1700 people below the gas level perished (Woodward, 1998).

In open field conditions, both integral and CFD models are expected to give similar results. However, the dispersion of pollutants in complex terrain is characterised by the interaction of atmospheric processes with local circulations originated by mechanical and thermal factors. It is noted an increase in use of CFD based mathematical modelling for dispersion of hazardous gas clouds in geometrically complex environments. For CFD modelling, Eulerian model is used to calculate all 3D wind field patterns and Lagrangian model is used more appropriately for the calculation of dispersion of species (or pollutant).

A comparison by applying the TOPSIS method to six Reynolds' Averaged Navier Stokes (RANS) models (RSM, standard k-ε, RNF k-ε, standard k-ω, SSTk-ω), shows that the Standard k-ε model (Equation 6) was the best suitable model under the simulation of heavy gas dispersion for hill-shaped terrains (Qingchun and Laibin 2011).

$$\frac{\partial}{\partial t}(\rho\phi) + (\rho\mu\phi) = (\Gamma grad\phi) + S_{\phi}$$

Equation 6

The four items from left to right on the style times were non-stationary items, convection and diffusion and source term.  $\phi$  is the general variable;  $\Gamma$  is a generalized diffusion coefficient.

Heavy gas dispersion modelling study using k-ε model, with the standard Jones and Launder values for the constants (ANSYS's FLUENT software) evaluated the cloud behaviour in presence of large obstacles (Derundi et. al 2014). The study concluded that the impact of obstacles in

dispersion of dense gas can be disregarded if the ratio of the obstacle and the cloud (unit less ratio  $R = h_{\text{obstacle}} / h_{\text{cloud}}$ ) is less than 0.25. However, when  $R > 1$ , the presence of the obstacle cannot be disregarded. This means, the effects of the obstacle shall be represented in the computational domain to estimate the effects.

## 2.8. Tool and relevant studies

A list of studies using different models, assumptions and tools used to predict discharge and dispersion of H<sub>2</sub>S rich releases is given in Table 11. The literature review findings are also included with the gaps in the studies and points out the disagreements.

**Table 11: Status of theoretical and numerical models and tools for H<sub>2</sub>S rich gas releases:**

	Study, Tool /Model, Assumptions	Findings and notes
1.	H <sub>2</sub> S gas dispersion potentials & release scenarios for pacific OCS; US DOI, MMS 2009-021 (Ricou and Spalding 1961)	
	<p>Release rate estimation: Chems-Plus (Arthur D Little Inc' model). Pacific Offshore Continental Shelf Region Oil &amp; Gas platforms &amp; pipelines located in the Santa Barbara channel and Santa Maria Basin, California, US Department of the Interior</p> <p>Modelling tool: ALOHA, by US EPA</p> <p>Validation/comparison of dispersion estimates between ALOHA and SLAB models.</p> <p>Three exposure concentrations (100, 300, and 1000ppm)</p> <p>Meteorology: Stable night-time conditions at 2m/s, neutrally stable at 5 m/s),</p> <p>Assumptions:</p> <ul style="list-style-type: none"> <li>i) Chemical mixture as Gaussian or heavy gas release.</li> <li>ii) The hazard area is directional in nature and only extends downwind.</li> <li>iii) Entire pipeline contents would be released at a constant pressure.</li> <li>iv) positive isolation as soon as the release is detected, 10 minutes for isolation and release; dispersion duration of 60 minutes</li> </ul>	<p>ALOHA limitation: the ALOHA model does not recommend using wind speeds less than 2 m/s.</p> <p>The ALOHA model bases its determination mainly on molecular weight, size of the release and temperature of the gas cloud to predict the dispersion of releases from the pipelines (connecting between assets) present a larger hazard area than that of the platforms they connect. The maximum 300 ppm H<sub>2</sub>S hazard zone distance estimated for a pipeline rupture was 2250 m whereas from platform, 300 ppm hazard area extends to maximum downwind distance of 400 m.</p> <p>Used the original pipeline pressure for the release duration, this is an extremely conservative assumption; so, the hazard zone distances estimated by the modelling and presented would be considered as extreme worst case.</p> <p>Detection and isolation (within 10 minutes) may not be possible for releases from onshore pipelines routed through remote locations; in those cases, potential exposure to smaller concentration for longer duration could be a concern.</p>

	Study, Tool /Model, Assumptions	Findings and notes
2.	Determine H <sub>2</sub> S emission factor for swine operations (O'Shaughnessy and Altmaier 2011)	
	<p>Modelling tool: AERMOD</p> <p>Inverse modelling approach used to determine H<sub>2</sub>S emission from concentrated animal feeding operations</p> <p>Average emission flux rate was determined</p> <p>Spatial distribution zone estimated using emission factor and compared against regulatory threshold criteria</p>	<p>Emission factor estimation was for highest downwind concentrations with non-local meteorological data.</p> <p>The estimations can produce relative error in concentrations below 50%, especially if there are areas with large elevation differences</p>
3.	CFD Simulations of H <sub>2</sub> S-Rich plumes from oil/gas well blowouts (Zemba et.al. 2014)	
	<p>Modelling tool: Fluidyn PANACHE</p> <p>Assumptions:</p> <p>i) Near field / near-source regions were simplified to determine worst-case release characteristics for far field modelling.</p> <p>ii) All liquid phase evaporated and results in the densest gas mixture possible; the release would be heavier than air (~suspended droplets).</p> <p>iii) Average molecular weight of the releases as 143.5 g/mol (5 times that of air, 28.9 g/mol)</p> <p>Gas phase 31.45 g/mol; Liquid phase 232.7 g/mol</p> <p>Blow out: Volume source (10 m<sup>3</sup>) at 5m above ground level</p> <p>Topography: 2000m above sea level (asl) near wellhead, 800m asl nearest village (4km away)</p> <p>Meteorology: Stable (E/F at 1m/s), Neutrally stable (D at 2 m/s), wind speed at 10m above ground level.</p> <p>Meshing: Unstructured, graduated spatial resolution.</p> <p>Model: The k-ε turbulence model was used for atmospheric dispersion. Time step of 1s</p> <p>A cloud convection parameter to assign a surface heat flux. 3D wind-field considering the terrain elevations was developed in the modelling domain.</p>	<p>PANACHE's dense gas algorithms evaluated against experimental data involving controlled releases of liquefied natural gas (LNG) and carbon dioxide – but not with sour natural gas release.</p> <p>Averaged molecular weight need not appropriately represent multi-component mixture dispersion.</p> <p>Near field / near-source regions complexities were not considered.</p> <p>Complex, two phase flow in the near source region was not examined; Justification: 100% vaporisation is not critical, due to high turbulence mixing in release region such that the overall excess density of the release is small.</p> <p>The level of gas density is generally predicted to dissipate rapidly, possibly from turbulent mixing. Elevated concentrations of H<sub>2</sub>S have the potential to persist for several kilometres downwind of source areas.</p> <p>Simulation exhibited some near-field influence of dense gas dispersion.</p> <p>Uncertainty in assigning wind boundary condition to the simulation domain (vertical domain in model = 2000m).</p> <p>Model validation difficult due to a lack of controlled monitoring studies of blowout releases in highly complex terrain.</p>

	Study, Tool /Model, Assumptions	Findings and notes
4.	Dispersion of accidental release of H <sub>2</sub> S on a gas production site followed in real-time by 3D modelling (Libre et.al. 2010)	
	<p>Developed a methodology for faster-than-real-time simulation, source term estimation from field detection and pre-solved simulations.</p> <p>Modelling tool: Fluidyn-PANEPR (part of PANACHE)</p> <p>Wind field pattern taking account of the details of the installations; Size of industrial site 1.8 x 1.3 km and size of domain 13.5 x 9.5 km</p> <p>Model solves the Navier-Stokes equations for atmospheric flow in a RANS formalism. It includes mass, momentum and enthalpy conservation, state law and equations of advection-diffusion in a finite-volume-based approach on a non-uniform mesh generator – takes account of the presence of obstacles or topographical features (i.e. with generation of a finer mesh in critical areas)</p> <p>A k-ε model used for turbulence simulations and micro meteorological model simulates the atmospheric temperature profile based on Monin-Obukov similarity theory.</p> <p>Eulerian mode to calculate all 3D wind field patterns; Lagrangian model is used more appropriately for the calculation of dispersion of species.</p> <p>Estimating obstruction dimension by combination of: (i) the Thales method, (ii) by shadow.</p>	<p>This study was carried out for 100% H<sub>2</sub>S emission (heavier than air). Sour gas (where H<sub>2</sub>S is minor composition in a mixture) dispersion could be different to 100% H<sub>2</sub>S</p> <p>The measurement is limited to the concentration up to 20ppm due to the detection sensor range; no useful information can be expected above these concentrations due to saturation.</p> <p>The location and intensity of the source term determined using a probabilistic approach making use of both real time measurements and pre-calculated concentration responses from unitary emissions (puffs) on sensors (Lagrangian puff dispersion).</p> <p>Influence of surface roughness on flow pattern set through a rugosity coefficient. All types of facilities that could interact with air displacement have been identified from GIS (French geographical institute). Effects of cooling towers etc. on plume accounted for.</p> <p>Bayesian inference with a random sampling approach was used to determine the source term in the complex situation of building and structure of the industrial site.</p>
5.	Validation of CFD tool to predict a real time drift of a toxic cloud on a complex industrial configuration Libre et.al 2011)	
	<p>Supported by two experimental campaigns for several Sulphur hexafluoride (SF<sub>6</sub>) releases.</p> <p>Modelling tool: Fluidyn-PANEPR (Part of PANACHE)</p> <p>Model solves the Navier-Stokes equations including mass, momentum and enthalpy conservation, state law and equations of advection-diffusion in a finite-volume-based approach; Structured and unstructured mesh</p>	<p>Good results for trends and mean values and little deviation figures between the model and the measurements.</p> <p>3D CFD deterministic models are the best-fitted models for accuracy of wind flows.</p> <p>Findings applicable for the trace gas emissions during unsettled meteorological conditions</p> <ul style="list-style-type: none"> <li>• Toxic cases limited to SF<sub>6</sub> release</li> </ul>

	Study, Tool /Model, Assumptions	Findings and notes
	<p>optimized to ensure numerical resolution of transport and diffusion equations.</p> <ul style="list-style-type: none"> <li>• Unsteady calculation of the 3D gas dispersion by an Eulerian solver</li> </ul> <p>A k-ε model used for turbulence simulations and micro meteorological model simulates the atmospheric temperature profile based on Monin-Obukov similarity theory.</p> <ul style="list-style-type: none"> <li>• Wind field pattern taking account of the details of the installations/obstructions and topographical features.</li> </ul> <p>Microscale short time natural wind fluctuations as observed, qualified by two criteria:</p> <ol style="list-style-type: none"> <li>1. The averaged behaviour (constant velocity and direction) of the flow considered as steady. The averaging time for such characteristics is around 10 minutes.</li> <li>2. The short time variations (Seconds to several minutes) around the mean value which are therefore tricky to model in details</li> </ol> <p>The finer the mesh and the higher the numerical scheme order, the closer the solution is to real atmospheric flow but the higher is also the CPU time.</p>	<ul style="list-style-type: none"> <li>• Trace gas emission only; emission from 10 to 30 minutes, with a constant mass flow rate 1.4 to 5.9 g/s (controlled releases of limited release rate, e.g., reliefs from pressure safety valves)</li> <li>• Boundary conditions (wind direction, speed, temperature, and turbulent parameters) are based on measured data from the 10m height mast height at site (With no significant effect of other structure influence is expected)</li> <li>• The wind speed and air temperature profiles are represented by logarithmic functions</li> <li>• The ground roughness is set up using a condition within which the wall shear stress and heat transfer in the boundary layer are computed from the standard logarithmic law of the wall and introduced into momentum and energy equations.</li> <li>• Size of industrial site 1.8 x 1.3 km and size of domain 13.5 x 9.5 km</li> <li>• All types of facilities that could interact with air displacement have been identified from GIS (French geographical institute)</li> </ul> <p>The emissions are evaluated through analytical models.</p>

Study #1 and #2 has used integral models (AERMOD, ALOHA) for dispersion modelling. The studies were primarily focusing on 100% H<sub>2</sub>S dispersion at lower release rates (emissions). The approach seems to meet the requirement for their respective objectives but has the following issues if considered for dispersion following higher release rates in rugged, mountainous terrains for the following:

- (a) ignore (does not rigorously consider) the channelling and confining effects due to terrain.
- (b) provide steady state concentration profile without taking account of turbulence in far-field dispersion; It also has limited accuracy in predicting the peak gas concentrations.
- (c) not validated for dispersion under stable low wind conditions.
- (d) does not account for natural gas as a mixture of multiple components.

Geometrically complex scenarios make integral models inaccurate and require CFD simulations to obtain reasonable data. As given in Studies #3 to #6, CFD models (like Fluidyn's PANCHE, and ANSYS's FLUENT) are often used to obtain numerical solutions for air entrainment and dispersion by solving the conservation equations for mass, momentum, and enthalpy in addition to the equations for concentration (Koopman et.al 1989). The review indicates that there are modelling tools and algorithms that can take account of H<sub>2</sub>S specific properties and well validated tools for generic hydrocarbon releases. It also is clear that few CFD codes can model complex thermodynamics processes during expansion of H<sub>2</sub>S rich hydrocarbons. The combination of expansion process and selection of EoS can lead to widely different input to dispersion in terms of temperature and composition, these subsequently affect the dispersion (Nilsen et al. 2014).

The studies using CFD models have made few assumptions that could result in giving substantially different results with respect to dispersion distances for the same accident scenario. The onsite emission modelling related studies were calibrated using the site gas detection system for trace gas emissions (low release rates) considering near field effects; however, the findings were not validated for far-field effects from catastrophic releases (larger release rates) due to lack of controlled monitoring studies or experimental data.

Study by Deng et al for H<sub>2</sub>S containing (up to 2%) with natural gas with concluded that the consequence distance does not vary linearly with pipeline pressure and the impact of real terrain around pipeline should be considered in dispersion modelling (Deng et al. 2018).

## 2.9. Numerical model validation

It is unlikely that we will ever be able to resolve the question "Just how reliable are the results?". Verification and validation are required at almost every level of consequence modelling predictions. Testing of consequence model is carried to 'verify' that the code correctly solves the mathematical model (i.e., that the calculated variables are a correct solution of the equations), and 'validates' against experimental data to show how closely the mathematical model agrees with the experimental result. Typically, the developers of the commercially available integral models demonstrate the tool applicability by validation against experiments. However, for CFD models used for specific consequence analysis application should be subjected to validation (including comparison with experiment and other models). This should be carried out prior to the actual situational application for ensuring the credibility of the model and the validity of the results. Model validation can be:

- 1) Scientific: examines formulas, assumptions, physics, and chemistry
- 2) Statistical: direct comparison with observed values
- 3) Operational: ease of use, model interface, output format, features

The range of application of models lies within the range of adjustment and validation. The selection of the series of measures on which the models are validated is made according to the quantity and quality of the information available. Comparisons can be made on the development of the concentration at a point as a function of time or the variation of the maximum concentration as a function of the distance from the source of emission. For dispersion, the modelling outputs subjected to validation are (Chang & Hanna 2004):

- 1) concentration over a sampling line
- 2) plume width along sampling line
- 3) maximum dosage along a sampling line
- 4) plume arrival and departure time-dependent

Various criteria for measuring agreement between predictions and full or model-scale measurements are available. These include (i) Scatter diagram, (ii) Classical Analysis of Variance (ANOVA), (iii) Pattern comparison and (iv) Weighted average fractional bias plots or a combination of these. The Standard criteria for statistical evaluation of model performance used are (Yadav and Sharan 1996, Olesen 2001, Chang and Hanna 2005):

- 1) Fractional bias (FB)

$$FB = \frac{(\overline{C_o} - \overline{C_p})}{0.5 (\overline{C_o} + \overline{C_p})}$$

Equation 7

- 2) Geometric mean bias (GMB)

$$GMB = \exp(\overline{\ln C_o} - \overline{\ln C_p})$$

Equation 8

- 3) Normalized Mean Square Error (NMSE)

$$NMSE = \frac{\overline{(C_o - C_p)^2}}{\overline{C_o - C_p}}$$

Equation 9

- 4) Geometric Variance (GV)

$$GV = \exp \left[ \overline{(\ln C_o - \ln C_p)^2} \right]$$

Equation 10

5) Correlation coefficient (R)

$$R = \frac{\overline{(C_o - \bar{C}_o)(C_p - \bar{C}_p)}}{\sigma_{C_p} \sigma_{C_o}}$$

Equation 11

6) Fraction within a factor of two (Fac2)

$$\text{Fraction of data that satisfy } 0.5 \leq \frac{C_{estimated}}{C_{observed}} \leq 2.0$$

Equation 12

Where,  $C_p$  denotes model predictions (estimated),  $C_o$  denotes observed values (in field trials/ experiments),  $\bar{C}$  overbar denotes the average over the dataset, and  $\sigma_c$  denotes the standard deviation over the dataset.

For a perfect model, FB and NMSE are equal to zero and GMB, GV and Fac2 are equal to one, implying that that observed and predicted values are identical (Chang and Hanna 2004). An acceptable model performance would have the following characteristics the fraction of predictions within

- A factor of two of the observed values should be more than 50% i.e.,
  - Fac2 > 0.5
- The mean bias is within +\_ 30% of the mean i.e.,
  - $0.0 < GMB < 1.3$  or
  - $-0.3 < FB < 0.3$
- The random scatter should be about a factor of two of the mean i.e.
  - $NMSE < 4$  or  $GV < 1.6$

Heavy gas dispersion models are distinguished from other dispersion models by three effects: (i) reduced turbulent mixing, (ii) gravity spreading, (iii) lingering (Chang & Hanna, 1993). The main parameters of interest in evaluations of these models are the maximum concentration, the average concentration over the cloud and the cloud width and height (all as a function of downwind distance, X). The ratio of predicted to observed variables and define several statistics, such as the mean and the variance.



One of the advantages of numerical modelling is that despite constraints associated with grid resolution, choice of time increments, turbulence model selection, or specification of boundary conditions, the simulation of atmospheric motions, plume transport or wind loading can be reproduced. One must also realize that validation is a learning process, and the process is never complete. Inherent uncertainties can exist in model physics, initial conditions, boundary conditions, and even turbulent randomness which can exist as a barrier to repeatability of both physical experiments and numerical comparisons. When considering numerical modelling, it is wise to remember that all such models are “virtual” reality; thus, they are only as accurate as the imagination and skill brought to the process.

### 2.10. Experiments and field trials

Literature review could not identify publicly available experimental data that can be used for validation of calculation tools, both for pure H<sub>2</sub>S gas and gas mixtures containing high concentrations of H<sub>2</sub>S. Cost of full-scale experiments are cost prohibitive at times. Unlike other fluids, the exposure impact from potential toxic exposure to gas containing H<sub>2</sub>S on public and environment prohibits from conducting large scale experiments/field trials. However, the literature study carried out by Nilsen. et. al revealed a relatively long list of experimental data, with various fluids, stagnant and ambient conditions that may be used for part validation (Nilsen et al 2014). Literature review identified a list of field trials for gas dispersion and a selected few for gas dispersion is given below:

- Dense gas continuous: Burro, Coyote, Desert Tortoise, Goldfish, Maplin Sands, Thorny Island
- Instantaneous dense gas: Thorny Island I
- Tracer gas (Passive) gas – Continuous: Prairie Grass, Hanford Kr
- Passive gas – Instantaneous: Hanford I

Some of the experimental campaigns relevant to natural gas releases are listed below (US EPA 2005, Ashrafi 2010):

- (a) Prairie grass field trials considered a standard database for evaluation of models for continuous plume releases near the ground over flat terrain (ASTM, 2000). Sulphur dioxide was used as tracer and for continuous 10-minute release.

- (b) Allen, Health and Safety Laboratory, United Kingdom – optical measurement of droplet size and velocity distributions in two-phase flashing propane jets (4 mm nozzle), using a diffraction-based technique.
- (c) INERIS Tests (large scale, 2004): 94 large-scale flashing jet releases. 64 tests were performed with propane and 30 tests with butane. The aim was to investigate the properties of flashing jets at a relatively large-scale closer to the industrial scales. The measurements included release parameters (e.g., liquid temperature and backing pressures, flammability and more) and environmental parameters. Temperature along the jet axis and jet edges was measured.
- (d) Joint Industry Project on flashing liquid jets and droplets modelling, phase II to IV, 2003 – 2012 – basis for the correlations used in PHAST. To a limited degree multi component releases were also included – in a number of gasoline (low volatility, mid boiling point 109oC, multicomponent) experiments.
- (e) Experimental data on phase equilibria for H<sub>2</sub>S/CO<sub>2</sub> systems. This was an experimental study on the system H<sub>2</sub>S/CO<sub>2</sub> from the critical region to the solid-liquid-vapour region. For seven mixtures individual phase diagrams were determined by the establishment of dew, volume percentage liquid, bubble, critical and triple points. Solid-liquid-vapour loci were found to meet at a minimum temperature, lower than either of the individual pure component triple points, due to the formation of a eutectic mixture consisting of 12.5 mole% CO<sub>2</sub>, thus a eutectic behaviour.

Though there are experimental studies for natural gas releases (primarily for Liquefied Natural Gas spills), it was primarily for 100% methane with specific properties as that for Liquefied Natural Gas (LNG) but no direct studies on sour natural gas releases. In the absence of experimental data, using data from unique and quality fundamental types of experiments has become increasingly acceptable (Kulfan 2012).

As per the screening studies (details in section #4) and the paper by Nair & Wen, H<sub>2</sub>S containing natural gas can behave as positively, neutrally, or negatively buoyant (Nair & Wen, 2019). The buoyancy characteristics of the field trail material (species) formed the key deciding factor for the selection. The specific gravity of a gas is the ration of the density of that gas to the density of air (at 16°C / 60°F). A gas with a specific gravity of less than 1.0 is lighter than air (buoyant) and will easily disperse in open or well-ventilated areas. A gas with specific gravity of greater than 1.0 is heavier than air (negatively buoyant). Thus, it will tend to stay near the ground and not

disperse easily into the air (IChemE 2007). The list of gas species and their respective molecular weight, density and specific gravity evaluated to select the appropriate field trial data for validating sour natural gas is given in Table 12.

**Table 12: Gases (species) used in field trials and their properties**

Species / gas (material) released	Molecular weight (g/mol)	Density (mass/unit vol.)	Specific gravity (Air = 1)
Methane (CH <sub>4</sub> )	16.04	0.657 to 0.717 kg/m <sup>3</sup>	0.5537
Hydrogen sulphide (H <sub>2</sub> S)	34.1	1.36 kg/m <sup>3</sup>	1.1895
Liquefied Natural Gas (LNG) initially heavier	20	430 to 470 kg/m <sup>3</sup>	Not applicable
Ammonia (NH <sub>3</sub> )	17.031	0.73 kg/m <sup>3</sup>	0.5970
Hydrogen fluoride (HF)	20.01	1.15 g/litre	0.98
Sulphur dioxide (SO <sub>2</sub> )	64.066 g/mol	2.63 kg/m <sup>3</sup>	2.927
Freon-12	120.91 g/mol	1400 kg/m <sup>3</sup>	1.35

In this research, scenarios from the project Prairie Grass field trials (Barad 1958) were used as the representative field trial data for validating the models for toxic natural gas dispersion.

### 2.10.1. Prairie Grass field trial project

The Prairie Grass (PG) field experiments were conducted in north-central Nebraska near the town of O’Neill (Latitude 42° 29.6’ North; Longitude, 98° 34.3’ West). The primary objective of the project was to determine the rate of diffusion of a tracer gas as a function of meteorological conditions. The site consisted of an agricultural field where the grass had been cut and was short dry stubble at the time of the experiments. The topography of the experimental site was very flat, within 3 feet of the mean elevation in the part of the section where readings were measured. The Prairie Grass field experiment is considered a standard database for evaluation of models for continuous plume releases near the ground over flat terrain (ASTM, 2000).

The fundamental data report is by Barad (1958), although there are many other published papers on this experiment and papers where the data was used for validation (Barad 1958a, Barad 1958b). The Project Prairie Grass data is available from [www.harmo.org/jsirwin](http://www.harmo.org/jsirwin). The concentrations of SO<sub>2</sub>, the tracer gas dispersed cloud were measured on arcs downwind. The gas was released continuously for 10 minutes from a source with 2-inch (51 cm) diameter, located near ground level at height 46 cm. The experimental set up is given in Figure 13.

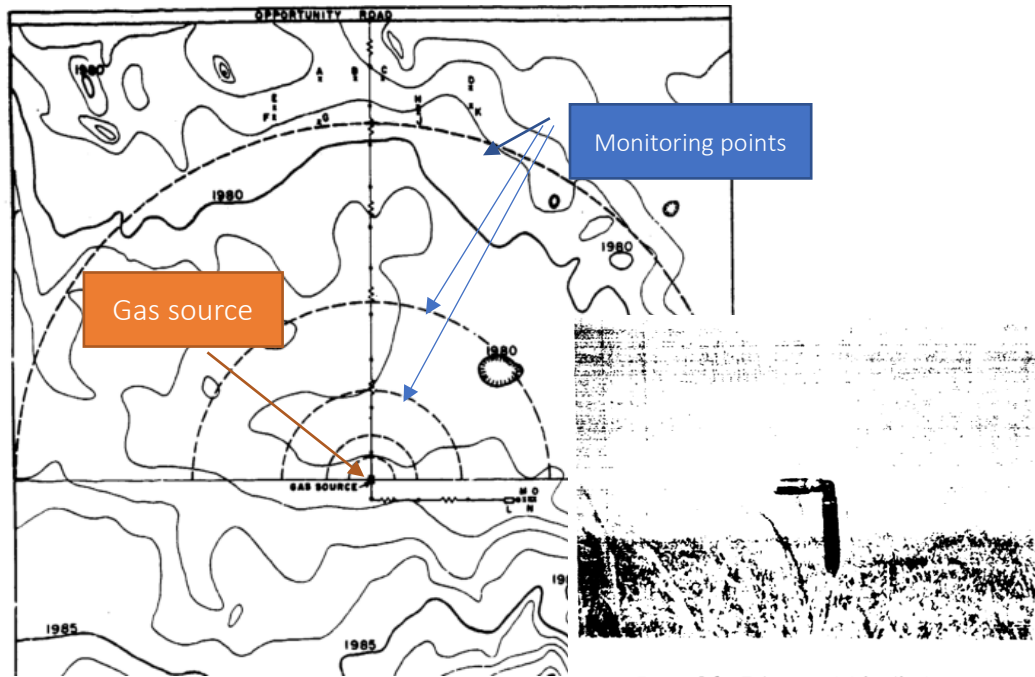


Figure 5.3 Release-point for the tracer.

Figure 13: Prairie Grass topography of field site and the release point

Source: Barad 1958

### 2.10.2. Prairie Grass field trial set up.

The project included 70 experiments over several days with different flow rates and measured  $\text{SO}_2$  concentration at 5 different distances from the point of injection. In the project set-up, a horizontal sampling array was arranged in five arcs (50, 100, 200, 400, 800m) downwind of the release. All sampled over a 180-degree arc centered on the release at a height of 1.5m. Sampling was along a semicircle from west (270 degrees) to north to east (90 degrees), with the release due south of the north point of the sampling array. The receptor spacing was every two-degrees on the inner four arcs (50, 100, 200 and 400 m), and every one-degree on the outer 800m arc. The distance between the monitoring points along the arcs are at 0.87m, 1.74m, 3.48m, 6.96m and 6.96m at 50m, 100m, 200m, 400m and 800m respectively. The location of the sampling point is represented in Figure 14.

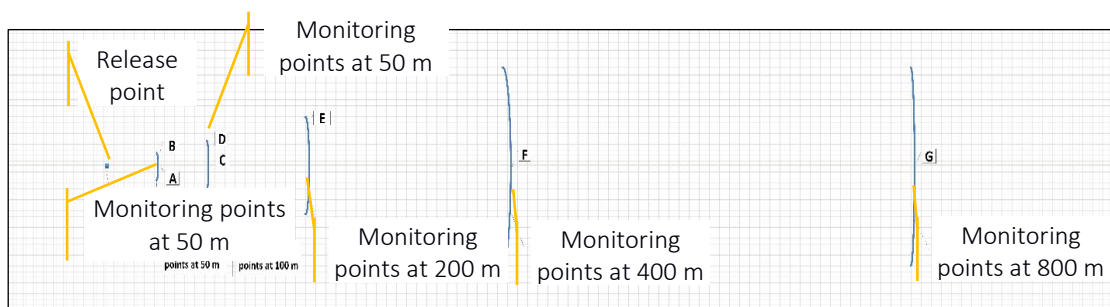


Figure 14: Release point and the monitoring points at radial distances

The vertical sampling array (for ambient conditions temperature, pressure and wind speed), six monitoring points positioned along the 100m arc with measurements at nine heights (0.5, 1.0, 1.5, 2.5, 4.5, 7.5, 10.5, 13.5, and 17.5m). The monitoring point towers were spaced at 14-degree intervals along the 100m arc at 325, 339, 353, 7, 21 and 35 degrees.

For the duration of the field experiments, mean horizontal wind direction and wind speed, and wind direction frequency (taken at 2.5s intervals) were collected at two locations: a) 25m west of the release location, and b) 450m downwind of the release and 30m west of the centerline of the receptor array. At both locations the instruments were 2m above ground. Results were tabulated for a 10-min and a 20-min period.

For 70 tracer data collection periods, air temperature and vapor pressure (8 heights), wind speed (7 heights), soil temperature (6 depths) were collected. Results were tabulated for the 10-min tracer sampling period and for a 20-min period that began 5-min prior to the beginning of the tracer sampling period. The tower location for these data was just beyond the 800m sampling arc.

### 2.11. Incidents, investigation, and analysis

Osman et al. has noted that efforts have been also made to review the damages observed (physical damage) after catastrophic events against the prediction by consequence modelling tools used for risk assessments (Osman 2015). The following session reviews a list of accidental releases and interpretations from related analysis.

Through literature search studies (limited) were found to have analysed the catastrophic release of hydrogen sulphide-bearing natural gas resulting in public/offsite effects; those are given in Table 13.

Table 13: Studies on accidental H<sub>2</sub>S rich gas releases:

Study- Tools and model	Findings and claims	Remarks and notes
1) Qingchun, M and Laibin, Z (2011) A simulation study of the Kaixian "12.23" incident (Kai County, Chongqing, Sichuan, China)- a sour gas well blowout in very complex geographical terrain. The release rate and duration of the incident	With faster downwind, the high-sulphur gas moves faster, especially through certain terrain types like canyon, valley. Hydrogen sulphide accumulation is possible at sag/low lying areas. The engineering case study shows that numerical	Qi et al prediction results of downwind gas concentrations close to ground level were in approximate agreement with the post-incident field data. Concentration of hydrogen sulphide exceeded 100 ppm at 300 to 500m (Xiaoyan village) Model estimation- Cloud with

Study- Tools and model	Findings and claims	Remarks and notes
<p>estimated post the event were used for the CFD simulation. The simulation results (toxic gas concentration at receptors) were compared with the toxic effects experienced in the surrounding area (field records). The case study demonstrates that numerical simulation provides an enhanced information on toxic gas dispersion which forms essential part for risk-based decision making, especially in engineering projects and emergency planning.</p> <p>Average elevation of the wellsite / release location is 470 to 540 m above sea level, relatively low-lying area. Kaixian County is mountainous with elevation ranges from 500 to 1000 m.</p>	<p>simulation based on k-ε model could take account terrain effects and wind speed. The sour gas cloud showed heavy gas characteristics in the dispersion.</p> <p>The cross-section surface of concentration at height of 100m and 200m above the well head shows the transmission range of gas was greater than it on the ground.</p> <p>Release rate equation of Canada EUB formula was used to determine release rate (0.02 m<sup>3</sup>/s).</p> <p>Standard kε model was selected for heavy gas dispersion for hill-shaped terrains. Large-eddy simulation (LES) can give high-accuracy simulation /computer precision of gas expansion</p>	<p>100 ppm H<sub>2</sub>S – farthest diffusion distance 500 to 1000 m</p> <p>Nearly 100% fatalities within 200 – 500m (Xiaoyan village)</p> <p>Longest distance noted for death – 1200 m</p> <p>Model estimation: 1000 ppm diffused to 231 m; 200 ppm diffused to 1271 m</p> <p>Study recommended further experimental work to characterize the physical process of sour vapour dispersion.</p>
<p>2) Yang et. al. (2006)</p> <p>Estimated Public Health Exposure to H<sub>2</sub>S Emissions from a Sour Gas Well Blowout</p> <p>CALPUFF coupled with MM5 model (for meteorological input)</p> <p>The model considers of detailed meteorological patterns, wet deposition, and chemical transformations.</p> <p>50 km x 50 km grid</p> <p>Single isolated point source with</p>	<p>H<sub>2</sub>S concentration distributions show spatial and temporary heterogeneity due to significant topographic diversity and wind fields variations over short distances. Mountain-valley features, especially during these cold, stable winter days contributed significant potential to elevated air pollution levels.</p> <p>The highest concentrations of H<sub>2</sub>S occur around the gas well within 1.5 km due to the sufficient source contribution.</p> <p>The model predicted relatively</p>	<p>The mortality due to the blowout was higher in the valley than the mountain; because H<sub>2</sub>S is heavier than air, it tends to accumulate in low-lying areas.</p> <p>In complex terrain lacking available observed meteorological data, the CALPUFF coupled with MM5 model can provide meaningful information for emergency management purposes.</p> <p>Uncertainties due to the estimation over 1 km x 1km grid cells</p>

Study- Tools and model	Findings and claims	Remarks and notes
<p>continuous H<sub>2</sub>S emission; 40 m/s 6 kg/s Calm conditions, surface-based upper air inversions and mesoscale, thermally driven wind flow, such as mountain-valley breezes are reasonable factors</p>	<p>high H<sub>2</sub>S concentrations along the valley due to the influence of slope flow.</p>	<p>Plausible cause for the difference is that the wet deposition as well as chemical formation of H<sub>2</sub>S might not be sufficiently represented in the model</p> <p>Emission rate varied from time to time and was not sufficiently accounted for in the emission scenario.</p>
<p>3) Zhang J. et. al. 2011 Analysis of chemical disasters caused by release of hydrogen sulphide-bearing natural gas Chemical hazards caused by leakage of natural gas with 9.02% hydrogen sulphide are analysed; High pressure (12 MPa, 298.15K) natural gas release from 1200mm pipe; mixture treated as neutral gas; Meteorology – Unstable (B at 3m/s) Gaussian dispersion model chosen to estimate the concentration of H<sub>2</sub>S at the ground level.</p>	<p>Probability of death = 1 within 300m for the two bigger hole release cases</p> <p>The paper recommends a risk-based approach to address sour gas hazards in handling.</p> <p>Suits for regulatory compliance in certain countries (risk-based process safety management)</p> <p>Method could be used to select between different options, for example to select a least risky pipeline route among many when it has to pass through populated areas (societal risk).</p>	<p>Focus on risk assessment methodology (linked to the frequency of severity); uncertainties in the consequence modelling tool, assumptions and limitations not addressed. Consequence on complex terrain remains a challenge</p>

The investigation and consequence modelling comparison for the post-incident analysis of the “12.23 disaster” is available in public domain. This can be used to evaluate the model with the findings with respect to H<sub>2</sub>S behaviour (like accumulation) observed during the incident. However, the comparison feature will be limited as the well blowout release case may not reflect the case considered (pipeline rupture at ground level). Alternatively, or in addition, validation of the models to be carried out against appropriate field trials or experiments. The analysis to be in a combined way by means of (i) Contours of velocity component, turbulent Kinetic Energy (TKE), Reynold stress component, (ii) Vertical and horizontal profiles of velocity component and TKE, (iii) Statistical analysis.

## 2.12. Uncertainties and sensitivity analysis

In consequence modelling, the results are estimated for a set of model input representing the initial conditions. It is unlikely that these input (initial) conditions exactly match the physical conditions, which may also vary during the dispersion duration, leading to the uncertainties. Sources of uncertainty in consequence modelling include:

- Discharge conditions to represent the actual release.
- Ambient conditions (wind speed, wind direction) do not stay constant over the duration of a release as is modelled.
- Integral and box models for dispersion with limited capability of turbulence due to obstructions and barriers (especially with porosity).

The consequences of parameter uncertainty to the model outcome can be determined with the use of sensitivity and uncertainty analysis. The uncertainty in models can partly be established by model validation studies (Uijt de Haag & Ale 2005). Sensitivity analysis presents robustness in the results based on variances in consequence modelling data, input and parameters. Sensitivities have to be determined to limit the uncertainties and produce robust conclusions (NORSOK 2001). For far-field dispersion calculations, the results are at the end of a chain of events and the uncertainties of the results are therefore relatively high.

## 2.13. Literature review summary

Risk assessments should be carried out as an integrated part of the field development project work, major modifications, change of area of application, or decommissioning and disposal of installations, as well as in connection with major changes in organisation and manning level. The results of risk assessments will always be associated with some uncertainty, which may be linked to the relevance of the data basis, the models used in the estimation, the assumptions, simplifications, or expert judgements that are made (NORSOK 2001).

Process risk assessments for natural gas exploration and production projects where the content of H<sub>2</sub>S containing natural gas have revealed toxic impact plays a major role. It is noted that it is common to assume that natural gas is lighter than air and the property of a mixture is determined by the mathematical average of the properties of the individual constituents. Such mathematical boldness and inconsistency of thought is detrimental to safety and must be qualified. It was observed that the computer tools can give substantially different results with respect to dispersion distances for the same accident scenario. The variations seem to be larger when the



stagnant conditions are liquid or 2-phase. Computational Fluid Dynamics based codes and simulation software can model the complex thermodynamic processes during expansion and diffusion of H<sub>2</sub>S rich natural gas. CFD can be used to effectively study how the wind and environment can interfere with the gas dissipation in the air. Extensive research is done on various heavy gas dispersion and vapour formation from liquefied natural gas. However, there are no dedicated experimental data H<sub>2</sub>S rich natural gas dispersion which can be used to validate the models. Several research successfully identified the parameters of sensitivity, application specific models and modifications for improvements. However, the available models and sensitivity to sour natural gas dispersion not addressed sufficiently.

### 3. Scenario definition, input parameters, and software tools

In Oil & Gas industry accidental releases happened when there is loss of integrity of the pipeline transferring natural gas. During such events the reservoir pressure or the system pressure drive the momentum release or the pressurised release. The pressure drops to atmospheric pressure; the gas cools rapidly as it expands, mixes with air and forms clouds. Liquid droplets (aerosols) can form and, in combination with the cooling, impact how the gas cloud subsequently disperses in the atmosphere. It is necessary to identify the physical phenomena preceding the formation of the cloud such as:

- Gas flow, possibly with jet effect.
- Single- or two-phase flow, possible with jet effect.
- Formation of pool and evaporation.
- Development of a gaseous cloud.

#### 3.1. Release scenario and the physics

The transformation of the fluid from its initial state to atmospheric conditions is normally evaluated in three different stages (i) Discharge, (ii) Expansion and (iii) Dispersion as illustrated in Figure 15.

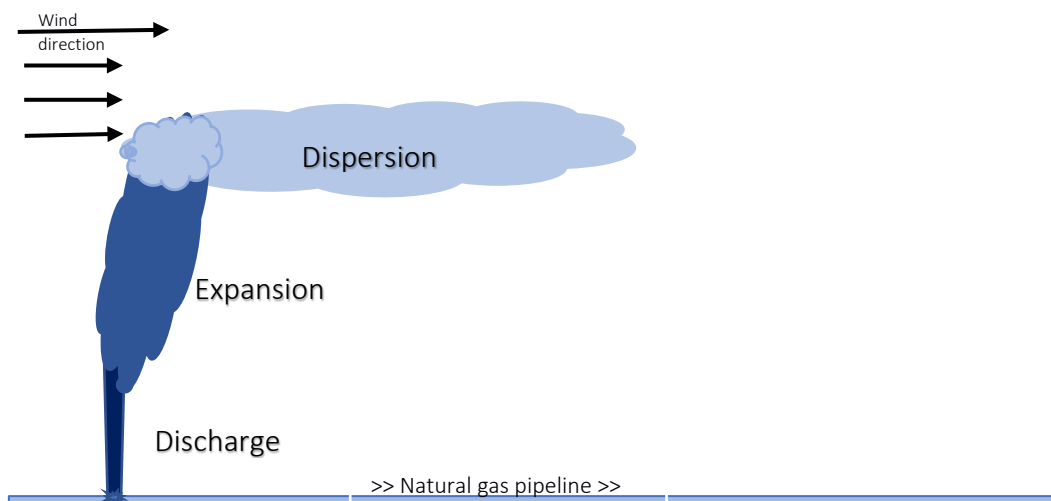


Figure 15: Scenario development – Discharge, Expansion, Dispersion

The calculation or assumption of how much natural gas can escape the containment must be addressed before one becomes concerned with the validity of the source term model which computes the vapour source term given a release scenario.

### 3.1.1. Discharge

The discharge and associated thermodynamics collectively known as the source term for consequence modelling. The influencing conditions and parameters that determine the phase of release and the characteristics of the fluid in near the release source dependent on (Fontaine and Hall, 1991):

- 1) the composition of the released material (the chemical components, density, and the mole %).
- 2) the initial physical state of the released material (single phase or multi-phase).
- 3) the rate or quantity of the release.
- 4) the duration of the release.

The release hole or aperture through which the release occurs may range from a large fraction of the containment (e.g., pipeline rupture where the release rate equals flow rate) to a small hole (e.g., puncture where release rate is less than flow rate). A very short duration release may be considered as instantaneous release (or also known as ‘puff’ release) and a prolonged discharge may be approximated as a continuous release (also referred as ‘plume’ release). It needs to be noted that the source terms are often idealizations of the actual situation (Mannan, 2014).

### 3.1.2. Expansion

The released material with jet momentum entrains air and expands to a larger cloud and reaches a point where the momentum is overtaken by the natural diffusion. The factors guiding expansion includes:

- 1) the momentum of the released material
- 2) near source obstructions
- 3) the ambient conditions (humidity, wind speed, temperature)

The momentum of the releases has a marked effect on the extent of air entrainment. If the kinetic energy is high, large quantities of air are entrained. The degree of air entrainment affects the density of the cloud and is important in its further dispersion.

### 3.1.3. Dispersion

Dispersion, or equivalently air entrainment, according to the theory of atmospheric turbulence, is a process of mixing in which turbulent eddies of large wavelength decay to eddies of ever smaller wavelengths (EPSC 1999). The dispersion process includes different phases (i) near source, (ii) interim and (iii) far-field. Dispersion can increase or decrease mass in a vapour cloud (Woodward 1998).

Depending on the gaseous mixture, gas properties, and ambient conditions, the sour natural gas cloud from a release could behave (i) positively buoyant (lighter than air; rises over time), (ii) neutrally buoyant (about the same weight as air; neither rises nor drops but disperses over time) or (iii) negatively buoyant or dense (heavier than air; drops over time). This is illustrated in Figure 16

The impact of source dimensions (area, height), humidity, temperature, wind speed, atmospheric stability and terrain effects are analysed for puff displacement, concentration distribution and parameter estimation. The negative buoyancy affects the dispersion of toxic gas cloud, and its modelling requires an approach different from positively buoyant or a passive gas. Dense gas cloud tends to hug the ground due to the gravity driven flow and does not disperse easily (Mohan 1995).

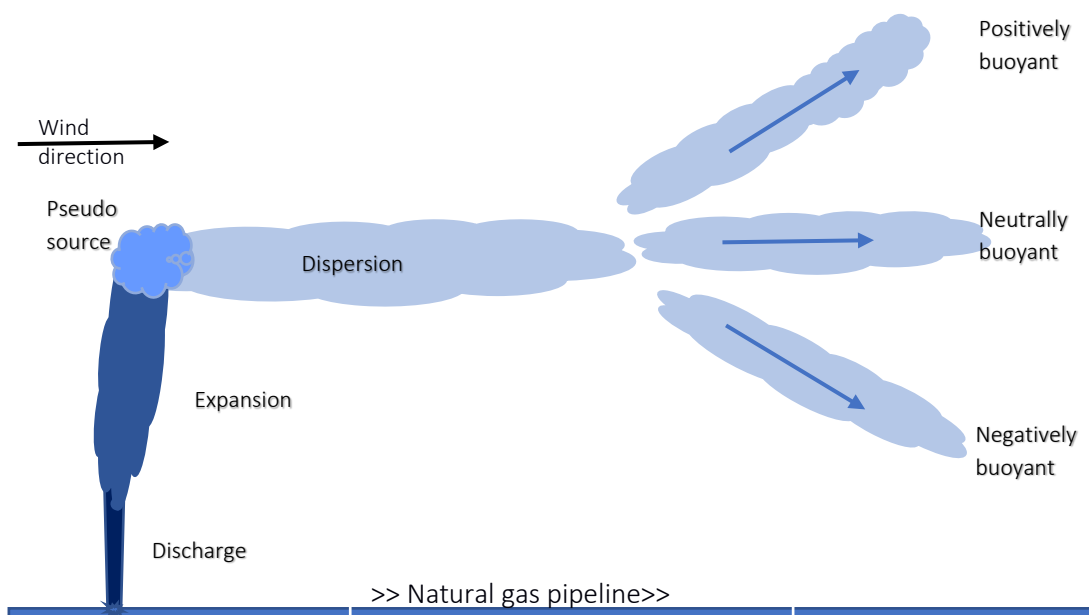


Figure 16: Buoyancy and Dispersion

During dispersion modelling process, the dispersion of pollutant or the vapour species of interest is tracked and the concentration is obtained. The key influencing factors in dispersion modelling can be classified as the physical processes and the guiding factors:

- 1) Physical process
  - Transport by wind and heat convection
  - Turbulent diffusion (random mixing of air mass)
- 2) Factors guiding dispersion
  - Cloud source (pseudo source) – mass or mass flow
  - Elevation (ground level or at height above ground) and dimensions of the source (pseudo source)
  - Weather conditions near the source and along the dispersion meteorology
  - Thermodynamic properties of the dispersed products
  - Topography (site, deposition, roughness etc.)

### 3.2. Natural gas composition

Natural gas contains many different compounds, the largest is methane, a compound with one carbon atom and four hydrogen atoms (CH<sub>4</sub>). Natural gas also contains smaller amounts of hydrocarbon with higher molecular weight, hydrocarbon gas liquids (also known as natural gas liquids) and nonhydrocarbon gases. Relative to air, methane is less dense, but the other hydrocarbon constituents of unrefined natural gas (i.e., ethane, propane, butane etc.) are denser than air (molecular weight 28.97 g/mol). The properties of constituents of commonly found sour natural gas (Airliquide 2016, Engineering ToolBox 2019) are given in Table 14.

Table 14: Properties of the main constituents of sour natural gas

	Methane	Ethane	Propane	Hydrogen sulphide	Carbon dioxide	Air
<b>Molecular formula</b>	CH <sub>4</sub>	C <sub>2</sub> H <sub>6</sub>	C <sub>3</sub> H <sub>8</sub>	H <sub>2</sub> S	CO <sub>2</sub>	
<b>Molecular mass (g/mol)</b>	16.043	30.069	44.096	34.081	44.01	28.97
<b>CAS number</b>	74-82-8	74-84-0	74-98-6	7783-06-4	124-38-9	
<b>Atmospheric boiling point (°C)</b>	- 161.5	- 88.5	-42.1	-60.3	-78.5	-194.4
<b>Liquid density @ boiling point (kg/m<sup>3</sup>)</b>	422.36	543.8	580.9	949.2	1150 (at 7bar, -49°C)	875.50
<b>Gas density @ boiling point (kg/m<sup>3</sup>)</b>	1.816	2.05	2.42	1.99	1.98	1.276 (at 0 °C, 1 bara)

	Methane	Ethane	Propane	Hydrogen sulphide	Carbon dioxide	Air
Gas density @ 15 °C (kg/m <sup>3</sup> )	0.678	1.28	1.89	1.45	1.87	
Specific gravity (gaseous phase)	0.555	1.05	1.52	1.19	1.53	1
Critical temperature (°C)	-82.59	32.2	96	100.2	30.98	-140
Critical pressure (bar)	45.99	48.8	42.58	89.7	73.8	37.36
Critical density (kg/m <sup>3</sup> )	162.7			348	467.6	

The phase diagram for methane and hydrogen sulphide is given in Figure 11 and Figure 12.

The density of the cloud in relation to the air is an important factor. Apart from the intrinsic density under normal temperature and pressure conditions, the following also matters (EPSC, 1999):

- Density at emission temperature (decrease in buoyancy through cold and increase in buoyancy through heat)
- Emission temperature, which may affect the temperature of the gas emitted at the source at the time of the thermodynamic flash
- Possibility of mist formation, depending on the humidity of the air and the temperature
- Source elevation (ground level or elevated) and dimensions of the source (pseudo source in the event of accidental natural gas leak occur in pipeline transfer).

The release density which impacts the cloud behaviour depends on the composition. For this research, the composition considered is limited to sour gas with the principal component CH<sub>4</sub> and the component of toxic concern, H<sub>2</sub>S. The effect of the composition in far-field dispersion behaviour, a range of H<sub>2</sub>S compositions were selected for evaluation.

### 3.3. Natural gas release - Source term

Natural gas travels from the reservoir wellhead to end consumers through a series of pipelines. These pipelines carry gas at varying rates of pressure. Among these, flowlines and gathering pipelines (2 to 12 inches diameter at 10 to 50 barg) and transmission pipelines (16 to 48 inches diameter at 15 to 150 barg) which transfer untreated gas from field to treatment facilities are the ones that handle sour natural gas (IOGP, 2010). The transfer under pressure could be single or multi-phase, but at the pseudo source for dispersion (following discharge and expansion) it will be gaseous phase. Even for two-phase discharge from a pipe of length greater than about 1

m, the assumption that phase equilibrium is achieved is justified (Woodward, 1998). The discharge and expansion evaluated as part of this research focuses on gaseous phase.

The dispersion is influenced by the initial conditions and require information on the discharge, which includes hole size (source physical dimensions), duration, rate, and quantity (Aloqaily 2018). The release hole size and release rate are estimated for a credible worst-case release event. The research scope is limited to long term (continuous) fixed release rates events. The potential changes in the release rate following detection and isolation of the source are not included in the current scope as these events can be at remote offsite locations without continuous monitoring and detection systems.

### 3.3.1. Discharge estimation

The discharge process determines the velocity, temperature, and mass flux of the released gas at release hole. Due to large pressure difference between the containment (pipeline) and atmosphere, natural gas forms jet flow in the vicinity of the release hole with a velocity of hundreds of meters per second. The gas temperature declines notably due to Joule-Thompson effect.

For assessing and calculating the surrounding area of concern and the distance from the leak site of a pipeline, one must evaluate the release rate of gas through the crack/hole in a highly pressurized pipeline. The release of natural gas from pipeline is a complex process (Zhang J. et.al. 2011) which includes:

- a) isothermal flow within the pipeline
- b) isentropic expansion at the leaking point
- c) jet release from the leaking point
- d) formation of the vapour cloud
- e) atmospheric dispersion.

The gas release rate through hole from a natural gas pipeline depends on time variant flow conditions, the nature of the hole (small, medium hole or large hole/rupture), the composition, initial physical state and the density of the gas, the pressure of the gas and the mass flow rate. Effective release rate can be estimated using the Equation 13 (Bariha et. al. 2016).

$$\dot{m}_{eff} = C_1 A_p \alpha p_0^{(1/2)} \times \max\left[0.25, \frac{1}{\sqrt{1 + C_2 \alpha^2 (L_d/d)}}\right]$$

Equation 13

Where,

- $\alpha$ , the ratio of hole area to the internal cross-sectional area of the pipeline

- $\gamma$ , the ratio of the specific heats of the gas at constant pressure and constant volume ( $C_p/C_v$ )
- $C$  is the decay coefficient
- $L_d$  is the length of the pipe from the source to release point (m)

Unit of measurements:

- mass flow rate (kg/s)
- density of the gas (kg/m<sup>3</sup>)
- pressure of the gas (bar)
- frictional pressure drop (decay coefficient, minimum is taken as 0.25)

The constant values to be used for the equation is given in Table 15.

**Table 15: Constant values for effective release rate estimation (Bariha et.al. 2016).**

Material	Density (kg/m <sup>3</sup> )	Gamma	C <sub>1</sub>	C <sub>2</sub>	C <sub>3</sub>	C <sub>4</sub>
Methane (CH <sub>4</sub> )	0.67	1.27	0.548	4.113E-3	0.57	1.85
Propane (C <sub>3</sub> H <sub>8</sub> )	1.18	1.13	0.989	3.947E-3	0.19	1.26

The release rates natural gas and its components, intrapolated from the graphs given in the paper by Bariha et al. is given in Table 16 and Table 17 (Bariha et.al. 2016). This approach can be used for estimating the mass rate at pseudo-source for dispersion modelling.

**Table 16: Mass release rates of natural gas – medium hole diameters (0.03 to 0.5 m)**

P (bar)	Hole dia. = 30mm; release rate $m_s$ (kg/s)	Hole dia. = 100mm; release rate $m_s$ (kg/s)	Hole dia. = 660mm; release rate $m_s$ (kg/s)	Hole dia. = 1000mm; release rate $m_s$ (kg/s)
1	4.07	13.6	89.5	136
3	7.04	23.5	155	235
5	9	30.33.	200	303
7	10.8	35.9	237	359
10	1.3	42.9	283	429

**Table 17: Mass release rates of methane and propane – rupture and large hole (diameter 1 m)**

P (bar)	Methane; alpha = 1 release rate $m_s$ (kg/s)	Propane; alpha = 1 release rate $m_s$ (kg/s)	Methane; alpha = 0.3 release rate $m_s$ (kg/s)	Propane; alpha = 0.3 release rate $m_s$ (kg/s)
30	16	30	13	24
70	25	44	20	36

Study by Stewart give solution for jet releases from rectangular shaped opening with possibilities of under expansion. Under-expanded jet forms when the rations between jet exit  $Pe/P_a > 1.8$



(Natural gas) where  $P_e$  is the exit pressure and  $P_a$  is ambient pressure. The CFD results show that for the 10:1 pressure ratio releases the hazard volume and hazard distance remain largely unaffected by nozzle shape. For the higher-pressure release, the hazard volume is larger for the rectangular nozzle releases than the equivalent release through a circular orifice, though the distance to lower flammability limit is comparable across the range of nozzle shapes considered. For both release pressures simulated the CFD results illustrate that a pseudo-source approach produces conservative results for all nozzle shapes considered. This finding has useful practical implications for consequence analysis in industrial applications, such as the assessment of leaks from flanges and connections in pipework (Stewart 2020).

Study by Ewan & Moodie demonstrates that pseudo source gives conservative predictions of the flammable volume and distance to  $\frac{1}{2}$  LFL. Compared to the jets modelled directly from the orifice, the pseudo source model gave  $\sim 15\%$  greater distance to  $\frac{1}{2}$  LFL (Ewan & Moodie 1986). Replacing the actual nozzle by a notional nozzle (often referred to as pseudo-diameter) occupying an area with the same flow rate as the real one has been demonstrated as an acceptable approach in various modelling applications (Venetsanos et. al. 2010, Papanikolaou and Baraldi 2011, Wen et. al. 2010). Nozzle shape may affect the resulting dispersion distance in the near field, whereas, far-field dispersion distances were not affected greatly by the nozzle shape (Stewart 2020). Using a pseudo source was considered as an appropriate means of modelling under-expanded jet releases from noncircular hole.

### 3.3.2. Expansion estimation

In expansion phase, the parameters of the pseudo source are obtained, where gas pressure approaches atmospheric pressure, which will later be regarded as the inlet boundary conditions for the dispersion process.

There are two methods to describe the expansion process (i) empirical correlations and (ii) numerical simulations. The numerical simulations can provide details of the gas flow, but the empirical method is convenient if the details are not required. The most used correlation for jet flow and expansion is the Birch model.

The continuity equation, momentum equation and gas EoS along with the temperature correlation are used to model the expansion (Nilsen et.al. 2014, Deng et.al. 2018).

$$\rho_a A_a U_a = \rho_e A_e U_e$$

Equation 14

$$\rho_a A_a U_a^2 = \rho_e A_e U_e^2 + (P_e - P_a) A_e$$

Equation 15

$$\rho_a = \rho(P_a, T_a)$$

Equation 16

$$T_a = T_e$$

Equation 17

Where,  $\rho_a$ ,  $P_a$ ,  $A_a$ ,  $u_a$  and  $T_a$  are the density, pressure, cross sectional area, velocity and temperature at the pseudo source respectively.  $\rho_e$ ,  $P_e$ ,  $A_e$ ,  $u_e$  and  $T_e$  are the corresponding parameters at the release hole, respectively.

The distance  $x_s$  between the pseudo source and release hole is given by Equation 18.

$$x_s = 6.45 d_e \sqrt{\frac{P_o}{P_a}}$$

Equation 18

Where,  $d_e$  is the diameter of release hole,  $P_o$ , is the pipeline pressure. The parameters of the pseudo source area obtained by solved above equations.

The initial momentum and the heat effect of gas jet leads the release gas to rise to a height and then spreads with wind direction, this phenomenon is known as uplift (Zhang J. et.al. 2014). The uplift height should be considered for defining the pseudo source as part of simulating gas dispersion. There are different equations used for estimating plume rise or the uplift height, key ones are (i) Carson and Moses equation, (ii) Smith equation, (iii) Holland formula, (iv) Concawe formula, (v) Thomas formula. Details of these approaches an analysis of estimating the uplift height using different equations is given in the study by Bhargava (Bhargava 2016). Study by Zhang determined that Holland formula was suitable for calculating the uplift height of the gas release driven by the momentum (Zhang et. al 2014). The Holland formula (Equation 19) is given in Equation 19.

$$H_r = \frac{u_s d}{u} \left[ 1.5 + 0.268 p d \left( \frac{T_s - T_a}{T_s} \right) \right]$$

Equation 19

Where,

$H_r$  elevated height (m)

$u_s$	flow rate of gas release (m/s)
$u$	velocity component, downwind (m/s)
$p$	Pressure (Pa)
$d$	Hole diameter (m)
$T_a$	Atmospheric temperature (K)
$T_s$	Source temperature (K)

The use of a pseudo source approach to represent an under expanded jet within a CFD model is also common and study by Papanikolaou et al. provide a review of its applications (Papanikolaou et al. 2012). If gas dispersion, rather than near field jet structures is of primary interest then a pseudo source term is used (Stewart 2020). For validation of the pseudo source estimation, the experimental data from Trans Canada pipeline Gas dynamic test can be utilized (Deng et al 2018).

### 3.4. Atmospheric conditions and parameters

The severity and area of effect of hazards could be significantly affected by the atmospheric conditions present at the time of the loss of containment. A release of gas that weighs about the same, turbulence created by higher wind speed tends to increase dispersion, resulting in a more rapid mixing of the gas with surrounding air. Ambient conditions (wind speed, wind direction) do not stay constant over the duration of the release as is modelled (IOGP 2010). In calm conditions, vapour clouds can travel very large distances on flat ground without showing high levels of dilution. If there is constraint on the gravity-driven flow in the far-field e.g., upward slopes or walls or perhaps dense high vegetation, then the flow will back-up, producing a deeper layer, again without significant dilution (Atkinson, 2017). Thus, gas cloud released under lower wind speed could result in larger hazard zones compared to a release under higher wind speed. However, it is also noted that for denser than air gas releases, higher wind speeds sometimes result in larger hazard zones, because the gas cloud is limited in its ability to spread (Chambers and Johnson, 2009). Dispersion modelling typically considers two cases (IOGP 2010, UK HSE 2022):

- (1) stable atmospheric conditions with low wind speeds, typically during dawn and dusk, and
- (2) neutral atmospheric conditions with higher wind speeds, typical day time

For modelling and analysis using integral tool, a low wind speed of 2 m/s was used for low wind stable conditions and 5 m/s was used for neutral conditions. Assumed 800 ft inversion layer for

the stable condition and assumed no inversion layer for neutral stability conditions. These assumptions are based on the consequence modelling guidance by IOGP 2010, UK HSE 2022.

### 3.5. Dispersion modelling end points

The risk to personnel is typically expressed as fatality risk or personnel injury and the calculations include response to personnel to the impacts from heat radiation, toxic gas, smoke, blast pressure (NORSOK 2001). The toxic effects of a material may be acute (high concentration over short period of time) or chronic (resulting from continuous exposure of lower concentration over longer period, could be routine exposure) (IOGP 2010). Consequence modelling provide estimates of the extent (ie hazard ranges and widths) and severity (i.e. how many people are affected, including the numbers of fatalities) of the consequences of each identified major accident hazard (UK HSE 2022). A number of regulators in different countries and industry peer groups including research laboratories have conducted experiments and have determined the toxicity data. For the application and use, the toxicity data is typically represented as (i) specified concentrations such as Immediately Dangerous Life and Health (IDLH) and (ii) concentration-lethality levels or Dangerous Toxic Load (DTL) (IOGP 2010).

#### 3.5.1. Hydrogen sulphide – specified end point values

The Emergency Response Planning Guidance (ERPG) by the Standards of the American Industrial Hygiene Association (AIHA) has set three exposure criteria levels for accidental releases and for exposure duration up to one hours (AIHA 2011). The ERPG values for H<sub>2</sub>S is given in Table 18.

Table 18: ERPG values for Hydrogen Sulphide

Classification	Exposure concentration	The maximum airborne concentration below which it is believed nearly all individuals:
ERPG-1	0.1 ppm	could be exposed for up to 1 hour without experiencing other than mild, transient adverse health effects or without perceiving a clearly defined objectionable odour
ERPG-2	30 ppm	could be exposed for up to 1 hour without experiencing or developing irreversible or other serious health effects or symptoms that could impair an individual’s ability to take protective action
ERPG-3	100 ppm	could be exposed for up to 1 hour without experiencing or developing life-threatening health effects

The Acute Exposure Guideline Levels (AEGL) by United States Environmental Protection Agency (US EPA) has set for single, non-repetitive exposures of air born chemicals for the public that don't exceed 8 hours. Three levels—AEGL-1, AEGL-2, and AEGL-3—are developed for each of five exposure periods (10 and 30 min and 1, 4, and 8 h) expressed as parts per million or milligrams per cubic meter (ppm or mg/m<sup>3</sup>) of a substance and are distinguished by varying degrees of severity of toxic effects (US EPA 2010). The AEGL values for H<sub>2</sub>S is given in Table 19.

**Table 19: AEGL values for Hydrogen Sulphide**

Classification	10 minutes	30 minutes	1 hour	4 hours	8 hours	End Point
<b>AEGL-1 (non-disabling, transient and reversible upon cessation of exposure)</b>	0.75 ppm (1.05 mg/m <sup>3</sup> )	0.60 ppm (0.84 mg/m <sup>3</sup> )	0.51 ppm (0.71 mg/m <sup>3</sup> )	0.36 ppm (0.50 mg/m <sup>3</sup> )	0.33 ppm (0.46 mg/m <sup>3</sup> )	Notable discomfort, irritation, or certain asymptomatic non-sensory effects (Headache in humans with asthma).
<b>AEGL-2 (Disabling)</b>	41 ppm (59 mg/m <sup>3</sup> )	32 ppm (45 mg/m <sup>3</sup> )	27 ppm (39 mg/m <sup>3</sup> )	20 ppm (28 mg/m <sup>3</sup> )	17 ppm (24 mg/m <sup>3</sup> )	irreversible or other serious, long-lasting adverse health effects or an impaired ability to escape.
<b>AEGL-3 (Lethality)</b>	76 ppm (106 mg/m <sup>3</sup> )	59 ppm (85 mg/m <sup>3</sup> )	50 ppm (71 mg/m <sup>3</sup> )	37 ppm (52 mg/m <sup>3</sup> )	31 ppm (44 mg/m <sup>3</sup> )	Life-threatening health effects or death

The Immediately Dangerous to Life or Health (IDLH) air concentration values developed by the National Institute for Occupational Safety and Health (NIOSH) characterize these high-risk exposure concentrations and conditions and are used as a component of respirator selection criteria. IDLH value for H<sub>2</sub>S is 100 ppm, IDLH values are established:

- (1) to ensure that the worker can escape from a given contaminated environment in the event of failure of the respiratory protection equipment, and
- (2) to indicate a maximum level above which only a highly reliable breathing apparatus, providing maximum worker protection, is permitted.

US EPA has identified approximately 400 Extremely Hazardous Substances (EHSs) and have developed acute exposure guideline levels. National Research Council (NRC) developed the guidelines for EHSs. Hydrogen sulphide is an EHS, and NRC used physiologically based

pharmacokinetic (PBPK) models to support the derivation of AEGs. The odour threshold is between 0.008 and 0.13 ppm, and olfactory fatigue, resulting in a lack of detection of odour, may occur at 100 ppm. Paralysis of the olfactory nerve has been reported at 150 ppm. Mean ambient air concentrations in the United States range between 0.00071 and 0.066 ppm (US EPA 2010).

### 3.5.2. Hydrogen sulphide – toxic load end point values

The toxic effects of a material (acute or chronic) can be estimated as a dose relationship or by the probit method.

- (i) Toxic dose is expressed by the concentration in the air (C) and the duration of exposure (t), known as the Haber law (UK HSE 2016). The dose (A) assuming that the concentration (C) remains constant over time (t) is given by concentration x time, and is known as Toxic Load.

$$A = C^n t$$

Equation 20

For number of gases, the relationship between C and t is simple (linear, where  $n = 1$ ). However, the 'n' value can vary and typically is determined by toxicological experiments (Franks et. al. 1996).

- (ii) Probit (Pr) expresses the fatality of a person from poisoning of H<sub>2</sub>S and can be estimated as the following equation:

$$Pr = a + b \ln(C^n t)$$

Equation 21

Where,  $a$ ,  $b$  and  $n$  are all material specific constants, for H<sub>2</sub>S, is -31.42, 3.008 and 1.43 respectively.

The Dangerous Toxic Load (DTL) describes the exposure conditions, in terms of airborne concentration and duration of exposure, which would produce a particular level of toxicity in the general population. DTL is a constant value for a given substance and is determined from the toxicology assessments (based on animal data and accidental chemical exposures to humans) as per the methodology is explained in Fairhurst and Turner (1993). UK HSE recommends using DTL for Specified Level of Toxicity (SLOT) for injury estimation and Significant Likelihood of Death (SLOD) for the fatality estimation in an evenly distributed population SLOD represents the mortality of 50% of an exposed population (UK HSE 2016).

DTL values is given in the UK HSE's Toxicity levels of Chemicals Table of SLOT DTL and SLOD DTL. The 'n' value in  $C^n t$  for Toxic dose for H<sub>2</sub>S is 4 and the DTL values for H<sub>2</sub>S is (UK HSE 2016)

SLOT DTL is  $2.0 \times 10^{12}$  ppm min

SLOD DTL is  $1.5 \times 10^{13}$  ppm min

Software tools like PHAST (by DNV) has the capability to estimate the dose (SLOD, SLOT) effects whereas CFD tools will provide the concentration as the output at any point. Contour plots of toxic lethality are not available from typical CFD software (IOGP 2010).

## 4. Consequence modelling input and parameter sensitivity

This session covers the part of the research where the following uncertainties related to consequence modelling were analysed:

- Release and dispersion of H<sub>2</sub>S containing natural gas with a range of density and properties.
- Release source terms including hole size, release fluid temperature and pressure, elevation and orientation of the release source.
- Sensitivity to the meteorological effects including wind speed, atmospheric stability, humidity.

The study is carried out in stages (Figure 17) using multiple tools; Chapter 5 and 6 explains the analysis using OpenFOAM, CFD tool. This Chapter includes the methodology and analysis using the following tools:

- (i) Aspen HYSYS, by AspenTech
- (ii) ALOHA, by US EPA
- (iii) Canary, by Quest

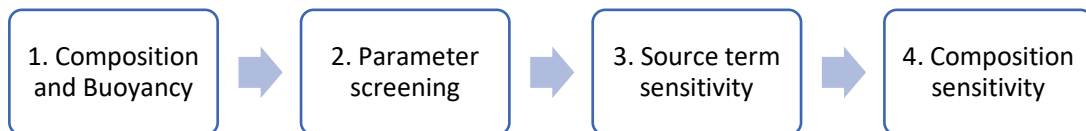


Figure 17: Input and parameter sensitivity analysis steps

### 4.1. Modelling tools

#### 4.1.1. Tool: Aspen HYSYS by AspenTech

Aspen's HYSYS is a chemical process simulator tool for oil and gas operations. It is used to mathematically model chemical processes, from unit operations to full chemical plants and refineries (Aspentech 2013). The software package is applicable over a wide range of conditions common to oil, gas and petrochemicals processes. The tool has a wide array of feature and functionalities which can be used to address engineering challenges in multi-phase flow modelling. In the study HYSYS is used to generate Pressure-Temperature (P-T) projection of the phase diagram of multi-component natural gas compositions.



Based on the phase diagram variations to the H<sub>2</sub>S containing natural gas is analysed to determine the buoyancy behaviour following release scenarios from pipeline. The analysis outcome was then used in the selection of the approach in the modelling tool, which is explained in the next sections.

#### 4.1.2. Tool: ALOHA by US EPA

The Aerial Locations of Hazardous Atmospheres (ALOHA) is an air dispersion model, which can be used as a tool for predicting the dispersion of gases (NOAA 2017). ALOHA is a program developed by the US EPA Chemical Emergency Preparedness and Prevention Office and the National Oceanic and Atmospheric Administration Office of Response and Restoration and is part of the agency's Computer-Aided Management of Emergency Operations (CAMEO) suite. CAMEO is a system of software applications used to plan for and respond to chemical emergencies. ALOHA is designed to produce reasonable results quickly enough to be of use to responders during a real emergency. Therefore, ALOHA's calculations represent a compromise between accuracy and speed (US EPA 2018).

ALOHA can predict the atmospheric dispersion rate and direction of vapours and can also generate a visual representation of the plume created by the chemical release (Figure 18). ALOHA uses the Gaussian model to predict how gases that are at or near the density of air will disperse in the atmosphere. The tool selects Gaussian (buoyant) or dense models depending on the properties of the released material. (US EPA 2018).

The Gaussian model predicts that the concentration distribution of a steady-state release of a neutrally buoyant gas will approach a Gaussian distribution with increasing down-wind distance. The model used to describe the dispersion is based on the model developed by Palazzi (NOAA 2013) and is described as:

$$C(x, y, z, t) = \begin{cases} \frac{\chi}{2} \left[ \operatorname{erf} \left( \frac{x}{\sigma_x \sqrt{2}} \right) - \operatorname{erf} \left( \frac{(x - Ut)}{\sigma_x \sqrt{2}} \right) \right] & (t \leq t_r), \\ \frac{\chi}{2} \left[ \operatorname{erf} \left( \frac{x - U(t - t_r)}{\sigma_x \sqrt{2}} \right) - \operatorname{erf} \left( \frac{(x - Ut)}{\sigma_x \sqrt{2}} \right) \right] & (t_r < t < \infty) \end{cases}$$

Equation 22

Where,

$\sigma_x, \sigma_y$ , and  $\sigma_z$  are the dispersion parameters,

$t_r$ , is the duration of the release.

$\chi$  represents the Gaussian distribution from a continuous steady-state point source (Hanna et. al. 1982).

The dispersion parameters depend upon the stability class and in some cases the surface roughness. Briggs developed formulas for estimating for each of the Pasquill-Guifford-Turner stability classes and for Urban (large surface roughness) and Rural (small surface roughness) conditions (Briggs 1973, Hanna et al. 1982, NOAA 2018). The Gaussian model is recommended when the pollutant cloud is less dense than air.

The Heavy gas dispersion calculations used in ALOHA are based on the DEGADIS model (NOAA 2013). The selection was based on for its general acceptance and the extensive testing carried out by DEGADIS authors (Havens and Spicer 1985, Spicer and Havens 1989 and Colenbrander 1980). Heavy gas model is designed to account for the gravitational effects on pollutant clouds with densities different than that of air.

In the default model, ALOHA incorporates a decision algorithm to choose between Heavy Gas and Gaussian models based on the Richardson's number. When Richardson's number is less than 1, ALOHA consider the gas to be passive and ALOHA computes dispersion using the Gaussian dispersion model (NOAA 2013).

ALOHA is used to model toxic gas clouds and flammable gas clouds. The key inputs for ALOHA model are , the release location information (site data), chemical (pollutant species), weather data (wind speed, wind direction), air temperature, humidity, surface roughness, release descriptions (source, inventory, area and type of leak, duration, temperature and pressure). The key output is the threat zone (hazard impact distance in downwind) which can be plotted for the levels of concern. The concentration of chemical at a specific point of interest (coordinates in map) is also an output from ALOHA.

The threat zone estimates are shown on a grid in ALOHA, and then plotted on maps in using [MARPLOT®](#), and Google Earth. [MARPLOT®](#) is the mapping program for the [CAMEO® software suite](#), which is used widely to plan for and respond to chemical emergencies. See example of the ALOHA outcome and results plotted using MARPLOT in Figure 18, the red threat zone represents the worst hazard level, and the orange and yellow threat zones represent areas of decreasing hazard. In this study, ALOHA version 5.4.7 was used for this research to estimate the release and dispersion of CH<sub>4</sub> and H<sub>2</sub>S.

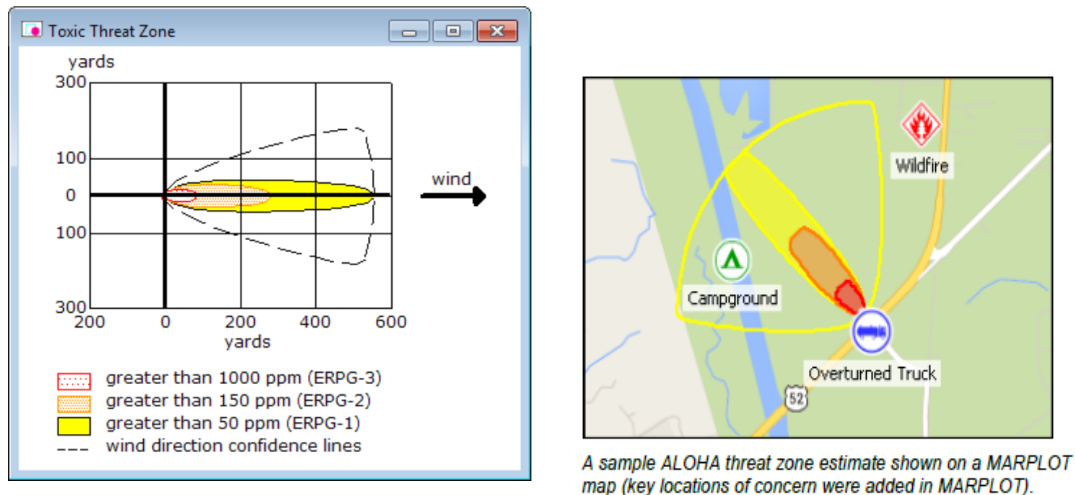


Figure 18: ALOHA output – graph for bell shaped dispersion and output on map using MARPLOT

#### 4.1.3. Tool: Canary by Quest

Canary by Quest is a regulator approved consequence assessment software which has a range of validated auxiliary models including models which integrates multicomponent thermodynamics into the time-varying fluid release simulation (Tauseef et.al. 2017). The base models in Canary are derived from DEGADIS and SLAB (available in public domain) and validated (US EPA, 2017). CANARY has auxiliary models to produce source term(s) required for consequence models such as multi-component thermodynamic calculation, liquid pool vaporization calculation and release rate calculation. CANARY allows the user to define the hazard endpoints (e.g. gas concentration, radiant flux, overpressure) that determine the extent of toxic or flammable gas clouds, radiation from several types of fire, or overpressure resulting from an explosion (UK HSE 2010).

For this study, Canary is used to determine the potential impact distance following sour natural gas release. By varying the input and parameters, the sensitivity is analysed. A typical output from Canary is given in Figure 19. The overhead (plan) view illustrates the toxic natural gas footprint of three H<sub>2</sub>S cloud concentrations in the downwind dispersion along the central line with the cloud width. The side view illustrates the elevation cross section of the cloud dispersion with the cloud height (black line indicates cloud central line). For the risk assessment application, the width of the cloud and the averaging time plays a significant role (US EPA 2017). The typical input required for Canary dispersion modelling are source terms (hole size, elevation, orientation), released material, operating conditions (temperature, pressure) ambient conditions, surface roughness.

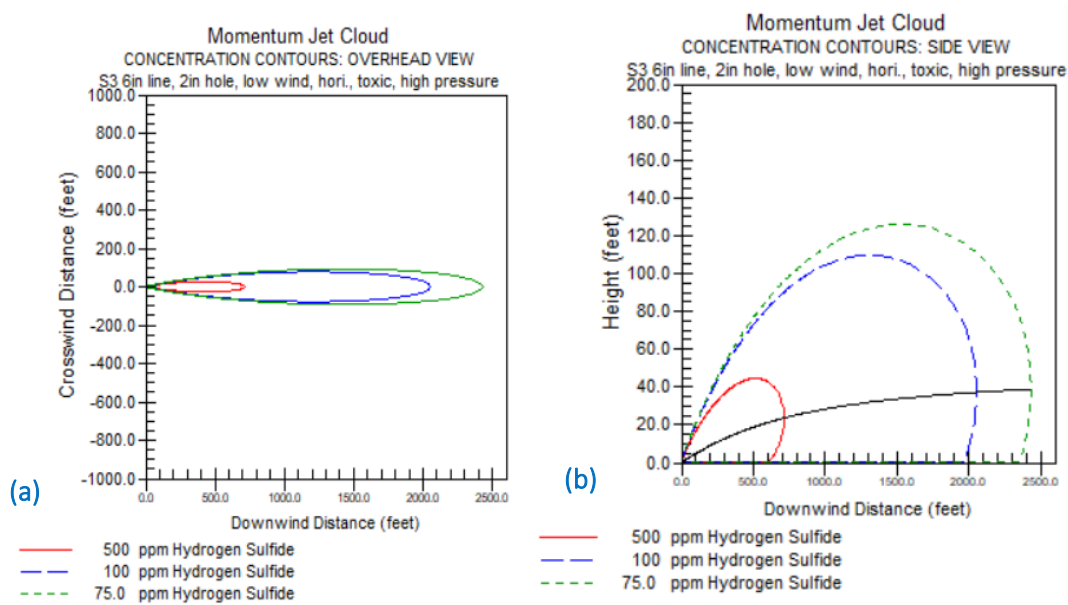


Figure 19: Hydrogen sulphide momentum jet cloud - dispersion isopleths (a) Overhead view (b) Side view

#### 4.2. Model selection based on buoyancy

For the initial screening, ALOHA is used to simulate the release and dispersion of  $\text{CH}_4$  and  $\text{H}_2\text{S}$  individually. The ALOHA model bases its determination mainly on molecular weight, size of the release, and temperature of the gas cloud. The molecular weight (mass of a molecule) of  $\text{H}_2\text{S}$  is 34.1 g/mol, and it is thus slightly heavier than air (molecular weight 28.97 g/mol) at standard conditions. During expansion from elevated pressure released  $\text{H}_2\text{S}$  will be colder and thus even heavier than air close to the release source with a high potential to accumulate in low-lying areas (AIHA 2011, Danielson et.al. 2009, Nilsen et.al. 2014, CCOHS 2016).

ALOHA has two separate dispersion models (i) Gaussian and (ii) Heavy gas, the selection is based on the relative density (to air), molecular weight, size of releases and temperature of the cloud (US EPA 2018). The user can manually choose whether to predict the dispersion of a chemical as a Gaussian or heavy gas release or allow ALOHA to choose automatically. A comparative study was carried out to analyse the automatic selection of the dispersion model by ALOHA.

The Project Prairies Grass (PG) Scenarios (Barad 1958) were used to evaluate the ALOHA model selection (see section 2.10 for details). The release source term and conditions for a set eight scenarios covering a range of atmospheric stability from A to F and material release temperature ranging from 20 °C to 32 °C selection for simulations in ALOHA is given in

Table 20.

Table 20: Prairie Grass field trial case data for ALOHA model selection

Prairie Grass Case	Wind speed (m/s)	Stability	Humidity	Ground Roughness (mm)	Air Temp (°C)	Source (kg/s)	Material temperature (°C)
PG07	4.93	B	20	6	32	0.0899	32
PG08	5.9	C	20	6	32	0.0911	32
PG09	8.4	C	20	6	28	0.092	28
PG10	5.4	B	20	6	31	0.0921	31
PG13	2.7	F	20	6	20	0.0611	20
PG15	4	A	20	6	22	0.0955	22
PG16	3.7	A	20	6	28	0.093	28
PG17	4.6	D	20	6	27	0.0565	27

Simulations were carried out using ALOHA for both Heavy gas and Gaussian models for the eight cases; Heavy gas was the default model selection by ALOHA. The estimated concentration for all the eight cases for both dispersion models were compared against the observed central line concentration from field trials (Table 21). The results indicate that Heavy gas model significantly overestimates the concentration and Gaussian model estimates are comparable.

Table 21: Comparison on the observed values vs estimated concentration

Case	Observed values					Estimated- Heavy gas model					Estimated- Gaussian				
	50 m	100 m	200 m	400 m	800 m	50 m	100 m	200 m	400 m	800 m	50 m	100 m	200 m	400 m	800 m
PG#07	36	9	1.6	0.3	0.0	337	85	22	5.8	1.6	53	13	3.4	0.8	0.2
PG#08	155	42	9.3	1.5	0.3	437	110	29	7.6	2.0	100	26	6.4	1.7	0.4
PG#09	72	20	5.0	1.0	0.2	299	77	20	5.4	1.4	70	18	4.5	1.2	0.3
PG#10	66	16	4.1	1.0	0.1	307	78	21	5.4	1.4	50	12	3.1	0.8	0.2
PG#13	-	-	-	46.7	37.1	-	-	-	45.9	13.6	-	-	-	47.	13.3
PG#15	147	39	7.8	1.7	0.2	295	74	19	5.1	1.3	29	7	1.8	0.5	0.1
PG#16	67	13	2.3	0.2	0.0	325	81	21	5.5	1.5	31	8	2.0	0.5	0.1
PG#17	235	98	30.8	9.5	3.5	553	142	37	9.8	2.6	154	40	10.7	3.0	0.9

The simulation results were analysed out using the ratio of maximum concentration to the release rate. The comparison using Fac2 numerical evaluation criteria is given in

Table 22.

Table 22: Comparison on the observed vs estimated concentration / release rate

Case	Observed values					Estimated- Heavy gas model					Estimated- Gaussian				
	50m	100m	200m	400m	800m	50m	100m	200m	400m	800m	50m	100m	200m	400m	800m
#07	404	95	18	3	0.3	3749	942	246	65	17	53	13	3	0.8	0.2
#08	1700	457	102	16	2.9	4797	1207	315	84	22	100	26	6	1.7	0.4
#09	779	221	54	11	2.1	3250	838	220	58	15	70	18	4	1.2	0.3
#10	719	172	45	11	0.7	3333	849	223	59	16	50	12	3	0.8	0.2
#13	-	-	-	764	607	-	-	-	751	223	-	-	-	47	13
#15	1539	406	82	18	2.1	3089	778	202	53	14	29	7	2	0.5	0.1
#16	725	137	25	2	0.2	3495	868	225	59	16	31	8	2	0.5	0.1
#17	4166	1738	545	168	62	9788	2513	655	174	46	154	40	11	3.0	0.9

The Fa2 comparison for Heavy gas model results is given in Figure 20 and for Gaussian model results is given in Figure 21. Criteria for a good dispersion model,  $Fac2 > 0.5$  represented by dashed lines corresponding to upper (twice) and lower (half) limits (Olesen 2001, Chang and Hanna, 2004). The ALOHA model selection analysis shows that for Heavy gas model simulations only 20% of the estimated results falls within  $Fac2$  whereas 65% of results falls within  $Fac2$  for simulations using Gaussian model.

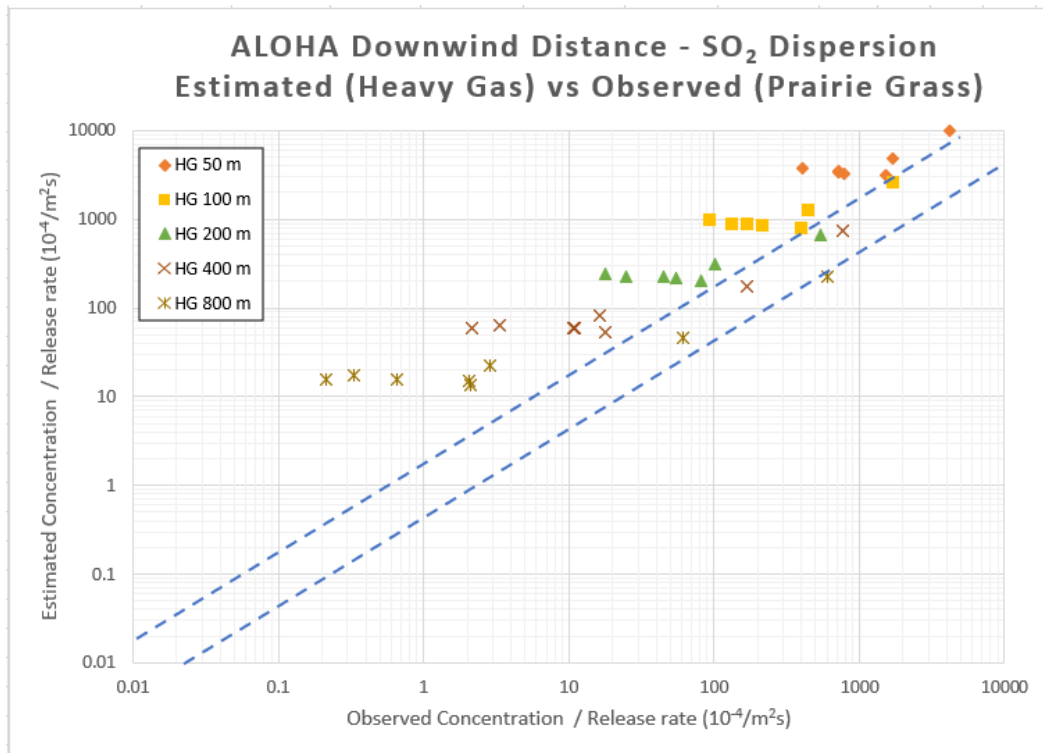


Figure 20: ALOHA verification – Heavy gas model results vs Prairie Grass field trial

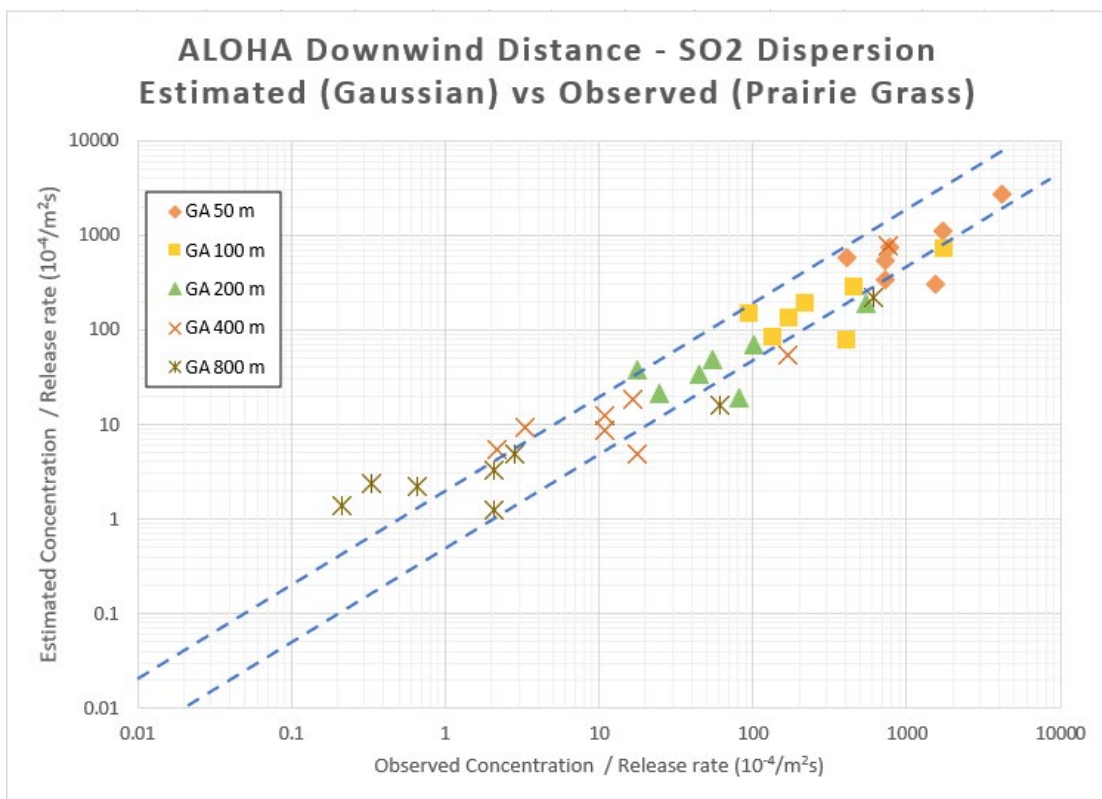


Figure 21: ALOHA verification – Gaussian model results vs Prairie Grass field trial

Based on the molecular weight, it is widely believed that SO<sub>2</sub> cloud is expected to behave as dense gas typically estimated using Heavy gas model. However, this verification study has shown that selection of Gaussian modelling for dispersion is better suited for SO<sub>2</sub> under the given release and dispersion condition. This evaluation Significance of risk analyst's understanding the cloud behaviour is critical for appropriate model selection.

### 4.3. Composition screening using HYSYS

Over the years, certain heuristics have been used as source term input parameters for modelling multiphase releases and ensuing dispersion. Examples of these heuristics include choosing a pure component of the same molecular weight in place of the mixture, distilling mixture composition to a handful of components, choosing to model natural gas as a pure methane, etc. Although convenient, these modelling assumptions can result in hazard estimations that diverge from reality with the biggest problem being the inability to accurately account for thermodynamic effects like phase splits and composition changes during release conditions (Johnson and Marx, 2003).

To determine the appropriate model, the characteristic of the multi-component sour natural gas need to be understood. HYSYS simulations are carried out to determine the sour natural gas characteristics. At first, the simulations were carried out only using methane (CH<sub>4</sub>) and hydrogen sulphide (H<sub>2</sub>S). In the second set of simulations, eight sour natural gas compositions were analysed. The density of the material is key factor for the selection of the dispersion modelling approach.

A knowledge of the phase behaviour in the critical region of multicomponent hydrocarbon mixtures is of value both in industrial processing operations and for the optimum operations of gas condensate reservoirs. The compressibility factor distinguishes natural gas from an ideal gas. Pipelines may operate at very high pressure (above 70 barg) to keep the gas in the dense phase, thus preventing condensation and two-phase flow. HYSYS modelling was carried out to estimate the phase equilibrium of natural gas for different H<sub>2</sub>S compositions at 30 barg. Natural gas (a non-ideal gas) obeys the modified gas law (Equation 23).

$$PV = nZRT$$

Equation 23

Where,



P = pressure

V = volume

T = absolute temperature (°K)

Z = compressibility

n = number of kilo-moles of the gas

A phase envelope (isopleths or contour plot) is the Pressure-Temperature (P-T) projection of the phase diagram of a multicomponent system of fixed composition (Figure 22). It is made up of two parts: (1) the bubble curve and (2) the dew curve. The bubble point curve is a curve that denotes the formation of the first bubble of vapour at a given pressure and temperature. Similarly, the dew point is a curve that denotes the formation of the first drop of condensate vapour at a given pressure and temperature. These two curves join at a critical point where the latent heat of vaporization is assumed to be zero denoting the co-existence of vapour, and liquid, phases. Transition from a liquid to a two phase and to vapour phase occurs in moving across from left to right.

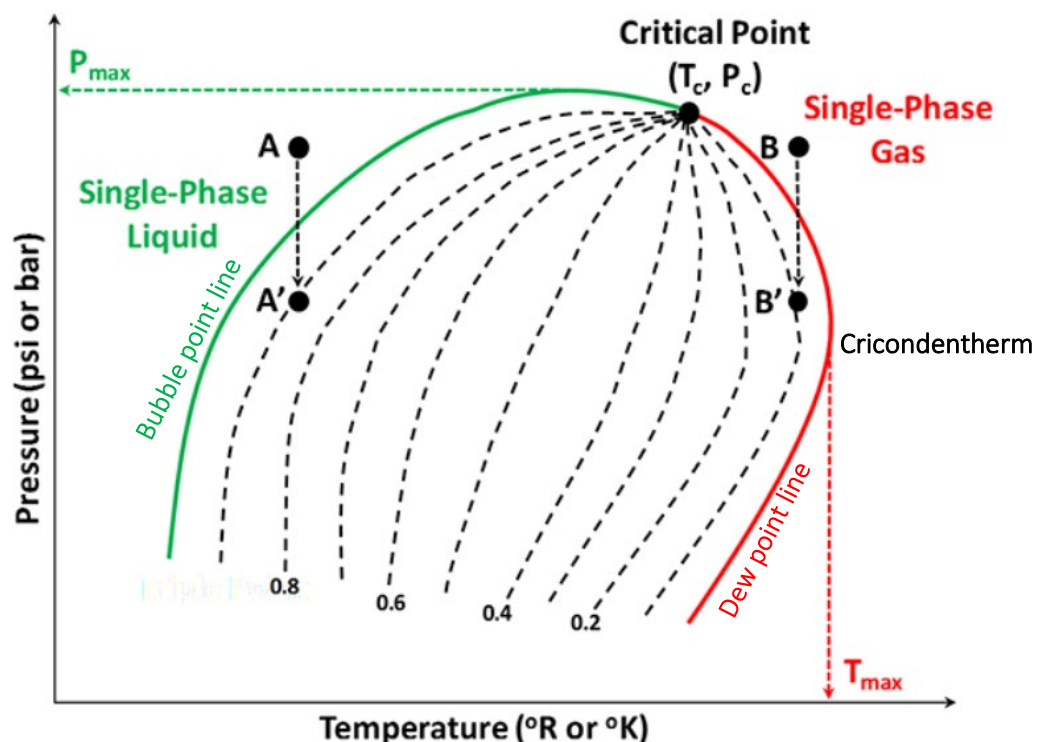


Figure 22: Multi-component Phase Diagrams

Source: PennState College of Earth and Mineral Sciences (PennState 2020)

The critical point for a multicomponent mixture is referred to as the state of pressure and temperature at which all intensive properties of the gas and liquid phases are equal. At the critical point, the corresponding pressure and temperature are called the critical pressure  $p_c$  and critical temperature  $T_c$  of the mixture. Cricondenbar is the maximum pressure above which no gas can be formed regardless of the temperature. The corresponding temperature is called cricondenbar temperature. Cricondenthem is the maximum temperature above which liquid cannot be formed regardless of the pressure. The corresponding pressure is called cricondenthem pressure.

For the simulations, the HYSYS process simulator was used to perform flash and property calculations to better understand fluid phase behaviour under process and release conditions. Cricondenthem and cricondenbar temperatures of multicomponent hydrocarbon mixtures is also estimated using HYSYS. The Peng-Robinson (PR) EoS, the model for non-ideal vapours was used. PR EoS in HYSYS rigorously solves any single, two-phase, or three-phase vapour-liquid-equilibrium (VLE) calculations with a high degree of reliability (Aspentech 2013). PR EoS provides better phase and equilibrium estimations close to/at the critical point as well provide better liquid densities estimations for gas and condensate systems when compared to Soave-Relich-Kwong EoS and Non-Random Two-Liquid EoS (Guerra 2006, Aspentech 2013). Furthermore, Aspentech, the licensor for the HYSYS software, has made several enhancements to the original PR EoS model to extend its range of applicability (Temperature, Pressure, and binary interaction parameters) to improve predictions of non-ideal systems (Aspentech 2013).

P-T projection of the phase diagram of a multicomponent system is compared against pure material (100% CH<sub>4</sub>) and simplified compositions (i) 78% CH<sub>4</sub>, 8% C<sub>2</sub>H<sub>6</sub>, 14% H<sub>2</sub>S and (ii) multicomponent composition S4 from Table 24. The P-T phase diagram illustration is given in Figure 24Figure 23.

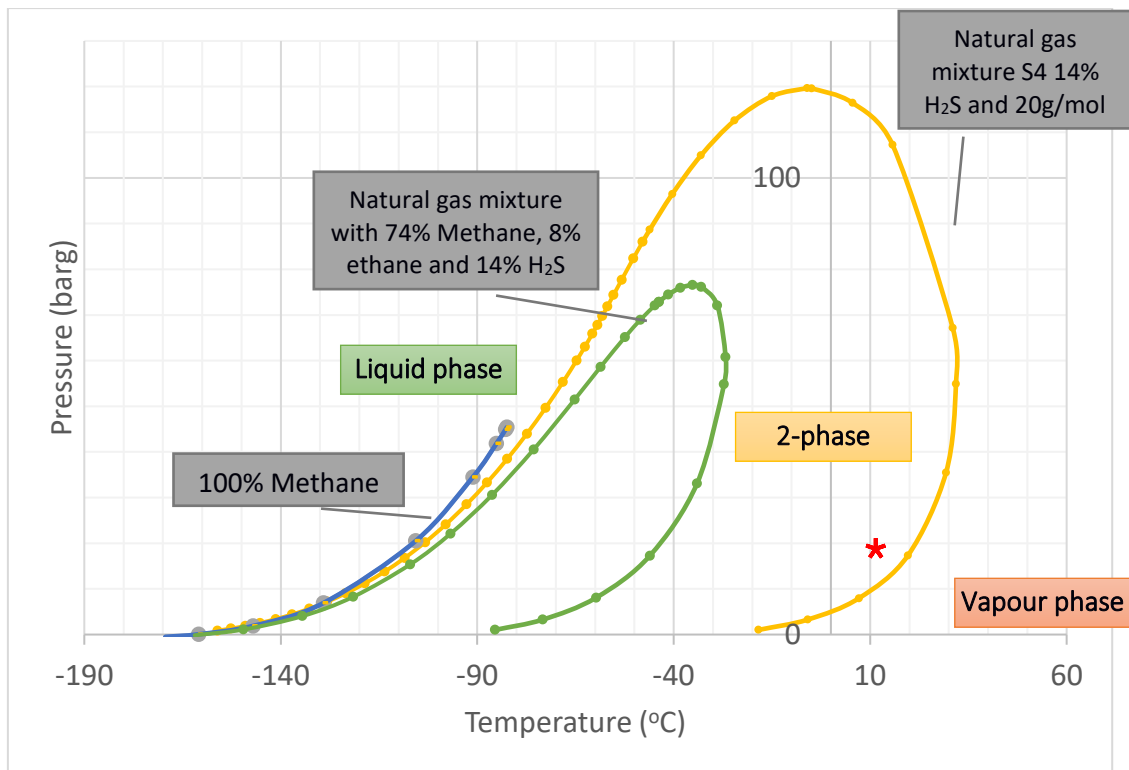


Figure 23: Phase equilibrium curves for methane (blue), Methane-ethane-Hydrogen sulphide (green), and S4 sample (yellow)

A typical set of natural gas pipeline transfer operating conditions are considered, 10 °C and 20 barg (red mark in the figure), is used for the comparison. Going by the popular heuristic of modelling natural gas as 100% methane (blue line), it was observed that at the pipeline operating conditions, the release is purely vapour with buoyant properties. Similarly, if the natural gas mixture with three components (78% CH<sub>4</sub>, 8% C<sub>2</sub>H<sub>6</sub> and 14% H<sub>2</sub>S) represented by the green line, at the pipeline vapour is mostly vapour too. However, a detailed composition of the mixture S4 reveals the release contains vapour, aerosol, and liquid phases which were missed in the prior two compositions. This analysis reveals the release contains vapour, aerosol, and liquid phases, which were missed earlier highlighting the importance of composition in dispersion modelling and the need to perform sensitivity analysis.

#### 4.3.1. HYSYS Simulations: CH<sub>4</sub> and H<sub>2</sub>S

Further analysis on the sour natural gas composition sensitivity was carried out. In the first step of composition simulations, HYSYS was used to estimate the phase equilibrium for H<sub>2</sub>S containing natural gas (CH<sub>4</sub>). The Cricondentherm and Cricondenbar values estimated for natural gas compositions with H<sub>2</sub>S concentrations 0%, 2%, 5%, 10%, 15%, 40%, 100% is given in Table 23. The phase equilibrium curves plotted is given in Figure 24.

Table 23: Natural gas phase equilibrium

	Cricondentherm (°C)	Cricondenbar (barg)
60% CH <sub>4</sub> and 40% H <sub>2</sub> S	25.99	1344
85% CH <sub>4</sub> and 15% H <sub>2</sub> S	-24.18	91.96
90% CH <sub>4</sub> and 10% H <sub>2</sub> S	-39.72	75.11
98% CH <sub>4</sub> and 2% H <sub>2</sub> S	-82.3	38.55
100% H <sub>2</sub> S	100.5	89.1

Phase equilibrium – impact of H<sub>2</sub>S in natural gas

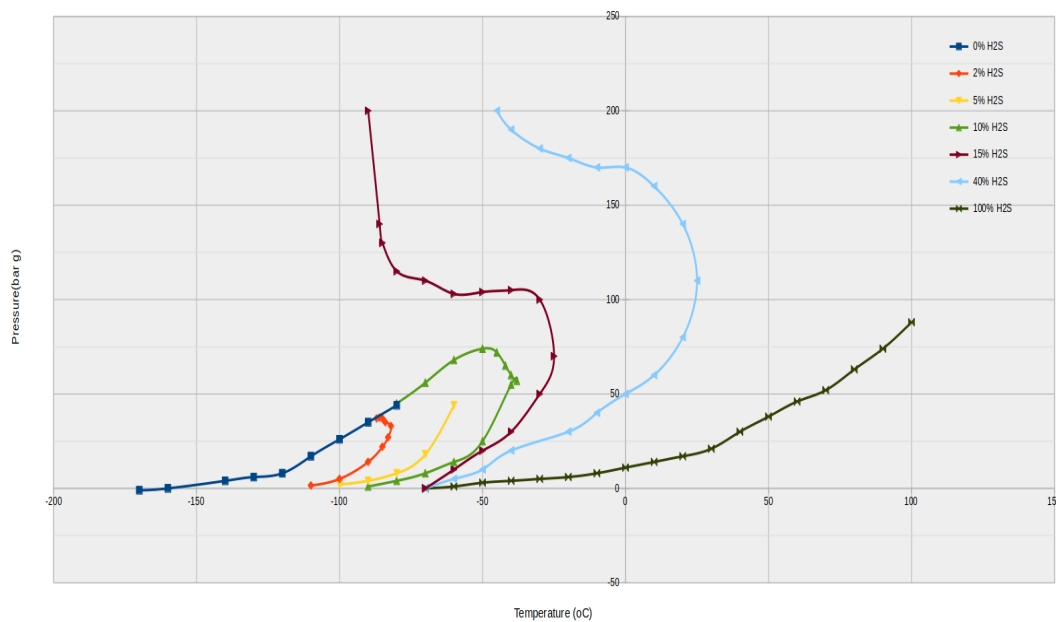


Figure 24: Phase equilibrium – impact of H<sub>2</sub>S concentration in natural gas (CH<sub>4</sub>)

From the plotting of the phase equilibrium curves from 0% H<sub>2</sub>S (i.e. 100% CH<sub>4</sub>) to 100% H<sub>2</sub>S (i.e. 0% CH<sub>4</sub>), it is observed that the lighter gas behaviour of the natural gas is followed for lower concentration of H<sub>2</sub>S; but, starts to change when the H<sub>2</sub>S concentration exceeds 10% and behaves more like dense gas when concentration exceeds 15%. Calculation results from the study by Nilsen et. al. for different sour gas compositions also concludes on a similar finding that significant differences in the discharge and dispersion for the combinations of EoS and expansion methods for varying concentration of sour components in natural gas (Nilsen 2014).

#### 4.3.2. HYSYS Simulations: multi-component sour natural gas

In the second set of screening for composition, eight sour natural gas compositions from gas production fields across the world were evaluated. The compositions are represented with references S1 to S8 and given in Table 24. The gas field name and location is not given due to commercial reasons. The compositions selection were to represent a range of H<sub>2</sub>S composition and the molar mass. The composition analysis selection has natural gas compositions with H<sub>2</sub>S

mol% ranging from 2.6% to 29.6% and the natural gas molar mass ranging from 20 g/mol to 38.7 g/mol. PR EoS was used, and the phase equilibrium simulations were carried out.

**Table 24: Multi-component compositions for release and dispersion modelling (mol %)**

Natural gas composition	S1	S2	S3	S4	S5	S6	S7	S8
H <sub>2</sub> S	2.6%	8.1%	10.4%	14.3%	14.6%	16.5%	17.8%	29.6%
CO <sub>2</sub>	5.5%	9.1%	12.1%	2.2%	3.4%	3.3%	8.8%	3.4%
CH <sub>4</sub>	14.3%	55.7%	54.5%	81.0%	66.1%	60.1%	19.2%	37.0%
C <sub>2</sub> H <sub>6</sub>	28.5%	11.3%	10.3%	0.8%	10.4%	11.0%	25.3%	15.5%
C <sub>3</sub> H <sub>8</sub>	32.8%	10.9%	9.0%	0.9%	4.3%	6.1%	20.6%	11.3%
C <sub>4</sub> H <sub>10</sub>	13.3%	4.9%	3.7%	0.8%	1.3%	3.1%	8.3%	3.3%
<b>Molar mass (g/mol)</b>	38.7	27.7	26.8	20.0	22.8	24.5	34.5	29.1
UFL	11.3%	15%	16%	16.6%	16.1%	15.8%	14.3%	16.6%
LFL	2.6%	4.0%	4.2%	4.8%	4.3%	4.1%	3.2%	3.7%

For this study, the compositions analysed include a range of sour (H<sub>2</sub>S rich) natural gases with molar mass in order to factor in the potential buoyancy effects in the toxic cloud dispersion in air. The phase envelope of eight compositions toxic natural gas given in Figure 25 illustrates that the phase of a multicomponent toxic natural gas could vary (liquid, 2-phase, or vapour) with a change in the composition, temperature, and pressure.

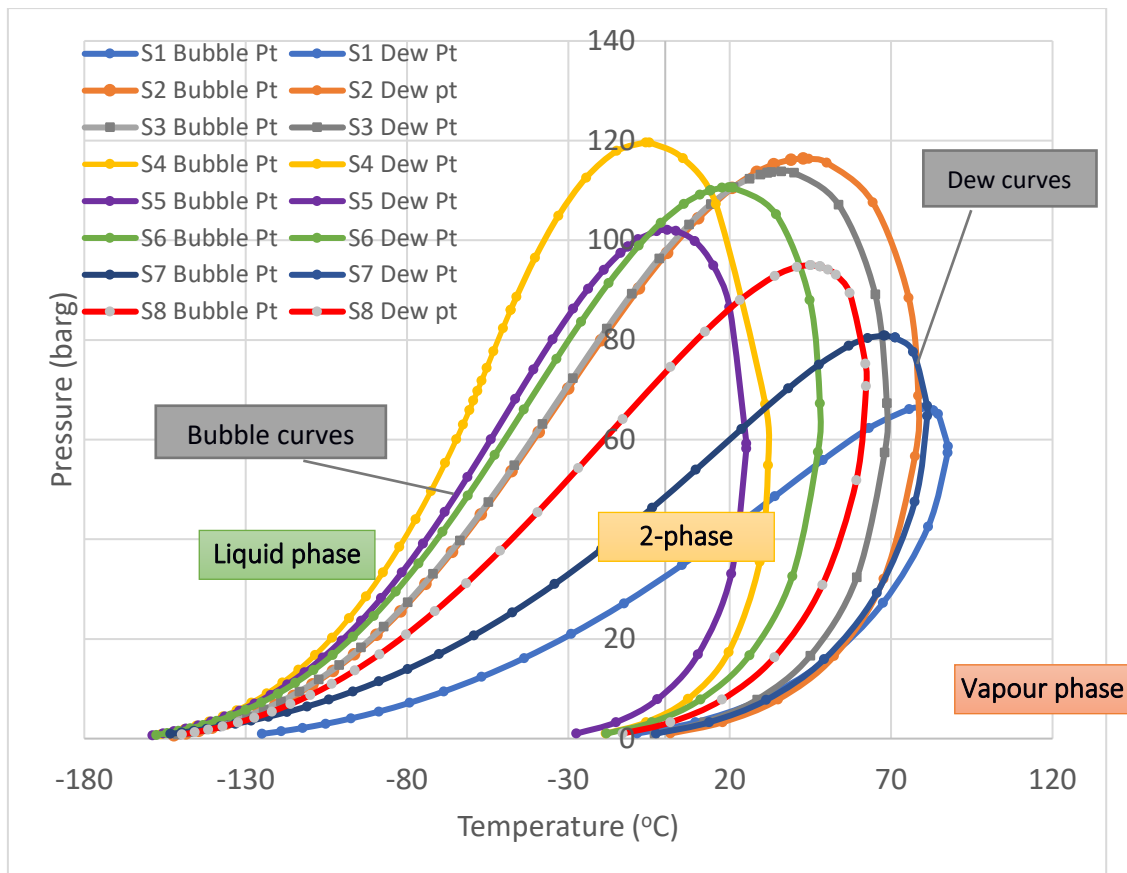


Figure 25: Phase equilibrium curve – toxic natural gas compositions

The phase envelope of eight toxic natural gas compositions given in Figure 25 illustrates that the phase of a multicomponent toxic natural gas could vary (liquid, 2-phase, or vapor) with a change in the composition, temperature, and pressure.

Density of fluid and related buoyancy (positive, neutral, negative) plays a major role in selecting the dispersion modelling approach (passive, dense etc) for estimating downwind distances (Nair & Wen, 2019). Released fluid density is driven by fluid's molar mass, release pressure and temperature. The Bubble curve and the Dew curves shift towards to right with an increase in molar mass (S1, S7, S8). This is due to the higher molar mass from higher composition of C4+ hydrocarbons and hydrogen sulphide contribution. The phase of the released material is critical since it determines the release and dispersion model used (e.g., heavy gas vs Gaussian); an inappropriate selection can lead to erroneous results. For example, the fluid phase of S5 (MW 24.2 g/mol) and S6 (MW 26.7 g/mol) with similar molecular mass could yield different results (dispersion distance) for a given pipeline operating pressure and temperature; for example, at 60 barg and 40 °C, composition S5 will be vapour, whereas composition S6 will be 2-Phase. Discussion on the sensitivity to the changes in temperature and operating pressure is included in section 4.4 and 4.5.

Using the phase envelope generated from HYSYS, the input compositions were modified to ensure similar sample molar mass and H<sub>2</sub>S composition which is acceptable for this comparative study. The analysis helped to understand the influence of user-adjustable parameters on model outputs.

#### 4.4. Impact of water vapour in natural gas

Well fluids may become saturated in the presence of produced water during production and transmission. As part of the analysis in this paper, the impact of water saturation on natural gas (with H<sub>2</sub>S) dispersion in the event of a release was studied. Using the water saturate tool in Aspen HYSYS, S6 natural gas sample (Table 24) was saturated at 7.9 barg (115 psig) and 25 °C (77 °F) to estimate the new composition given in Table 25.

Table 25: Wet (saturated) and Dry base – natural gas (S6) compositions (mol%)

Component	Dry basis	Wet basis
H <sub>2</sub> O	0.00%	<b>0.15%</b>
Nitrogen	1.00%	1.00%
H <sub>2</sub> S	15.68%	15.66%
CO <sub>2</sub>	3.10%	3.09%
Methane	57.34%	57.25%
Ethane	10.49%	10.47%
Propane	5.79%	5.79%
i-Butane	1.30%	1.30%
n-Butane	3.00%	2.99%
n-Pentane	1.80%	1.80%
n-Hexane	0.50%	0.50%

Consequence modelling was performed using Canary to assess the impact of water saturation on downwind dispersion to H<sub>2</sub>S hazard level dispersion distance (see Figure 26).

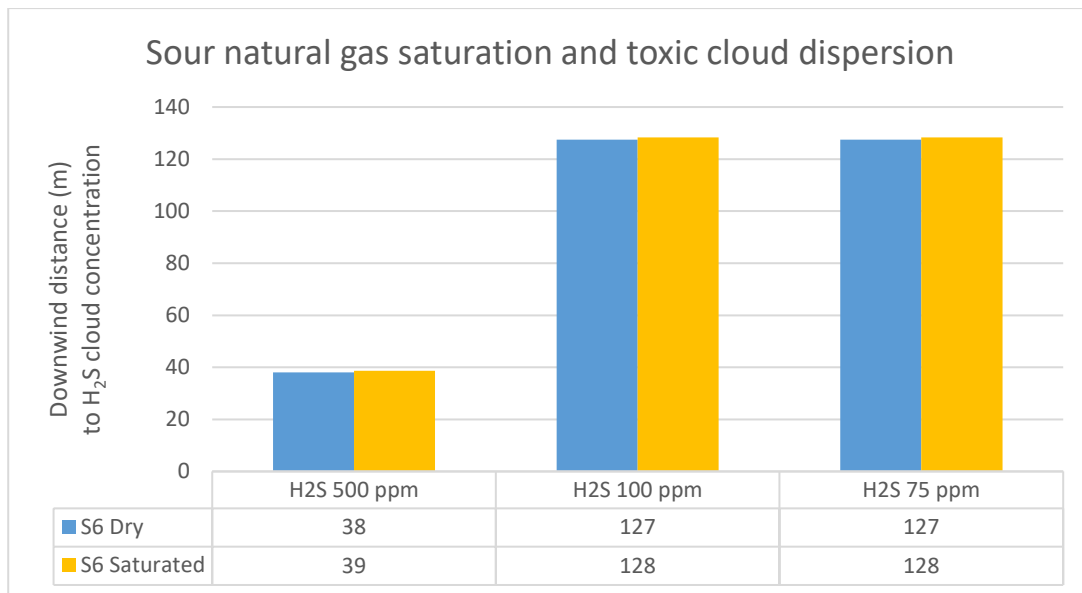


Figure 26: Sensitivity – natural gas saturation: Downwind distance to H<sub>2</sub>S concentration

The difference in the estimated downwind distances (about 1%) for the dry and saturated natural gas is not significant for the process risk management purposes. The results suggest that water saturation of natural gas is not a significant parameter in downwind dispersion to H<sub>2</sub>S hazard levels.

#### 4.5. Parameter screening using ALOHA

ALOHA calculates and plots the maximum downwind distance to each of the levels of concern (concentrations). The release and dispersion modelling using ALOHA is limited to one component at a time. Though natural gas consists of a range of constituents, for this analysis, modelling and results for two components only were evaluated. Release and dispersion modelling was carried out for 100% CH<sub>4</sub> and 100% H<sub>2</sub>S as separate cases.

For the comparison of the integral tool results against incident impact distance, the release rates and related parameter values was estimated on the conditions of natural gas pipeline like the conditions for Kaixian, Kai County, China. The toxic cloud hazardous level distance estimation is validated against the actual monitored values from Kaixian (“12.23” disaster) given in the case study by Qingchun and Laibin (Qingchun and Laibin 2011). The estimated release rate from the blowout was 98.5 kg/s. A set of release cases with a range of release rates, wind speeds and weather stability were selected; the input data for the base case and sensitivity cases for ALOHA are listed in Table 26.



Table 26: ALOHA Simulation: Model input for base case and sensitivities

Description	Release conditions	Atmospheric stability and wind speed	Ambient temperature and humidity	Inversion layer height and surface roughness
<b>Base case</b>	Release from 6" pipeline at ground level; continuous release from rupture in vertical orientation at 30 barg (CH <sub>4</sub> ); at 12.4 barg (H <sub>2</sub> S)	F stability (typical night-time / stable); 1 m/s	8 °C 50% humidity	No specific inversion height (end of momentum jet); Terrain similar to open country (minimum turbulence from obstacles)
<b>Sensitivity</b>	Release rate similar to Kaixian blowout- 100 kg/s	D stability (typical day time / neutral); 5 m/s	25 °C 99% humidity	Inversion at 1000 m, 100 m, 15 m; Terrain to represent urban or forest

Three hazardous concentration criteria levels are set and the threshold criteria values for CH<sub>4</sub> and H<sub>2</sub>S as given in Table 27. When the volume of methane in air ranges from 5% to 15% (LFL to UFL), the occurrence of fire or an explosion becomes very high. However, the methane concentration higher than 5% is considered high. For alerting personnel for emergency response 10% LFL is typically used. Inversion refers to a layer of air (change in temperature at altitude) that resists upward motion of air. This phenomenon (entrapment) could impact the distance compared to free dispersion

Table 27: Hazardous levels of pipeline release of sour natural gas

Component	Accidental consequence	Level-3	Level-2	Level-1
<b>Methane (CH<sub>4</sub>)</b>	Flash fire (flammable vapour cloud distance)	LFL (50,000 ppm)	60% LFL	10% LFL
<b>Hydrogen sulphide (H<sub>2</sub>S)</b>	Toxic concentrations of significance	400 ppm	200 ppm	100 ppm

The list of simulation cases for the release scenarios and sensitivities and the two previously discussed sets of meteorological conditions (*i.e.*, stable night-time with 1 m/s wind, neutral stability with 5 m/s wind). The hazardous level distances estimated for CH<sub>4</sub> (flammable cloud) is given in Table 28.

Table 28: Base case and sensitivity results – CH<sub>4</sub>

Case reference	ALOHA file	Wind velocity (m/s)	Stability	Ambient temperature (°C)	Release rate (kg/s)	Distance (m) to LFL	60% LFL	10% LFL
Base case	ALOA02	1	F	8	14.06	884	1200	3800
Stability D	ALOA01	1	D	8	14.06	273	359	620
Pressure 70 barg	ALOB01	1	F	8	32.43	430	573	1700
Wind speed	ALOA03	5	D	8	14.06	121	158	416
Amb. Temp	ALOA04	1	F	25	13.6	899	1200	3900
Inversion at 15 m	ALOA05	1	F	8	14.05	918	1400	7700
Urban or forest	ALOA06	1	F	8	14.05	460	616	1800
Humidity 99%	ALOA07	1	F	8	14.05	884	1200 <td 3800	

A representative illustration of un-ignited gas cloud (ALOA02) to downwind direction for three CH<sub>4</sub> flammable concentration levels of interest plotted on a geographical location in Kaixian County is given in Figure 27.

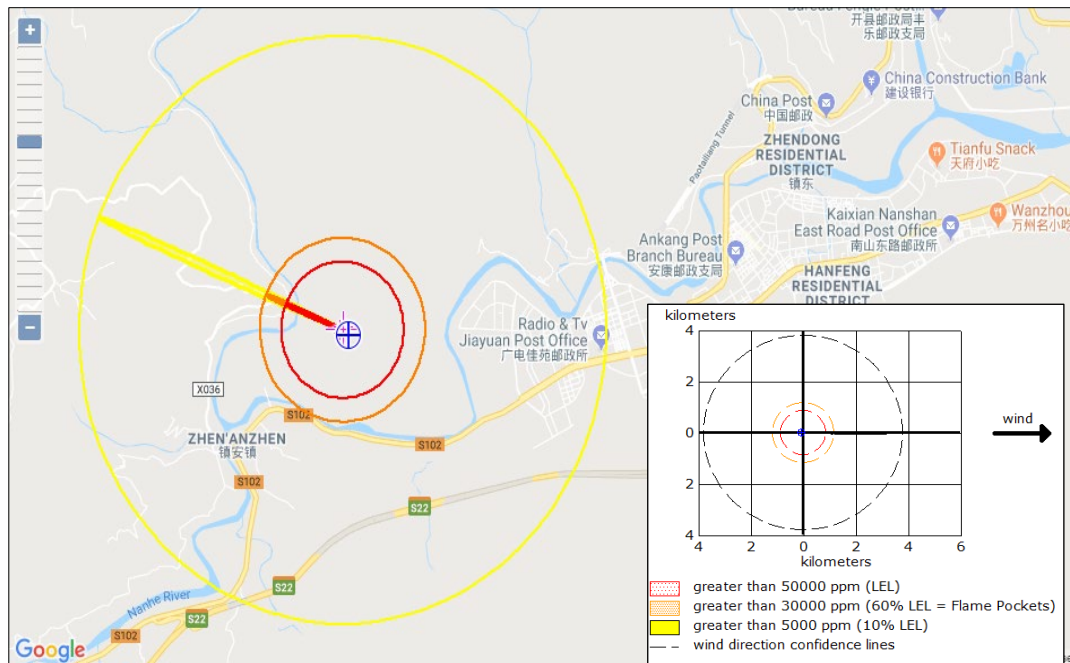


Figure 27: ALOHA estimated Methane (flammable) Hazard zones

The hazardous level distances estimated for H<sub>2</sub>S (toxic cloud) is given in Table 29.

Table 29: Base case and sensitivity results – H<sub>2</sub>S

Case reference	ALOHA file	Wind velocity (m/s)	Stability	Ambient temperature (°C)	Release rate (kg/s)	Distance (m) to 400 ppm	200 ppm	100 ppm
Base case	AL1A02	1	F	8	8.7	2100	3000	4400
Stability D	AL1A01	1	D	8	8.7	1400	2000	3000
Wind speed	AL1A03	5	D	8	8.7	838	1200	1700
Amb. Temp 25 oC	AL1A04	1	D	25	8.43	2100	3100	4500
Inversion at 15 m	AL1A05	1	F	8	8.7	2100	3000	4400
Urban or forest	AL1A06	1	F	8	8.7	1600	2300	3500
Humidity 99%	AL1A07	1	F	8	8.7	2100	3000	4400

A representative illustration of un-ignited gas cloud (AL1A02) to downwind direction for three H<sub>2</sub>S toxicity concentration levels of interest plotted on a geographical location in Kaixian County is given in Figure 28.

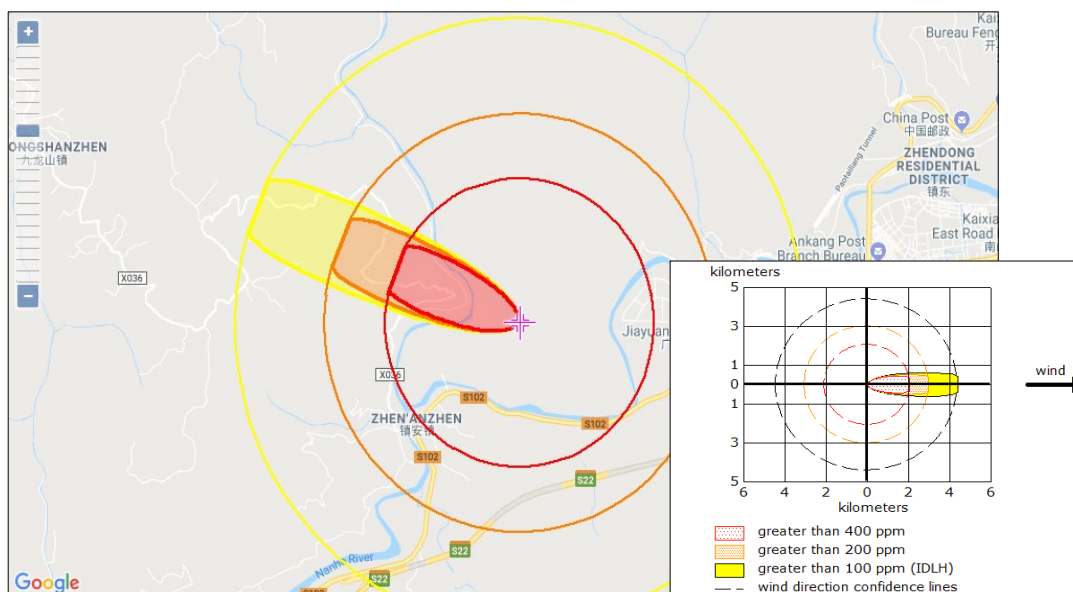


Figure 28: ALOHA estimated Hydrogen sulphide (toxic) Hazard zones

The area shaded and outlined by red represents the area downwind of the release point that could contain released gas with a concentration of 1,000 ppm or more H<sub>2</sub>S. The area shaded and outlined by orange represents the area downwind of the release point that could have released gas with a concentration of  $\geq 400$  ppm H<sub>2</sub>S. Finally, the area shaded and outlined by yellow represents the area downwind of the release point with a concentration of  $\geq 100$  ppm H<sub>2</sub>S. Dashed or solid lines along both sides of the yellow threat zone indicate uncertainty in the wind direction. Since the wind rarely blows constantly from any one direction, ALOHA displays "uncertainty lines" around the largest threat zone, which in this case is 100 ppm. The area located within the "uncertainty lines" is where ALOHA predicts the gas cloud to remain for 95% of the time, based on variable and uncertain wind directions.

As given in Chapter #2, an instantaneous exposure to a gas cloud having a concentration of  $\geq 1,000$  ppm H<sub>2</sub>S, or a 30-minute exposure to a gas cloud having a concentration of  $\geq 400$  ppm, can be fatal. Exposure to a gas cloud with a concentration of 100 ppm H<sub>2</sub>S is thought to be the level that the public can be exposed to for up to 60 minutes without experiencing any serious health problems.

The comparison and analysis indicate that the hazardous level distance and the area under impact for toxic consequences from H<sub>2</sub>S dispersion (400 ppm) is longer and wider than flammable zone (LFL). It is noted that in ALOHA Gaussian (passive dispersion) model was run for CH<sub>4</sub> and heavy gas (gravity slumping) model was run for H<sub>2</sub>S based on the release characteristics and the density of the released material.

The hazardous level distances for the same set of discharge conditions are sensitive to dispersion parameters and as a result the cloud dispersion can vary significantly. A comparison of the results from the sensitivity analysis for the input parameters listed is given in Figure 29 and Figure 30 .

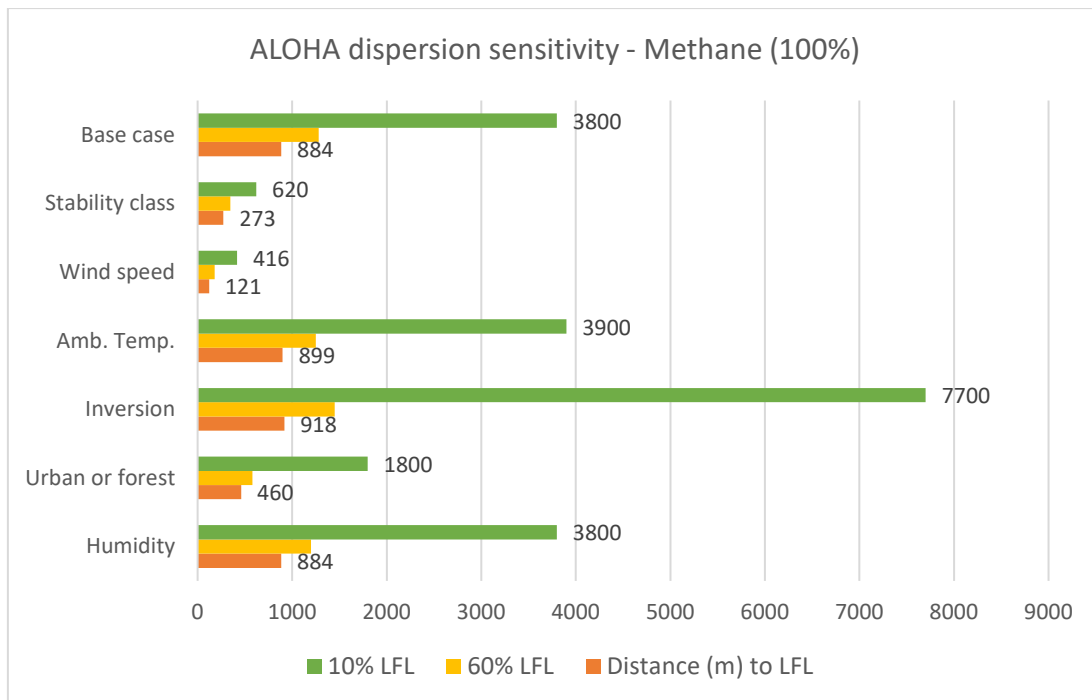


Figure 29: ALOHA: Methane dispersion - sensitivity

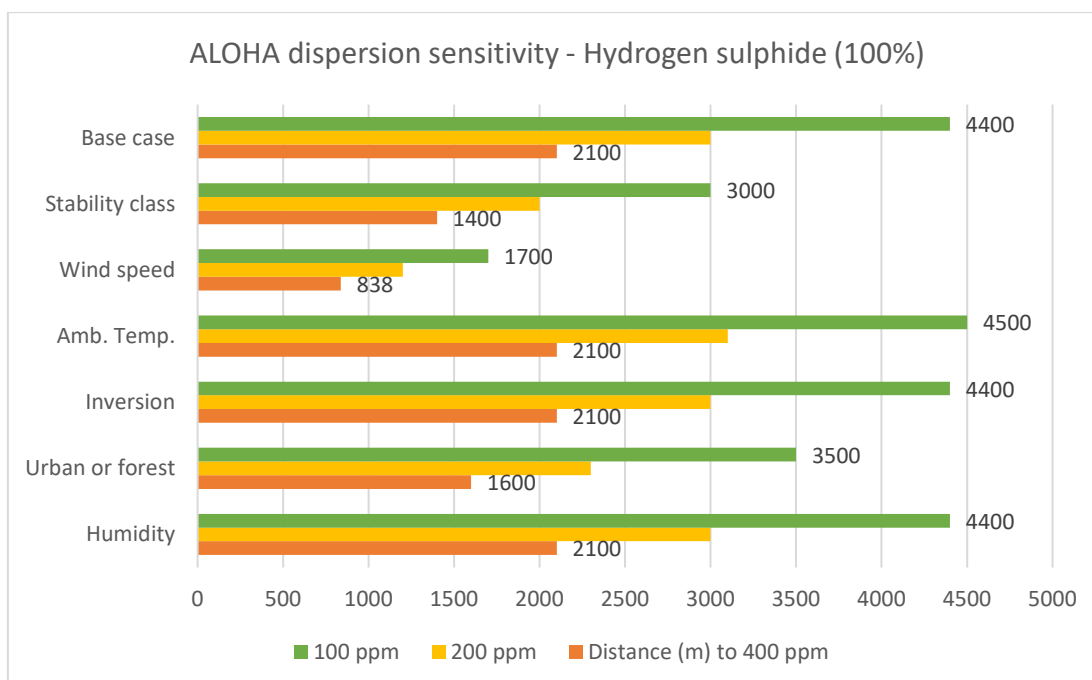


Figure 30: ALOHA: Hydrogen sulphide dispersion – sensitivity

It is observed that the hazardous level distance (LEL) for lighter gas ( $\text{CH}_4$ ) ranges from 120 m to 920 m and for heavier gas ( $\text{H}_2\text{S}$ ) the 400 ppm distance ranges from 840 m to 2100 m. By analysis of the ALOHA dispersion results, following conclusions were arrived:

1. Dispersion of  $\text{CH}_4$  and  $\text{H}_2\text{S}$  are not significantly sensitive to the changes in humidity and ambient temperature.

2. H<sub>2</sub>S (heavier gas) is not sensitive to inversion layer height, but CH<sub>4</sub> (lighter than air) is very sensitive to inversion layer height, and it is observed that the downwind distance can be longer (see inversion Figure 3a) if the discharged material (momentum jet) reaches the inversion layer (lower inversion levels heights are likely during calm night-time conditions).
3. Both positive (lighter gas) and negative buoyant (denser gas) cloud dispersion is sensitive to the turbulence related parameters, i.e. stability class, wind speed and surface roughness.

Hazardous level distances estimated using ANSYS FLUENT (Qingchun and Laibin, 2011) based on the impact from Kaixian “12.23” incident is used for comparison to the ALOHA predicted H<sub>2</sub>S dispersion results at similar release and atmospheric conditions. The post-incident field data indicates nearly 100% fatalities within 200 – 500 m (Xiaoyan village) and the longest distance noted for death as 1200 m. The prediction results of downwind hazardous level distances close to ground level are not in agreement with the available incident data; FLUENT estimated 200 ppm reaching 1270 m whereas ALOHA estimated 200 ppm reaching 2000 m, a summary of the comparison is given in Table 30.

**Table 30: Hazardous level distance – ALOHA validation**

Case description	Results to H <sub>2</sub> S concentration	400 ppm	200 ppm	100 ppm
<b>FLUENT, Kaixian 16H well blowout; natural gas</b>	Mass flow at 98.8 kg/s; 16% H <sub>2</sub> S (Mass%: 68% CH <sub>4</sub> and 7% CO <sub>2</sub> )	0.62 km	1.27 km	2.15 km
<b>ALOHA, this study; 100% H<sub>2</sub>S</b>	Mass flow at 15.4 kg/s representing 16% mass flow rate of H <sub>2</sub> S in natural gas.	1.3 m	2.0 km	3.2 km

Parameters were changed in ALOHA to calibrate the terrain and weather sensitivity to match Kaixian characteristics. However, the limitation of ALOHA to model only single component (in this case H<sub>2</sub>S) affects the estimation of the results in comparison to the results from FLUENT where three components were considered for modelling.

Toxic – H<sub>2</sub>S: The modelling estimated that the maximum potential downwind distance for the 1000 ppm concentration H<sub>2</sub>S gas hazard zone is 422 m. This distance is less than the established U.S. Coast Guard Safety Zone for these platforms. For the 300 ppm H<sub>2</sub>S concentration hazard zone, the estimated distance is 1.4 miles (2250 m) under stable atmospheric conditions, which typically only occur during the night.

Flammable – CH<sub>4</sub>: The larger flammable gas cloud hazard distances, under neutral atmospheric conditions, were estimated to be 139 m to 146 m and 200 m to 232 m for the 100% LFL and 60% LFL, respectively. Under stable atmospheric conditions, which only occur at night, the maximum hazard zones for flammable gas were estimated to range between 78 m to 81 m and 125 m to 145 m for the 100% LFL and 60% LFL, respectively.

The FLUENT simulation results of the gas (with high H<sub>2</sub>S) dispersion after the well blowout shown the characteristics of heavy gas. The incident and the case study also confirm that the high-sulphur gas is affected by terrain, wind speed and move quickly along valleys. ALOHA overestimates by 40% in comparison to FLUENT, the comparison of the results shows that a simple tool like ALOHA, designed for emergency responses with conservative results, is not suitable for detailed engineering and emergency response planning considering weather and terrain effects. Further analysis was carried out to determine the concentration of H<sub>2</sub>S (sourness) in natural gas that initiates the dense-gas behaviour.

From the simulations carried out using ALOHA, it is evident that the existing so called simple models and algorithms cannot adequately consider H<sub>2</sub>S specific properties for the toxic natural gas dispersion.

#### 4.6. Parameter screening using Canary

This section reports the results of the simulations and discuss the sensitivity to the input and parameters. The aim is to identify the most important parameters from amongst a large number that affect model outputs. This will help in optimizing the time and resource usage for consequence modelling in risk assessment. The analysis is carried out on two sets:

- Material and release conditions (Source term): fluid composition, hole size, temperature, pressure, release orientation
- Environmental conditions: atmospheric stability, wind speed, humidity, terrain

The CANARY consequence modelling software package is incorporating both source term calculations for natural gas release and a dispersion model. CANARY is one of the few general package software tools that account for the composition of the gas. Toxic and flammable cloud dispersion to concentrations of personnel impact (injury, fatality) is analysed through modelling. The hazardous concentration levels (to determine the distance to the dispersion end points) used for this study is given in Table 31. A 100% mortality is expected for personnel above flammable

limit (Level 3, Level 2) which is typical for estimating Flash fire (Cornwell and Marx 1996). 50% LFL (Level 1) is considered as an additional criteria to address modelling uncertainties, if any (UK HSE, 2022).

**Table 31: Canary - Hazardous levels of pipeline release of natural gas**

Component	Accidental consequence	Level-3	Level-2	Level-1
<b>Natural gas</b> (see values in Table 24)	Flash fire (flammable vapor cloud distance)	UFL Methane (CH <sub>4</sub> ) 15% Propane (C <sub>3</sub> H <sub>8</sub> ) 9.5%	LFL CH <sub>4</sub> 5% C <sub>3</sub> H <sub>8</sub> 2%	50% LFL CH <sub>4</sub> 2% C <sub>3</sub> H <sub>8</sub> 1%
<b>Hydrogen sulphide</b> (H <sub>2</sub> S)	Toxic concentrations of exposure results in health effects or death	500 ppm potential for respiratory arrest, loss of consciousness	100 ppm IDLH, coughing, dizziness	75 ppm AEGL #3; loss of sense of smell in minutes

The study focuses on a selected set of scenarios to represent the release from a toxic natural gas transfer pipeline to treatment plants in the onshore natural gas exploration and production. Consequence modelling (release and dispersion) from 2-inch hole in horizontal direction at ground level for stable wind condition. The flow through pipeline is fixed at 22.68 kg/s (50 lb/s) and release from a hole is assumed to be continuous (60 minutes) and disperses in an open field (no impingement). The number of components in the toxic natural gas compositions was optimized (given in Table 24) for more accurate phase representation within the Canary multi-component model. The results of dispersion were recorded for the maximum concentration along downwind central line concentration for an averaging time of 60 seconds.

#### 4.6.1. Source term parameters and sensitivity

##### Source term sensitivity to release rate:

The necessity of natural gas composition accuracy to the Canary model input values release hole size, temperature and pressure is evaluated in this section. Base case scenario is a release from 50 mm (2 inch) hole in horizontal direction at ground level. The flow through pipeline is fixed at 22.68 kg/s (50 lb/s) with operating temperature 25 °C (77 °F) and pressure 7.9 bara (115 psia). Sensitivity simulations were carried out for higher and lower values for base case source term conditions:



- (i) release hole sizes 76 mm (3 inch) and 25.4 mm (1 inch)
- (ii) fluid release pressures 34.5 bara (500 psia) and 3.45 bara (50 psia)
- (iii) fluid temperatures 49 °C (120 °F) and -6.7 °C (20 °F)

The above input were considered to represent the typically design and operating parameters for onshore gas production and transfer operations. The release rates estimated for the eight natural gas compositions for the source term sensitivity values are given in Table 32.

Table 32: Canary - Comparison of release rate (kg/s) for hole size, pressure, and temperature

Natural gas	Molar mass	H <sub>2</sub> S mol%	Base Case	Release hole		Pressure (bara)		Temperature	
			51 mm, 25 °C, 7.9 bara	High (67 mm)	Low (25 mm)	High (34.5)	Low (3.45)	High (49 °C)	Low (-6.7 °C)
S1	38.57	(2.6%)	5.35	9.75	1.34	22.68 <sup>1</sup>	1.36	5.35	7.35
S2	27.65	(8%)	2.59	5.76	0.64	12.70	1.13	2.59	2.83
S3	26.83	(10%)	2.68	5.76	0.65	12.70	1.13	2.68	2.83
S4	19.95	(14%)	2.31	5.22	0.58	10.43	1.00	2.31	2.47
S5	22.81	(15%)	2.45	5.53	0.61	11.34	1.04	2.45	2.63
S6	24.48	(16%)	2.54	5.72	0.64	12.02	1.09	2.54	2.74
S7	34.52	(18%)	3.04	6.80	0.75	22.68 <sup>1</sup>	1.27	3.04	5.58
S8	29.05	(29%)	2.77	6.21	0.70	22.68	1.18	2.77	2.99

Note: For S1 and S7 composition release under high pressure, the release will be two-phase.

A comparison of the molar mass and H<sub>2</sub>S composition (Table 32) shows that the molar mass of the toxic natural gas is not directly proportional to H<sub>2</sub>S mol% nor to any one pure hydrocarbon component. The following observations were inferred from the simulation results:

Release rate comparison for release hole sizes (1, 2 and 3 inch):

- (i) Release rates grow significantly with increase in hole size irrespective of the composition. For S1 composition, the release rates varied from 1.34 kg/s (2.9 lb/s) to 9.75 kg/s (21.5 lb/s).
- (ii) Release rates were higher for compositions with larger molar masses (S1, S7) and the difference is significant for larger hole sizes.
- (iii) Comparable release rates 2.31 kg/s to 2.68 kg/s (2-inch hole size) for compositions with molar mass less than 27 g/mol (S2, S3, S4, S5, S6). This was observed for all hole sizes.

However, significantly higher release rate (9.75 kg/s) was estimated for S1 with molar mass 39 g/mol.

Release rate comparison for operating pressures (3.45 bara, 7.9 bara, 34.5 bara):

- (i) For low pressure, the release rates were between 1 to 1.36 kg/s (2 to 3 lb/s) for all the eight compositions.
- (ii) For medium pressure, the release rates ranged from 2.3 to 2.68 kg/s (5.1 to 5.9 lb/s) for all compositions (S2 to S6) with molar mass less than 29 g/mol, but higher 5.35 kg/s (11.8 lb/s) for S1 with the highest molar mass.
- (iii) For high pressure, the compositions (S1, S7, S8) with higher molar mass (>29 g/mol) have significant higher release rates (>38 lb/s) compared to the compositions (S2, S3, S4, S5, S6) with lower molar mass (<29 g/mol).

Release rate comparison for operating temperature (-6.7 °C, 25 °C, 49 °C):

- (i) For medium and high temperature conditions, the release rates are similar irrespective of the compositions.
- (ii) Similar release rates, approximately 2.6 kg/s (~5 lb/s), were estimated for compositions with molar mass 29 g/mol and less for the range of temperatures evaluated.
- (iii) Significantly higher release rates were estimated for compositions with molar mass greater than 30 g/mol under low temperature conditions.

**Source term sensitivity to downwind dispersion:**

Dispersion modelling was carried out with base case inputs for all eight toxic natural gas compositions (Table 32) using Canary by Quest. Sensitivity simulations were carried out for higher and lower values for base case source term conditions:

- (i) Release hole sizes 76 mm (3 inch) and 25.4 mm (1 inch)
- (ii) Fluid operating (release) pressures 34.5 bara (500 psia) and 3.45 bara (50 psia)
- (iii) Fluid operating temperatures 49 °C (120 °F) and -6.7 °C (20 °F)

In addition, sensitivity to the release orientation also was evaluated. Two directions, horizontal and upwards (release at 45 deg from horizontal) was considered. The downwind dispersion distance to concentrations of concern were estimated for the eight natural gas compositions and discussed in this section.

Composition sensitivity to dispersion:

The estimated downwind distances (impact zones) to toxicity and flammability criteria (Table 31) is given in Table 33.

Table 33: Comparison of downwind distance to flammable and toxicity hazard levels

Natural gas	Molar mass	H <sub>2</sub> S mol%	Distance downwind (m) to H <sub>2</sub> S concentration			Distance downwind (m) to flammable concentration		
			500 ppm	100 ppm	75 ppm	UFL	LFL	0.5 LFL
S1	38.57	(2.6%)	113	338	338	6	18	34
S2	27.65	(8%)	80	250	250	3	10	17
S3	26.83	(10%)	98	294	294	2	9	16
S4	19.95	(14%)	124	361	361	2	8	15
S5	22.81	(15%)	125	363	363	2	8	15
S6	24.48	(16%)	137	392	392	2	9	17
S7	34.52	(18%)	146	404	404	3	12	21
S8	29.05	(29%)	204	541	541	2	10	18

The downwind dispersion distances for the eight toxic natural gas compositions to toxic and flammable hazard levels are given in Figure 31.

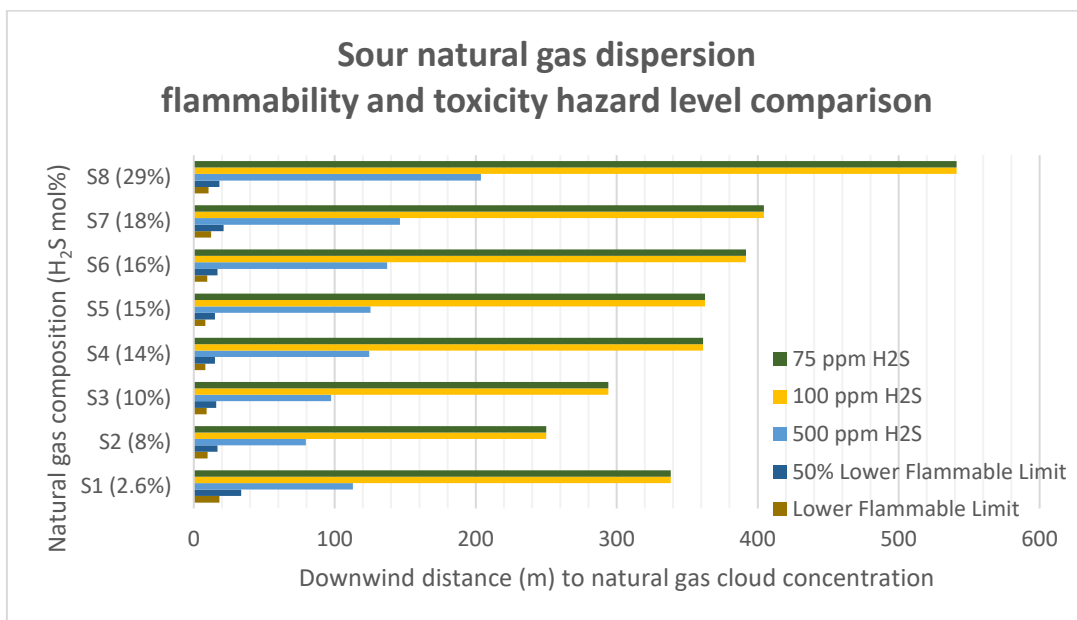


Figure 31: Canary - Sensitivity composition: Comparison of downwind distance to flammable and toxicity hazard levels

The downwind distances for LFL ranges from 8 m (S4, S5) to 18 m (S1) and H<sub>2</sub>S 100ppm cloud ranges from 250 m (S2) to 540 m (S8). The following observations inferred from the results:

- i. Distance to H<sub>2</sub>S toxic hazard level is significantly larger than flammability hazard levels. For example, results of toxic gas composition S2, toxicity downwind distance to 500 ppm = 80 m and 100 ppm = 250 m whereas the flammable cloud downwind distance UFL = 2.5 m and LFL = 9 m.
- ii. Downwind distance of toxic dispersion is maximum for those release with higher compositions of H<sub>2</sub>S (S7, S8) and with higher molar mass (S8, S7, S1).
- iii. Downwind distance of toxic cloud dispersion is higher for toxic gas with higher H<sub>2</sub>S composition (S8) while the downwind distance of flammable cloud dispersion is higher for composition with higher molar mass (S1, S7).

Downwind dispersion comparison for release hole sizes ((1, 2 and 3 inch):

The downwind dispersion distance to 500 ppm and 100 ppm H<sub>2</sub>S concentration for three release hole sizes were estimated and were compared (Figure 32).

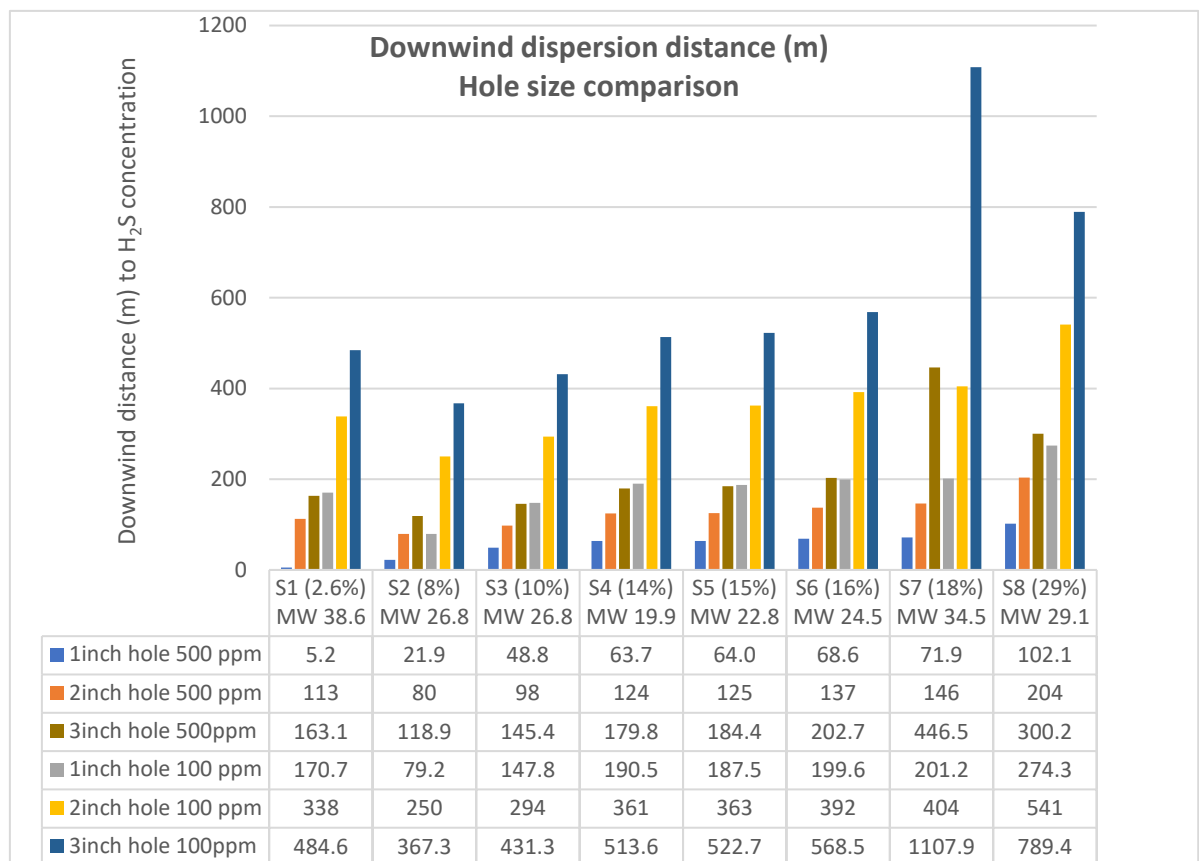


Figure 32: Canary - Sensitivity of downwind distance (H<sub>2</sub>S Concentration) to Release hole size

For the eight compositions considered, the releases from 1 inch, 2 inch and 3 inch hole sizes, the downwind distances for H<sub>2</sub>S 500 ppm the cloud ranges from 5 m to 446 m and for H<sub>2</sub>S 100 ppm the cloud ranges from 79 m to 1108 m. The following observations inferred from the results:

- (i) Downwind dispersion distance to 500 ppm H<sub>2</sub>S concentration from small (1-inch) hole releases was noted as proportional to the H<sub>2</sub>S composition. However, for larger hole sizes the increase in downwind distance was not proportional to the change in hole size.
- (ii) Longest downwind dispersion reported (3inch releases), for 500 ppm H<sub>2</sub>S concentration was for S8 composition (28% H<sub>2</sub>S, molar mass = 29 g/mol), while 100 ppm was for S7 (18% H<sub>2</sub>S, molar mass = 34 g/mol). Downwind dispersion following release from larger hole sizes are influenced by H<sub>2</sub>S concentration and molar mass.

Downwind dispersion comparison for operating pressures (3.45 bara, 7.9 bara, 34.5 bara):

The downwind dispersion distance to 500 ppm and 100 ppm H<sub>2</sub>S concentration for releases from 2-inch hole at three operating pressures were estimated (Figure 33).

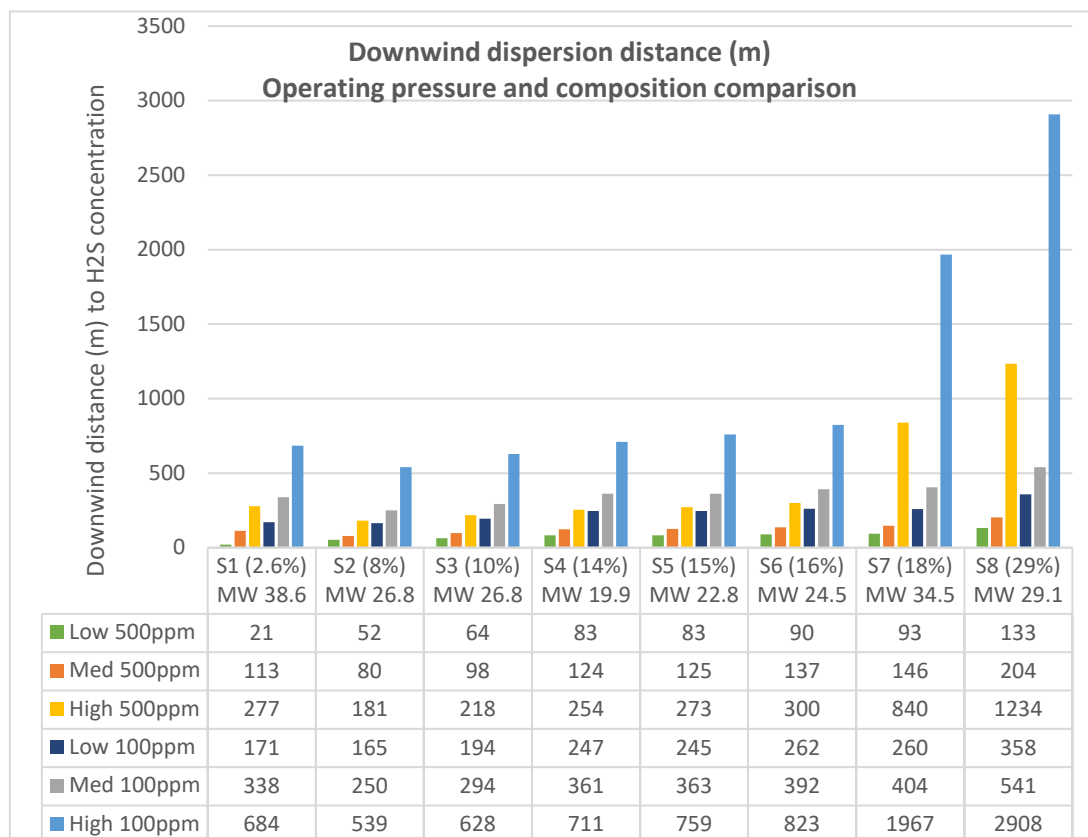


Figure 33: Canary - Sensitivity of downwind distance (H<sub>2</sub>S Concentration) to Operating pressure

The downwind distances for H<sub>2</sub>S 500 ppm cloud ranges from 21 m to 1234 m and H<sub>2</sub>S 100ppm cloud ranges from 171 m to 2908 m. For high H<sub>2</sub>S compositions (S7, S8), the dispersion distances were significantly longer for high pressure releases, 100 ppm exceeds 1900 m compared to less than 830 m for natural gas composition with less than 18% H<sub>2</sub>S.

During expansion from elevated pressure, released toxic gas could be colder and heavier than air close to the release source with the potential to accumulate in low-lying areas (Nair and Wen, 2019b). From the simulations, it is established that the cloud dispersion behaviour changes to dense gas for natural gas with H<sub>2</sub>S compositions higher than 18 mol%.

Downwind dispersion comparison for operating temperature (-6.7 °C, 25 °C, 49 °C):

The downwind dispersion distance to 500 ppm and 100 ppm H<sub>2</sub>S concentration for releases from 2-inch hole at three operating temperatures were estimated (Figure 34).

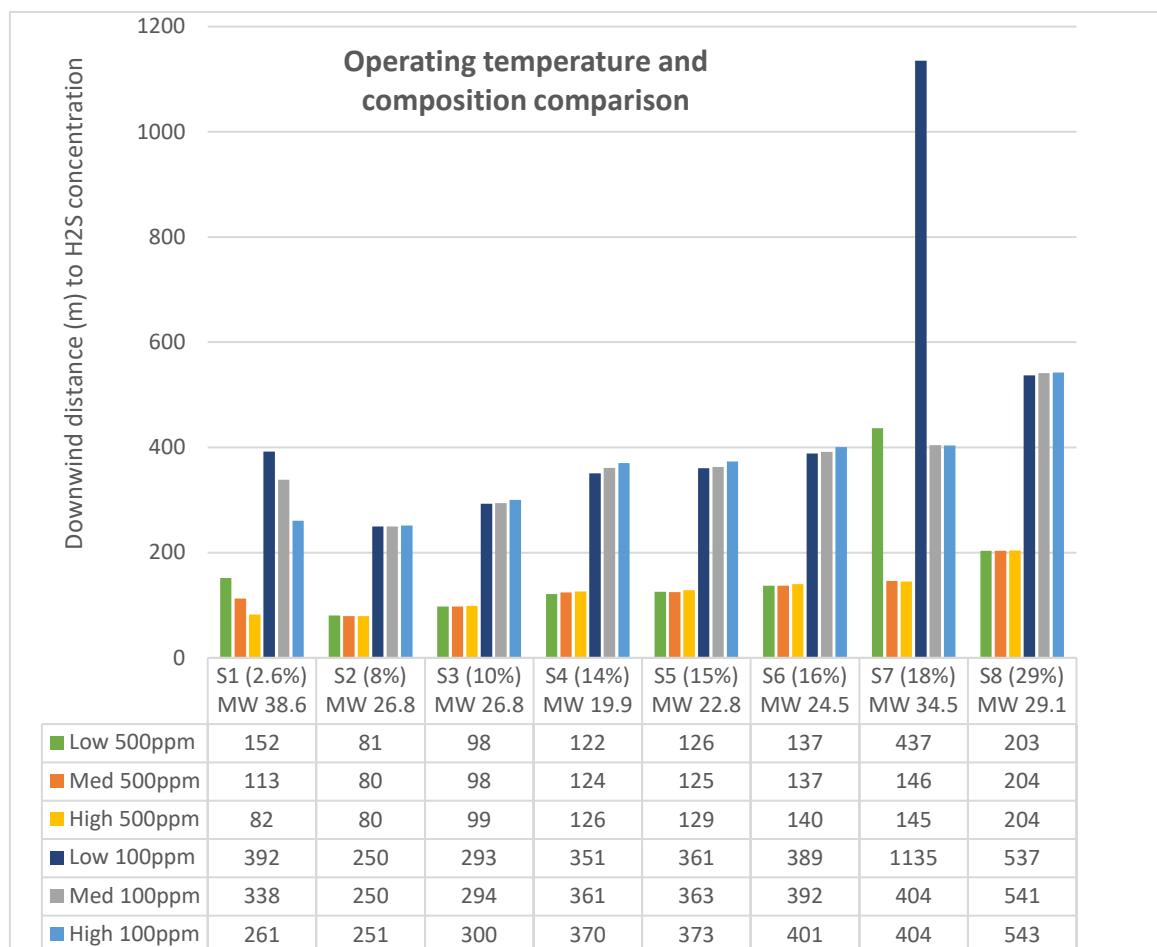


Figure 34: Canary - Sensitivity of downwind distance (H<sub>2</sub>S Concentration) to Operating temperature

The downwind distances for H<sub>2</sub>S 500 ppm cloud ranges from 80 m to 200 m and H<sub>2</sub>S 100ppm cloud ranges from 250 m to 1135 m. For all the three temperature conditions, the downwind dispersion distances estimated was similar for all the compositions with molar mass less than 30 g/mol. However, for composition with greater than 30 g/mol (S1, S7), the downwind dispersion distances estimated were significantly higher for low temperature releases. The natural gas

releases at low temperature is observed to be slumping down and entraining less air for dilution, as a result the cloud travels to longer downwind dispersion distances. For the dispersion modelling of compositions with molar mass > 30 g/mol, sensitivity for operating temperature should be included.

Downwind dispersion comparison for release orientation:

Release and dispersion from two release orientations, horizontal and upwards (at 45deg inclination from grade) for the eight natural gas compositions and from 2-inch hole at 77oF and 115psia were compared.

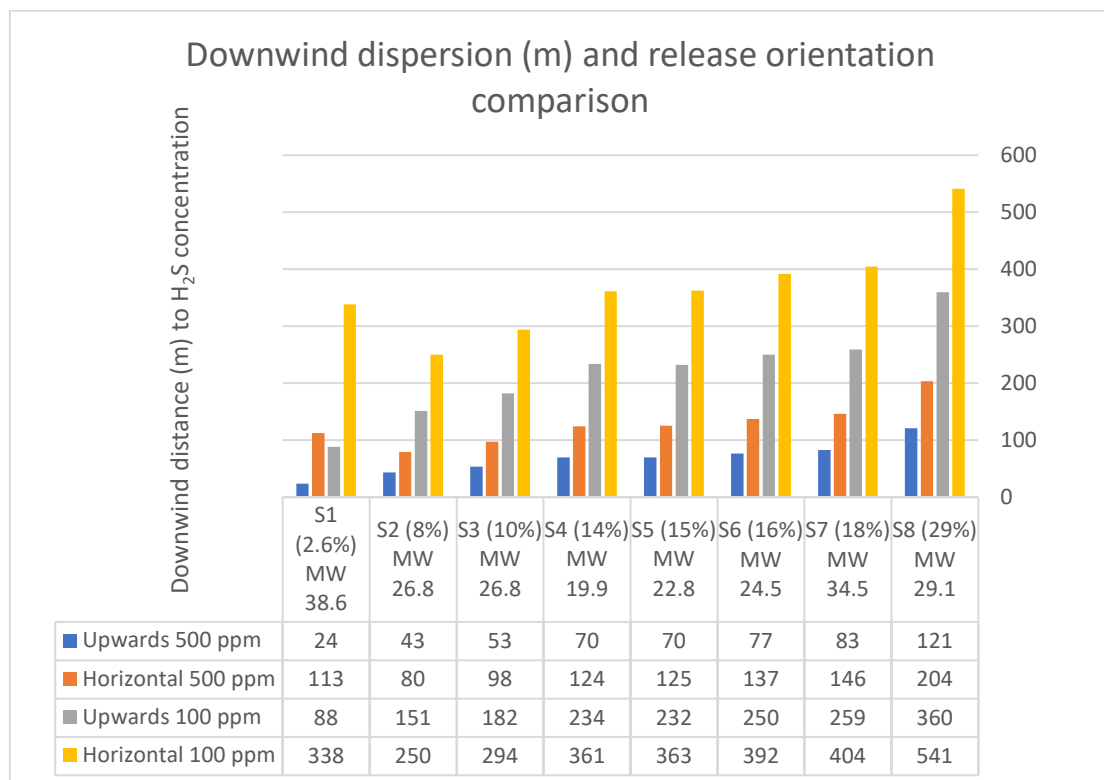


Figure 35: Canary - Sensitivity of downwind distance (H<sub>2</sub>S Concentration) to Release orientation

Following observations are inferred from the results given in Figure 35:

- (i) Downwind dispersion distances are higher for horizontal orientation compared to upwards orientation for all compositions.
- (ii) For both orientation, downwind dispersion distances for 500 ppm and 100 ppm were similar for compositions with H<sub>2</sub>S concentrations 14% to 18% (S4, S5, S6, S7), but significantly lower for compositions with low (20%) H<sub>2</sub>S concentrations (S8).

(iii) For dispersion from upwards releases, the downwind dispersion distance increases with the increase in H<sub>2</sub>S concentration. For dispersion from horizontal release, S1 with 2.6% H<sub>2</sub>S (highest molar mass and release rate) dispersion distances are higher than S2 (8% H<sub>2</sub>S) and S3 (10% H<sub>2</sub>S).

Appropriate orientation based on the failure mode and expected location (elevation) of the receptors of concern should be used for consequence modelling.

#### 4.6.2. Environmental parameters and sensitivity

##### Downwind dispersion sensitivity to atmospheric stability and wind speed:

Dispersion for set of eight natural gas compositions and from 2-inch hole at temperature 25 °C (77 °F) and pressure 7.9 bara (115 psia) over three atmospheric stability conditions and wind speeds (3.4F: stable and low wind speed, 13D: Neutral and medium wind, 20C: slightly unstable and high wind) were compared (Figure 36).

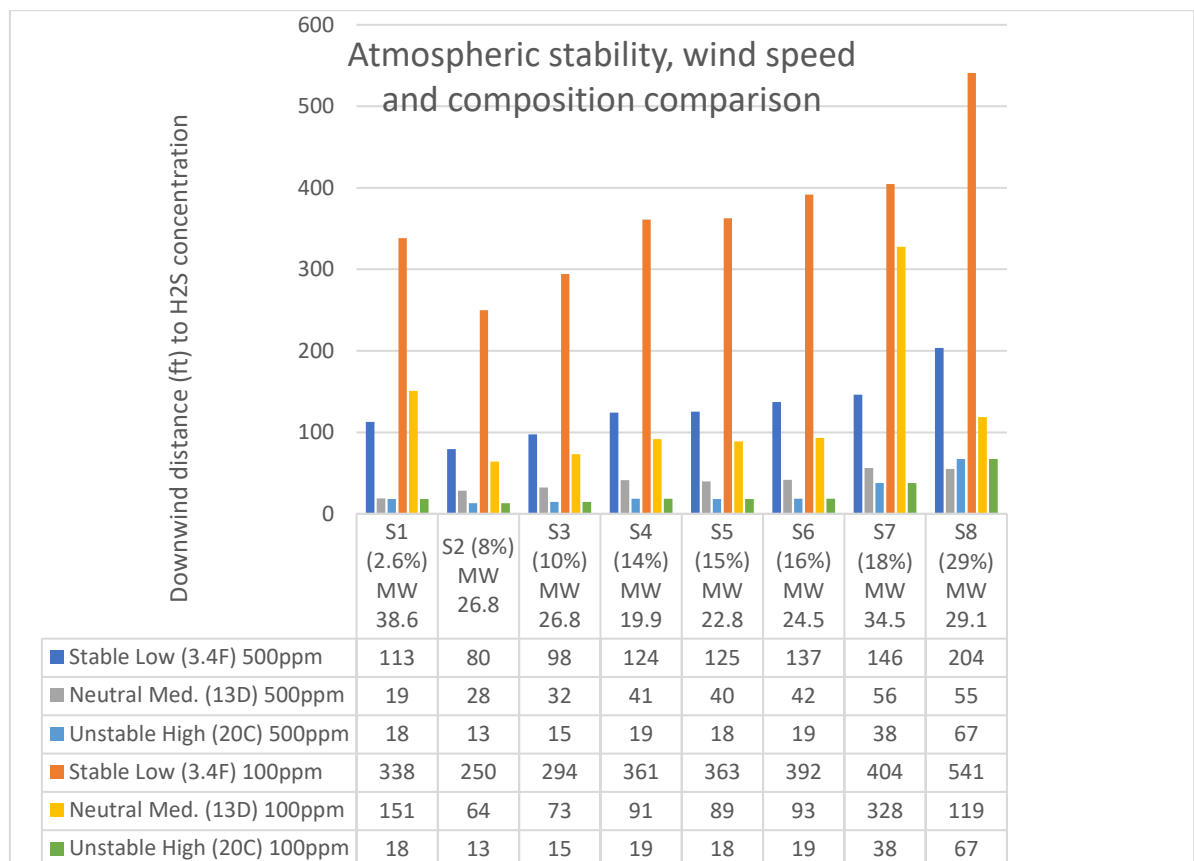


Figure 36: Canary - Sensitivity of downwind distance (H<sub>2</sub>S concentration) to Atmospheric stability and wind speed

Canary tool couples (transition) from jet dispersion to heavy gas dispersion when the central line touches ground level (Quest 2020). This modelling factor is reflected in results for S7 under 13D conditions and for all compositions under 20C conditions.



Following observations are inferred from the results given in Figure 36:

- (i) The longest downwind dispersion irrespective of the composition was recorded for stable conditions and low wind speed.
- (ii) For dense gas (negatively buoyant) compositions (S1, S7) with higher molar mass ( $>29$  g/mol), the downwind dispersion for Neutral and Medium wind (13D) was significantly higher.
- (iii) For lightly unstable and high wind (20C) conditions, the downwind distances for 100 ppm were less than 61 m for all compositions whereas for stable and low wind speed (3.4F) conditions, the distances exceeded 244 m.
- (iv) For compositions with molar mass  $<29$  g/mol (positively buoyant), the downwind distances for 20C conditions were higher than 13D conditions. Under these conditions, the cloud is behaving more as heavy gas and closer to ground level, whereby higher concentration cloud travels further downwind.

For higher  $H_2S$  concentration (S8 composition), the downwind distance to 100 ppm extends to 541 m at low wind and stable conditions (3.4F) compared to 119 m and 67 m for neutral stability and higher wind speeds. For a location with predominant neutral stability and medium wind speed (like 13.4D), if the risk management bases the impact zone distance worst-case stability and wind (541 m) which is about 5 times typical (119 m), then the risk management (e.g., emergency planning) incur significantly higher cost and effort.

#### **Downwind dispersion sensitivity to terrain:**

Dispersion for different toxic gas compositions and from 2-inch hole at temperature  $25\text{ }^\circ\text{C}$  and pressure 7.9 bara over three different terrains (mud flat, level country or cut grass, urban area) were compared. The terrain effects were modelled using the surface roughness parameters option in the tool. The surface roughness value 0.01 mm, 5.1 mm and 99mm were used respectively for mud flat, cut grass and urban area. Comparison of the downwind distances to the  $H_2S$  concentrations of interest is given in Figure 37.

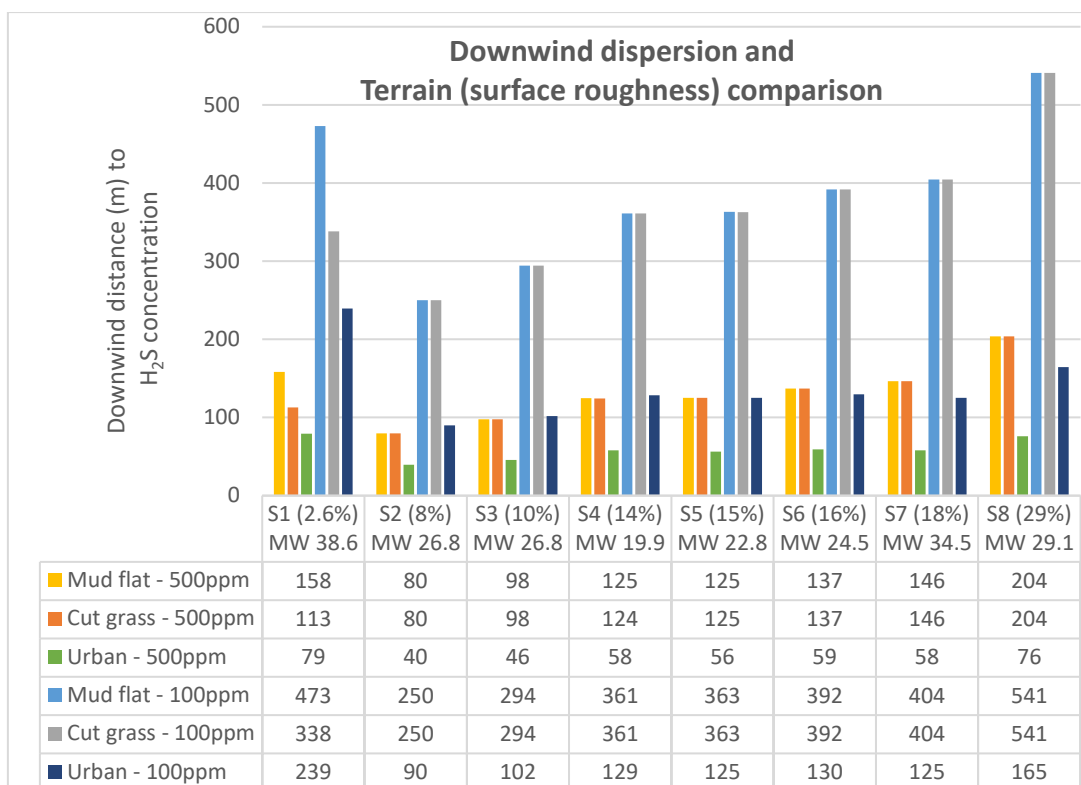


Figure 37: Canary - Sensitivity of downwind distance (H<sub>2</sub>S Concentration) to Terrain

The terrains were considered flat (without obstructions) and the turbulence from terrains were addressed by surface roughness parameter as given in Table 10. Following observations are inferred from the results given in Figure 37:

- (i) With increase in surface roughness, the downwind dispersion decreases. Downwind dispersion distances for Urban area were significantly lower than (1/3rd) for all compositions except S1.
- (ii) Downwind dispersion distances for Mud flat and Cut grass is similar for all compositions except S1 with the highest molar mass.

This implies that dispersion of toxic gas with less than 35 g/mol molar mass is not sensitivity to surface roughness 5 mm (<0.2 inch).

**Downwind dispersion sensitivity to humidity:**

Dispersion for the eight toxic gas compositions and from 2-inch hole at operating temperature 25 °C (77 °F) and pressure 7.9 bara (115 psia) at three humidity conditions (low =20%, medium = 50%, high =80%) were compared. The downwind distance to H<sub>2</sub>S concentration of interest is given in Figure 38.

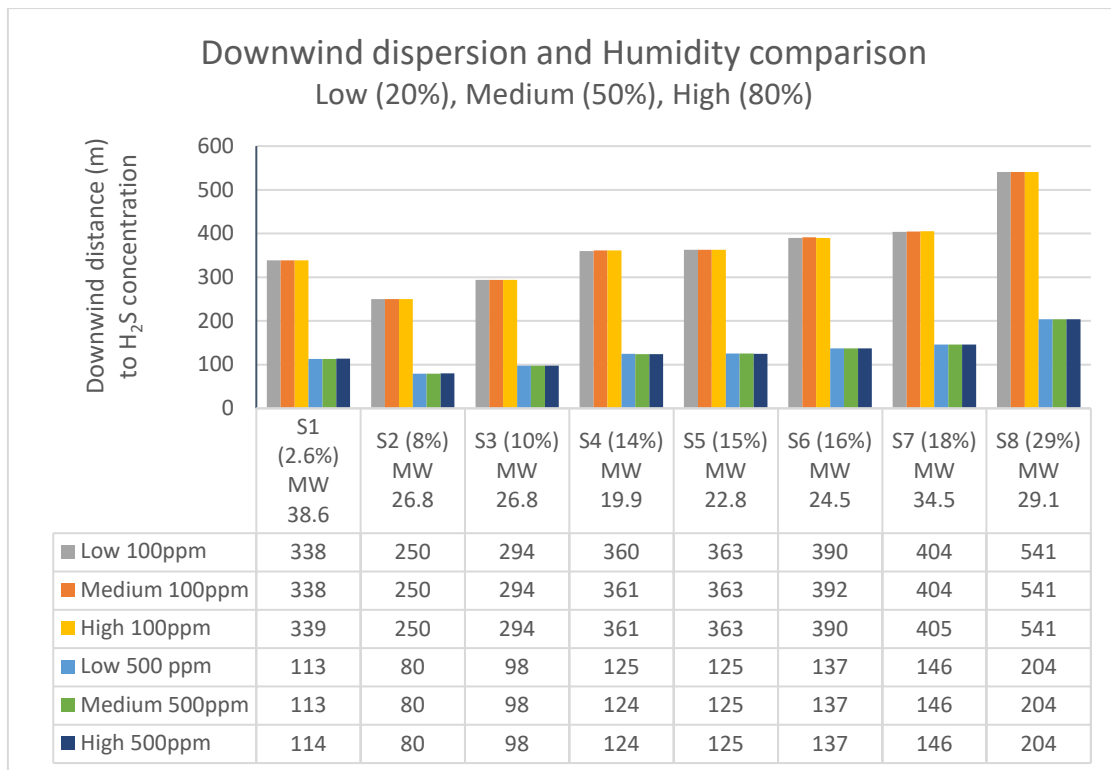


Figure 38: Canary - Sensitivity of downwind distance ( $H_2S$  Concentration) to Humidity

The difference in the downwind distance of concern is within 1%. The results given in Figure 38 implies that changes in humidity values have no significant impact on the downwind dispersion of toxic natural gas.

### 4.6.3. Discussion

There are several tools and methodologies available to determine the release and dispersion characteristics of the loss of containment and determine the hazardous level distances. Whichever approach is adopted, it should be used with an understanding of its range of validity, its limitations, the input data required, the sensitivity to the different input data, and how the results can be verified. From the range of simulations (using HYSYS) and consequence modelling (using Canary), it was concluded that for a similar type of release event, the toxic hazard impact zone could be orders of magnitude different.

Comparative study was carried out for eight different toxic natural gas compositions with  $H_2S$  concentration ranging from 2.6% to 29%. It was observed that the downwind distance to hazardous levels ranges from less than 15 m to more than 1500 m for a loss of containment from toxic natural gas pipeline transfer line. The range of results were obtained by varying input on the release (source term) conditions and certain environment conditions. From the parametric

sensitivity analysis for a release event from a natural gas transfer pipeline at ground level using eight different compositions, the following are the observations and related guidance for toxic natural gas consequence modelling:

- Phase equilibrium properties of the release should be considered in determining the release phase as low temperature and high-pressure releases can have longer impact zone distances. Detailed review (prior to implementing risk mitigation) should be carried out for high pressure releases of compositions with >18 mol% H<sub>2</sub>S & molar mass >29 g/mol and for low temperature releases of compositions with molar mass >30 g/mol.
- Downwind dispersion of toxic cloud is dependent on hole size, release rate and composition. The failure mechanism and related hole size for larger releases need to appropriately be determined. Dispersion from small hole releases is not sensitive to the composition of natural gas.
- Release rates and downwind dispersion are sensitive to low temperature for those compositions with >30 g/mol. For such cases with significantly higher impact zone, further analysis should be carried out before implementing risk reduction measures.
- Downwind dispersion for high pressure releases is sensitive for compositions with greater than 18% H<sub>2</sub>S content. For such cases with significantly higher impact zone, further analysis should be carried out before implementing risk reduction measures.
- The analysis implies that downwind dispersion is sensitive to the orientation of release; distance to H<sub>2</sub>S concentration was note higher for composition S1 with 2.6% H<sub>2</sub>S (highest molar mass and release rate) in comparison with the composition with higher H<sub>2</sub>S compositions like S2 (8% H<sub>2</sub>S) and S3 (10% H<sub>2</sub>S). Release orientation also has significance in relation to the receptor of concern. So, a site-specific orientation shall be selected (not necessarily the worst case).
- Dispersion if natural gas with high toxic concentration has significant effect on wind speed and stability. For risk assessment purposes, it is advisable to have a range of stability and wind speed to represent the variations for 24 hours and through the year (Pandya 2012, US EPA 2017).
- Variation in humidity has no significant impact on the downwind dispersion of toxic natural gas.

#### 4.7. Application of the consequence modelling results in risk assessment:

Significance of the consequence modelling results in the risk management efforts is analysed with the methodology, software and inputs were applied to a credible release event from pipeline routed through a populated area (a scenario reasonable to expect to happen during the operational life of the asset). The results from the parameter sensitivity analysis for natural gas composition S4 transposed to geographical location as pointed in

Figure 39. The potential impact to public (personnel) corresponding to each impact zone radius was estimated for comparing the levels of risk. A comparison with composition S7 and possible risk management considerations are also discussed. The downwind distances to 100 ppm H<sub>2</sub>S cloud are summarized in Table 34.

Table 34: Natural gas (S4) compositions (mol%) and downwind distance to 100ppm H<sub>2</sub>S

Case sensitivity (distance in m)	S4	S7
Molecular weight	19.95	34.52
Base case (2in, 3.4F, 25 °C, 5 barg)	361	404
Sensitivity: Temperature – Low (-6.5 °C)	351	1135
Sensitivity: Pressure – High (35 bara)	710	1966
Sensitivity: Wind & Stability – Medium, Neutral	91	328
Sensitivity: Surface roughness – High (0.1m)	128	125

Impact zones for selected few cases are illustrated in

Figure 39., the yellow pin corresponds to the release point and the coloured circles represents the impact zone for different set of input and parameters are given in Table 34. The impact area for a release event will be a section of the circle with orientation dependent on the wind direction.

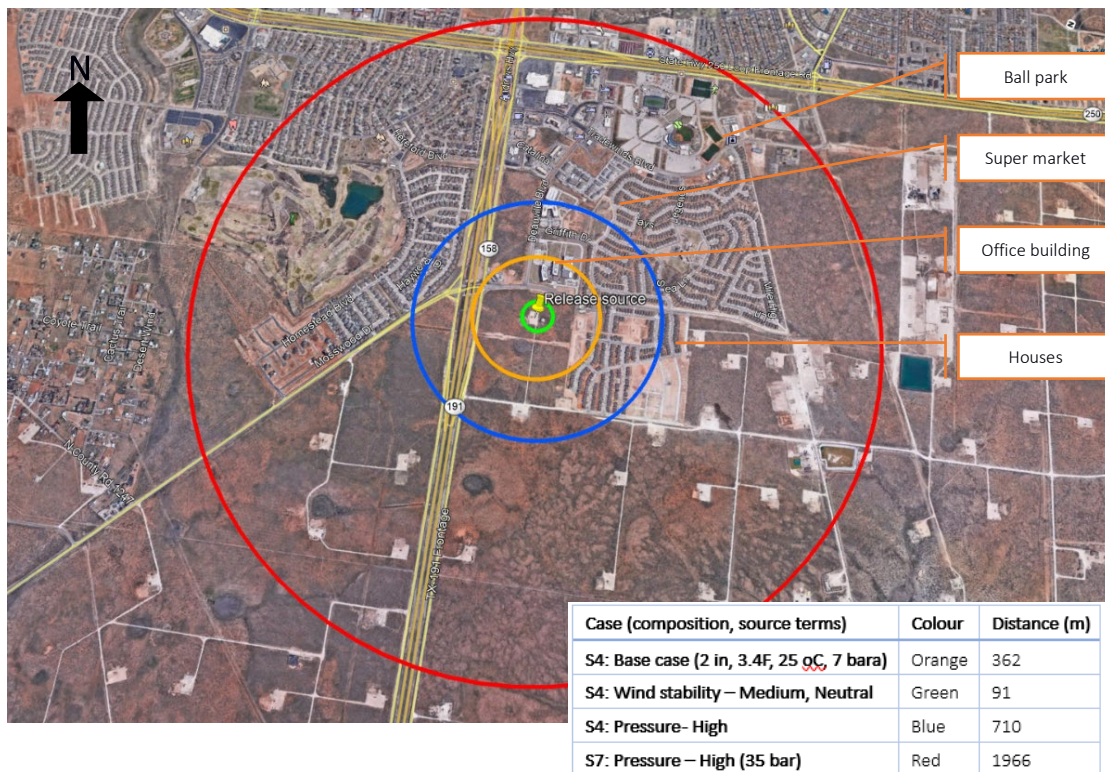


Figure 39: Parameter sensitivity application example - H<sub>2</sub>S downwind distances and potential impacts

The representative set of cases with impact zones, corresponding potential consequence and risk management considerations are given in Table 35. The base case impact zone (Orange colour and radius 362 m), the 100 ppm H<sub>2</sub>S cloud (IDLH – concentration level) could reach an office building or residential area. This implies that in the event of a release under the given base case conditions and Southerly (towards North) wind, more than 500 personnel could be exposed to natural gas cloud with 100 ppm or more for a period until the release is isolated and such an exposure could result in coughing and dizziness. Risk reduction measure considerations should be to reduce the impact zone radius including reducing the pipeline diameter or restricting the horizontal release orientation (e.g., laying pipeline underground). However, modelling using the site-specific representative wind speed and atmospheric stability (13D - medium and neutral) instead of worst-case conditions (3.4F – stable and low wind conditions), the impact zone estimated was much smaller (91 m, green colour). The impact zone was limited to the facility surroundings (without personnel exposure) and whereby the risk management limits were limited to maintaining the exclusion zone (restricting personnel access / habitats). Similarly, for the impact zone and potential consequences for operating under higher pressure or for S7 composition is given in Table 35.

Table 35: Natural gas impact zone – parameter sensitivity and risk management considerations

Case sensitivity	Colour	Consequence / concern	Risk management considerations
<b>S4: Base case (2 in, 3.4F, 25 oC, 7 bara)</b>	Orange	500+ (1 x Office, 30 houses)	Perform site specific assessment Risk reduction through buried lines, smaller diameter pipeline
<b>S4: Wind stability – Medium, Neutral</b>	Green	Environmental impact	Manageable risk, maintain exclusion zone
<b>S4: Pressure- High</b>	Blue	2000+ (2 x office, 100+ houses)	Operational controls (e.g., at lower pressure)
<b>S7: Pressure – High (35 bar)</b>	Red	25,000+ (Ball Park, Supermarket, 500+ houses)	Elevated risk, consider alternate route

A worst-case consequence modelling estimate may not be the best for risk management, instead a ‘credible’ worst-case scenario needs to be determined and subjected to consequence modelling. The credibility of a set of modelling input should be determined considering the site-specific operating conditions, fluid characteristics, and types of failure and likelihood of environmental conditions. Once the risk levels are evaluated, sensitivity analysis for the key modelling inputs and parameters as given in this study should be used further to determine the risk management efforts.

## 5. OpenFOAM model set-up and validation

### 5.1. Computational fluid dynamics – methodology and model development

Computational Fluid Dynamics (CFD) is the process of mathematically modelling a physical phenomenon involving fluid flow and solving it numerically. CFD is used worldwide to solve variety of fluid flow problems including aerodynamics, marine engineering, semiconductor industry, wind engineering, hydrology, meteorology, and nuclear power. The concept of CFD is to solve the equations of fluid dynamics using discretization process (Anderson 1995). In the discrete domain, each flow variable is defined only at the specified points called as grid points.

In a CFD solution, the equations are solved for the relevant flow variables at the grid points (typically several million within a domain). Objective is to give a solution that satisfies governing equations and the boundary conditions. Setting up the discrete system and solving it involves a very large number of repetitive calculations and is done by the digital computer. Larger number of grid points gives better accuracy. Multiple equations (multiple variables) are solved simultaneously. CFD software tools are available to analyse the fluid flow using a mathematical model of the physical case and a numerical method. In recent years, the exponential growth of computing performance combined with the increased availability of large-scale computing resources enabled researchers and engineers to analyse complex problems in realistic time scales (Lawson et al 2012).

In this chapter, fluid dynamics concepts, fundamentals of CFD and specifics of the open source CFD software OpenFOAM used for this study is given. The steps involved in the simulation model build, including the selection of the solver, and setting the boundary conditions are mentioned. Mesh independence and validation against field trial is also demonstrated in this chapter. The results from the sour natural gas OpenFOAM modelling are given Chapter 6.

#### 5.1.1. Fluid flow fundamentals and Governing equations

A fluid is a substance that flows or deforms under applied shear stress. The fluid flow examination is directed by governing equations that are based on the conservation law of fluid's physical properties. In general, a fluid flow is described by the continuity, momentum and energy equations which describe the conservation of mass, momentum, and total energy.



The basic equations are the three laws of conservation:

Conservation of Mass	: Continuity Equation
Conservation of Momentum	: Newton's Second Law
Conservation of Energy	: First Law of Thermodynamics or Energy Equation

These principles state that mass, momentum, and energy are stable constants within a closed system. Basically, everything must be conserved. These are collectively known as the Navier-Stokes equations and are highly nonlinear second order Partial Differential Equations (PDEs) with four independent variables (three spatial coordinates and one temporal coordinate). The choice of models is based on the type of fluid flow:

- Laminar and Turbulent
- Steady and Unsteady
- Compressible and In-compressible
- Uniform and Non-uniform

### Laminar and turbulent flow

Laminar fluid flow is defined as the type of flow in which the fluid particles move along well-defined paths or streamlines, and all streamlines are straight or parallel. Laminar flows are characterised by smoothly varying velocity fields in space and time in which individual "laminae" (sheets) move past one another without generating cross currents.

Turbulent fluid flow is defined as the type of flow in which the fluid particles move in a zig-zag way, the eddies formation takes place which is responsible for high energy loss. Turbulent flows are characterised by large, nearly random fluctuations in velocity and pressure in both space and time. In turbulent flows, particles exhibit additional transverse motion which enhances the rate of energy and momentum exchange (increasing heat transfer, friction coefficient).

Reynolds number is a dimensionless quantity that is used to determine the type of flow pattern as laminar or turbulent while flowing through a passageway like a pipe. Reynolds number ( $Re$ ) is the ratio of fluid momentum force (inertial forces) to viscous shear force (Equation 24).

$$Re = \frac{\rho V D}{\mu}$$

Equation 24

where,

$\rho$  is the density of the fluid

$\mathcal{V}$  is the velocity of the flow (where it is well-defined and undisturbed)

$\mathcal{D}$  is the diameter of the passageway

$\mu$  is the viscosity of the fluid

$Re$  sets the criteria that defines if a flow is turbulent or laminar.

Flow is turbulent if,  $Re > Re_{critical}$

Flow is laminar if,  $Re < Re_{critical}$

Flow is critical if,  $Re > 2000$  and  $Re < 4000$

### Steady and unsteady flow

There are two general types of flow, steady and unsteady flow. For steady flow, all fluid flow properties are independent of time. That is

$$\frac{\partial \phi}{\partial t} = 0$$

Equation 25

Where,  $\phi$  represents a fluid property (e.g., velocity, temperature, pressure and density). The properties, however, may vary from point to point.

For unsteady flow, the fluid properties are function of time. For example, the temperature for unsteady flow however will vary as time changes.  $T = T(x, y, z, t)$ . Unsteady flows can be further classified to periodic flow, non-periodic flow, and random flow.

$$\frac{\partial \phi}{\partial t} \neq 0$$

Equation 26

As a result, it is normally much more difficult to analyse a problem where unsteady flow is occurring. In fluid mechanics study, it is often assumed that the flow is steady to simplify the analysis.

### Compressible and incompressible fluid

The volume of real fluids changes when they are expanded or compressed by an external force or by the change of pressure or temperature. The property of volume change is called compressibility.

Compressible fluid flow is defined as the flow in which the density is not constant, a fluid whose volume changes is called compressible fluid.

Incompressible flow is constant density flow, which means the density of the fluid does not change from point to point, i.e.,  $\rho = \text{constant}$ .

An incompressible fluid without viscosity is called an ideal fluid or perfect fluid. An ideal fluid does not exist, however is used in fluid dynamics due to the ease to handle theoretically.

### Uniform and non-uniform fluid flow

Uniform fluid flow is defined as the type of flow in which the velocity at any given time does not change with respect to space (i.e., length of direction of the flow).

Non-uniform fluid flow is defined as the type of flow in which the velocity at any given time changes with respect to space (i.e., length of the direction of the flow).

### 5.1.2. Conservation principles and governing equations

There are two different approaches to describe the conservation laws (i) Lagrangian approach and (ii) Eulerian approach. In the Lagrangian approach, the fluid is divided into fluid parcels that are tracked as they move through time and space. The Eulerian approach focuses on a specific volume element through which the fluid flows over time. Reynolds Transport Theorem is used to describe the change of material volume in the Eulerian specification.

Newton's laws of motion are applicable for particles and not for control volume.

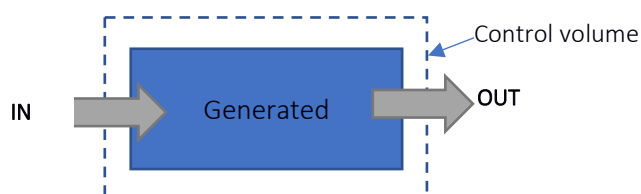


Figure 40: CFD - Control volume

$$\text{Rate of (in - out + generated)} = \text{Rate of (change)}$$

Control volume = identified region in space

Newton's laws of motion are developed for identified states of particles (Lagrangian). Basic equations are not applicable for the control volume. Reynolds transport theorem is applied for converting Lagrangian to Eulerian.

### Conservation of mass:

The continuity equation describes the conservation of mass, meaning without sources or sinks, an object will have a constant mass. This follows the chemical principle that mass is neither created nor destroyed.

$$\left\{ \begin{array}{l} \text{Rate of accumulation} \\ \text{of mass in} \\ \text{the control volume} \end{array} \right\} = \left\{ \begin{array}{l} \text{rate of} \\ \text{inflow mass} \end{array} \right\} - \left\{ \begin{array}{l} \text{rate of} \\ \text{outflow mass} \end{array} \right\} + \left\{ \begin{array}{l} \text{any source of mass} \\ \text{(not relevant for} \\ \text{non - nuclear)} \end{array} \right\}$$

For a fluid of density  $\rho$  and velocity  $\mathbf{U}$ , the conservation of mass is expressed by:

$$\frac{\partial \rho}{\partial t} + \nabla \cdot (\rho \mathbf{u}) = 0$$

Equation 27

In Eulerian system, it can be written as:

$$\frac{\partial \bar{\rho}}{\partial t} + \nabla \cdot [\bar{\rho} \tilde{U}_j] = 0$$

Equation 28

### Conservation of momentum:

Newton's second law of motion correlates the change in momentum of an object to the external force applied to it.

*Momentum = mass x velocity*

$$\left\{ \begin{array}{l} \text{Rate of accumulation} \\ \text{of momentum} \\ \text{in the control volume} \end{array} \right\} = \left\{ \begin{array}{l} \text{Rate of inflow} \\ \text{of momentum} \end{array} \right\} - \left\{ \begin{array}{l} \text{rate of} \\ \text{outflow} \\ \text{of momentum} \end{array} \right\} + \left\{ \begin{array}{l} \text{net external} \\ \text{forces in the} \\ \text{control volume} \end{array} \right\}$$

$$\frac{\partial \bar{\rho} \tilde{u}_i}{\partial t} + \frac{\partial \bar{\rho} \tilde{u}_i \tilde{u}_j}{\partial t} = \frac{\partial}{\partial x_j} \left( \bar{\rho} (v + v_t) \left( \frac{\partial \tilde{u}_i}{\partial x_i} + \frac{\partial \tilde{u}_j}{\partial x_j} - \frac{2}{3} \frac{\partial \tilde{u}_k}{\partial x_k} \delta_{ij} \right) \right) - \frac{\partial \bar{\rho}}{\partial t} + \bar{\rho} g_i$$

Equation 29

## Conservation of energy

Energy is conserved, meaning that the energy rate of change in a material particle is equal to the energy received by heat and work to the particle.

$$N = E \text{ (total energy)}$$

$$= \text{Internal energy} + \text{kinetic energy} + \text{Potential energy}$$

First law of thermodynamics is applicable for moving fluids (Anderson 1995, Wendt 2009)

$$\left\{ \begin{array}{l} \text{Rate of change of} \\ \text{energy inside} \\ \text{the fluid volume} \end{array} \right\} = \left\{ \begin{array}{l} \text{Net flux of heat} \\ \text{into the volume} \end{array} \right\} + \left\{ \begin{array}{l} \text{Rate of working done} \\ \text{on the volume to body} \\ \text{and surface forces} \end{array} \right\}$$

There are many possible forms of energy equations in terms of enthalpy  $h$  or total enthalpy ( $h + V^2/2$ )

$$\text{Mechanical energy} = \text{Total energy} - \text{Thermal energy}$$

Conservation of sensible enthalpy:

$$\frac{\partial \bar{\rho} \bar{h}_s}{\partial t} + \frac{\partial \bar{\rho} \bar{u}_j \bar{h}_s}{\partial x_j} = \frac{D\bar{p}}{Dt} + \frac{\partial}{\partial x_j} \left( \bar{\rho} \left( D_{th} + \frac{v_t}{Pr_t} \right) \frac{\partial \bar{h}_s}{\partial x_j} \right) - \frac{\partial \bar{q}''}{\partial t} + \bar{\omega}_{h_s}'''$$

Equation 30

Conservation of species mass fraction:

$$\frac{\partial \bar{\rho} \bar{Y}_k}{\partial t} + \frac{\partial \bar{\rho} \bar{u}_j \bar{Y}_k}{\partial x_j} = \frac{\partial}{\partial x_j} \left( \bar{\rho} \left( D_k + \frac{v_t}{Pr_t} \right) \frac{\partial \bar{Y}_k}{\partial x_j} \right) - \bar{\omega}_{h_s}'''$$

Equation 31

In this study, Eulerian approach is used to calculate all the wind field patterns and Lagrangian approach is used for the calculation of dispersion of species.

### 5.1.3. Turbulence models

The integral models for dispersion modelling are well-known for the ability to account for the stability-class approach whereas most of the commercial CFD software usually do not provide specific turbulence model for simulating atmospheric stratification effects. In this work, a new approach to take account of atmospheric features in CFD simulations has been developed and validated by comparison with available experimental data.

Turbulence models in CFD are methods to include the effect of turbulence in the simulation of fluid flows. Increase in turbulence increases convective heat transfer, increases mass transfer and mixing, reduces drag. Effect of turbulence increases with velocity and decreases with viscosity. These characteristics make the modelling more complex and computationally challenging. An unstable atmosphere enhances mechanical turbulence, whereas a stable atmosphere inhibits turbulence and neutral atmosphere neither enhances nor inhibits turbulence. The turbulence of the atmosphere is by far the most important parameter affecting dilution of a gas (Ricou & Spalding 1961). In the literature, a large variety of turbulent models can be found. The applicability depends on the type of problem analysed and on the accuracy of the problem solution to be achieved. In OpenFOAM, Turbulence modelling methods include RANS, LES and DNS.

### **Reynolds-Averaged Navier-Stokes (RANS)**

RANS approach calculates a time average of the Navier-Stokes (conservation) equations in order to obtain a mean value for the physical variables (Launder & Spalding 1972, Pope 2002). This approach is primarily used to describe turbulent flows. In order to be capable of performing the calculations, closure models have to be provided. For turbulent combustion, a turbulence model to capture the flow dynamics is combined with a model for turbulent combustion, which considers the chemical species conversion and the heat release. Such a simulation can be interpreted as if the average of different realizations (or cycles for periodic flows) is calculated. The computational cost for this simulation type is smaller in comparison to DNS and LES (Reynolds 1895).

### **Large Eddy Simulation (LES)**

In LES, the large turbulent structures (eddies) are resolved whereas the smaller scales are modelled. It was developed based on the paper released by Smagorinsky (1963). The larger scales, which contain most of the energy, are computed while the smaller scales, which are thought to be more predictable are modelled, instead (Pope 2002). Equally as for the turbulent structures, the large-scale contribution is captured by the LES equations. A sub-filter model is often provided to consider the effects of the small scales of turbulence. In LES, variables are time dependent quantities, averaging is performed locally over space (a small zone around each point). In comparison to RANS, LES approach gives higher accuracy (reduced influence of the turbulence model), but with higher computational cost. In RANS codes,  $k$  and  $\epsilon$  values need to be provided at the inlet whereas in LES codes, turbulence need to be generated explicitly.

Study by Fransen et. al. to compare LES with RANS and experiments for aerodynamic and heat transfer predictions have determined that LES need more development to achieve better predictions on wall regions, reduce the computational cost and improve the quality of the results (Fransen et al 2012).

### **Direct Numerical Simulation (DNS)**

DNS model solves the full instantaneous Navier-Stokes equations without any turbulence or chemical model. It involves the numerical solution of the instantaneous equations that govern fluid flows. Small turbulence requires a very fine mesh, fine enough to be able to solve the smallest dissipative scales (Kolgomorov scales), which renders very accurate solutions (Pope 2002). In spite of increase in the availability of computational resources, the DNS simulations are restricted to simple domains and low Reynolds numbers.

### **Linear and hybrid**

Linear models contain simple turbulence and roughness models, providing fast and accurate results for simple cases. The code starts not to be accurate when the terrain is hilly, and it is known to poorly predict flow separation and recirculation.

Hybrid of flow averaged and subgrid, Detached Eddy Simulation (DES): It is a modification of the RANS, where RANS model is used and only separated regions are modelled by LES. This hybrid model between RANS and LES permits the user to have the advantages of both programmes at the same time (Pope 2002, Heinz 2020).

#### **5.1.4. CFD Turbulence models**

A turbulence model is a computational procedure to close the system of mean flow equations. For most engineering applications it is unnecessary to resolve the details of the turbulent fluctuations. Turbulence models allow the calculation of the mean flow without first calculating the full time-dependent flow field. Turbulence models use different methods to model fluctuations inherent in the full Navier-Stokes equations. RANS based turbulence models are used to compute the Reynolds stresses and the different categories include (i) Linear eddy viscosity models, (ii) Nonlinear eddy viscosity models and (iii) Reynolds stress model. Linear eddy viscosity models are modelled by a linear constitutive relationship with the mean flow. These are sub-categorised, based on the number of transport equations solved for to compute the eddy viscosity coefficient, (i) algebraic (zero-equation) models, (ii) one-equation models and (iii) two-equation models and (iv) second-order closure models (Yusuf et. al 2020).

## Two-equation models

Two-equation models have been most popular for engineering application and has been subjected to development through research. These models provide independent transport equations for both the turbulent kinetic energy and the turbulence length scale (or an equivalent parameter). A selection of two-equation turbulence models was compared for the applicability and suitability the current application (Table 36).

Table 36: Two equation turbulence models

Turbulence model	Description
<b>Standard k-epsilon model (k-ε)</b>	<p>Used to simulate mean flow characteristics for turbulent flow conditions. Two equation linear eddy viscosity RANS approach,</p> <ul style="list-style-type: none"> <li>- The first transported variable is the turbulent kinetic energy (k).</li> <li>- The second transported variable is the rate of dissipation of turbulent kinetic energy (ε).</li> </ul> <p>Assumes turbulent viscosity is isotropic (i.e., ratio between Reynolds stress and mean rate of deformation is the same in all directions). It is usually useful for free-shear layer flows with relatively small pressure gradients as well as in confined flows where the Reynolds shear stresses are most important. It can also be stated as the simplest turbulence model for which only initial and/or boundary conditions needs to be supplied.</p> <p>In the derivation of the k-ε model, the assumption is that the flow is fully turbulent, and the effects of molecular viscosity are negligible. The standard k-ε model is therefore valid only for fully turbulent flows.</p> <p>k-ε model takes account of buoyancy and suitable for turbulence in the presence of large adverse pressure gradients such as regions where the flow detaches from a wall.</p>
<b>Realizable k-ε</b>	<p>The term “realizable” means that the model satisfies certain mathematical constraints on the Reynolds stresses, consistent with the physics of turbulent flows. The realizable k-ε model differs from the standard k-ε model in two ways:</p> <ul style="list-style-type: none"> <li>(a) Contains an alternative formulation for the turbulent viscosity. <math>C_\mu</math> is not a constant like in the standard model but a variable.</li> <li>(b) A modified transport equation for the dissipation rate, <math>\epsilon</math>, has been derived from an exact equation for the transport of the mean square vorticity fluctuation.</li> </ul> <p>It provides improved predictions for the spreading rate of both planar and round jets. It also exhibits superior performance for flows involving rotation, boundary layers under strong adverse pressure gradients, separation, and</p>



Turbulence model	Description
	recirculation. In virtually every measure of comparison, Realizable $k-\epsilon$ demonstrates a superior ability to capture the mean flow of the complex structures (Soe & Khaing 2017,).
<b>k-Omega model (k-<math>\omega</math>)</b>	Two-equation turbulence model that is used as an approximation for the RANS equations. The model attempts to predict turbulence by two partial differential equations for two variables, $k$ and $\omega$ , with the first variable being the turbulence kinetic energy ( $k$ ) while the second ( $\omega$ ) is the specific rate of dissipation (of the turbulence kinetic energy $k$ into internal thermal energy). $k-\omega$ is suitable and widely used for the flows where wall effects are predominant (Wilcox, 2008).
<b>k-Omega Shear Stress Transport (k-<math>\omega</math> SST)</b>	A two-equation eddy-viscosity model with Shear Stress Transport (SST) formulation combines both $k-\epsilon$ and $k-\omega$ . The model switches between the formulations based on the dominance of wall effects. $k-\omega$ SST has higher accuracy compared to standard $k-\epsilon$ model. The $k-\omega$ SST model does produce a bit too large turbulence levels in regions with large normal strain, like stagnation regions and regions with strong acceleration (Menter, 1994).

A comparison by applying the Technique for Order of Preference by Similarity to Ideal Solution (TOPSIS) method to six RANS models (RSM, standard  $k-\epsilon$ , RNF  $k-\epsilon$ , standard  $k-\epsilon$ , SST  $k-\epsilon$ ), shows that the standard  $k-\epsilon$  model was the best suitable model under the simulation of heavy gas dispersion for hill-shaped terrains (Qingchun and Laibin, 2011). Wang et al. study has used the modified Realizable model of standard  $k-\epsilon$  model (Wang et. al. 2016).

Adiabatic effectiveness simulations revealed that using the standard  $k-\omega$  model resulted in the closest agreement with experimentally determined laterally averaged adiabatic effectiveness, and the realizable  $k-\epsilon$  model agreed and best with centreline values (Harrison and Bogard, 2008).

A comparison of standard  $k-\epsilon$  and realizable  $k-\epsilon$  turbulence models in curved and confluent channels showed the better performance of the standard  $k-\epsilon$  model in curved channels and the realizable  $k-\epsilon$  model in confluent channels (Shaheed et. al 2019). The turbulence model selection was carried out by running simulations for standard  $k-\epsilon$ ,  $k-\omega$  SST and realizable  $k-\epsilon$  turbulence models (See section 5.3.4.5).

### DES and DDES

At higher Reynolds number, spatial scales in flows become to be too small to be resolved by the normal grid spacing and more powerful turbulent approaches need to be applied (Frana and Honzejk 2010). Detached Eddy Simulation (DES) proposed by Spalart et al. (1997) and its

improved version, Delayed DES (DDES) Spalart et al. (2006) are seamless methods, designed to treat the entire boundary layer using a RANS model. Classic DES approach suffers from various deficiencies, for example, early separation causing switch between LES and URANS (in hybrid model), especially in low Reynolds number region. As per the study by Frana and Honzejek (2010), DDES, the improved version of DES, can reach results that were in better agreement to the experiments and other numerical simulations in respect to the velocity field and Reynolds stress tensors.

### **Synthetic turbulence**

For the detailed analysis of unsteady flows, turbulent motions (random fluctuation of velocity) are necessary and are critical especially for the wind movement. To ensure velocity fluctuation is continuously available, turbulence is generated (synthesis of realistic turbulence). This is critical for the wind movement and associated dispersion of the specie. Synthetic turbulence generation (STG) has become a valuable tool for providing unsteady turbulent boundary conditions by spatially evolving boundary layers (Patterson et. al. 2021). The goal of an STG is the synthetic generation of velocity fluctuations with respect to the correct representation of integral quantities like length and time scales (Matha et al., 2018). The impact of ensuring continuous velocity fluctuation is investigated using STG.

In Synthetic Eddy Method (SEM) method, a control volume is defined and it generates a a set of eddies with random intensities. These eddies, which represent the velocity fluctuations defines the velocity distribution around the eddy, create the turbulent velocity field which is then used as inlet for the simulation (Jarrin et. al. 2009). Divergence Free SEM (DFSEM) is an improved version of SEM where the eddies are modelled such that a divergence free fluctuating velocity is created (Poletto 2013).

### **5.1.5. Numerical modelling for fluid dynamics**

In CFD, for solving the problem, a specific set of equations need to be chosen based on assumptions on the fluid type, flow properties like 2D flow, compressible, isothermal etc. Incorrect selection of the mathematical model and simplifications may lead to wrong results.

Inherent uncertainties can exist in model physics, initial conditions, boundary conditions, and even turbulent randomness which can exist as a barrier to repeatability of both physical experiments and numerical comparisons (Atkinson, 2017). In comparison to experimental analysis, numerical modelling of the basic physics of the phenomena are not limited by scale

constraints. However, there are issues related to CFD solutions, such as grid resolution, choice of time increments, turbulence model selection, or specification of boundary conditions. In this application, in addition to the species transportation, the simulation of all aspects of atmospheric motions, plume transport or wind loading is produced.

For a numerical simulation to become accurate and to overcome the constraints, the method is to go through some basic steps such as set-up a computational grid, selection of the discretization method, mathematical model, finite approximations of physical quantities, a solution method and a convergence criterion. The sequence of steps is given in Figure 41.

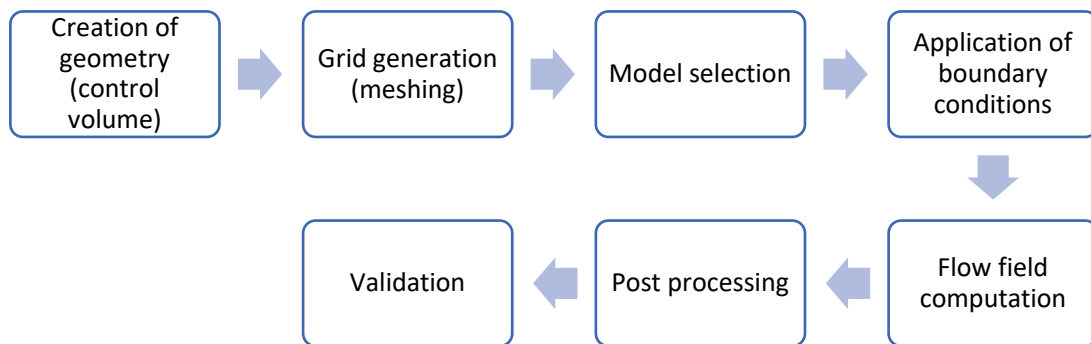


Figure 41: CFD methodology - Sequence of steps

### Computational grid – Geometry and meshing

A computational geometry model is a mathematical representation of the objects and the domain where the simulations are run. This computational grid is created using a separate Computer Aided Design (CAD) package, for example Opensource packages like Blender, Salome, FreeCAD or commercial packages like AutoCAD, CATIA. The geometry created should be reviewed and cleaned up prior to mesh generation. A mesh divides a geometry into many elements. These are used by the CFD solver to construct control volumes. Meshing can be done using the grid generator CAD tool / generation packages or by using the CFD tool itself. Mesh resolution, type of mesh and computational resources are to be considered when generating a mesh. The grids can be structured, block structured, unstructured or hybrid. Some cases can be reduced to simplified (representative) systems by taking advantage of dimensionality, symmetry, and cyclic behaviour. Commonly used meshing terminology is given in Table 37.

Table 37: Meshing terminology

Mesh term	Description
Cell	control volume into which domain is broken up
Node	grid point
Cell centre	centre of a cell
Edge	boundary of a face
Face	boundary of a cell
Zone	grouping of nodes, faces, cells
Domain	group of node, face and cell zones

Effective use of turbulence models requires close attention to their respective meshing requirements, particularly in near-wall regions. For viscous calculations, a boundary layer mesh also has to be constructed and the distance to the wall of the first cell in the boundary layer mesh depends on the near-wall treatment of the turbulence model (Lee and Moser 2015).

Not all meshes have the same likelihood of a successful modelling outcome. Some of the key aspects of effective meshing:

- Keep it simple (not to include minor details that will have little or no impact to the results but which may increase the computational time significantly)
- High aspect ratio surfaces: Long, thin surfaces will require very many mesh elements to capture and may add little to the final solutions. Should be blended out or removed completely.
- Shallow angles: At meeting points of two surfaces at an acute angle or where an arc asymptotically touches a straight line, the mesh will have problems fitting into the corner. Ensure the element volume does not tend to zero.

Meshing is a key initial step in successful CFD simulations, the following quotes highlights this message.

“A good mesh might not lead to the ideal solution, but a bad mesh will always lead to a bad solution.” P. Baker – Pointwise

“Who owns the mesh, owns the solution.”

H. Jasak – Wikki Ltd.

“Garbage in – garbage out. As I am a really positive guy I prefer to say, good mesh – good results.” J. G. – WD

## Discretisation of the Partial Differential Equations (PDE)

Discretisation is the process of transferring continuous functions, models, variables, and equations into discrete counterparts. This process is usually carried out as a first step toward making them suitable for numerical evaluation and implementation on digital computers. Numerical solutions give answers of the PDEs at discrete points in the domain, called as grid points. Characteristics of discretization of PDE:

- Continuum field or domain subdivided into elements or cells, which form a grid.
- Solution belongs to a function space and for an integral form of the PDE with higher order accuracy and with the ability to incorporate differential type boundary conditions

Analytical solutions of PDEs involve closed-form expression which give the variation of the dependent variables continuously throughout the domain. There is a wide range of approaches that lead to different discretization methods, the commonly used ones are Finite Volume Method (FVM), Finite Element Method (FEM) and Finite Difference Method (FDM).

A **FDM** discretization is based upon the differential form of the PDE to be solved. Each derivative is replaced with an approximate difference formula (that can generally be derived from a Taylor series expansion). The computational domain is usually divided into hexahedral cells (the grid), and the solution will be obtained at each nodal point. The FDM is easiest to understand when the physical grid is Cartesian, but through the use of curvilinear transforms the method can be extended to domains that are not easily represented by brick-shaped elements. The discretization results in a system of equation of the variable at nodal points, and once a solution is found, then we have a discrete representation of the solution.

A **FEM** discretization is based upon a piecewise representation of the solution in terms of specified basis functions. The computational domain is divided up into smaller domains (finite elements) and the solution in each element is constructed from the basic functions. The actual equations that are solved are typically obtained by restating the conservation equation in weak form: the field variables are written in terms of the basic functions, the equation is multiplied by appropriate test functions, and then integrated over an element. Since the FEM solution is in terms of specific basis functions, a great deal more is known about the solution than for either FDM or FVM. This can be a double-edged sword, as the choice of basic functions is very important and boundary conditions may be more difficult to formulate. Again, a system of equations is obtained (usually for nodal values) that must be solved to obtain a solution.

A **FVM** discretization is based upon an integral form of the PDE to be solved (e.g. conservation of mass, momentum, or energy). The PDE is written in a form which can be solved for a given finite volume (or cell). The computational domain is discretized into finite volumes and then for every volume the governing equations are solved. The resulting system of equations usually involves fluxes of the conserved variable, and thus the calculation of fluxes is very important in FVM. The basic advantage of this method over FDM is it does not require the use of structured grids, and the effort to convert the given mesh in to structured numerical grid internally is completely avoided. As with FDM, the resulting approximate solution is a discrete, but the variables are typically placed at cell centres rather than at nodal points. This is not always true, as there are also face-centred finite volume methods. In any case, the values of field variables at non-storage locations (e.g., vertices) are obtained using interpolation.

Comparison of the three discretisation methods is difficult, primarily due to the many variations of all three methods. FVM and FDM provide discrete solutions, while FEM provides a continuous solution. FEM & FVM can have unstructured mesh and curved cells, whereas FDM can have only structured mesh. FVM and FDM are generally considered easier to program than FEM, but opinions vary on this point.

### Boundary conditions

When solving the equations in CFD, appropriate initial conditions and boundary conditions need to be applied. Those cells in the computational grid which are not surrounded by other cells are called boundary cells. The CFD modeller or the user need to provide the values on such faces. These values are called as boundary conditions and to be set to represent the computational model, the closest possible to the real one. In general, the conditions set such that boundaries classified to:

- (i) a fixed value [Dirichlet BC], Specify the value e.g.,  $U = \text{constant}$  (fixed pressure, constant velocity etc.)
- (ii) a fixed gradient or specify the gradient derivative [Newumann BC] e.g.,  $\frac{\partial u}{\partial x} = C_2$
- (iii) mixed (a linear combination of fixed value and gradient). [Robin BC] e.g.,  $au + b \frac{\partial u}{\partial x} = C_3$

In the absence of sources and sinks, system behaviour is driven by its boundary conditions. Boundary conditions need to be appropriately selected and such that the predictions are physical correct (in many cases, ill-posed combinations lead to solver failure). For the computer flow field, there are two sets for boundary conditions (i) physical set by the nature and (ii) numerical.

(i) Physical boundary conditions:

For a viscous fluid, the boundary conditions on a surface assumes no relative velocity between the surface and the gas immediately at the surface. This is called the no-slip conditions. If the surface is stationary, with the flow moving past it, then  $u = v = w = 0$  at the surface (for viscous flow)

For an inviscid flow, the flow slips over the surface (there is no friction with surface); hence the flow is tangent to the surface.  $\vec{V} \cdot \vec{n} = 0$  at the surface (for an inviscid flow), where,  $\vec{n}$  is a unit vector perpendicular to the surface. The boundary conditions elsewhere in the flow depend on the type of problem being considered, and usually pertain to inflow and outflow boundaries at a finite distance from the surfaces, or an 'infinity' boundary condition far from the surfaces.

(ii) Numerical boundary conditions:

Computed flow field is driven by the numerical boundary conditions and the accuracy and appropriateness is very important in CFD. Frequently used boundary conditions are inlet, outlet, wall, symmetry planes, periodic planes or an axis for axis-symmetrical computations and coupled boundary conditions.

### Numerical stability and convergence

CFD simulations should follow some rules in order to obtain the appropriate solution to the problem. This is achieved through convergence, consistency, and stability (Macchi 2015). A numerical method is referred to as being stable when the iterative process converges and as being unstable when it diverges. A common strategy for steady problems (in CFD codes) is to solve the unsteady equations and march in time until the solution converges to a steady state (Bhaskaran and Collins 2018).

A numerical method is considered:

- (i) as convergent, if the solution is exact with the grid spacing and time step tending to zero.
- (ii) as consistent if the truncation error tends to zero and time step tending to zero
- (iii) as stable if an error in the solution is not magnified during the calculation process.

For computational efficiency, large time-step  $\Delta t$  to reach the steady state in the least number of time-steps is to be determined. If  $\Delta t > \Delta t_{\max}$ , the numerical errors will grow

exponentially in the time causing solution to diverge from the steady state result. The value  $maxDeltaT (\Delta t_{max})$  depends on the numerical discretisation scheme used. CFD codes allows to set the Courant number,  $C_o$ , when using time-stepping (Courant-Friedrichs-Lewy or CFL condition). Larger time-steps leads to faster convergence to the steady state, so it is advantageous to set the Courant number as large as possible within the limits of stability.

$$C_o = \frac{U\Delta t}{\Delta x}$$

Equation 32

The Courant number depends on the local cell velocity  $U$ , the time step  $\Delta t$  and the distance between the cells  $\Delta x$  (computational grid). In FVM, the calculation is based on the cell volume and not on the distance  $\Delta x$ . Based on formula, we can derive the following aspects:

The higher the local cell velocity  $U$ , the larger the Courant number,

The larger the time step  $\Delta t$ , the larger the Courant number,

The smaller the distance  $\Delta x$ , the larger the Courant number.

The main aspect here is, that if we refine the mesh, increase the velocity or the time step, the Courant number will increase. To fulfil the criteria in above equation, the time step has to be adjusted based on the mesh size and the velocity.

Note: For simplicity, keep CFL number below 2.0 and preferably less than 1. The criteria have to be fulfilled for each cell. That means, that one bad cell can limit the whole simulation.

### 5.1.6. High Performance Computing (HPC)

The University of Warwick provides high performance computing (HPC) facilities for researchers at Warwick. The service and support are managed by the Scientific Computing Research Technology Platform (SCRTP). HPC includes a cluster of UNIX workstations. Cluster is a collection of more or less ordinary computers networked together. Each computer called a “node”. Number of nodes,  $n_{tasks}$  per node, memory per CPU and run time to be requested/ set. This study has used ORAC with access and parallelism managed through MPI (message passing interface) codes.

## 5.2. OpenFOAM fundamentals

This study uses CFD toolbox OpenFOAM to evaluate and minimize the knowledge gap and uncertainty with the consequence calculations. OpenFOAM is a free object oriented and an



open-source version of FOAM (acronym for Field Operation and Manipulation), a CFD software package available under the GNU General Public License through [www.openfoam.com](http://www.openfoam.com) (Maintained by ESI-OpenCFD Ltd) or through [www.openfoam.org](http://www.openfoam.org) (Maintained by OpenFOAM Foundation). OpenFOAM with a large user base across most areas of engineering and science has origin from the Imperial College London. OpenFOAM is used by both commercial and academic organisations to solve complex fluid flows involving chemical reactions, turbulence and heat transfer. The toolbox contains a selection of pre-configured solvers, utilities and libraries; and permits code customisation to suit the problem. Parallel processing utilities and option to export to other visualisation software also adds to the favour of choosing OpenFOAM.

OpenFOAM has an extensive range of features to solve anything from complex fluid flows involving chemical reactions, turbulence, and heat transfer, to solid dynamics and electromagnetics. The software package features advanced meshing capabilities, including adaptive mesh and unstructured mesh, offering up to second order accuracy, predominantly using collocated variable arrangements and parallel computing capability. Since its release as an open-source platform in 2004, the package added extensive range of features and now have applications extended to solid dynamics and electromagnetics. In this study, the OpenFOAM version v17.12 was used.

### 5.2.1. Introduction

OpenFOAM is a C++ based toolbox which allows the development of solvers for fluid and continuum mechanical problems. OpenFOAM includes an extensive collection of library functionality covering most aspects engineering flow problems through Physical modelling, Boundary conditions, Numerics, Meshing and Solvers. OpenFOAM is designed as a toolbox that is easily customisable. OpenFOAM also includes many tools to derive additional data from the calculations and generate set-ups for batch-driven processes.

The model is based on conservative Finite Volume Method (FVM) to discretise systems of partial differential equations. OpenFOAM applications are designed for use with unstructured polyhedral grid meshes, offering up to second order accuracy, predominantly using collocated variable arrangements. A number CFD studies have been published recently based on *OpenFOAM* toolbox, such as Doolan (2012), Lysenko et. al. (2010), Flores et. al. (2014), ESI (2020), Liu Q et.al. (2016), Zang (2018), Yusuf (2020). A significant number of the studies focus on incompressible flow phenomena and fluid-structure interactions. Utilizing OpenFOAM-based compressible solvers for compressible flows has gained remarkable traction over the past few

years as well. Some of these works would include studies conducted by Shen et. al. (2013). The expressions syntax enables users to define custom expressions for use in a variety of scenarios, including input dictionaries, boundary conditions and utilities, e.g., setting field values. The workflow of using OpenFOAM is like conventional CFD programs, and it is categorized as pre-processing, solving and post-processing. Details of OpenFOAM fundamentals is given in Appendix G.

For the CFD model workflow, first the geometry to appropriately represent the scenario with the surrounding conditions is established, then generate mesh (using blockMesh, snappyHexMesh). A suitable solver to solve the specific computational continuum mechanics is then selected from the set of libraries in OpenFOAM. Simulations are run and the computed results are subjected to post-processing, especially for data visualization is achieved by program ParaView. The workflow is summarised in Figure 42.

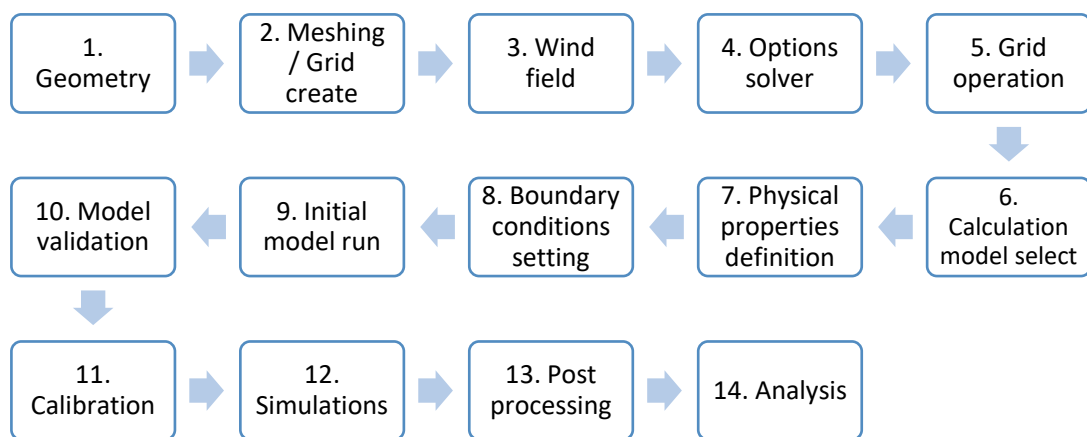


Figure 42: OpenFOAM workflow steps

### 5.2.2. Pre-processing

#### Computational grid – meshing

Mesh is generated using the OpenFOAM utilities like *blockMesh*, *snappyHexMesh* or by conversion using utilities like *fireToFoam*, *fluentMeshToFoam*, *gmsHToFoam* etc. *checkMesh* is used to check quality of the mesh which includes skewness, orthogonality, and aspect ratio.

The patch (list of face labels) types are specified in the mesh and field files of OpenFOAM case. The base type is specified under the type of keyword for each patch in the boundary file, located

in the constant/polyMesh directory. Initial meshing input sensitivity run details are given in Appendix A and the model input on the meshing is given in Appendix B.

### Parallel simulation

Parallel processing functionality is available and helps in optimising the model run time. When running a simulation in parallel, the geometry must first be decomposed (segmented) into individual geometries for each MPI process. These separate geometries are connected together with special processor boundary patches. The execution is done using utilities *decomposePar* (split the mesh and fields for parallel execution) and *reconstructPar* (merge decomposed fields from parallel runs). *reconstructParMesh* is a utility to merge decomposed mesh and data (simulated files from parallel processors) into a single set of files.

OpenFOAM has a range of decomposition methods and interfaces for example simple, hierarchiacal, structured, multilevel.

#### 5.2.3. Post-processing

Post processing in OpenFOAM like other CFD tools is to derive the results in the form of customized values, field properties and images. OpenFOAM includes utility *paraFoam* for post-processing. A widely used alternative for post-processing is *paraView*, an open source, multi-platform data analysis and visualisation application. *paraView* is a cross platform application with Python scripting and batch processing capabilities.

#### 5.2.4. Solving

OpenFOAM includes a wide range of options for solution, monitor solution progress and scheme controls, these are listed as [<https://www.openfoam.com/documentation/guides/>];

**Numerical schemes:** The treatment of each term in the system of equations is specified in the *fvSchemes* dictionary. This enables fine-grain control of e.g., temporal, gradient, divergence and interpolation schemes.

**Linear equation solvers Solution methods:** Case solution parameters are specified in the *fvSolution* dictionary. These include choice of linear equation solver per field variable, algorithm controls e.g., number of inner and outer iterations and under-relaxation.

**Finite volume options:** Additional run-time selectable physical modelling and general finite terms are prescribed in the *fvOptions* dictionary, targeting e.g., acoustics, heat transfer, momentum sources, multi-region coupling, linearised sources/sinks.

## Numerical schemes

The value for the variables is usually stored at the cell center so if the value at the face is needed (e.g., convection term), it must be computed from the interpolation of cell center values. There are several schemes that can be used in order to interpolate. Collaboration diagram for Finite volume numerical schemes is given in Figure 43.

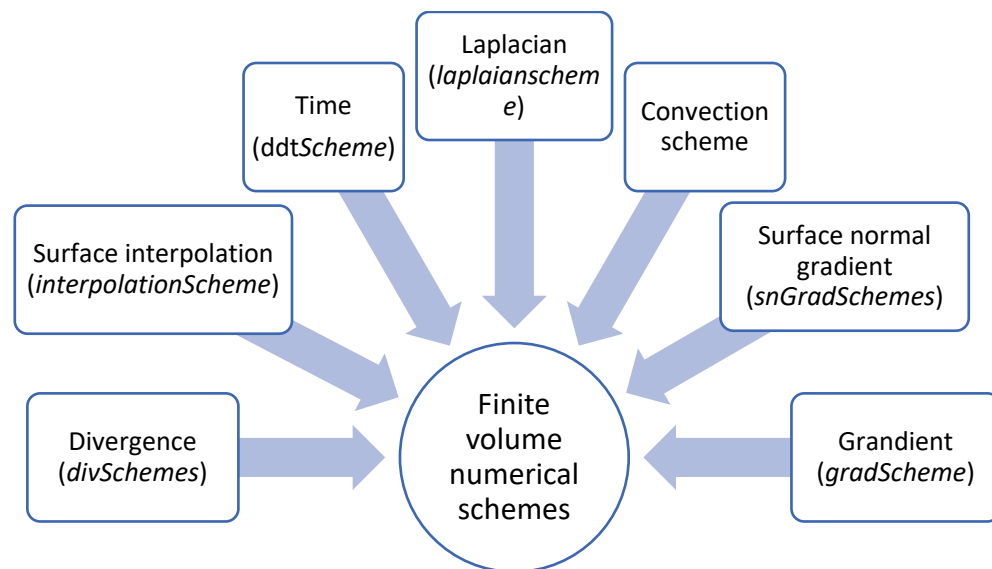


Figure 43: OpenFOAM collaboration diagram for Finite volume numerical schemes

Models are implemented using an equation syntax that closely follows the mathematical notation; for example, OpenFOAM syntax for some operators are given below:

- time rate of change:  $\partial\phi/\partial t$ 
  - `fvc::ddt(phi)`
- gradient:  $\nabla\phi$ 
  - `fvc::grad(phi)`
- divergence:  $\nabla\cdot\phi$ 
  - `fvc::div(phi)`
- laplacian:  $\nabla^2\phi$ 
  - `fvc::laplacian(phi)`

As the order of the scheme is increased, the accuracy is increased but being increased the required computational resources as well. For the first order upwind discretization, the variable is considered constant inside the cells, thereby, the value at the face is the same as the value at the cell center. For second order upwind discretization, the variable changes are considered linearly inside the cell, thereby, the following formula (Equation 33) is used in order to get the value at the face:

$$\theta_{face} = \theta_{center} + \nabla\theta \cdot \vec{r}$$

Equation 33

As can be seen such method requires a previous gradient calculation  $\nabla\theta \cdot \vec{r}$  is referred to the displacement vector from the upstream cell centroid to the face centroid.

### Solution, control and monitoring

The equation solvers, tolerances and algorithms are controlled from the *fvSolution* dictionary in the system directory. *fvSolution* includes sub-dictionaries for controlling under-relaxation, tolerances and algorithms. Most fluid dynamics solver applications in OpenFOAM use the pressure-implicit split-operator (PISO) or semi-implicit method for pressure-linked equations (SIMPLE) algorithms. These algorithms are iterative procedures for solving equations for velocity and pressure, PISO being used for transient problems and SIMPLE for steady state.

Successful running of OpenFOAM includes monitoring and managing jobs. It is an iterative process and may require periodic review of the progress reporting, correcting the input and debugging. A separate *log* file can be generated for review and record.

### Discretisation

To solve the fluid problem, the FVM Volume method is applied. The computational domain is divided into a finite number of volumes, also called mesh. The method is based on the partial differential equation of the general law of conservation (Equation 34).

$$\frac{\partial \bar{u}}{\partial t} + \nabla \cdot f(u) = \Gamma$$

Equation 34

Where,  $f$  is the flux of the conserved state and  $\Gamma$  (gamma) is the source term. By applying Gauss's theorem (Equation 35),

$$\int_V \nabla \cdot \bar{F} dV = \oint_S \bar{F} \cdot \bar{n} dS$$

Equation 35

To the divergence term, the change of a quantity within a volume can be described by integrating over all fluxed through the volume faces (Equation 36):

$$\int_{V_i} \frac{\partial u}{\partial t} dV + \oint_{S_i} f(u) \cdot \bar{n} dS = \gamma$$

Equation 36

where,  $V_i$  is the total volume and  $S_i$  the total surface area of a cell.

Different schemes can be used to discretize and solve the parts of this equation. Detailed discussion of the schemes can be found in Moukalled et. al. (2015).

### 5.2.5. Models and physical properties

OpenFOAM includes a number of solvers that are able to model basic flow, compressible or incompressible fluids, with heat transfer capabilities, combustion, and multi-phase / phase changes. A solver has to meet a number of requirements to be suitable for the given application. The classification of commonly used OpenFOAM solvers for Flow related problems are Basic, Incompressible, Compressible, Heat transfer, Multiphase, Lagrangian particles, Combustion.

Selection of solver along with the parameters and physical properties are required to define the case. The conditions and common models are explained in this section.

#### Thermophysical models in OpenFOAM

Thermophysical models are used to describe cases where energy, mass transfer or compressibility is important. OpenFOAM includes a large set of pre-compiled combinations of modelling, built within the code using C++ templates. This coding approach assembles thermophysical modelling packages beginning with the equation of state and then adding more layers of thermophysical modelling that derive properties from the previous layer(s).

The *thermophysicalProperties* dictionary is read by any solver that uses the thermophysical model library which is constructed in OpenFOAM as a pressure-temperature ( $p - T$ ). There is one compulsory dictionary entry called *thermoType* which specifies the package of thermophysical modelling that is used in the simulation. The keyword entries in *thermoType* reflect the multiple layers of modelling and the underlying framework in which they combined. Additional layers include transport and mixture modelling. An example is given in Appendix G.

#### Turbulence modelling

OpenFOAM includes supports RAS, DES and LES turbulence modelling [Ref: OpenFOAM: User Guide: Turbulence]. Turbulence generation is driven by the velocity gradient. Errors arising from the gradient calculation, e.g., due to poor quality meshes, can lead to spurious turbulence predictions and solver instability. This effect can be partly compensated by the application of

limited schemes. Turbulence models are specified in ‘constant’ folder. An example of specifying the turbulence for RAS  $k\omega$ - SST is given in Appendix G.

### Boundary conditions

Setting up of appropriate boundary conditions is vital for successful simulation, to minimize solver failure and optimize the computational time. OpenFOAM offers a wide range of boundary conditions which can be categorized to (OpenFOAM 2019):

- (i) basic like *fixedValue*, *fixedGradient*, *zeroGradient*,
- (ii) geometric constraints like *symmetry*, *wedge*, *empty*, *cyclic*, and
- (iii) derived like *slip*, *noSlip*, *fixedProfile*, *inletOutlet*.

The commonly used boundary conditions are Inflow (inlet) conditions, Wall, Outflow (outlet) conditions, symmetry condition, and periodic condition. Boundary conditions are assigned in the *boundaryField* section of the field files within each time directory for each mesh patch. The format is given in Appendix G.

### In OpenFOAM: atmBoundaryLayer Class reference (turbulence models at inlet)

Base class to set log-law type ground-normal inlet boundary conditions for wind velocity and turbulence quantities for homogeneous, two-dimensional, dry-air, equilibrium, and neutral atmospheric boundary layer (ABL) modelling (Richards & Hoxey 1993, Hargreaves & Wright 2007, Yang et. al. 2009a, Yang et. Al. 2009b, Emeis 2013).

The ground-normal profile is derived from the friction velocity, flow direction and ‘vertical’ direction (Equation 37):

$$U = \frac{U^*}{\kappa} \ln \left[ \frac{z - z_g + z_0}{z_0} \right] \tag{Equation 37}$$

$$k = \frac{(U^*)^2}{\sqrt{C_\mu}} \tag{Equation 38}$$

$$\epsilon = \frac{(U^*)^3}{\kappa(z - z_g + z_0)} \tag{Equation 39}$$

$$U^* = \kappa \frac{U_{ref}}{\ln \left( \frac{z_{ref} + z_0}{z_0} \right)} \tag{Equation 40}$$

Where,

- $U$  = Ground-normal streamwise flow speed profile [m/s]
- $k$  = Ground-normal turbulent kinetic energy (TKE) profile [ $m^2/s^2$ ]
- $U^*$  = Friction velocity [m/s]
- $\kappa$  = von Kármán constant [-]
- $C_\mu$  = Turbulent viscosity coefficient, empirical model constant [-]
- $z$  = Ground-normal (vertical) coordinate component [m]
- $z_g$  = Ground-normal displacement height, minimum z-coordinate.[m]
- $z_0$  = Surface roughness height / aerodynamic roughness length [m]
- $U_{ref}$  = Reference velocity at  $Z_{ref}$  [m/s]
- $Z_{ref}$  = Reference height [m]

### OpenFOAM Solvers

OpenFOAM comes with a range of solvers. Each solver is coded to simulate a specific flow phenomenon ranging from compressibility to reacting and fluid-structure interaction. As an open-source tool, it constantly expands and improves upon the available solvers.

The list of solvers and the flow modelling capabilities (OpenFOAM 2019) is listed in Table 38.

Table 38: Capability matrix: Flow characteristics vs Solvers

Solver	tra	cor	tur	tra	bu	cor	mu	par	dvr	reg	fvC
	tra	cor	tur	he	bu	cor	mu	par	dvr	mu	fvC
<a href="#">simpleFoam</a>			✓								✓
<a href="#">pimpleFoam</a>	✓		✓						✓		✓
<a href="#">icoFoam</a>	✓										
<a href="#">interFoam</a>	✓		✓				✓		✓		✓
<a href="#">pisoFoam</a>	✓		✓								✓
<a href="#">buoyantPimpleFoam</a>	✓	✓	✓	✓	✓						✓
<a href="#">buoyantSimpleFoam</a>		✓	✓	✓	✓						✓
<a href="#">chemFoam</a>	✓			✓		✓					
<a href="#">fireFoam</a>	✓	✓	✓	✓	✓	✓				✓	✓
<a href="#">reactingFoam</a>	✓	✓	✓	✓		✓					✓



Solver	tra	cor	tur	tra	he	bu	cor	mu	pa	dvi	reg	mu	fvC
<a href="#">rhoCentralFoam</a>	✓	✓	✓	✓									
<a href="#">rhoPimpleFoam</a>	✓	✓	✓	✓						✓			✓
<a href="#">rhoSimpleFoam</a>		✓	✓	✓									✓

In the Navier-Stokes system, the form of the equations shows linear dependence of velocity on pressure and vice-versa. This inter-equation coupling is called velocity pressure coupling. Semi-Implicit Method for Pressure Linked Equations (SIMPLE) for steady state and Pressure Implicit with Splitting of Operators (PISO) for transient are the pressure-velocity algorithms in OpenFOAM. Combination algorithms like PIMPLE (PISO and SIMPLE), SIMPLER are also available. The list of the solvers evaluated for the dispersion of toxic natural gas is given in Table 39.

Table 39: OpenFOAM solver and description

Solver name	Category	Description
<b>boundaryFoam</b>	Incompressible	Steady-state solver for incompressible, 1D turbulent flow, typically to generate boundary layer conditions at an inlet, for use in a simulation.
<b>fireFoam</b>	Combustion	Transient solver for fires and turbulent diffusion flames with reacting particle clouds, surface film and pyrolysis modelling; it is specialized in simulating heat and smoke transport in fires, and it is a LES solver for incompressible flow
<b>mppicFoam</b>	Particle tracking flows	Transient solver for the coupled transport of a single kinematic particle cloud including the effect of the volume fraction of particles on the continuous phase. Multi-Phase Particle In Cell (MPPIC) modelling is used to represent collisions without resolving particle-particle interactions.
<b>rhoReactingFoam</b>	Combustion	Solver for combustion with chemical reactions using density-based thermodynamics package
<b>rhoReactingBuoyantFoam</b>	Combustion	Solver for combustion with chemical reactions using a density-based thermodynamics package with enhanced buoyancy treatment
<b>rhoSimpleFoam</b>	Compressible	Steady-state solver for turbulent flow of compressible fluids

Solver name	Category	Description
<b>rhoPimpleFoam</b>	Compressible	Transient solver for turbulent flow of compressible fluids for HVAC and similar applications, with optional mesh motion and mesh topology changes
<b>sonicFoam</b>	Compressible	Transient solver for trans-sonic/supersonic, non-isothermal, single phase, turbulent flow of a compressible gas
<b>simpleFoam</b>	Incompressible	Steady-state solver for incompressible, turbulent flow, using the SIMPLE algorithm
<b>pimpleDyMFoam</b>	Incompressible	Transient solver for Newtonian fluids in a moving mesh with PIMPLE (PISO-SIMPLE) algorithm
<b>interDyMFoam</b>	Incompressible	Isothermal for immiscible fluids with Volume of fluid (VOF) phase-fraction adaptive remeshing
<b>buoyantSimpleFoam</b>	Compressible	Steady-state solver for turbulent flow of compressible fluids

From literature review for the solver choice for the natural gas dispersion modelling application, simulations were carried out using *fireFoam*, *simpleFoam*, *rhoSimpleFoam*, *rhoPimpleFoam*, *rhoReactingFoam* and *rhoReactingBuoyantFoam*. This includes establishing an initial flow field (e.g. velocity field  $U$ ) prior to the release and dispersion of the species. For  $U$ ,  $k$  and  $e$  ABL conditions are established. Input, set-up, validation for the initial runs is given in Appendix A.

In OpenFOAM, there is option to use the real fluid property value, where the phases are not distinguished by the solver. In such cases, the fluid properties are stored in tables by pressure and temperature and are interpolated by a custom OpenFOAM library during the simulation run. The fluid properties can be obtained from the NIST Chemistry WebBook (Linstrom & Mallard 2017).

If the density ratio is large, and accuracy is important, the study by Bogaers et. Al suggests that a compressible solver is necessary. The validation and comparison between different OpenFOAM solvers have concluded that *rhoReactingBuoyantFoam* is a suitable solver (Bogaers & Jansen van Rensburg 2018). It is recommended as good solver for large density ratio models requiring higher accuracy. The suitability of *rhoReactingBuoyantFoam* for modelling the dispersion of  $H_2S$  bearing natural gas is further evaluated in the next subsection of this Chapter.

“*rhoReactingBuoyantFoam*” is an OpenFOAM, density based, fully compressible, combustion solver which includes chemical reactions using a density-based thermodynamics package with enhanced buoyancy treatment [OpenFOAM user guide]. *rhoReactingBuoyantFoam* includes

compressible continuity and momentum equations, a scalar advection-diffusion transport equation with chemical reactions, an energy equation, a state equation and a pressure-temperature thermophysical model. By turning off (False) chemical reaction equation, the solver has shown good functionality for accurately approximating gas dispersion (Fiates et. al. 2016, Bogaers & Jansen van Rensburg 2018). The conservation of mass is expressed in Equation 27, the general set of equations are as follows:

Momentum equation for a non-constant density

$$\frac{\partial}{\partial t}(\rho \mathbf{u}) + \nabla \cdot (\rho \mathbf{u} \mathbf{u}) = -\nabla p + \nabla \cdot \boldsymbol{\sigma} + \rho \mathbf{g} + \mathbf{S}$$

Equation 41

Scalar advection-diffusion transport equation

$$\frac{\partial}{\partial t}(\rho Y_i) + \nabla \cdot (\rho \mathbf{u} Y_i) = \nabla \cdot \mathbf{J}_i + S_i + R_i$$

Equation 42

Energy equation is given by

$$\frac{\partial}{\partial t}(\rho h) + \nabla \cdot (\rho h \mathbf{u}) + \frac{\partial \rho K}{\partial t} + \nabla \cdot (\rho \mathbf{u} K) - \frac{\partial \rho}{\partial t} = \nabla \cdot \mathbf{q} + \nabla \cdot (\boldsymbol{\tau} \cdot \mathbf{u}) + \rho r + \rho \mathbf{g} \cdot \mathbf{u}$$

Equation 43

Where,

$h$  is the system's enthalpy (the sum of the systems internal energy and dynamic pressure).

$\nabla \cdot \mathbf{q}$  is the heat flux

$\rho r$  is the heat source for any specific heat source  $r$

$K$  is the specific heat energy, defined as  $|\mathbf{u}|^2/2$

$\boldsymbol{\tau}$  is the viscous stress tensor

$$\boldsymbol{\sigma} = \boldsymbol{\tau} - p\mathbf{I}$$

For weakly compressible formulation and assuming a perfect gas formulation, density can be related to temperature via:

$$\rho = \frac{PM}{RT}$$

Equation 44

Where,

$M$  is the combined fluid mixtures molar weight

$R$  is the universal gas constant

Dynamic viscosity defined by Sutherland transport model as,

$$\mu = \frac{A_s \sqrt{T}}{1 + T_s/T}$$

Equation 45

Where,

$A_s$  and  $T_s$  are constants, default values used in OpenFOAM

$$A_s = 1.67212 \times 10^{-6}$$

$$T_s = 170.672$$

The ideal gas law for rhoReactingBuoyantFoam is invoked as follows (Equation 46):

$$p = \rho R_{spec} T$$

Equation 46

Where,

U = velocity vector

p = pressure

T = temperature

$\rho$  = flow density

### 5.3. CFD model and validation

An important element in the development of a CFD model for an analysis involves the validation (and calibration) of the methodology using experimental or using other computational data. The model validation can be scientific examination, statistical comparison and also for operational easiness like interface and user friendliness. This section describes the model set up and the associated validation of the CFD model for sour natural gas dispersion. Model set up in OpenFOAM includes solver selection, defining physical model, establishing boundary conditions, pressure-velocity coupling, selecting numerical discretization schemes and defining the convergence criteria.

The various types of validation using experiment process include full or major configuration studies, and when possible, fundamental flow physics studies. The model set up and validation is carried out in steps (Figure 44).

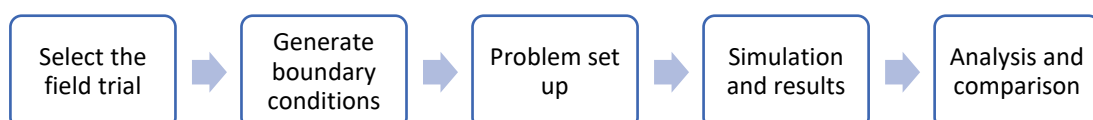


Figure 44: OpenFOAM model set up and validation steps

### 5.3.1. Prairie Grass field trial project

In the present study, observations from Prairie Grass (PG) field trials have been used to validate the OpenFOAM model for toxic natural gas dispersion. The project conducted about 70 experiments over several days with different flow rates and measured SO<sub>2</sub> concentration at 5 different distances from the point of injection. A horizontal sampling array was arranged in five arcs (50, 100, 200, 400, 800m) downwind of the release. The details of the experimental setup and the monitoring point information is given in Section 2.10.

The Field trial case Test No- 09 set of results (Volume I – Table 3.1, Volume II pages 55 and 210) were used for this validation (Barad 1958). The test was performed at 1600 hours with Air Temp 28.33 °C, wind speed (recorded at source) was 6.88 m/s with Wind direction 204 deg. The air and soil temperature and the wind profile along vertical is given in Table 40 and Table 41 respectively for Case 09.

**Table 40: Prairie Grass Field Trail – Temperature profile**

Height (m)	16	8	4	2	1	0.5	0.25	0.12	-0.03	-0.06	-0.12
Temperature (°C)	25.76	26.25	26.61	27.39	28.19	28.75	29.53	29.82	26.64	24.48	23.14

**Table 41: Prairie Grass Field Trail Case 09 – Vertical wind profile**

Height (m)	16	8	4	2	1	0.5	0.25	0.12
Wind speed (cm/sec)	884	842	709	700	611	533	533	450

The vertical velocity and temperature profiles need to be established in the OpenFOAM model and maintained in the solution domain. The emission release rate (source strength, Q), for test 09 is 92 g/s from 2-inch pipe and the diffusion measurement obtained are given Volume I – Table 5.1 and Table 42 (pages 96-97) respectively (Barad 1958). Atmospheric transport and dispersion processes include stochastic components.

The transport downwind follows a serpentine path, being influenced by both random and periodic wind oscillations, composed of both large- and small-scale eddies in the wind field (Barad, 1958). The maximum concentration measured at the concentric sampling arcs are given in Table 42.

Table 42: Prairie Grass Field Trail Case 09 diffusion results – maximum concentration along the sampling arcs

Data	50 m	100 m	200 m	400 m	800 m
	83° – 149°	89°-147°	95°-145°	99°-145°	100°-139°
Max at	109°	107°	107°	105°	105°
Value (ppm)	200	56.1	14.2	2.90	0.52

The input (solution parameters) and boundary conditions (*turbulentInlet*) for the field trail case model were developed using a simplified tunnel model. By this two-step approach, modelling time can be saved, and more options can be evaluated using the simplified tunnel model.

### 5.3.2. Simplified tunnel model for input and boundary conditions

Geometry and Mesh: The total computational domain for the simplified tunnel model (box dimensions in x, y and z directions) are 1100m in length, 14m in width and 40m in height and as given in Figure 45.

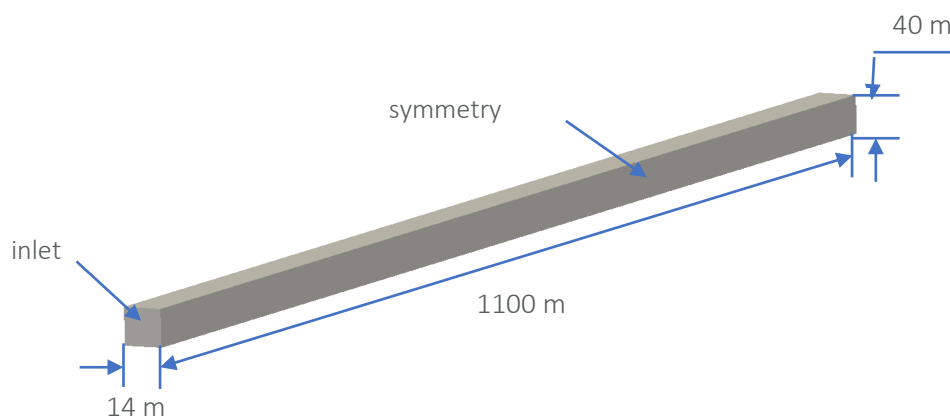


Figure 45: Simplified tunnel – Geometry

During the simulation the inlet velocity profile needs to be maintained throughout the simulation domain. Vertical velocity profile along with other scalar variables are taken at 4 different distances from inlet (i.e.,  $X = -90$  m, 400 m, 700 m, 990 m as given in Figure 46). They are compared with the experimental data given in Table 40 and Table 41. The test problem, along with the computational grid is illustratively shown in Figure 47.

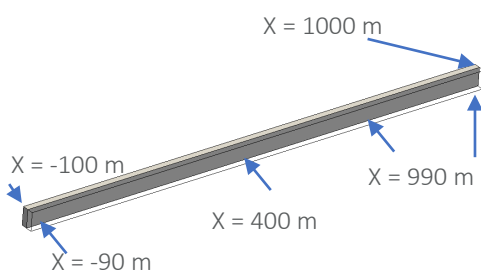


Figure 46: Simplified tunnel – monitoring points

The computational domain was divided into 23500 mesh as represented in Figure 47 .

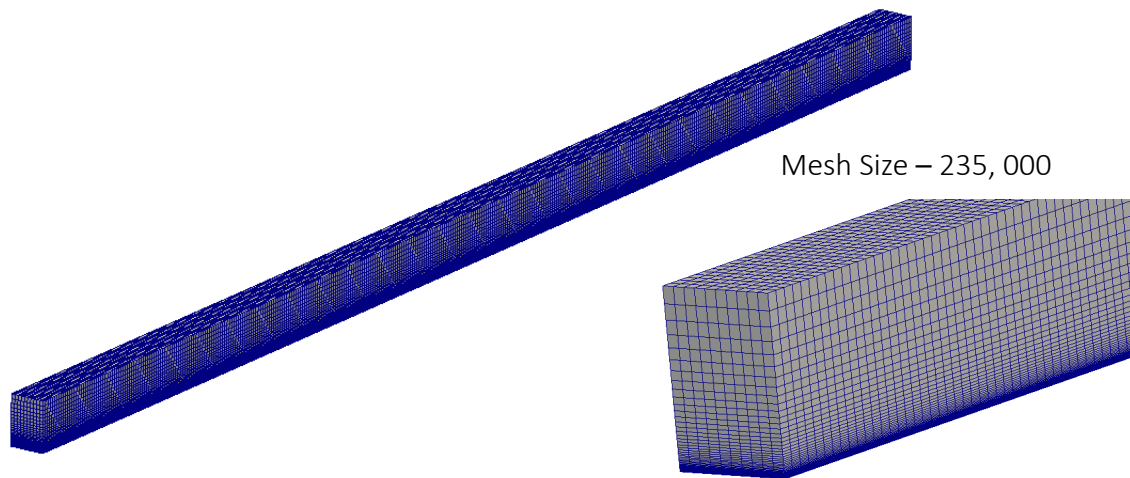


Figure 47: Simplified tunnel – Mesh

Velocity ranges from 4.5 m/s to 8.84 m/s for heights ranging from 0.25 m to 16 m above ground level. To account for the turbulence, the vertical velocity and temperature profiles were established and validated in the solution domain.

The simplified tunnel is run in steady-state and then run in transient with fluctuating *inlet bc* to check whether the model has been able to keep the profile intact over the simulation domain and time. The vertical velocity profile is plotted to check the consistency. *rhoSimpleFoam* and *rhoPimpleFoam* solver have been used for steady-state and transient runs respectively.

OpenFOAM's boundary condition *atmBoundaryLayerInletVelocity* was used to generate the vertical velocity profile in the solution domain. For the top plane *fixedShearStess* bc used.

#### Steady-state simulation:

OpenFOAM has a substantial number of turbulence models available. Two models k-Omega SST (k- $\omega$  SST) and Realizable k- $\epsilon$  were studied. A comparison of the vertical velocity profile (U) along the four monitoring points using both turbulence models was carried out. The results of the comparison along the vertical provide is given in Figure 48.

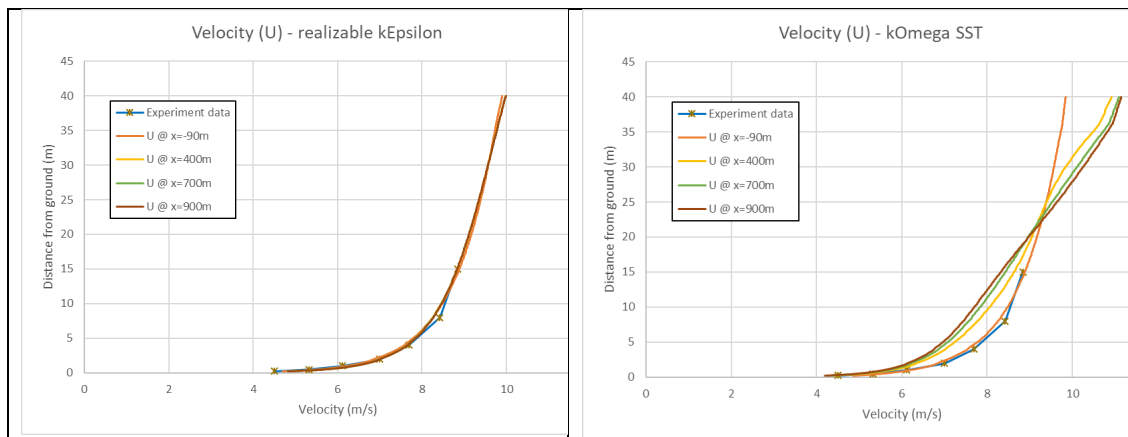


Figure 48: Vertical velocity profile comparison between realizable k-ε and k-ω SST

It is evident from the velocity profile comparison that Realizable k-ε preserve the vertical velocity much better as compared to k-ω SST model. So Realizable k-ε is chosen as the turbulence model. The velocity profile along the symmetry plane is given in Figure 49.

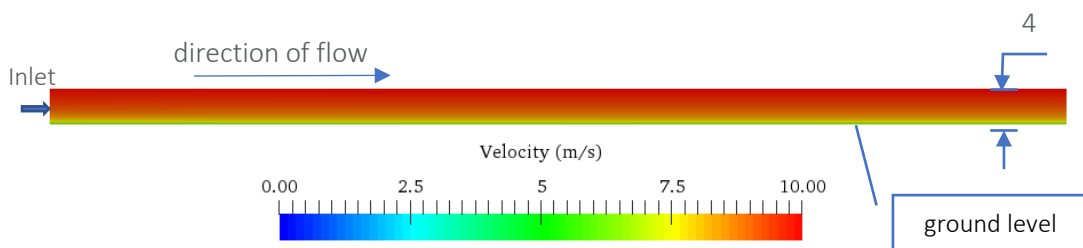


Figure 49: Simple tunnel velocity profile along symmetry plane

The selected turbulence model with a steady state velocity, temperature, Kinetic energy, and dissipation rate (Epsilon) values along the vertical profile at the monitoring points were compared against the experimental values. The results of the comparison for the steady state are given in Figure 50 to Figure 53.



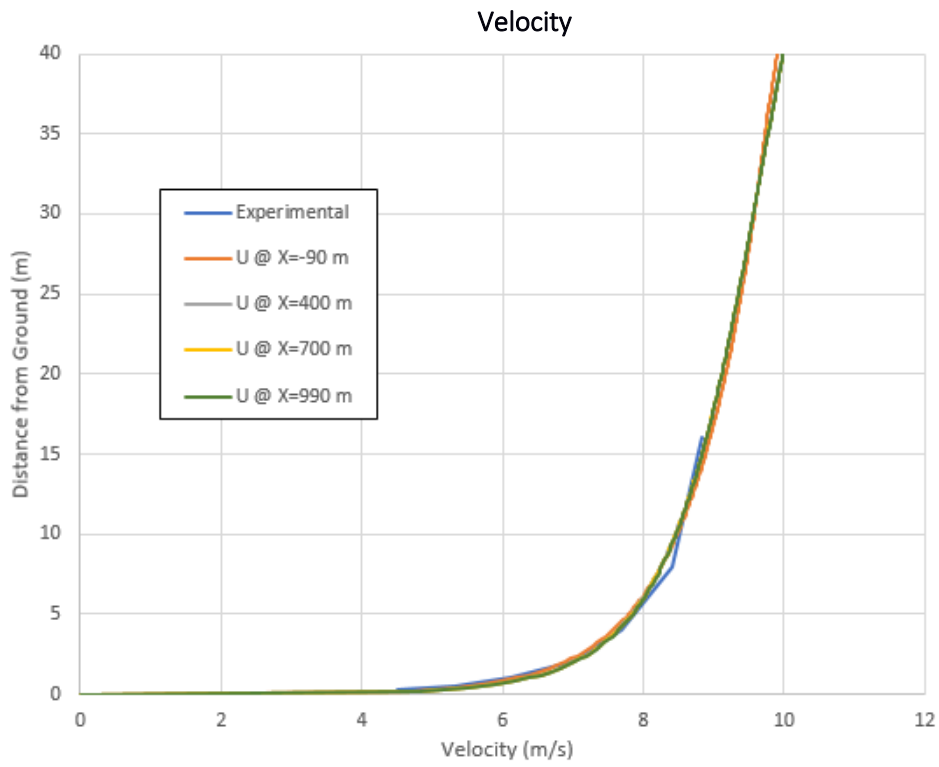


Figure 50: Simplified model - Steady state Velocity profile comparison

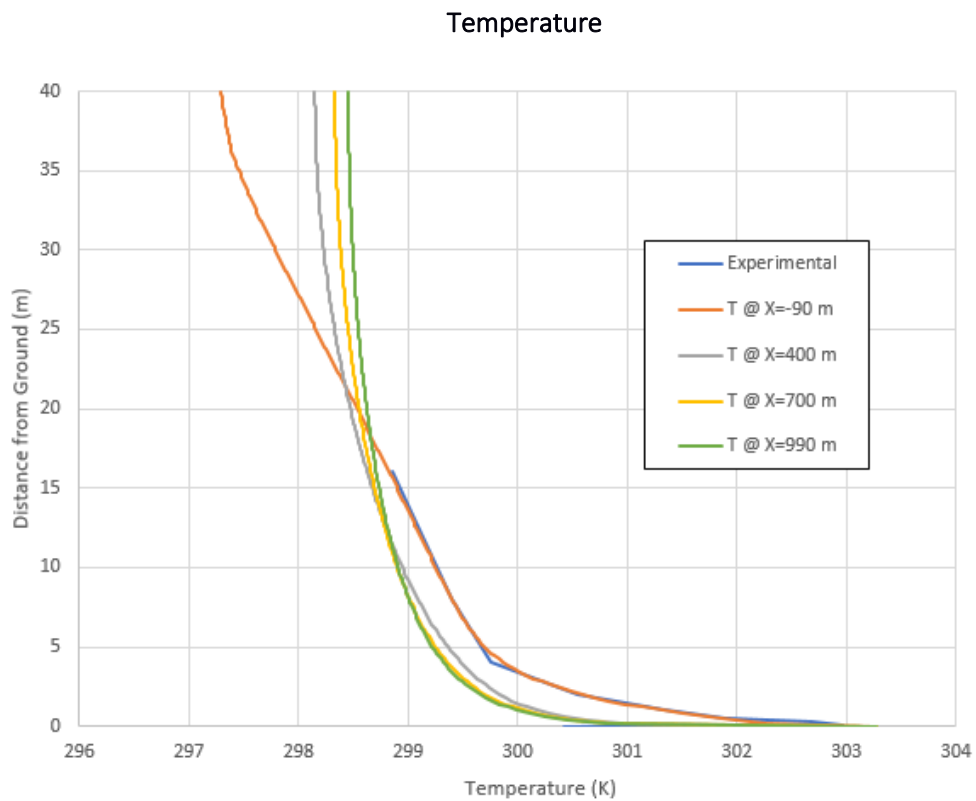


Figure 51: Simplified model - Steady state Temperature profile comparison

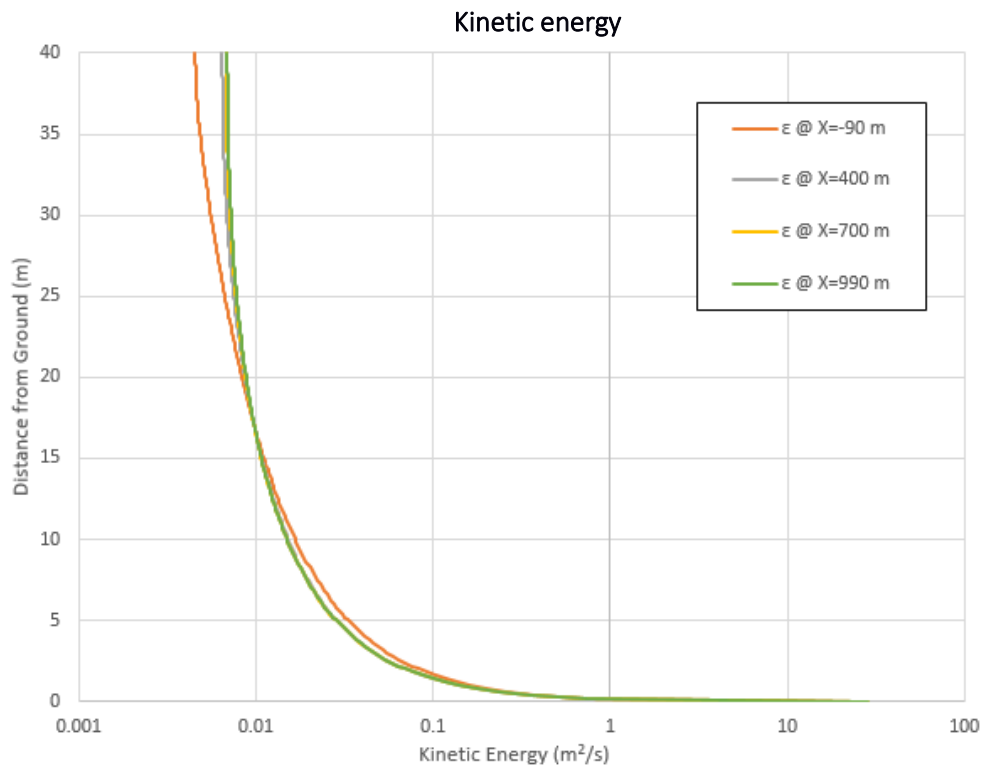


Figure 52: Simplified model - Steady state Kinetic energy comparison

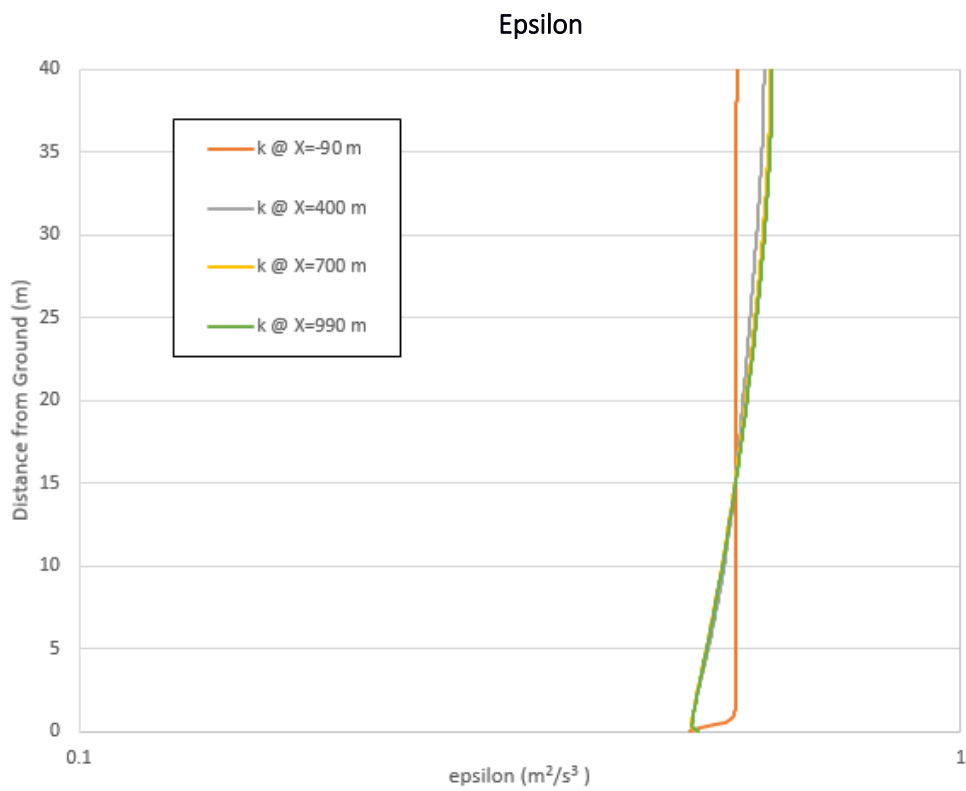


Figure 53: Simplified model - Steady state Epsilon comparison

The results show that the OpenFOAM boundary conditions chosen are able to maintain velocity, kinetic energy and dissipation rate (to a lesser extent). The estimated temperature along vertical at 90m is not maintained but the deviation is within 2Kelvin. The boundary conditions chosen are given below:

#### ABLConditions

```

kappa          0.41;
cmu           0.09;
Uref         6.88;
Zref         2;
zDir         (0 0 1);
flowDir      (1 0 0);
z0           uniform 0.002;
d            uniform 0.0;
zGround      constant 0;

```

#### k (kinetic energy)

```

inlet
{
  type          atmBoundaryLayerInletK;
  #include      "include/ABLConditions";
  value        uniform 100;
}
outlet
{
  type          inletOutlet;
  inletValue   uniform 100;
  value        uniform 100;
}
ymin
{
  type          symmetry;
}
ymax
{
  type          symmetry;
}
zmax
{
  type          zeroGradient;
  value        uniform 0.005;
}
releasePoint
{
  type          turbulentIntensityKineticEnergyInlet;
  intensity    0.1;
  value        uniform 1.0e-16;
}

```

#### T (temperature)

```

inlet
{
  type          timeVaryingMappedFixedValue;
  offset        0;
  setAverage   off;
}
outlet
{
  type          inletOutlet;
  inletValue   uniform 301.48;
  value        uniform 301.48;
}

```

U (velocity)

```

inlet
{
  type          atmBoundaryLayerInletVelocity;
  #include      "include/ABLConditions"
  value        uniform (0.001 0 0);
}
outlet
{
  type          pressureInletOutletVelocity;
  value        uniform (0 0 0);
}
ymin
{
  type          symmetry;
}
ymax
{
  type          symmetry;
}
zmax
{
  type          fixedShearStress;
  tau           (0.193876 0 0);
  value        uniform (0 0 0);
}
releasePoint
{
  type          flowRateInletVelocity;
  massFlowRate constant 0.092;
  rho           rhoInlet;
  rhoInlet     2.652;
  extrapolateProfile false;
  value        uniform (0 0 0);
}

```

Simulating SO<sub>2</sub> mass flow rate

Epsilon

```

inlet
{
  type          atmBoundaryLayerInletEpsilon;
  #include      "include/ABLConditions"
  value        uniform 100;
}
outlet
{
  type          inletOutlet;
  inletValue   uniform 100;
  value        uniform 100;
}
ymin
{
  type          symmetry;
}
ymax
{
  type          symmetry;
}
zmax
{
  type          zeroGradient;
  value        uniform 0.1;
}
releasePoint
{
  type          turbulentMixingLengthDissipationRateInlet;
  mixingLength 0.051;
  phi           phi;
  k            k;
  value        uniform 100;
}

```

## Transient Turbulence - Simplified tunnel

Tests for turbulent boundary conditions: OpenFOAM have different types of transient turbulent model, i.e., Unsteady RANS, DDES, IDDES and LES. For DDES, IDDES and LES type of models' user need to define the inlet velocity fluctuations. In OpenFOAM, there are two options, i.e., Divergence Free Synthetic Eddy Model (DFSEM) and Digital Filter based inlet boundary condition. However, the DDES types of models require very fine mesh to resolve major eddies. So, for the huge domain dimension (1100 m X 240 m X 40 m) and time (600 sec), it will be very computational resource intensive to run model. Unsteady RANS with Realizable k- $\epsilon$  model has been chosen.

Values from the final time step of Steady-state simulation were manually copied over and were used for the transient simulation.

From the final time step (600 seconds) of the steady state simulation is given below:

```
(1.17316 2.53087e-07 -1.10448e-08)
(2.21335 2.59172e-07 3.03958e-06)
(1.17324 -1.30372e-07 2.81791e-05)
(1.17317 -1.76797e-07 -4.19296e-08)
(1.17323 1.61451e-07 2.88252e-05)
)
;

boundaryField
{
    inlet
    {
        type                atmBoundaryLayerInletVelocity;
        z0                  constant 0.002;
        flowDir             constant (1 0 0);
        zDir                constant (0 0 1);
        kappa               0.41;
        Cmu                 0.09;
        Uref                constant 6.88;
        Zref                constant 2;
        zGround             constant 0;
        value               nonuniform List<vector>
600
(
(9.81324 0 0)
(9.81324 0 0)
(9.81324 0 0)
(9.81324 0 0)
(9.81324 0 0)
(9.81324 0 0)
(9.81324 0 0)
(9.81324 0 0)
(9.81324 0 0)
(9.81324 0 0)
(9.71251 0 0)
(9.71251 0 0)

```

The transient simulation with *turbulentInlet* bc, the boundary condition for inlet is given below.

```
(1.17316 2.53087e-07 -1.10448e-08)
(2.21335 2.59172e-07 3.03958e-06)
(1.17324 -1.30372e-07 2.81791e-05)
(1.17317 -1.76797e-07 -4.19296e-08)
(1.17323 1.61451e-07 2.88252e-05)
)
;

boundaryField
{
    inlet
    {
        type                turbulentInlet;
        fluctuationScale     (0.6 0.6 0.6);
        alpha                0.5;
        referenceField       nonuniform List<vector>
600
(
(9.81324 0 0)
(9.81324 0 0)
(9.81324 0 0)
(9.81324 0 0)
(9.81324 0 0)
(9.81324 0 0)
(9.81324 0 0)
(9.81324 0 0)
(9.81324 0 0)
(9.81324 0 0)
(9.71251 0 0)
(9.71251 0 0)

```

*turbulentInlet* bc need these reference field from steady-state

To mirror the field trial settings, the simulation has been done as it is in an open ground. There is a lot of atmospheric turbulence that affects the local velocity field and dispersion of the species (SO<sub>2</sub>). To take account of the impact of atmospheric turbulence, a hypothetical inlet turbulence has been generated using *turbulentInlet* boundary condition. Series of simulations run to find out proper parameters for the *turbulentInlet* boundary condition and by ensuring velocity profile can be maintained. This boundary condition generates a fluctuating inlet condition by adding a random component to a reference (mean) field (Equation 47).

$$x_p = (1 - \alpha)x_p^{n-1} + \alpha(x_{ref} + sC_{RMS}x_{ref})$$

Equation 47

where,

- X<sub>p</sub> = patch values
- X<sub>ref</sub> = reference patch values
- n = time level
- α = fraction of new random component added to previous time value
- C<sub>RMS</sub> = RMS coefficient
- s = fluctuation scale

The patch for the boundary condition in OpenFOAM.

```
myPatch
{
    type            turbulentInlet;
    fluctuationScale 0.1;
    referenceField  uniform 10;
    alpha           0.1;
}
```

For atmospheric turbulence generation using *turbulentInlet* boundary condition, *fluctuationScale* and *alpha* values are required. A series of simulations were run to determine appropriate *fluctuationScale* and *alpha* values to the Standard deviation ( $\sigma$ ) for velocity as per Run No.#9 in Table 17.2 of Prairie Grass Trials (Barad 1958b). The combinations and the result comparisons are given in the Appendix C. Based on the analysis, this study further utilized *fluctuationScale* of (0.95 0.95 0.95) and *alpha* of 0.75.

#### Summary: Simplified tunnel

A two-step approach proved to be useful where at first the model is run in steady-state mode and the velocity profile for the domain is established. This velocity profile is used in transient state simulations to mimics the real field prior to the release of the species. From the different types of transient turbulence model in OpenFOAM, Unsteady RANS with Realizable k- $\epsilon$  model has been chosen as it preserves the velocity profile much better as compared to SST k- $\omega$ . To represent the atmospheric turbulence that effects the local velocity field, a hypothetical inlet turbulence is generated using *turbulentInlet* boundary condition.

### 5.3.3. Full domain OpenFOAM model for Prairie Grass Field trial

The total computational domain (box dimensions in x, y and z directions) is 1100m in length, 300m in width and 50m in height. The location of release point is set at a release point at 100m from inlet, middle of the width and at 0.45m height. The test problem, along with the computational grid is illustratively shown in Figure 54.

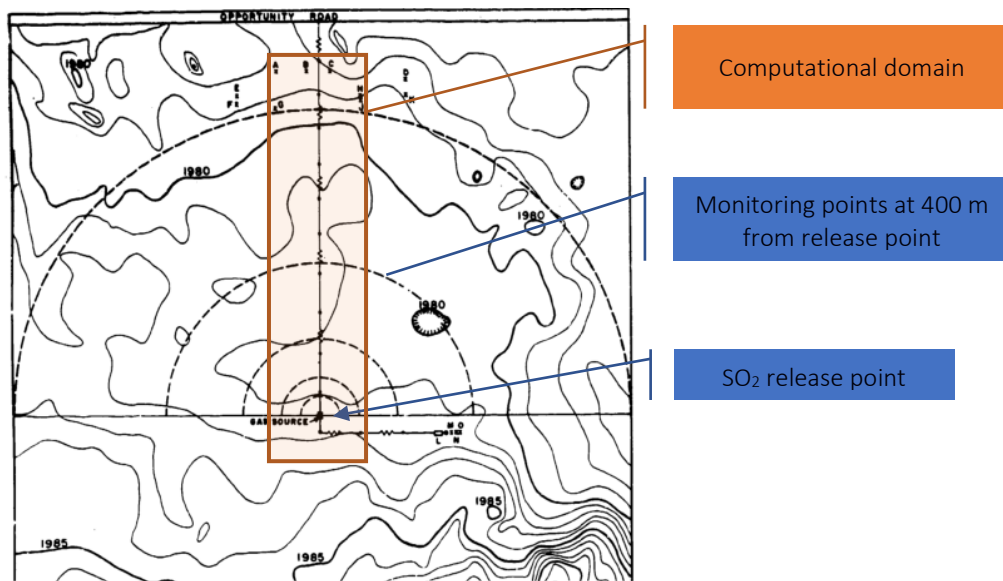


Figure 54: Schematic of the Prairie Grass Experiment setup along with an illustration of the computational domain

The modelling boundary (computational domain) was selected to include all the monitoring points at five distances downwind with the observed concentrations. The estimated values were then compared against the observed values to select the OpenFOAM solver, turbulence model, velocity profile and temperature.

The simulations were run at two stages as explained in the ‘Simplified tunnel’ in session 5.3.3; a wind velocity flow field was established prior to the  $\text{SO}_2$  dispersion modelling. Steady state run was initially carried out to get the inlet conditions and the flow field, which is fed as input to Transient simulations. This approach establishes the flow field in the solution domain like the field trial ground conditions. For steady-state simulation, *buoyantSimpleFoam* was used as variable  $p$  and  $p\_rgh$  are required for the species simulation solver *rhoReactingBuoyantFoam* (*rhoSimpleFoam* do not output  $p\_rgh$  values). Turbulence model Realizable  $k\varepsilon$  was selected. Session 5.3.3.5 includes the validations for the input conditions and boundary.

**Geometry:** The dimensions of the computational domain are 1100 m (L) by 240 m (W) by 40 m (H). The X-axis is in the horizontal streamwise direction, i.e., parallel to the wind direction. The Y-axis is lateral and perpendicular to the wind direction while the Z-axis is in the vertical direction (Figure 55).



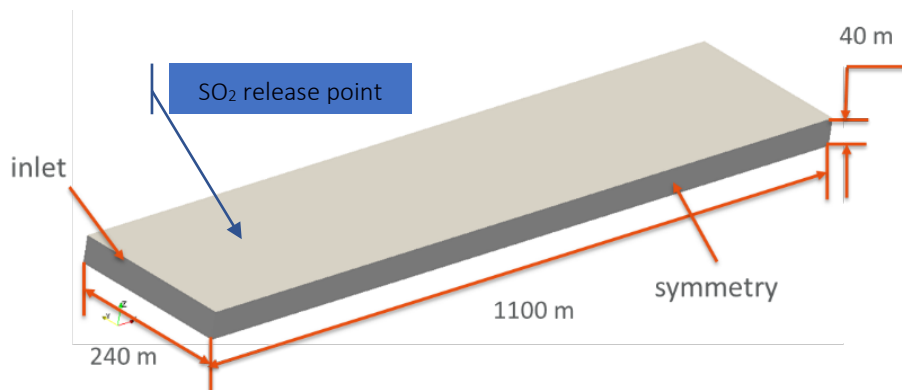


Figure 55: Computational domain geometry for PG case simulation

**Meshing:** Meshing of the domain was carried out using the following commands.

```

surfaceFeatureExtract
blockMesh
topset
createPatch -overwrite
decomposePar -force
snappyHexMesh -overwrite

```

```

snappyHexMeshDict
  addLayers
  nCellsBetweenLevel
  resolveFeatureAngle
  snapControls

```

The file information of *blockMeshDict* and the *snappyHexMeshDict* are given in [Appendix B](#).

In *blockMeshDict*, the *vertices* define the geometry and *block* defines the mesh resolution.

*blockMesh* settings used for this study is given here.

```

vertices
(
  (0 300 50)
  (1000 300 50)
  (1000 0 50)
  (0 0 50)
  (0 300 0)
  (1000 300 0)
  (1000 0 0)
  (0 0 0)
);

blocks
(
  hex (0 1 2 3 4 5 6 7) 125 38 16) simpleGrading 1 1 0.1
);

```

In *snappyHexMeshDict*, '\*.stl' files define the geometry types. The *releasePoint.stl* defines the inlet for species (pollutant gas), the *releaseTube.stl* is set for flow detachment around inlet and *ground.stl* defines the refinement close to the ground. The settings used in the study is given below.

```

releasePoint.stl
{
    type          triSurfaceMesh;
    name          releasePoint;
}
releaseTube.stl
{
    type          triSurfaceMesh;
    name          releaseTube;
}
ground.stl
{
    type          triSurfaceMesh;
    name          ground;
}
dirRefineBox
{
    type searchableBox;
    min (99 149 0.0);
    max (101 151 1);
}

```

The refinement closer to surfaces and edges are of higher order. This is done by setting the level in *refinementSurface* as given below. The sensitivity of the values of these levels were validated and used to increase or decrease the number of cells. Representative set of values and the corresponding mesh refinement is illustrated in Figure 56 and Figure 57.

```

features
(
    {
        file "releasePoint.eMesh";
        level 7;
    }
    {
        file "releaseTube.eMesh";
        level 3;
    }
);
refinementSurfaces
{
    releasePoint
    {
        level (7 7);
    }
    releaseTube
    {
        level (3 3);
    }
    ground
    {
        level (2 2);
    }
}

```

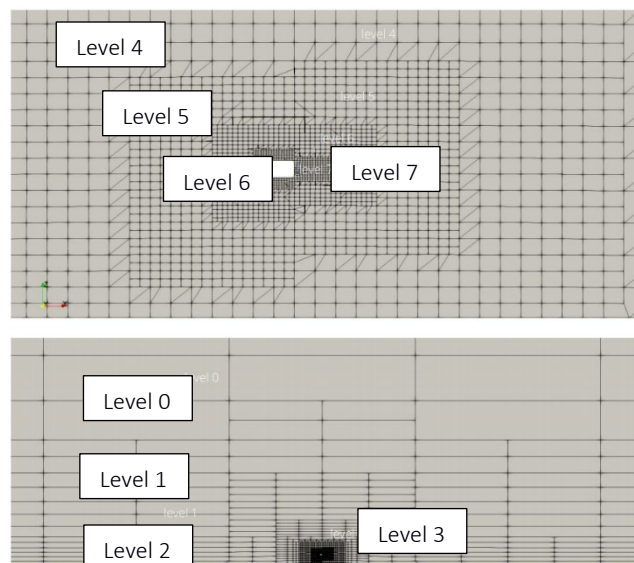


Figure 56: Mesh refinement – representative set

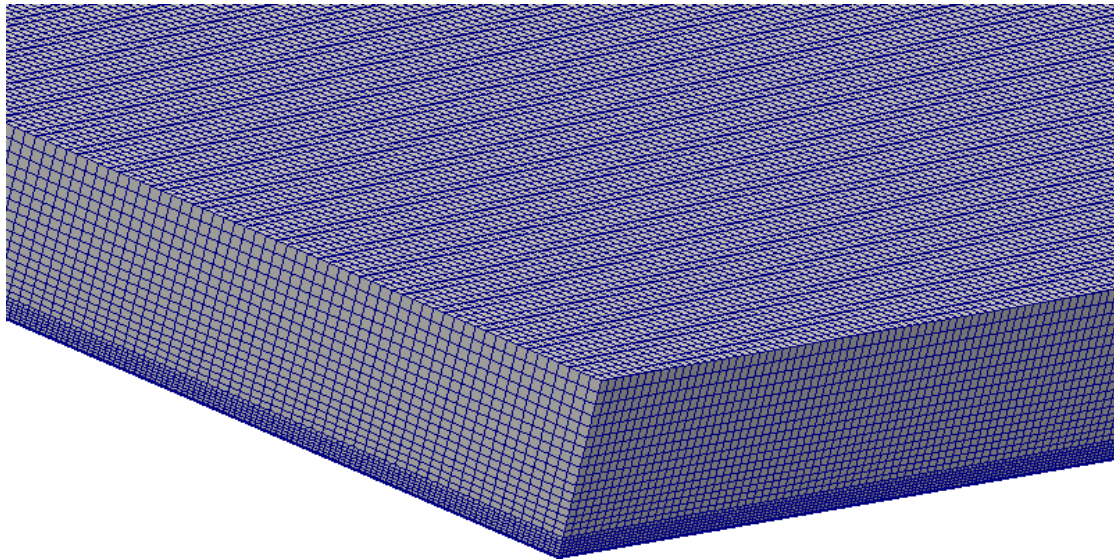


Figure 57: Meshed domain – full model

The directional refinement within box and in specified direction is defined using *dirRefineBox*. The release point (at 0.46m) and the release orientation with respect to the wind direction is illustrated in Figure 58.

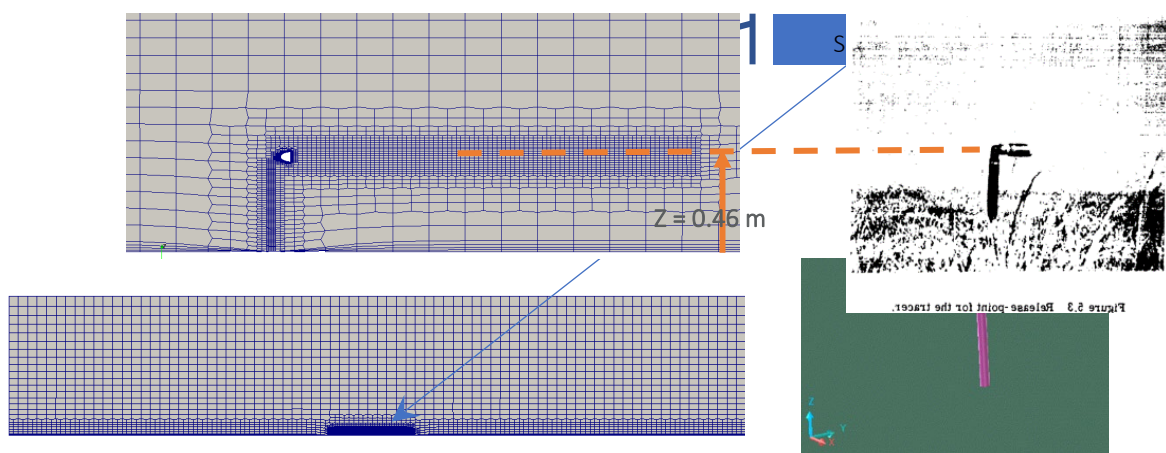


Figure 58: The meshed domain with location of the release source compared with the field trial set up

In the field trial, the wind direction was  $204^\circ$  on the day of No.09 test case. In order to reflect the wind direction impact on the dispersion of the species ( $\text{SO}_2$ ), gas release was introduced as an angle. The release was set at  $24^\circ$  (with respect to the release orientation) as illustrated in Figure 59.

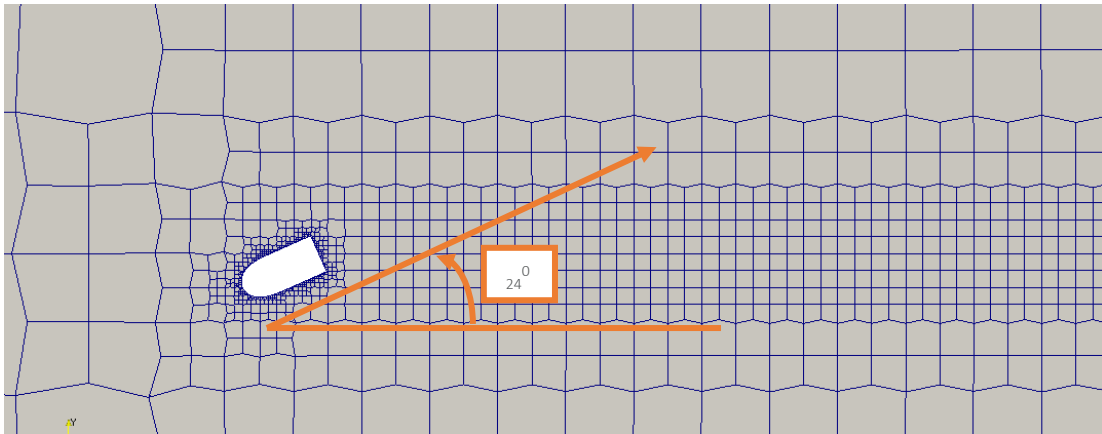


Figure 59: Release orientation with respect to the wind direction (horizontal cross section at 0.46m)

In order to achieve mesh independence, simulations for multiple mesh sizes (Meshing sensitivity) were carried out and the details are given in Section 5.3.8.

### Initial and Boundary conditions

The vertical velocity and temperature profiled need to be maintained in the solution domain. To approximate velocity profile at inlet, OpenFOAM specific boundary conditions *atmBoundaryLayerInletVelocity* was used along with *fixedShearStress* boundary condition at the top plane. The solid surfaces selected Wall function with no slip condition. Prescribed velocity (from the field trial run 09) was used for the species. *maxCo* number of 30 and *maxDeltaT* of 0.001 sec is used for accuracy and solver stability; (*maxCo* is the maximum Courant number allowed and *maxDeltaT* is the maximum time step allowed in transient simulation).

*rhoReactingBuoyantFoam*, transient solver for trans/super-sonic, turbulent flow of a compressible gas was selected and the reaction source term was switched off. The boundary condition is exactly similar to the simplified model. Only the release tube for SO<sub>2</sub> ejection has been introduced. After the steady-state simulation is done, then the inlet velocity boundary condition is copied across to the transient model inlet time 0 condition. The species / gas source release with respect to the wind direction is illustrated in Figure 60.

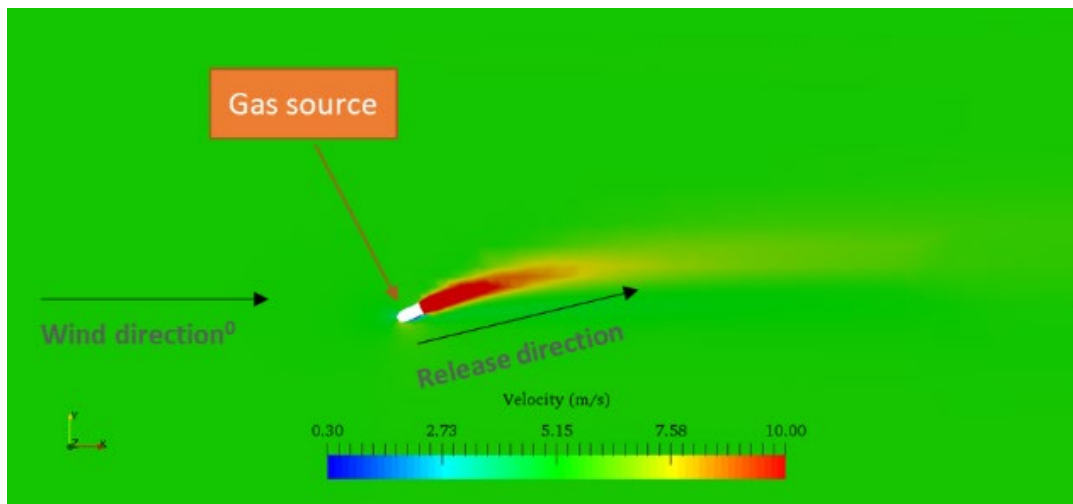


Figure 60: Species release with respect to the wind direction (horizontal cross section at 0.46m)

For each radial distance from the SO<sub>2</sub> release point, a total of 6 points on each side and 1 on the centerline, a total of 13 points are probed for SO<sub>2</sub> concentration. OpenFOAM gives the concentration in mass fraction. The unit has been changed to mg/m<sup>3</sup> using Equation 48 (Lenntech 2020)

$$\text{Concentration (value in } \frac{mg}{m^3} = 1.29 \times 10^6 \text{ (mass fraction))}$$

Equation 48

The simulation has been run for 600 sec and the average over the time-period of the pollutant dispersion has been taken. A comparison of the estimated concentration with averaged over 100 seconds and 600 seconds is given in Appendix. The concentration profile of SO<sub>2</sub> (mg/m<sup>3</sup>) along the horizontal cross section at 0.46m along z axis (above ground level) at sequence of time steps is given in Figure 61.

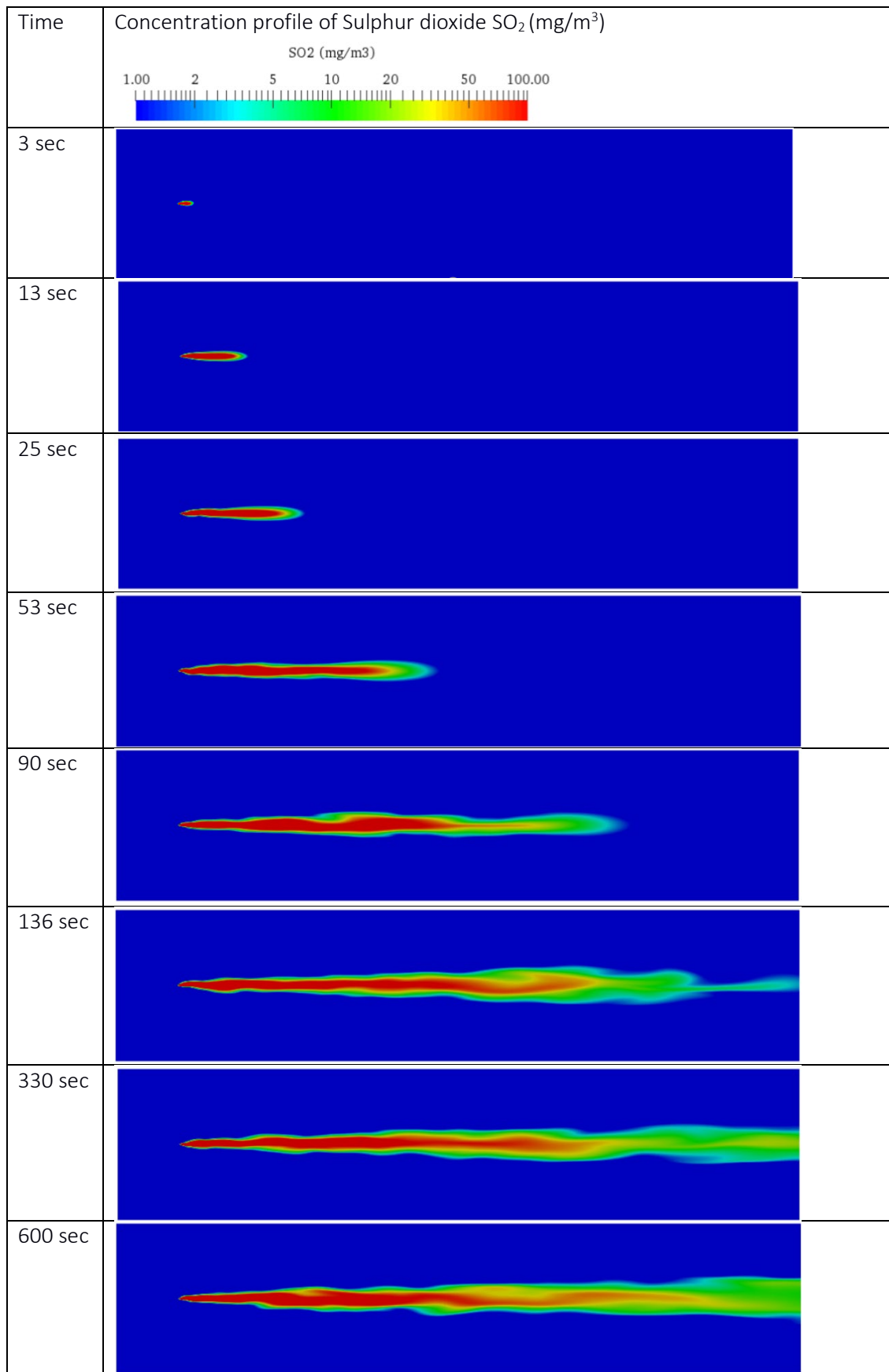


Figure 61: Dispersion of SO<sub>2</sub> representation from OpenFoam at time steps

### 5.3.4. Results along the monitoring points and comparison with field trial

A series of runs corresponding to Prairie Grass experiments #9 were completed using the University of Warwick's High-performance computing – ORAC. The estimated species concentration at the monitoring points (13 probes) along five arcs downwind from the release source averaged over 10 minutes (600 seconds) is compared with the field trial overserved concentration. The monitoring point locations and orientation with respect to the release point are given in Figure 13. The concentration comparison using scatter plot representation and to satisfy Factor of two (Fac2) criteria as given in Equation 12. Details of the experimental setup and the monitoring points is given in Section 2.10.

An example of the SO<sub>2</sub> concentration (mg/m<sup>3</sup>) estimated using *rhoReactingBuoyantFoam* k- $\omega$  SST for the 13 probe locations at 100 m downwind arc from the source is compared against the observed maximum value (56.1 mg/m<sup>3</sup>) is given in chart below Figure 62.

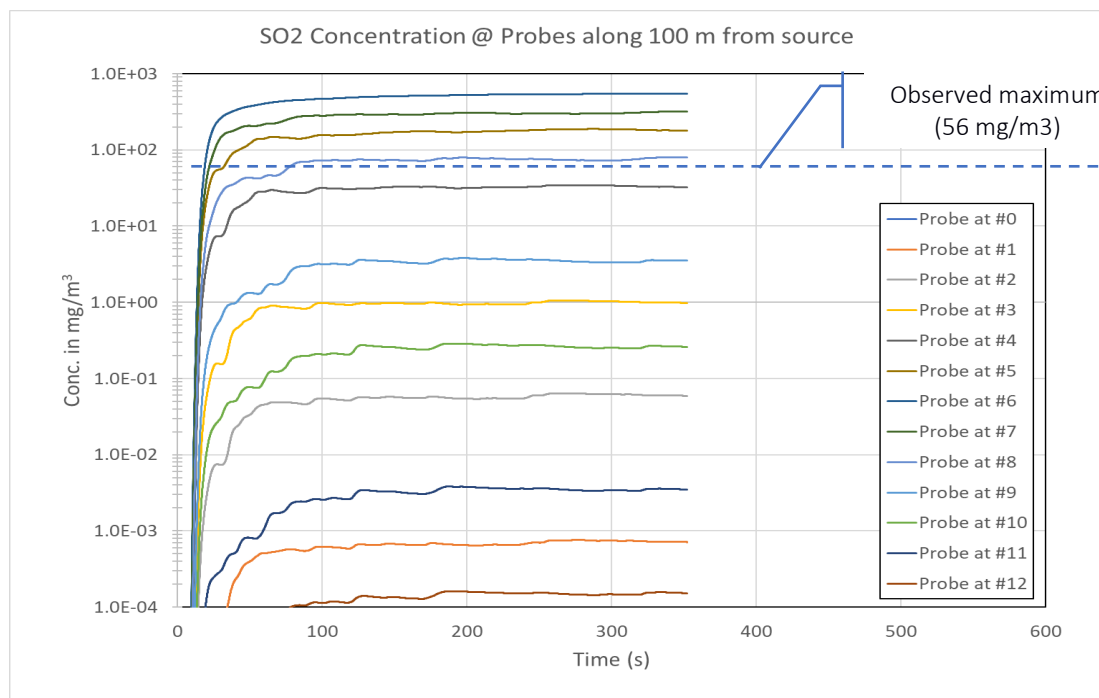


Figure 62: Concentration (SO<sub>2</sub>) estimated (OpenFOAM) at probes along 100m arc

The estimated results were averaged for 600 seconds. Monitoring point #6 is the central line along downwind, #0 towards left and #12 towards right from the source towards downwind.

### 5.3.5. Sensitivity: Mesh independence

For successful CFD simulations, meshing is a key initial step. The model validation should be carried out for adequacy of the mesh (domain, grid) and the results should be independent of the number of grids. The meshing should be fine enough such that any further improvement in the meshing with potential increase in computational cost is not proportional to the improvement in the results. A grid sensitivity study has been conducted with four different mesh resolutions. Mesh#0, Mesh#1, Mesh#2 and Mesh#3 with 0.9M, 1.3M, 2.0M and 2.3M cells. The number of cells, faces, points and faces per cell for each of the mesh is given in Table 43.

Table 43: Mesh attributes

	Cells	Faces	Points	Faces per cell
<b>Mesh#0 (0.9M)</b>	899,737	2805949	1007942	6.09
<b>Mesh#1 (1.3M)</b>	1,339,626	4159693	1481903	6.0821
<b>Mesh#2 (2.0M)</b>	2,055,428	6356387	2247355	6.0742
<b>Mesh#3 (2.3M)</b>	2,536,142	7832811	2762476	6.0706

The meshes were generated using '*snappyHexMesh*' and included six levels. The inner most level closest and around the release point with highest density of the cells as explained and illustrated in 5.3.4.2. This grid sensitivity study was conducted for mesh independence with the following objectives:

- Use mesh sensitivity analysis to derive the optimum meshing for results and run time.
- Good geometry (unique clean, watertight, without shared angles) is needed for good mesh.
- Keep the skewness, orthogonality, aspect ratio, minimum face area and growth rate low

For all four meshes, the results for checking faces in errors is given below:

- non-orthogonality > 65 degrees : 0
- faces with face pyramid volume < 1e-30 : 0
- faces with face-decomposition tet quality < 1e-30 : 0
- faces with concavity > 80 degrees : 0
- faces with area < 1e-30 m<sup>2</sup> : 0
- faces with skewness > 4 (internal) or 20 (boundary) : 0
- faces with interpolation weights (0..1) < 0.05 : 0
- faces with volume ratio of neighbour cells < 0.01 : 0



- faces with face twist < 0.02 : 0
- faces with triangle twist < 0.001 : 0
- faces on cells with determinant < 0.001 : 0

The quality of the mesh was evaluated for the following criteria (OpenFOAM 2019) and the results are reported in Table 44.

- Maximum face non-orthogonality angle [deg]: the angle made by the vector between the two adjacent cell centers across the common face and the face normal; < 65 can be used for simulation.
- Skewness: higher values may impair quality (accuracy) of the results, a reasonably high value (<20) of skewness parameter can be used for simulation.
- High aspect ratio cells usually appear in very fine boundary layers. It is not fatal for the solver stability, but can significantly decrease convergence speed (i.e., faces with skewness > 4 (internal) or 20 (boundary)). The aspect ratio close to the release point need to be good for good results whereas further away with higher aspect ratio to optimise the run time.

Table 44: Meshing – Quality criteria evaluation attributes

	Max. aspect ratio	Max skewness Criteria <4	Non-orthogonality (Max) Criteria <65
Mesh#0 (0.9M)	44.48	3.699	57.33
Mesh#1 (1.3M)	25.807	2.20579	49.68
Mesh#2 (2.0M)	39.874	2.08468	50.42
Mesh#3 (2.3M)	38.701	2.21445	52.22

All the four Meshes considered for the sensitivity checks meet the quality criteria.

### Grid Sensitivity Check 01: Comparison with Mesh#2 as base to the other three Meshes

In this sensitivity check, the SO<sub>2</sub> concentration estimated for the four different meshing (Grids) at the selected monitoring points (as in Figure 14). The percentage difference with SO<sub>2</sub> Concentrations with Mesh#2 ( $C_{M2}$ ) as the base is given in Table 45.

Table 45: Summary of the grid sensitivity in percentage difference

Monitoring point	SO <sub>2</sub> concentration (mg/m <sup>3</sup> ) at 1.5 m height				$\frac{C_{M0} - C_{M2}}{C_{M2}}$	$\frac{C_{M1} - C_{M2}}{C_{M2}}$	$\frac{C_{M3} - C_{M2}}{C_{M2}}$
	$C_{M0}$	$C_{M1}$	$C_{M2}$	$C_{M3}$			
<b>A</b>	957.96	1017.65	1000.73	999.84	-4%	2%	0%
<b>B</b>	137.57	143.84	149.44	158.84	-8%	-4%	6%
<b>C</b>	394.34	463.30	438.29	455.93	-10%	6%	4%
<b>D</b>	172.24	191.38	205.34	193.10	-16%	-7%	-6%
<b>E</b>	0.03	0.03	0.03	0.03	-1%	-7%	4%
<b>F</b>	75.58	60.31	78.18	81.87	-3%	-23%	5%
<b>G</b>	9.97	10.14	9.86	10.40	1%	3%	5%

The largest of the differences between the estimations of the Mesh#2 and Mesh#3 is 6% for one point and less than that for all other monitoring points.

### Grid Sensitivity Check 02: Averaged SO<sub>2</sub> concentration comparison between the field trail data and the meshing options

The averaged SO<sub>2</sub> concentration using different meshing compared against the observed (field trail) values along the five arcs downwind is given in Figure 63.

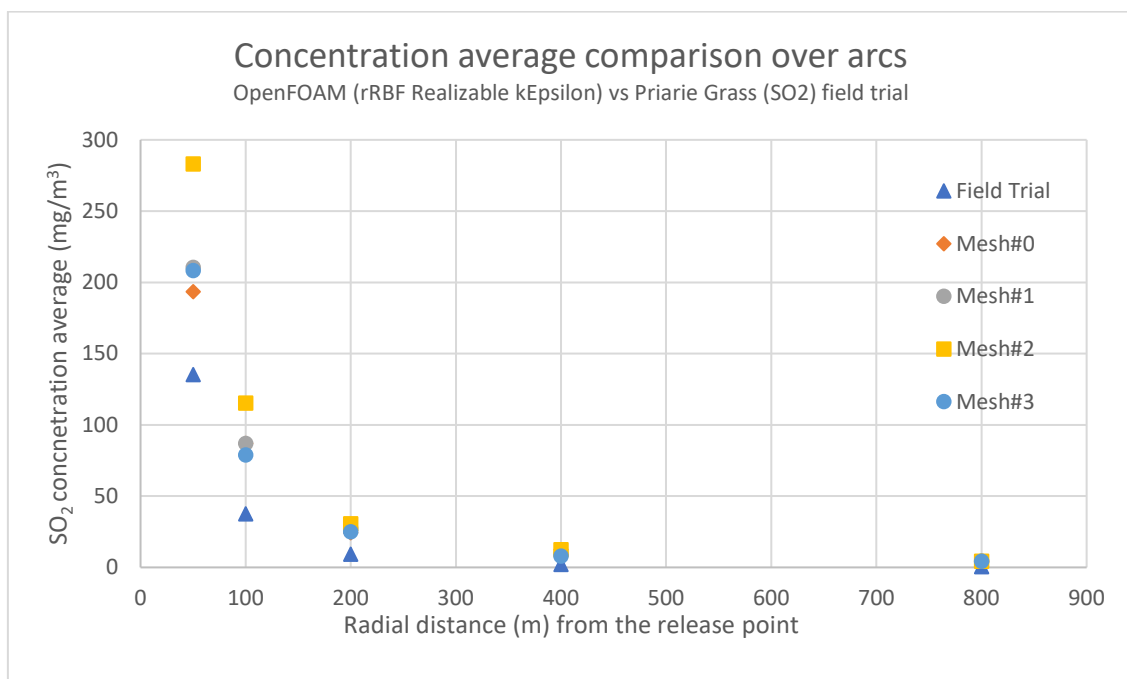


Figure 63: Comparison between the observed (field trial) and estimated (Mesh##) SO<sub>2</sub> concentration averaged over radial distances (arcs) from the release point

The model predictions (for all four Meshes) over-estimates the concentrations nearer the release points (along the arcs at 50m and 100m), but are in reasonably good agreement 200m, 400m and 800m as shown in Figure 14. For the research study purpose, the focus is on far

field estimations (to determine the impact to public from accidental releases) for which the observed and estimated results agree.

### Grid Sensitivity Check 03: Factor of data comparison between the field trail and the four meshes

Model simulation (estimated) results for all four meshes compared with the observed (field trial) concentrations using fraction of data that satisfy (references: Olesen 2001, Chang and Hanna, 2004).

Factor of two (Fac2):

$$0.5 < \frac{C_{estimated}}{C_{observed}} < 2$$

and,

Factor of five (Fac5):

$$0.2 < \frac{C_{estimated}}{C_{observed}} < 5$$

The concentration at monitoring points in comparison to the observed concentration falling within Fac2 and Fac5 for all four meshing is illustrated in figures given below.

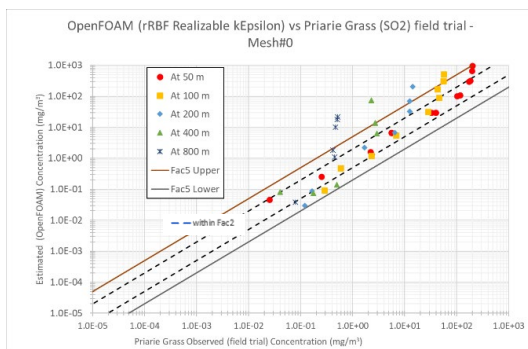


Figure 64: Grid Sensitivity, estimated (Mesh#0) vs observed concentrations within the Fac2 and Fac5

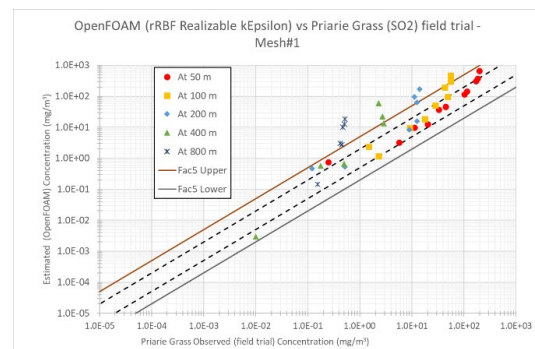


Figure 65: Grid Sensitivity, estimated (Mesh#1) vs observed concentrations within the Fac2 and Fac5

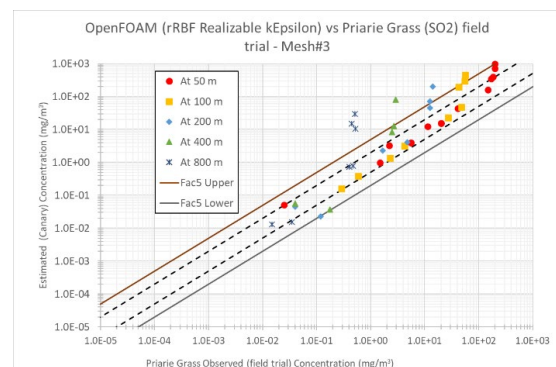
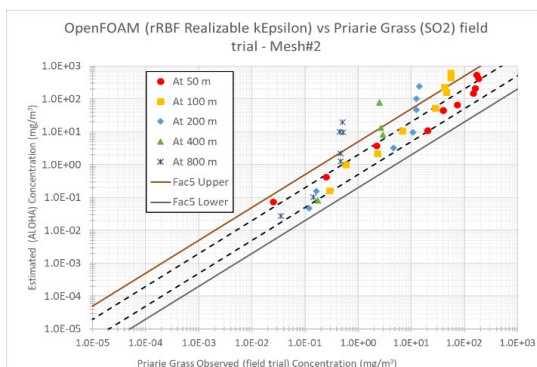


Figure 66: Grid Sensitivity, estimated (Mesh#3) vs observed concentrations within the Fac2 and Fac5

Figure 67: Grid Sensitivity, estimated (Mesh#3) vs observed concentrations within the Fac2 and Fac5

Summary of the results with the percent of estimated vs observed concentrations within Factor of Two and Factor of Five is given in Figure 68.

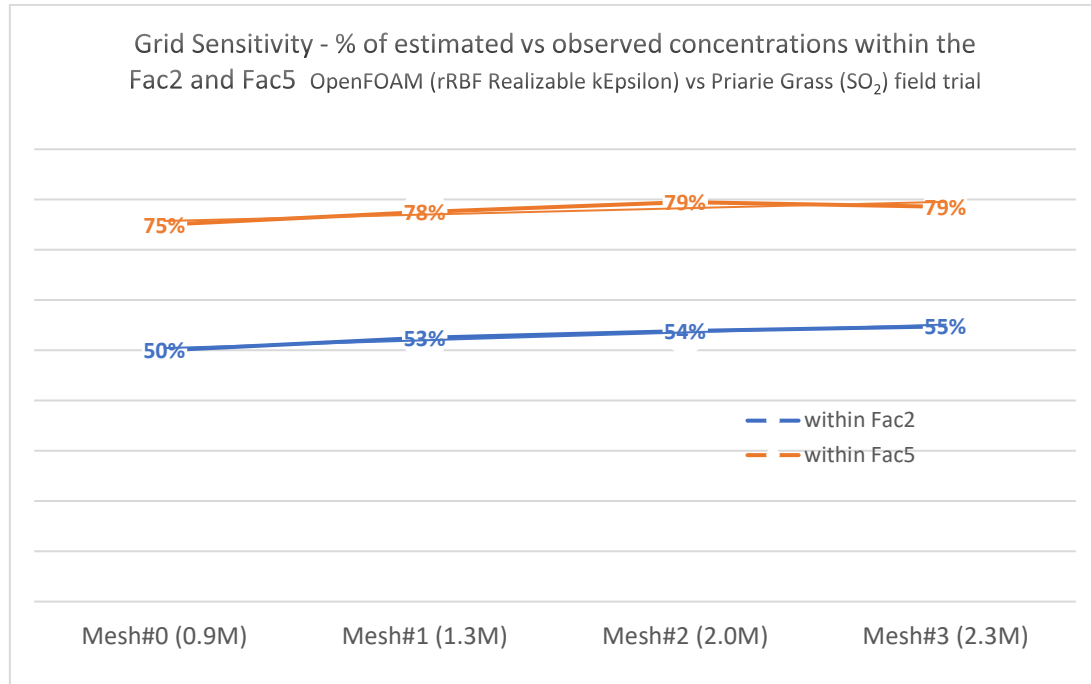


Figure 68: Grid Sensitivity, percent of the estimated vs observed concentrations within the Fac2 and Fac5

The results indicate that the estimations improve with the increase in the mesh size, i.e., with an increase in mesh from 0.9M to 2.3M, the Fac2 improved from 75% to 79% and Fac5 improved from 50% to 55%. However, it is noticed that for an increase from 2.0M to 2.3M (Mesh#2 and Mesh#3), the improvement is not significant and for the study purpose they can be considered as identical.

#### Grid Sensitivity Check 04: SO<sub>2</sub> concentration comparison along the crosswind profile between the field trail and four meshing options

Figure 69 and Figure 70 illustrates the observed concentrations seen along a sampling arc at 50m and 100m respectively. The figures show that the maximum concentration is along the central with gradual decrease towards the sides.

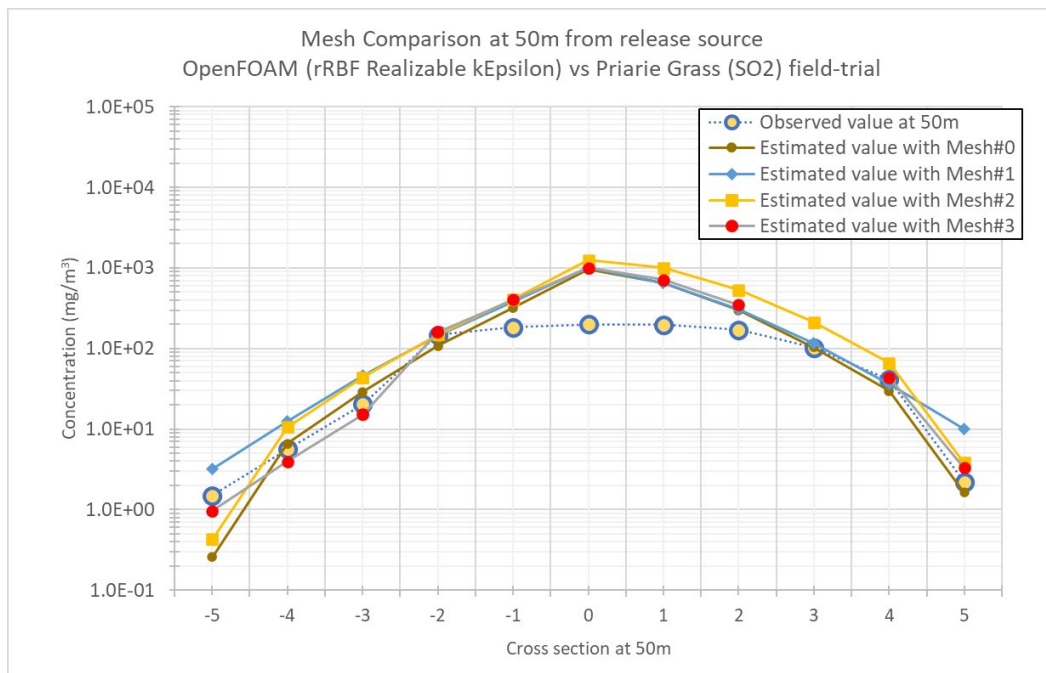


Figure 69: Grid Sensitivity - Crosswind profile of the plume dispersion at 50m

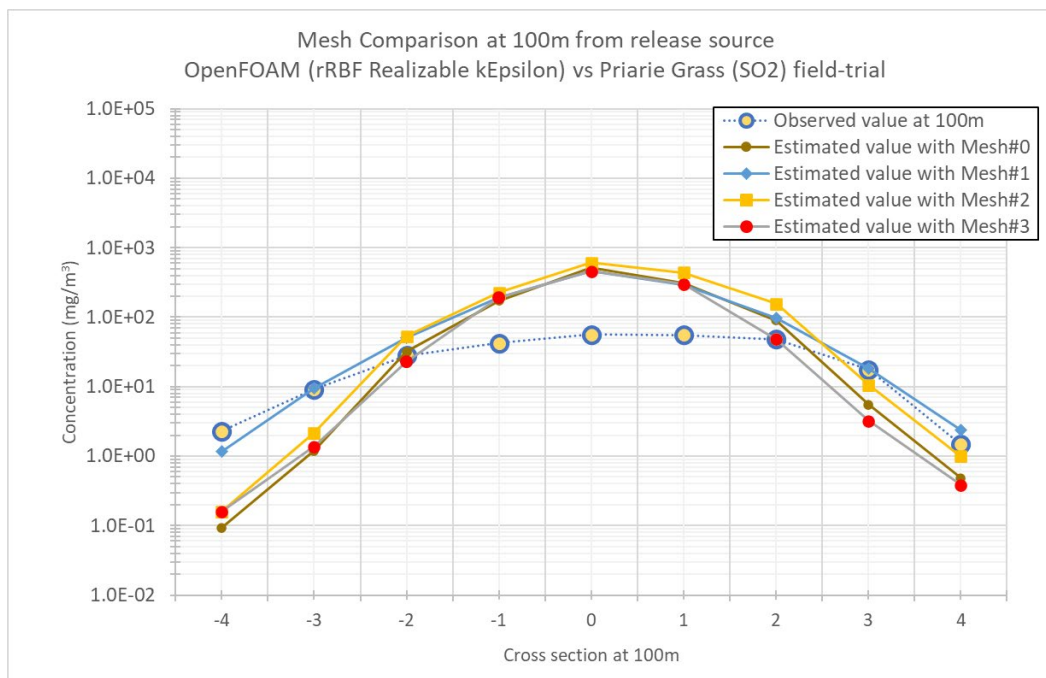


Figure 70: Grid Sensitivity - Crosswind profile of the plume dispersion at 100m

The illustrations shows that the improvement in the concentration estimation at all the 13 points improved when Mesh size increased but noticed no significant improvements when the mesh size increases from 2.05M to 2.3M.

### **Results discussion:**

The model estimation is compared to one realization out of the ensemble of all possible realizations, the discrepancy between the model estimations and the experimental measurements cannot be smaller than the expected fluctuations of the individual realizations about the ensemble mean. Therefore, it is impossible for even a perfect model to give a greater precision in its predictions of the concentration than the expected concentration variability from realization to realization in the atmospheric dispersion (Wen et. al. 2016). As noted by Cleaver et al. (2007) for the simulations of large-scale dispersions of a liquefied natural gas spill, there appeared to be a degree of consensus that the better of the more, practical models (box or similarity models) should be within a factor of 2 of the observed concentrations for a straight-forward situation within the bounds covered by the experimental data. Similar comments were also reported by Hanna et al. (1993) and Daish et al. (2000).

As noted by Wen et. al. (2016), the transport downwind follows a serpentine path, being influenced by both random and periodic wind oscillations, composed of both large- and small-scale eddies in the wind field. It is noted that in interpreting the level of agreement between the estimations and the observations (experimental measurements), one needs to recognize that the measurements of the short time-averaged concentrations obtained correspond to one realization of the instantaneous dispersion, whereas the model predictions correspond to an ensemble-averaged concentration (and as such, is associated with an average over an ensemble of realizations of the instantaneous dispersion).

The model estimations were carried out for four different mesh resolutions (0.9M, 1.3M, 2.05M and 2.3M). The model estimations improved with increased mesh resolution and are comparable for the runs with highest resolution 2.05M and 2.3M. The agreement between the data averaged over the arcs from estimations and observed is validated (Figure 63 to Figure 68). In this mesh sensitivity study, the estimated results were time averaged for 600s.

Based on the results, it was decided that the 2.05M grid resolution is used for the parametric studies to investigate the effects of concentration and wind speed for sour natural gas dispersion. For Mesh#2 (2.05M), the maximum cell aspect ratio is 39.8, the maximum grid skewness is 2.08 and the mesh non-orthogonality is 6.7 (averaged) with a maximum of 50. Atmospheric transport and dispersion processes include stochastic components.

### 5.3.6. Sensitivity: Transient Turbulence Eddy simulation

To further evaluate the potential improvement in the predictions which can be achieved by the use of Synthetic turbulence, Divergence Free Synthetic Eddy Method (DFSEM), was carried out for inflow turbulence and to maintain turbulence through the field (OpenFOAM 2019). The geometry with 2.05 million cell grid resolution was used for this sensitivity. The results comparison between k-omega Shear Stress Transport ( $k\omega$ -SST) Delayed Detached Eddy simulation (DDES) and DFSEM  $k\omega$ -SST is given in Table 46 and Table 47, the scatter plots are given in Figure 71 and Figure 72.

**Table 46: Turbulence model sensitivity concentration (SO<sub>2</sub>) Observed vs Estimated for DDES  $k\omega$ -SST**

Monitoring point	Observed	Estimated	Observed	Estimated	Observed	Estimated	Observed	Estimated	Observed	Estimated
	At 50 m		At 100 m		At 200 m		At 400 m		At 800 m	
0	56.1	0.03	9.18	0.00	0.12	0.00				
1	67.2	0.19	17.3	0.00	1.68	0.00			0.035	
2	93.5	6.25	26.9	0.06	4.67	0.00			0.055	
3	115	29.23	28.2	0.98	8.93	0.02	0.175		0.135	0.00
4	148	114.7	32.9	32.48	9.83	1.70	1		0.255	0.00
5	183	355.3	42.6	179.9	12.5	32.65	2.48	0.00	0.415	0.00
6	200	1101	56.1	547.8	14.2	209.2	2.9	0.00	0.52	0.01
7	198	759.8	55.7	317.1	11.3	55.28	2.14	0.00	0.46	0.49
8	171	336.3	45.9	79.12	10.9	3.72	2.26	0.00	0.44	8.06
9	159	108.5	44.4	3.51	12.2	0.05	2.29	0.04	0.47	22.24
10	130	28.19	48.5	0.26	12.6	0.00	2.53	5.46	0.47	8.80
11	123	1.23	41.3	0.00	10.6	0.00	2.68	76.53	0.45	0.76
12	114	0.22	38.7	0.00	9.73	0.00	2.63	7.45	0.405	0.01

**Table 47: Turbulence model sensitivity concentration (SO<sub>2</sub>) Observed vs Estimated for DFSEM  $k\omega$ -SST**

Monitoring point	Observed	Estimated	Observed	Estimated	Observed	Estimated	Observed	Estimated	Observed	Estimated
	At 50 m		At 100 m		At 200 m		At 400 m		At 800 m	
0	56.1	1.63	9.18	0.00	0.12	0.00				
1	67.2	5.24	17.3	0.06	1.68	0.00			0.035	
2	93.5	48.22	26.9	2.33	4.67	0.01			0.055	0.00

Monitoring point	Observed	Estimated	Observed	Estimated	Observed	Estimated	Observed	Estimated	Observed	Estimated
	At 50 m		At 100 m		At 200 m		At 400 m		At 800 m	
3	115	105.7	28.2	10.67	8.93	0.48	0.175		0.135	0.00
4	148	211.5	32.9	83.03	9.83	9.78	1		0.255	0.03
5	183	333.3	42.6	167.3	12.5	42.82	2.48	0.00	0.415	0.27
6	200	568.4	56.1	280.8	14.2	96.67	2.9	0.00	0.52	2.02
7	198	546.5	55.7	270.2	11.3	80.18	2.14	0.00	0.46	4.94
8	171	437.7	45.9	165.5	10.9	27.37	2.26	0.00	0.44	6.88
9	159	281.5	44.4	45.23	12.2	2.03	2.29	0.32	0.47	7.96
10	130	149.9	48.5	8.66	12.6	0.03	2.53	7.17	0.47	2.77
11	123	27.46	41.3	0.36	10.6	0.00	2.68	31.65	0.45	0.21
12	114	8.54	38.7	0.05	9.73	0.00	2.63	21.28	0.405	0.03

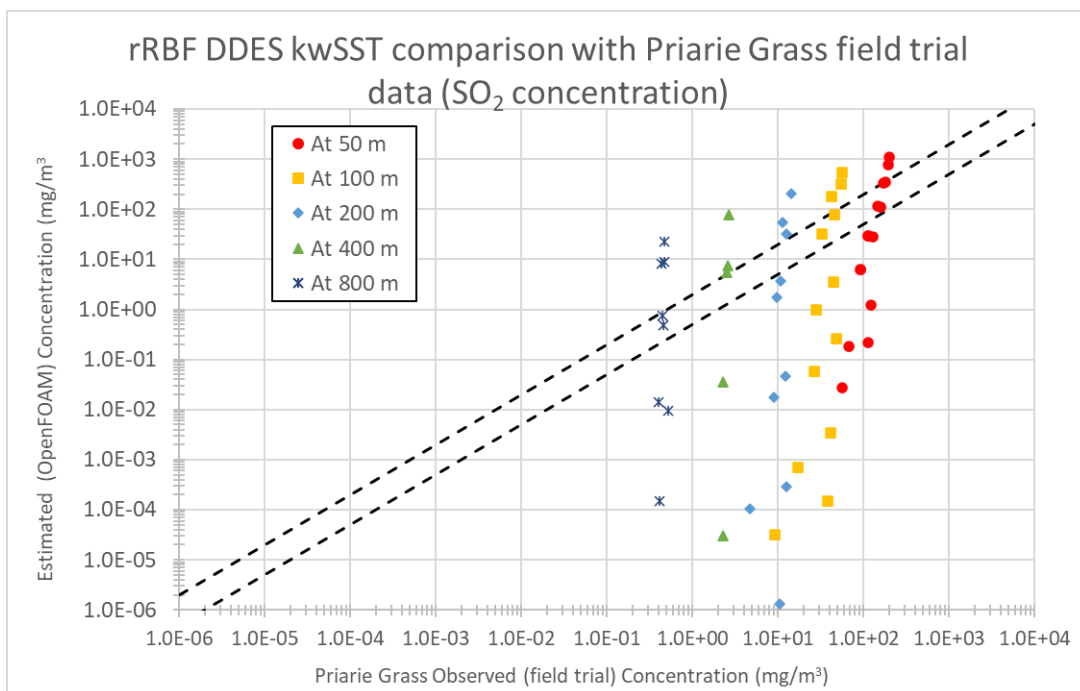


Figure 71: Turbulence model sensitivity, Concentration (SO<sub>2</sub>) scatter plot - observed vs estimated comparison for DDES  $k\omega$ -SST

Interpretation of the results, grouped into three sets:

1. The estimated concentration along the central line of the downwind dispersion of the toxic cloud is higher than observed (above the dashed line in Scalar plot).



2. Comparable or similar values on either side of the central line (within the two dashed line in scalar plot), good model to have most of the results in this area.
3. The estimated concentration is lesser than observed (below the dashed line in Scalar plot).

From the comparison, the CFD (OpenFOAM) estimated cloud concentration is higher along the central line (traveling further downwind) and the crosswind dispersion is lesser compared to the field trial observed values. This difference is due to the modelling capability and differences in the turbulence generation and estimation for lower averaging time (less than 1 hour); Prairie Grass observations were made for short averaging time (10 minutes). It is also noted that the estimated concentrations at the outer envelope of the cloud is of very low concentrations (<1 ppm) and hence the comparison results is not of significance in the toxic risk management. In this study, some of those noises (results of non-significance) is scrubbed from the graphs in the next sections.

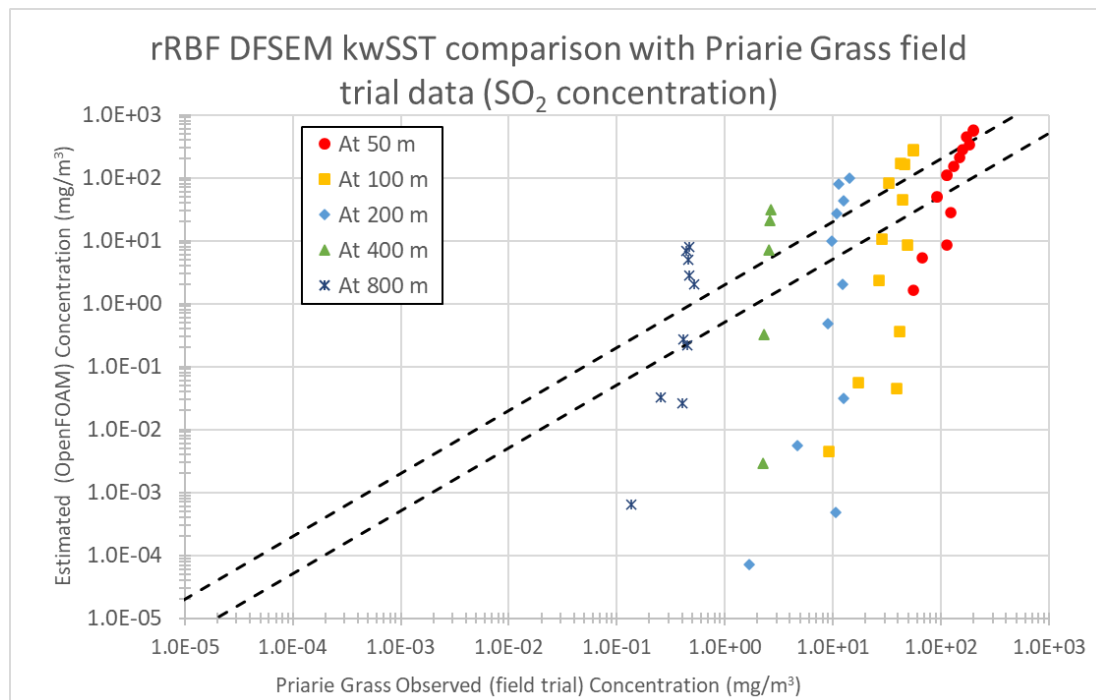


Figure 72: Turbulence model sensitivity, Concentration ( $\text{SO}_2$ ) scatter plot - observed vs estimated comparison for DFSEM  $k\omega$ -SST

DFSEM (*turbulentDFSEMInlet*) condition generates turbulent eddies that are continuously evolved across an inlet patch, based on the Reynolds stresses, velocity profile and eddy length scales. Eddies are injected to generate coherent flow structures that persist into the domain, aiding the process of establishing a fully developed turbulent flow. Through this approach,

marginally higher wind velocity (>1 m/s) was maintained at farther downwind distances (e. @800 m) from the inlet and source. However, the runs require higher mesh refinement, higher computational power (7 days for with DFSEM synthetic turbulence compared to 1 day otherwise). A comparison of the wind velocity estimations along X, Y and Z for the two turbulence model approaches are given in Figure 73 to Figure 78 .

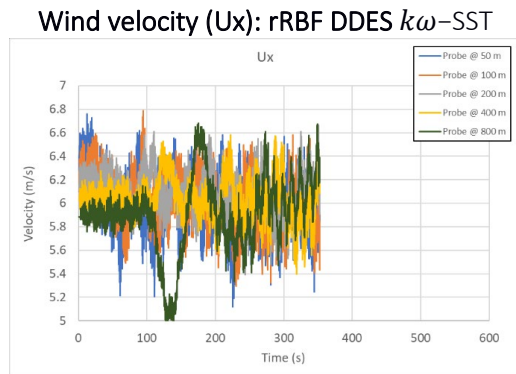


Figure 73: Wind velocity along  $x$  direction for rRBF DDES  $k\omega$ -SST

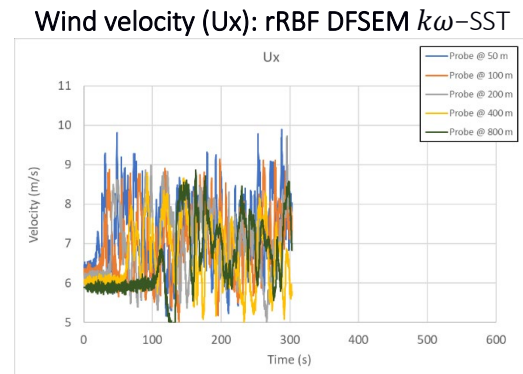


Figure 74: Wind velocity along  $x$  direction for rRBF DFSEM  $k\omega$ -SST

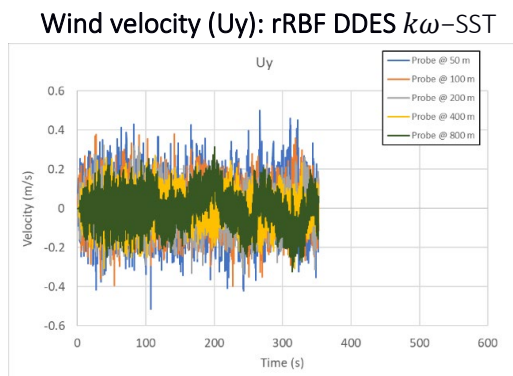


Figure 75: Wind velocity along  $y$  direction for rRBF DDES  $k\omega$ -SST

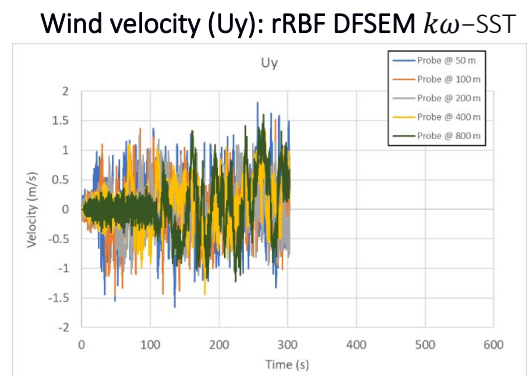


Figure 76: Wind velocity along  $y$  direction for rRBF DFSEM  $k\omega$ -SST

**Wind velocity (Uz): rRBF DDES  $k\omega$ -SST**

**Wind velocity (Uz): rRBF DFSEM  $k\omega$ -SST**

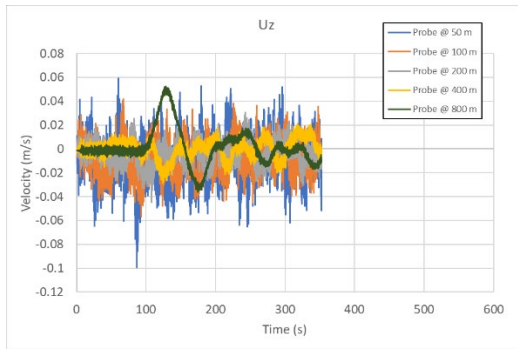


Figure 77: Wind velocity along z direction for rRBF DDES  $k\omega$ -SST

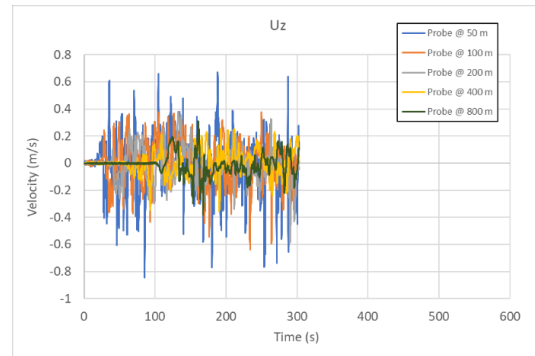


Figure 78: Wind velocity along z direction for rRBF DFSEM  $k\omega$ -SST

Both turbulence eddy simulation approach estimations are similar for concentration and velocity profile. However, it is noted that with synthetic turbulence (DFSEM) the computational time and resource is significantly higher, but the estimates are not significantly different.

### 5.3.7. Sensitivity: Transient Turbulence Models

A comparison study was carried out between Unsteady Reynolds Averaged Simulation (RAS) models Realizable  $k\epsilon$  ( $k\epsilon$ ) model and  $k\omega$ -SST. The results for transient turbulence model  $k\epsilon$  for *rhoReactingBuoyantFoam* (rRBF) solver is given in Table 48 and the concentration comparison scatter plot in Figure 79. The results is comparison with  $k\omega$ -SST DDES (Table 46 and Figure 71).

Table 48: Turbulence model sensitivity concentration ( $SO_2$ ) Observed vs Estimated for realizable  $k\epsilon$

Monitoring point	Observed	Estimated	Observed	Estimated	Observed	Estimated	Observed	Estimated	Observed	Estimated
	At 50 m		At 100 m		At 200 m		At 400 m		At 800 m	
0	56.1	0.07	9.18	0.00	0.12	0.00				
1	67.2	0.43	17.3	0.00	1.68	0.00			0.035	
2	93.5	10.65	26.9	0.16	4.67	0.00			0.055	
3	115	43.87	28.2	2.16	8.93	0.05	0.175		0.135	0.00
4	148	149.4	32.9	53.03	9.83	3.18	1		0.255	0.00
5	183	408.7	42.6	225.3	12.5	46.75	2.48	0.00	0.415	0.00
6	200	1247.9	56.1	610.3	14.2	238.9	2.9	0.00	0.52	0.03
7	198	1000.7	55.7	438.3	11.3	99.28	2.14	0.00	0.46	1.28
8	171	536.0	45.9	156.1	10.9	9.46	2.26	0.00	0.44	9.54
9	159	211.4	44.4	10.61	12.2	0.16	2.29	0.08	0.47	19.71
10	130	66.03	48.5	1.00	12.6	0.00	2.53	8.19	0.47	9.86

Monitoring point	Observed	Estimated	Observed	Estimated	Observed	Estimated	Observed	Estimated	Observed	Estimated
	At 50 m		At 100 m		At 200 m		At 400 m		At 800 m	
11	123	3.83	41.3	0.02	10.6	0.00	2.68	78.18	0.45	2.16
12	114	0.76	38.7	0.00	9.73	0.00	2.63	13.10	0.405	0.10

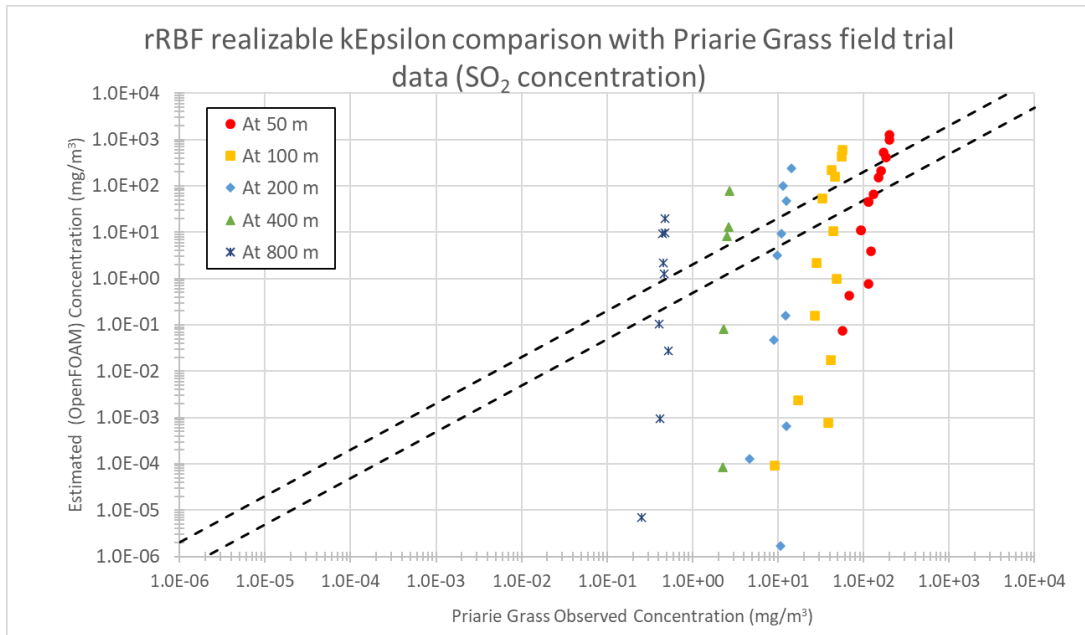


Figure 79: Turbulence model sensitivity, Concentration (SO<sub>2</sub>) scatter plot - observed vs estimated comparison for kEpsilon ( $k\varepsilon$ )

A summary of the sensitivity to the turbulence models, time averaging and the release orientation with respect to the wind direction comparisons is given in Table 49.

Table 49: Concentration (SO<sub>2</sub>) at 50 m Observed vs Estimated for sensitivity comparison summary

Monitoring point	Observed (Prairie Grass run #09)	rRBF DDES- $k\omega$ -SST ABL	rRBF DDES- $k\omega$ -SST ABL (10min ave.)	#1: rRBF DDES $k\omega$ -SST (@ 24°)	#4: rRBF realizable $k\varepsilon$
0	56.1	0.00	0.00	0.03	0.07
1	67.2	0.01	0.01	0.19	0.43
2	93.5	0.86	0.79	6.25	10.65
3	115	6.26	5.84	29.23	43.87
4	148	39.60	37.67	114.67	<b>149.44</b>
5	183	204.79	198.48	355.63	408.68
6 (Central line)	200	1459.17	1438.35	1100.62	1247.97
7	198	805.65	781.85	759.74	1000.73
8	171	239.64	227.77	336.31	536.00
9	159	49.08	45.71	108.46	211.43

Monitoring point	Observed (Prairie Grass run #09)	rRBF DDES- $k\omega$ -SST ABL	rRBF DDES- $k\omega$ -SST ABL (10min ave.)	#1: rRBF DDES $k\omega$ -SST (@ 24 <sup>0</sup> )	#4: rRBF realizable $k\varepsilon$
10	130	7.98	7.32	28.19	66.03
11	123	0.14	0.12	1.23	3.83
12	114	0.02	0.01	0.22	0.76

A summary of the averaged concentration across all the monitoring points (probes) along the downwind distance arcs for the sensitivity runs compared to the average of the observed concentration ( $\text{SO}_2$  in  $\text{mg}/\text{m}^3$ ) is given in Table 50.

Table 50: Averaged concentration ( $\text{SO}_2$ ) along the downwind arc of monitoring points (across all 13 probes)

Monitoring point	Observed (Prairie Grass run #09)	rRBF DDES, $k\omega$ -SST ABL	rRBF DDES- $k\omega$ -SST ABL (10min ave.)	#1: rRBF DDES $k\omega$ -SST (@ 240)	#4: rRBF realizable $k\varepsilon$
Ave. at 50m	135.2154	216.40	211.07	218.519622	283.069
Ave. at 100m	37.51385	99.16	96.24	89.32742	115.1578
Ave. at 200m	9.173846	27.45	26.17	23.27691	30.59446
Ave. at 400m	2.1085	-	14.96	11.18489	12.44371

Through these sensitivity checks, it is demonstrated that OpenFOAM with *rhoReactingBuoyantFoam* solver with Realizable  $k\varepsilon$  DDES turbulence can be used to predict the gas dispersion of interest in this study.

### 5.3.8. Validation modelling summary

OpenFOAM model simulation was carried out for Prairie Grass ( $\text{SO}_2$ ) field trial data for Run #9. The model performance statistics for stable conditions were satisfactory at the 400m and 800m arcs.

- Inlet velocity boundary condition for transient runs were determined using a separate steady-state simulation.
- *rhoReactingBuoyantFoam* (rRBF) solver and four options evaluated for turbulence
  - rRBF realizable  $k\varepsilon$  estimations provided the closest for velocity profile.
  - rRBF DFSEM DDES  $k\omega$ -SST estimations provided the closest to observed field trial concentrations.

- Estimated results comparable to observed values (meeting quality criteria) for monitoring points nearside of the central line.
- The results the model seems to be over-predicting the concentration near the centerline and under-predicting further away from centerline (cross-diffusion not correctly modelled).

## 6. Sour Natural Gas dispersion modelling results and analysis

Dispersion behaviour analysis is a critical topic to study in the consequence modelling and risk management of natural gas pipeline transportation. Natural gas leakage accidents of major scale have occurred in the Chongqing onshore facility, China in 2003 (Nair & Wen, 2019b) and Kab-121 platform in the Gulf of Mexico in 2007 (Zhu et.al., 2010). Since these accidental gas releases contained hydrogen sulphide, the events resulted in fatalities and mass evacuation. Therefore, studying the toxic gas release and dispersion is quite important to prevent and control similar accidents. In the paper by Yang et.al, the results demonstrate that gas composition is a driving factor for dispersion characteristics of blowout gas in an offshore environment (Yang et al., 2019).

Taking a representative sour natural gas (hydrogen sulphide-containing gas) leakage accident as an example, the hydrogen sulphide diffusion process is simulated using OpenFOAM and the sensitivity to the composition is evaluated. Natural gas ( $\text{CH}_4$ ) with three  $\text{H}_2\text{S}$  compositions (5%, 15% and 20%) were evaluated for downwind dispersion concentrations. The geometry, meshing, solver, and boundary conditions validated (given in Chapter 5) is used for the simulations. A study by Gupta and Chan evaluated the models for the leakage and dispersion of gas with a time-varying leakage rate confirms that using the constant leakage rate may be relatively reasonable for systems with slow depressurization rates (Gupta and Chan, 2016). A small sized release from a long-distance pipeline carrying natural gas, it is appropriate to consider that the depressurization rate is not significant. This study uses a constant release rate of sour natural gas.

### 6.1. Case Study

For the case study, a continuous natural gas release of 92 g/s from 2-inch diameter source located near ground level (at height 46 cm) was used as the leak source. The gas temperature 28 °C, wind speed 6.8 m/s (at source), wind direction 204° and surface roughness 5 mm was used as the input to the model set up. The release conditions and the OpenFOAM model set-up used for the validation was used for the  $\text{H}_2\text{S}$  bearing natural gas dispersion sensitivity case study. A vertical temperature and wind velocity profile was established prior to the dispersion modelling simulation. The velocity profile details at the probes is given in Appendix. The main simulation parameters are summarised in Table 51.

Table 51: OpenFOAM Natural Gas dispersion – Simulation parameters

Meteorological conditions	Atmospheric temperature	Wind speed	Wind direction
	25.7 °C to 28.7 °C	4.5 m/s to 8.8 m/s	204°
Emission conditions	Latitude	Longitude	Pollutant species
	42° 29.6' North	98° 34.3' West	Methane (CH <sub>4</sub> ) and Hydrogen sulphide (H <sub>2</sub> S)

The computational domain (geometry) extends 1100 m in x direction (length), 240 m in y direction (width) and 40 m in z direction (height). The release source is at the point of 100 m, 120 m, 0.46 m (x, y, z). The geometry with 2.05 million cell grid resolution was used for this sensitivity assessment of natural gas composition. The natural gas downwind dispersion as the concentration of Methane (CH<sub>4</sub>) and Hydrogen sulphide (H<sub>2</sub>S) at 13 probes (locations) at 1.5 m height, spread across the cloud width along the downwind arcs set at 50 m, 100 m, 200m, 400 m, 800 m was estimated. The concentrations estimated and averaged over 600 seconds; the results were analysed using the flammable and toxic exposure criteria.

## 6.2. Toxicity and flammability concentrations of interest

To provide the decision support, for the natural gas processing facility site selection and the emergency response planning, the dispersion modelling should be carried out to the concentrations specified by the standards or by the regulators. The following H<sub>2</sub>S airborne concentration from different standards group are adopted in this study.

- 0.51 ppm, AEGL-1, for exposure period 60 minutes
- 17 ppm, AEGL-2, for exposure period 8 hours
- 30 ppm, ERPG-2, for exposure period of 60 minutes
- 100 ppm, IDLH, for any length of time unless equipped and protected to be in that environment.

AEGL-1 and AEGL-2, by US EPA, are the airborne concentration of a substance above which it is predicted that the exposed population, could experience notable discomfort and irreversible health effects (or an impaired ability to escape) respectively.



ERPG-2, by AIHA, is the maximum airborne concentration below which it is believed nearly all individuals could be exposed for up to 1 hour without experiencing or developing irreversible or other serious health effects or symptoms that could impair an individual’s ability to take protective action.

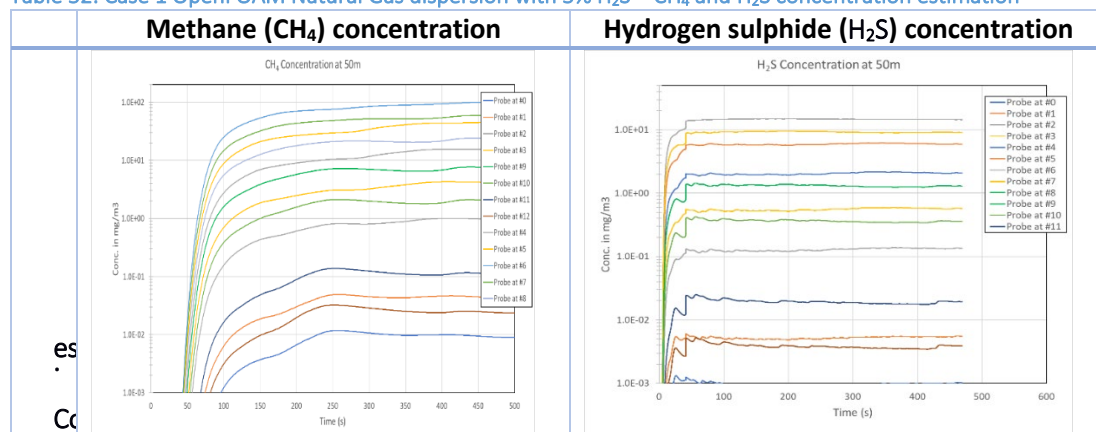
IDLH limit, by NIOSH, represents the concentration of a chemical in the air to which healthy adult workers could be exposed (if their respirators fail) without suffering permanent or escape-impairing health effects.

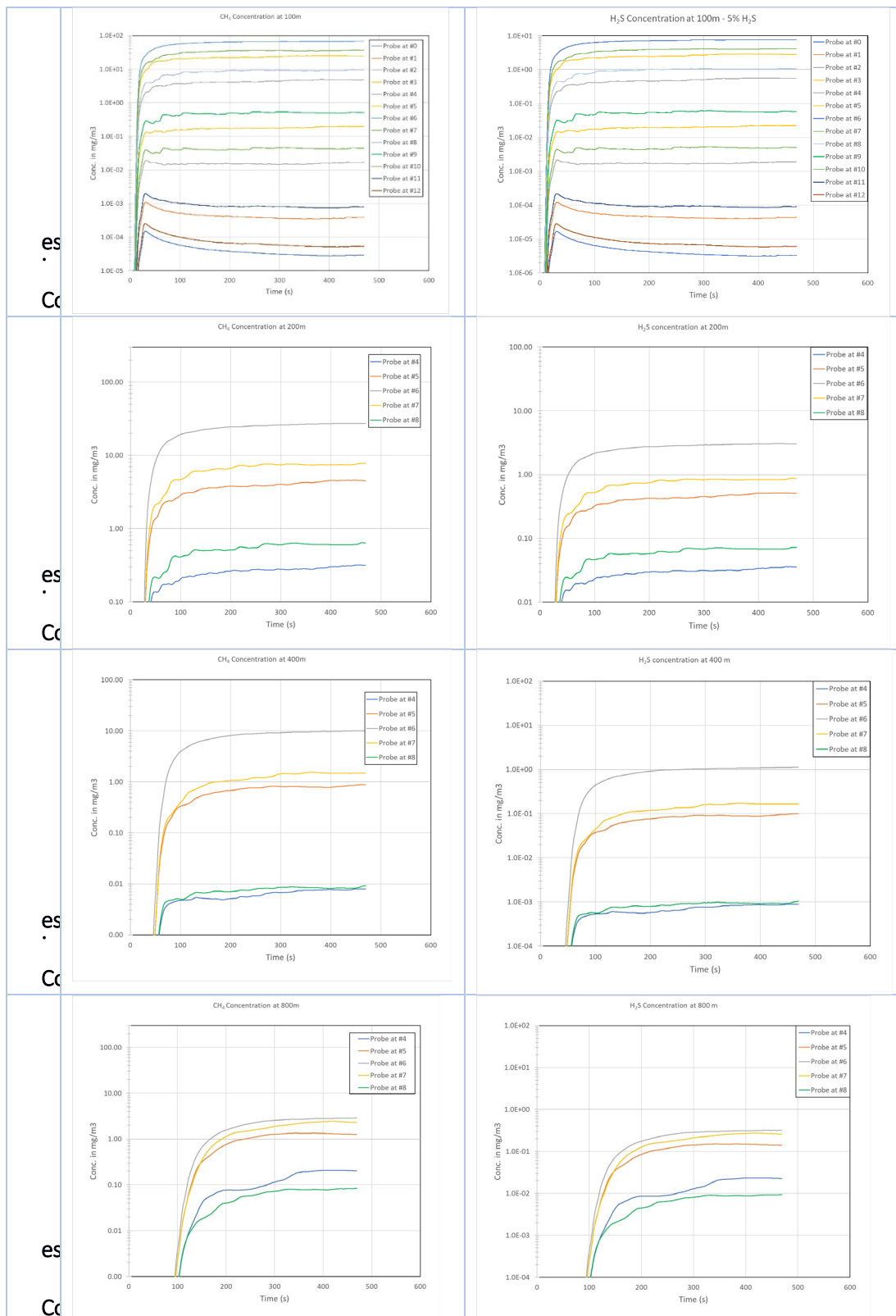
Similarly, the flammability/explosion limits of flammable gases are important parameters to measure the possibility of the fire/explosion of flammable gas under certain initial conditions, which defines the range of fuel concentrations for flame propagation to occur. The lower flammable limit (LFL) and upper flammable limit (UFL) are the minimum and maximum composition limits, respectively, which a flame can propagate. The lower flammability limit (LFL) of methane is 5 % in volume or 50,000 ppm. For early detection and emergency planning purposes, 10% of LFL (5000 ppm) is typically used for alarms and 25% LFL for initiating process-plant trip actions.

### 6.3. Case 1: Natural gas with 5% H2S

The first case evaluated was the natural gas composition with 95% CH<sub>4</sub> and 5% H<sub>2</sub>S. The CH<sub>4</sub> and H<sub>2</sub>S concentrations were estimated at the 13 probes (locations) along the five downwind arcs. The concentration of both species, estimated at each probe with the progression of time is given in Table 52.

Table 52: Case 1 OpenFOAM Natural Gas dispersion with 5% H<sub>2</sub>S – CH<sub>4</sub> and H<sub>2</sub>S concentration estimation





The CH<sub>4</sub> concentration estimated (time averaged) from the natural gas dispersion is given in Table 53 and the CH<sub>4</sub> concentration in the cloud along the probes is illustrated in Figure 80.

Table 53: Case 1 OpenFOAM Natural Gas dispersion with 5% H<sub>2</sub>S – CH<sub>4</sub> concentration at the probes

Methane (CH <sub>4</sub> ) concentration – time averaged over 600 seconds													
probe at	0	1	2	3	4	5	6	7	8	9	10	11	12
50 m	0.0	0.0	1.2	5.1	18.4	52.3	127	79.2	33.8	11.2	3.1	0.2	0.0
100 m	0.0	0.0	0.0	0.2	4.8	24.9	67.1	36.6	9.4	0.5	0.0	0.0	0.0
200 m	0.0	0.0	0.0	0.0	0.3	4.5	27.2	7.8	0.6	0.0	0.0	0.0	0.0
400 m	0.0	0.0	0.0	0.0	0.0	0.9	10.1	1.5	0.0	0.0	0.0	0.0	0.0
800 m	0.0	0.0	0.0	0.0	0.2	1.3	2.9	2.3	0.1	0.0	0.0	0.0	0.0

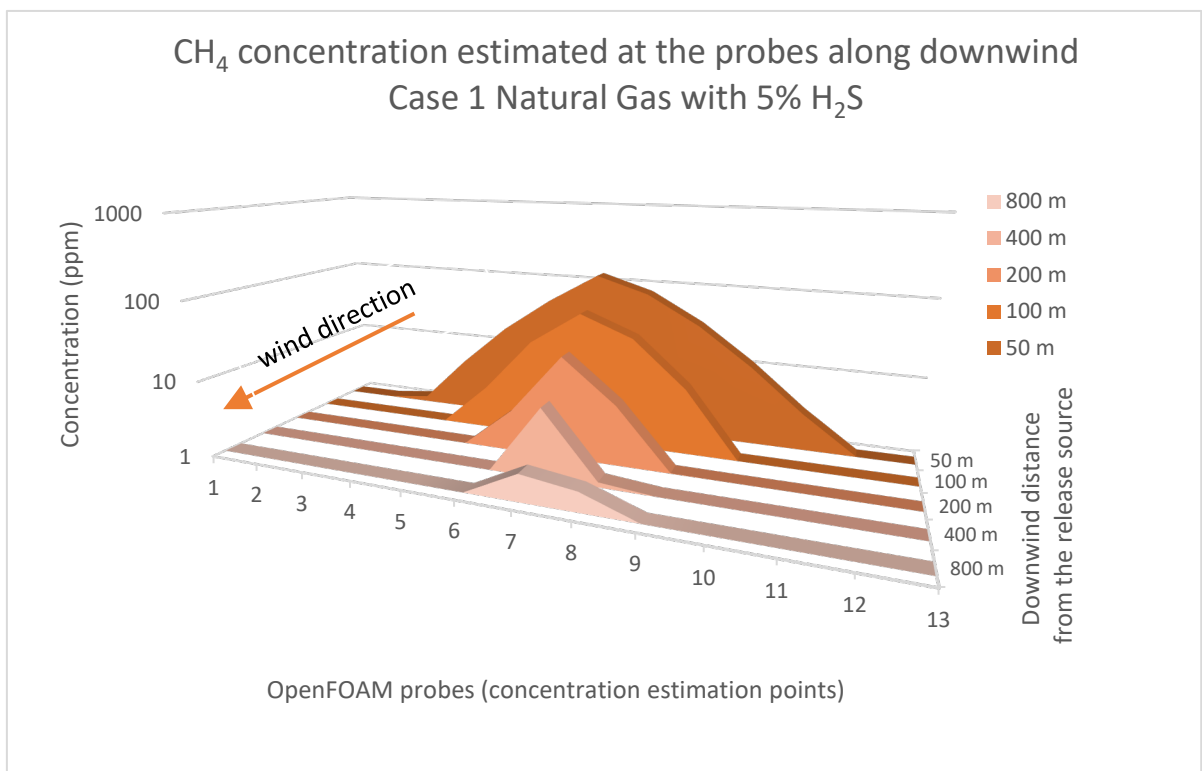


Figure 80: Case 1 OpenFOAM Natural Gas dispersion with 5% H<sub>2</sub>S - downwind dispersion of CH<sub>4</sub> concentration

5000 ppm (10% LFL) concentrations of Methane not predicted at any of the monitoring points. The results imply that the flammability hazard from this release is not of any significant concern.

The H<sub>2</sub>S concentration estimated at the 13 probes (locations) along the downwind arcs for Case 1 (natural gas composition 95% CH<sub>4</sub> and 5% H<sub>2</sub>S) is given in Table 54 and the H<sub>2</sub>S concentration in the cloud along the probes is illustrated in Figure 81.

Table 54: Case 1 OpenFOAM Natural Gas dispersion with 5% H<sub>2</sub>S – H<sub>2</sub>S concentration at the probes

Hydrogen sulphide (H <sub>2</sub> S) concentration													
probe at	0	1	2	3	4	5	6	7	8	9	10	11	12
50 m	0.0	0.0	0.1	0.6	2.1	5.9	14.5	9.1	3.9	1.3	0.4	0.0	0.0
100 m	0.0	0.0	0.0	0.0	0.6	2.8	7.7	4.2	1.1	0.1	0.0	0.0	0.0
200 m	0.0	0.0	0.0	0.0	0.0	0.5	3.0	0.9	0.1	0.0	0.0	0.0	0.0
400 m	0.0	0.0	0.0	0.0	0.0	0.1	1.1	0.2	0.0	0.0	0.0	0.0	0.0
800 m	0.0	0.0	0.0	0.0	0.0	0.1	0.3	0.3	0.0	0.0	0.0	0.0	0.0

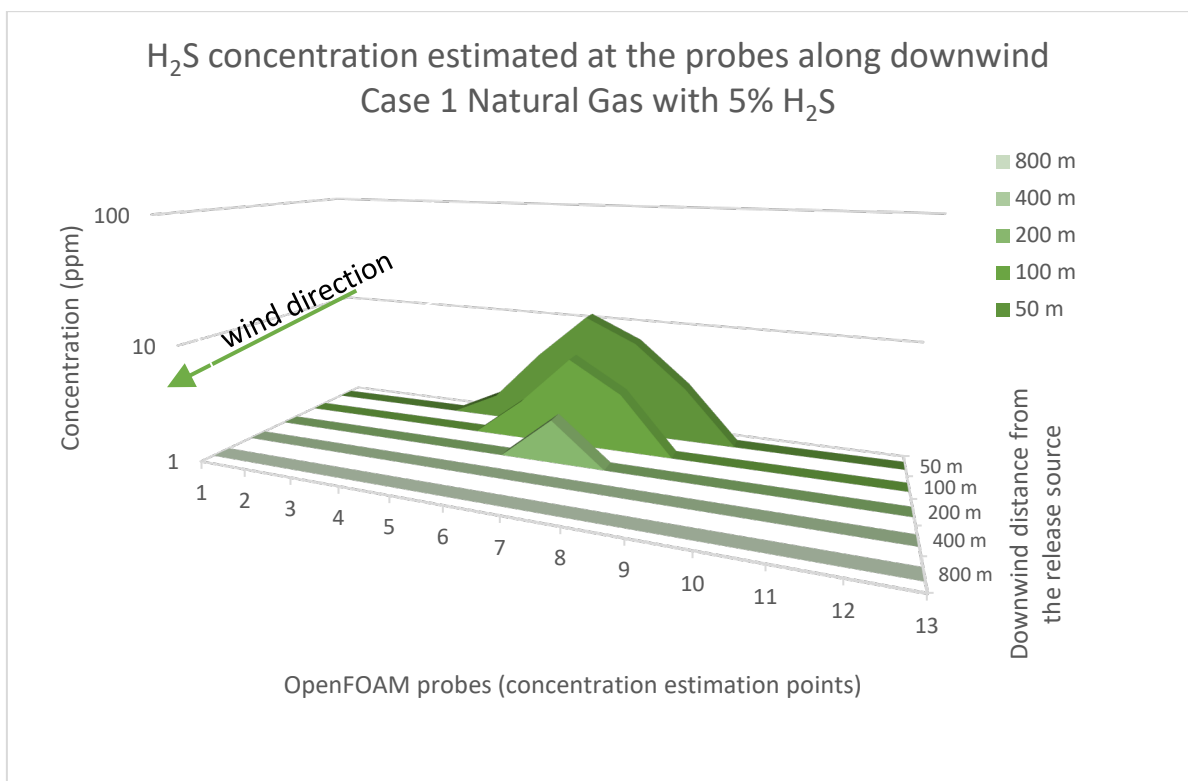


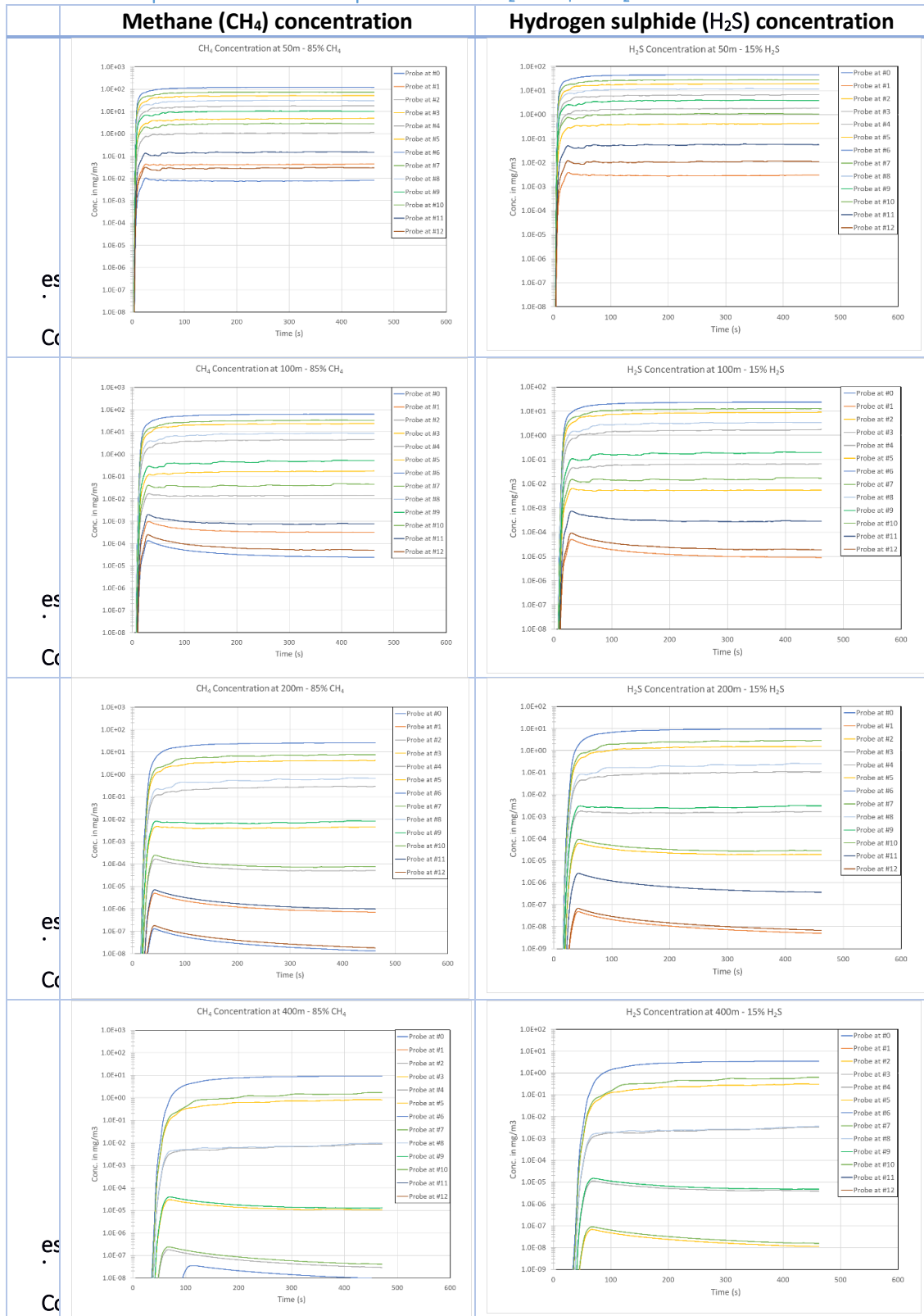
Figure 81: Case 1 OpenFOAM Natural Gas dispersion with 5% H<sub>2</sub>S - downwind distribution of H<sub>2</sub>S concentration

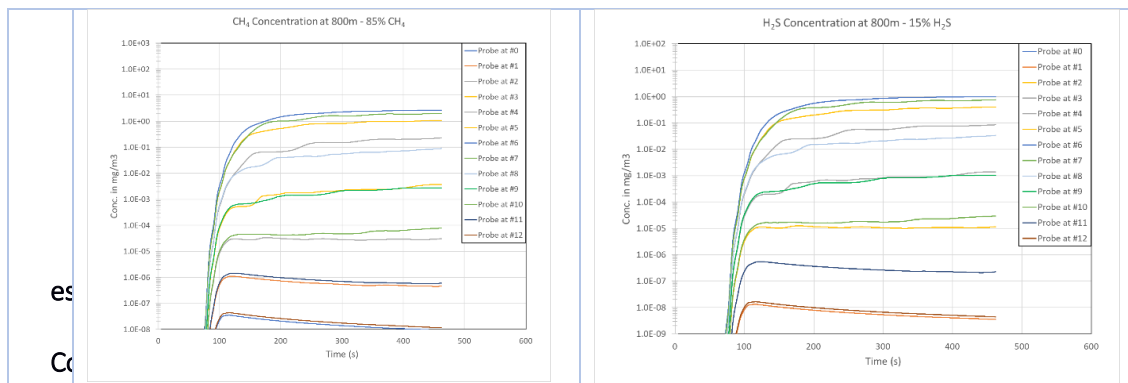
Natural gas with H<sub>2</sub>S concentration 0.51ppm (AEGL-1) was estimated to disperse beyond 400m downwind. The maximum concentration estimated at 50 m was 14.5 ppm and at 800m was 0.14 ppm.

#### 6.4. Case 2: Natural gas with 15% H<sub>2</sub>S

The second case evaluated was the natural gas composition with 85% CH<sub>4</sub> and 15% H<sub>2</sub>S. The CH<sub>4</sub> and H<sub>2</sub>S concentrations were estimated at the 13 probes (locations) along the downwind arcs. The concentration of both species, estimated at each probe with the progression of time is given in Table 55.

Table 55: Case 2 OpenFOAM Natural Gas dispersion with 15% H<sub>2</sub>S – CH<sub>4</sub> and H<sub>2</sub>S concentration estimation





The CH<sub>4</sub> concentration estimated (time averaged) from the natural gas dispersion is given in Table 56 and the CH<sub>4</sub> concentration in the cloud along the probes is illustrated in Figure 82.

Table 56: Case 2 OpenFOAM Natural Gas dispersion with 15% H<sub>2</sub>S – CH<sub>4</sub> concentration along monitoring points

Methane (CH <sub>4</sub> ) concentration – time averaged over 600 seconds													
probe at	0	1	2	3	4	5	6	7	8	9	10	11	12
50 m	0.0	0.0	0.9	3.8	13.9	39.8	92.1	55.8	23.5	7.7	2.2	0.1	0.0
100 m	0.0	0.0	0.0	0.1	3.6	18.7	48.2	25.7	6.8	0.4	0.0	0.0	0.0
200 m	0.0	0.0	0.0	0.0	0.2	3.2	19.6	5.8	0.5	0.0	0.0	0.0	0.0
400 m	0.0	0.0	0.0	0.0	0.0	0.6	7.2	1.3	0.0	0.0	0.0	0.0	0.0
800 m	0.0	0.0	0.0	0.0	0.2	0.8	2.0	1.5	0.1	0.0	0.0	0.0	0.0

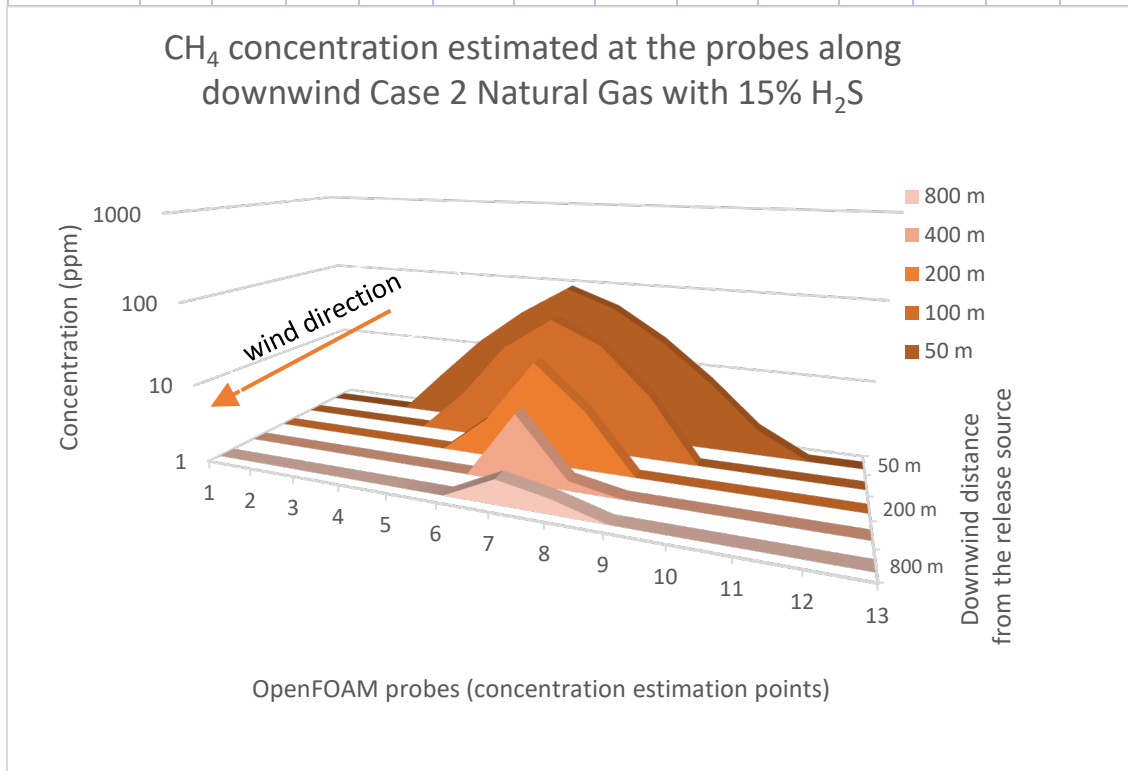


Figure 82: Case 2 OpenFOAM Natural Gas dispersion with 15% H<sub>2</sub>S - downwind dispersion of CH<sub>4</sub> concentration

Methane concentration for flammability alarm level (10% LFL = 5,000 ppm) not predicted at any of the monitoring points. The results imply that the flammability hazard from this release is not of any significant concern.

The H<sub>2</sub>S concentration estimated at the 13 probes (locations) along the downwind arcs for Case 2 (natural gas composition 85% CH<sub>4</sub> and 15% H<sub>2</sub>S) is given in Table 57 and the H<sub>2</sub>S concentration in the cloud along the probes is illustrated in Figure 83.

**Table 57: Case 2 OpenFOAM Natural Gas dispersion with 15% H<sub>2</sub>S – H<sub>2</sub>S concentration at the probes**

Hydrogen sulphide (H <sub>2</sub> S) concentration													
probe at	0	1	2	3	4	5	6	7	8	9	10	11	12
50 m	0.0	0.0	0.4	1.9	6.8	19.4	44.8	27.2	11.4	3.8	1.0	0.1	0.0
100 m	0.0	0.0	0.0	0.1	1.7	9.1	23.6	12.6	3.3	0.2	0.0	0.0	0.0
200 m	0.0	0.0	0.0	0.0	0.1	1.5	9.6	2.8	0.3	0.0	0.0	0.0	0.0
400 m	0.0	0.0	0.0	0.0	0.0	0.3	3.4	0.6	0.0	0.0	0.0	0.0	0.0
800 m	0.0	0.0	0.0	0.0	0.1	0.4	1.0	0.7	0.0	0.0	0.0	0.0	0.0

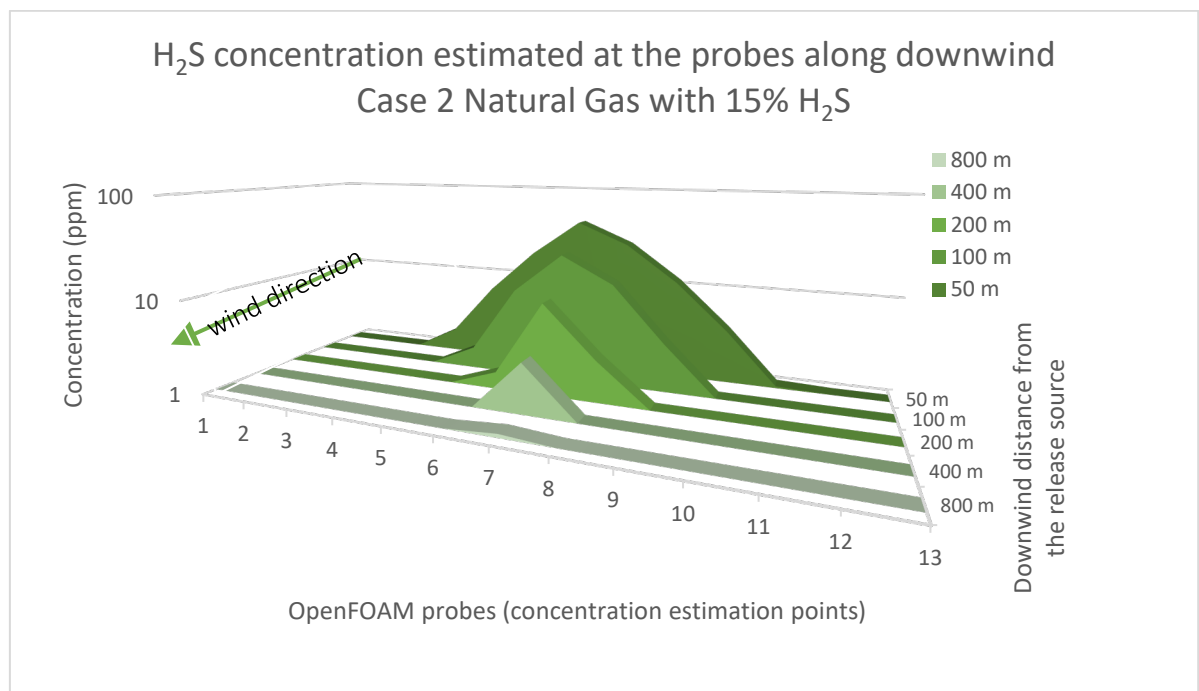


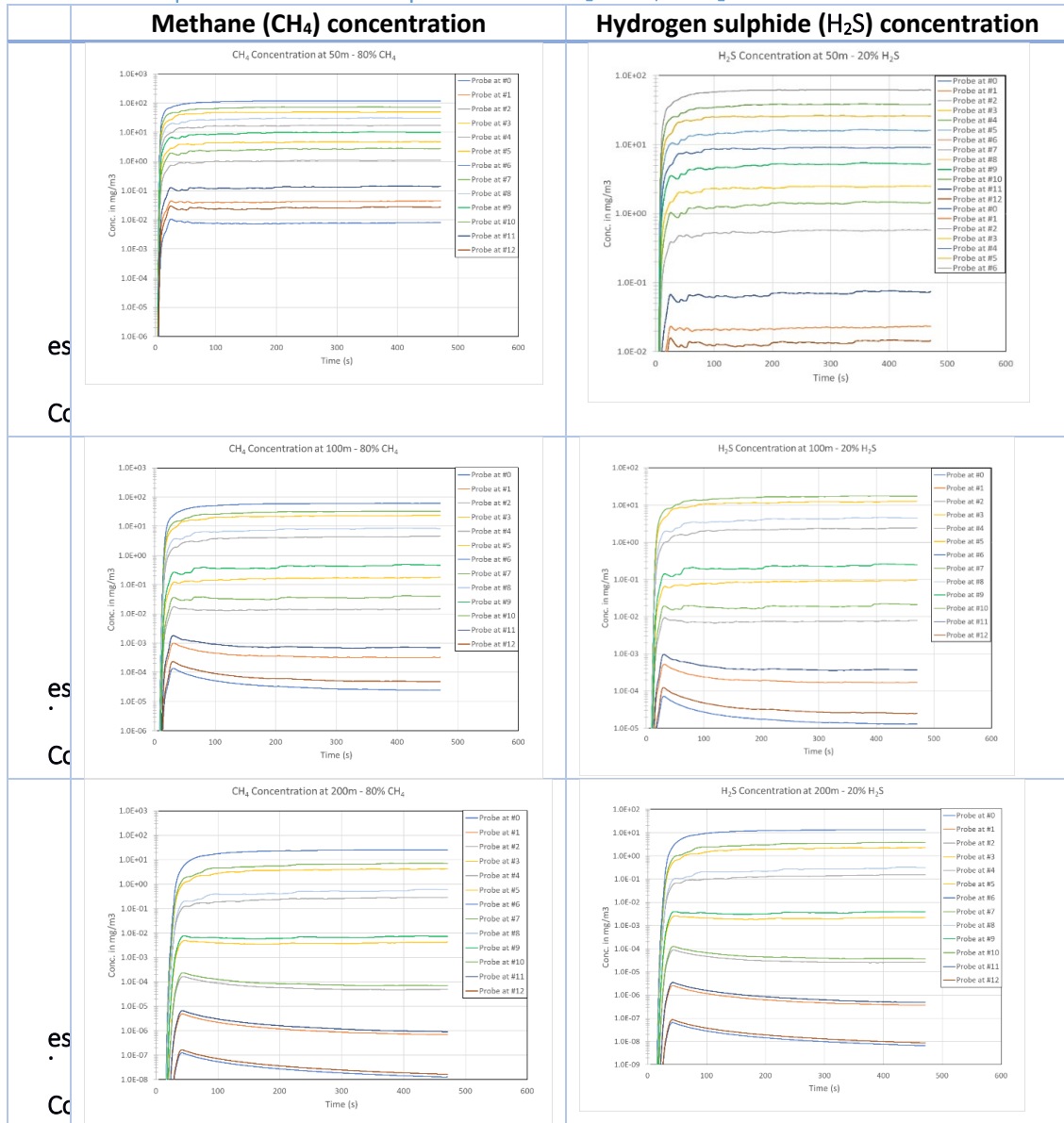
**Figure 83: Case 2 OpenFOAM Natural Gas dispersion with 15% H<sub>2</sub>S - downwind distribution of H<sub>2</sub>S concentration**

Natural gas with H<sub>2</sub>S concentration exceeding 0.51 ppm (AEGL-1) was estimated to disperse beyond 800 m downwind. The maximum concentration estimated at 50 m was 44.7 ppm and at 800 m was 1 ppm.

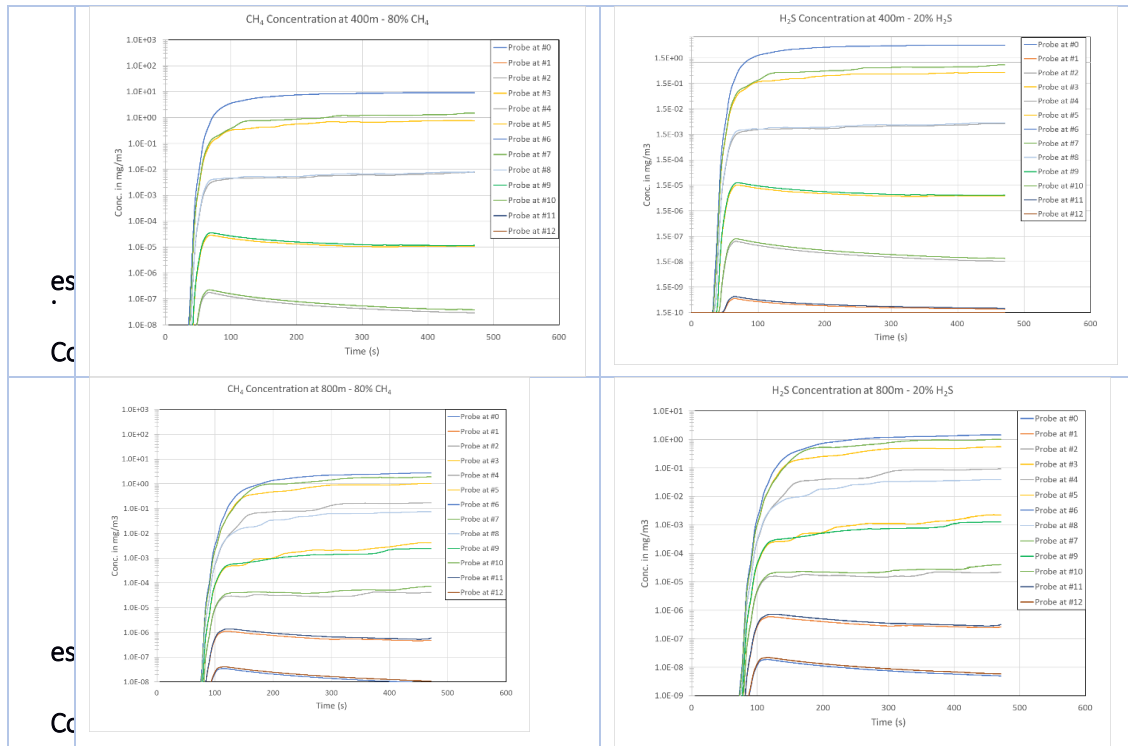
### 6.5. Case 3: Natural gas with 20% H<sub>2</sub>S

The third case evaluated was the natural gas composition with 80% CH<sub>4</sub> and 20% H<sub>2</sub>S. The CH<sub>4</sub> and H<sub>2</sub>S concentrations were estimated at the 13 probes (locations) along the downwind arcs. The concentration of both species, estimated at each probe with the progression of time is given in Table 58.

Table 58: Case 3 OpenFOAM Natural Gas dispersion with 20% H<sub>2</sub>S – CH<sub>4</sub> and H<sub>2</sub>S concentration estimation







The CH<sub>4</sub> concentration estimated (time averaged) from the natural gas dispersion is given in Table 59 and the CH<sub>4</sub> concentration in the cloud along the probes is illustrated in Figure 84.

Table 59: Case 3 OpenFOAM Natural Gas dispersion with 20% H<sub>2</sub>S – CH<sub>4</sub> concentration along monitoring points

Methane (CH <sub>4</sub> ) concentration – time averaged over 600 seconds													
probe at	0	1	2	3	4	5	6	7	8	9	10	11	12
50 m	0.0	0.0	0.9	3.8	13.9	39.8	92.1	55.8	23.5	7.7	2.2	0.1	0.0
100 m	0.0	0.0	0.0	0.1	3.6	18.7	48.2	25.7	6.8	0.4	0.0	0.0	0.0
200 m	0.0	0.0	0.0	0.0	0.2	3.2	19.6	5.8	0.5	0.0	0.0	0.0	0.0
400 m	0.0	0.0	0.0	0.0	0.0	0.6	7.2	1.3	0.0	0.0	0.0	0.0	0.0
800 m	0.0	0.0	0.0	0.0	0.2	0.8	2.0	1.5	0.1	0.0	0.0	0.0	0.0

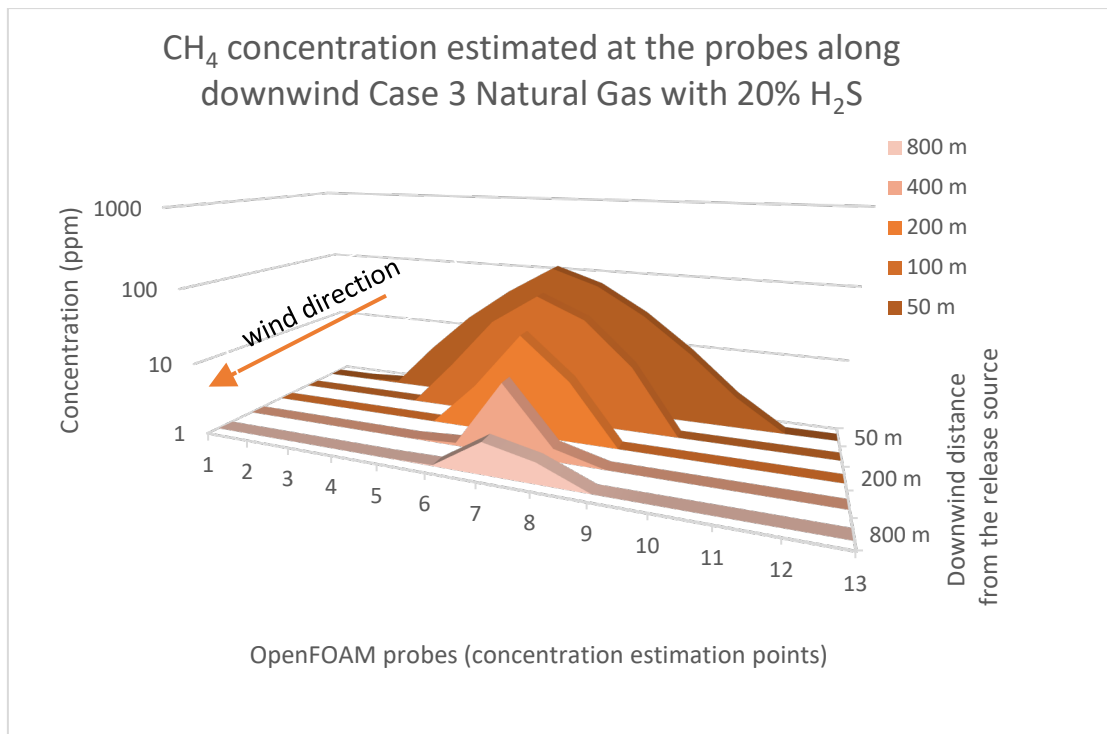


Figure 84: Case 3 OpenFOAM Natural Gas dispersion with 20% H<sub>2</sub>S - downwind dispersion of CH<sub>4</sub> concentration

The H<sub>2</sub>S concentration estimated at the 13 probes (locations) along the downwind arcs for Case 3 (natural gas composition 80% CH<sub>4</sub> and 20% H<sub>2</sub>S) is given in

Table 60 and the H<sub>2</sub>S concentration in the cloud along the probes is illustrated in Figure 85.

Table 60: Case 3 OpenFOAM Natural Gas dispersion with 20% H<sub>2</sub>S – H<sub>2</sub>S concentration along monitoring points

Hydrogen sulphide (H <sub>2</sub> S) concentration													
probe at	0	1	2	3	4	5	6	7	8	9	10	11	12
50 m	0.0	0.0	0.6	2.5	9.0	25.8	61.7	38.0	16.1	5.3	1.5	0.1	0.0
100 m	0.0	0.0	0.0	0.1	2.4	12.5	32.5	17.2	4.4	0.2	0.0	0.0	0.0
200 m	0.0	0.0	0.0	0.0	0.2	2.2	13.4	3.7	0.3	0.0	0.0	0.0	0.0
400 m	0.0	0.0	0.0	0.0	0.0	0.4	4.9	0.8	0.0	0.0	0.0	0.0	0.0
800 m	0.0	0.0	0.0	0.0	0.1	0.6	1.4	1.0	0.0	0.0	0.0	0.0	0.0

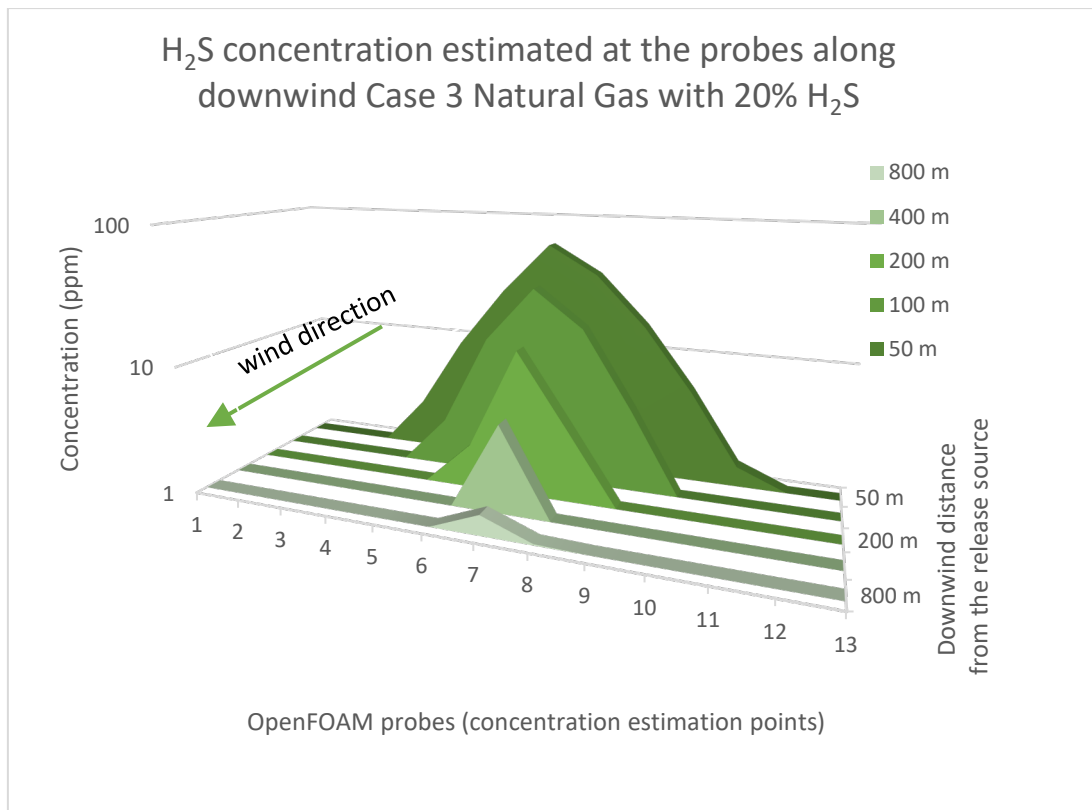


Figure 85: Case 3 OpenFOAM Natural Gas dispersion with 20% H<sub>2</sub>S - downwind distribution of H<sub>2</sub>S concentration

Natural gas with H<sub>2</sub>S concentration 0.51ppm (AEGL-1) was estimated to disperse beyond 800 m downwind. The maximum concentration estimated at 50 m was 61.7 ppm and at 800 m was 1.4 ppm.

## 6.6. Analysis of the results – sensitivity to natural gas composition

From the literature review and the initial screening study (dispersion modelling) using general purpose consequence modelling software tools (see Chapter 4), it is evident that the composition (H<sub>2</sub>S content) can impact the natural gas dispersion both downwind and crosswind. In the paper Nair et al. demonstrates that the cloud behaviour changes from passive to dense when the composition of H<sub>2</sub>S increases higher than 15% (Nair et al. 2022). As per the study by Yang et al., the natural gas composition affects the dispersion behaviour and accumulation characteristics of H<sub>2</sub>S. As the dispersion height of hydrogen sulphide decreases, the critical time of the H<sub>2</sub>S spreading to the inhabited area decreases whereby reducing the time to respond in an emergency (Yang et al 2019).

### 6.6.1. Toxicity – Hydrogen sulphide

For all the natural gas compositions evaluated, hydrogen sulphide concentrations that can impact personnel (toxicity) were predicted at downwind distances. The maximum hydrogen

sulphide concentration at the probes (monitoring points) for the three compositions evaluated is summarised in Table 61 .

**Table 61: OpenFOAM Natural Gas dispersion – maximum H<sub>2</sub>S concentration at downwind monitoring arcs**

Maximum concentration along the monitoring point arcs	at 50 m	at 100 m	at 200 m	at 400 m	at 800 m
Natural gas with 5% H <sub>2</sub> S	14.5 ppm	7.7 ppm	3.1 ppm	1.1 ppm	0.14 ppm
Natural gas with 15% H <sub>2</sub> S	44.7 ppm	23.5 ppm	9.5 ppm	3.4 ppm	1 ppm
Natural gas with 20% H <sub>2</sub> S	61.7 m	32.5 ppm	13.4 ppm	4.9 ppm	1.4 ppm

A comparison of the hydrogen sulphide concentrations estimated along the 13 probes at five arcs downwind from the release source for the three compositions are given in Figure 86 to Figure 90.

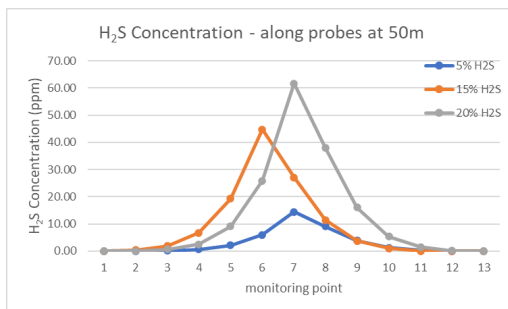


**Figure 86: H<sub>2</sub>S concentration comparison along probes at 50 m**

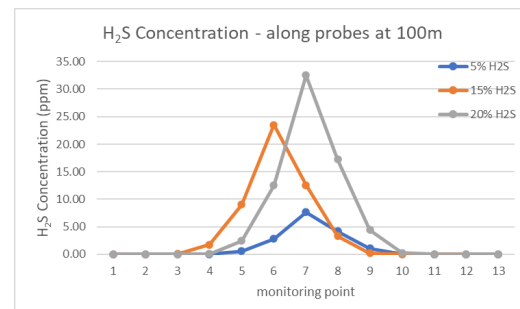


**Figure 87: H<sub>2</sub>S concentration comparison along probes at 100m**

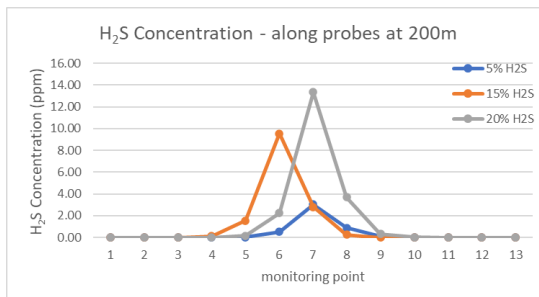


**Figure 88: H<sub>2</sub>S concentration comparison along probes at 200m**

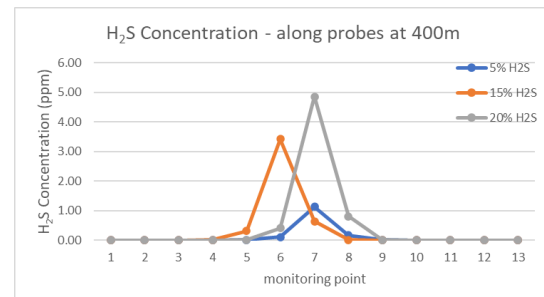


**Figure 89: H<sub>2</sub>S concentration comparison along probes at 400m**

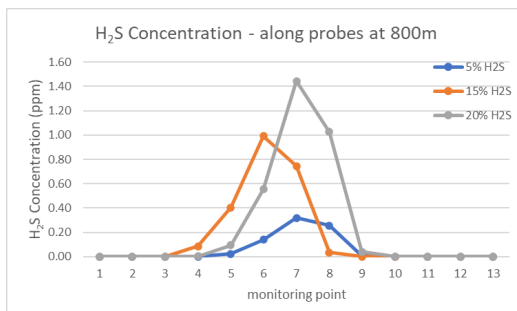


**Figure 90: H<sub>2</sub>S concentration comparison along probes at 800m**

The following are observed from the analysis of the distribution of the estimated hydrogen sulphide concentration along the probes at five downwind distances:

- (i) The maximum concentration at all the five downwind arcs for 15% H<sub>2</sub>S and 20% cases were significantly higher compared to the concentration estimated for 5% H<sub>2</sub>S case. This implies that the cloud dispersion downwind increases significantly for H<sub>2</sub>S compositions in the natural gas exceeding 15%.
- (ii) The maximum width for all the H<sub>2</sub>S concentrations at the monitoring points for all the compositions is comparable, which indicates the cloud spread horizontally is not impacted by the composition of H<sub>2</sub>S-composition in the natural gas.
- (iii) The maximum concentration downwind is not always in the central line (varies from probe 6 to 7), the meandering implies the effect of wind on the dispersion. This has an impact on the toxic dose (exposure to specific concentration over a duration) estimations and the impact to personnel.

The leakage and dispersion of hydrogen sulphide-containing natural gas threatens the energy industry, especially in the gas transfer from the production field to the gas processing facilities. The pipelines may pass through communities with the public signifying the importance of emergency response planning and preparedness. The toxicity impacts for the public exposure and emergency response criteria for the three compositions is given in Table 62.

**Table 62: Toxicity impact comparison for natural gas compositions**

	5% H <sub>2</sub> S	15% H <sub>2</sub> S	20% H <sub>2</sub> S
<b>AEGL-1: 0.51ppm, 60 minutes</b>	Beyond 400 m	Beyond 800 m	Beyond 800 m
<b>AEGL-2: 17 ppm, 8 hours</b>	Not reached	Beyond 100 m	Beyond 100 m
<b>ERPG-2: 30 ppm, 60 minutes</b>	Not reached	Beyond 50 m	Beyond 100 m
<b>IDLH: 100 ppm</b>	Not reached	Not reached	Not reached

Being exposed to 0.51 ppm of hydrogen sulphide more than 1 hour, the respiratory tract and eyes of people will be injured. Being exposed to 17 ppm of hydrogen sulphide for more than 8 hours will cause irreversible effects on the human body. Exposure to 30 ppm exceeding 60 minutes can impair the ability to take protective action. From the figures and tables, the toxic cloud size increases significantly for 15% and 20% H<sub>2</sub>S. Based on the potential exposure level concentrations, the area surrounding the potential releases could be divided into the safety

zone, warning area and dangerous area for land use planning and minimising exposure in the event of accidental release.

### 6.6.2. Flammability – Methane

CFD simulation study using FLACS by Yang et al. specifies that the gas composition affects the dispersion behaviour and accumulation characteristics of the flammable cloud and the influenced area of flammable cloud increases as the blowout gas becomes heavier (Yang et al. 2019). A comparison of the flammable cloud (maximum methane concentration) along monitoring point arcs for the three compositions is summarised in Table 63.

Table 63: OpenFOAM Natural Gas dispersion – maximum CH<sub>4</sub> concentration at downwind monitoring arcs

Maximum concentration along the monitoring point arcs	at 50 m	at 100 m	at 200 m	at 400 m	at 800 m
Natural gas with 95% CH <sub>4</sub>	127 ppm	67 ppm	27 ppm	10 ppm	2.9 ppm
Natural gas with 85% CH <sub>4</sub>	116 ppm	61 ppm	25 ppm	9.1 ppm	2.7 ppm
Natural gas with 80% CH <sub>4</sub>	92 ppm	48 ppm	20 ppm	7.2 ppm	2.1 ppm

A comparison of the methane concentrations estimated along the 13 probes at five arcs downwind from the release source for the three compositions are given in Figure 91 to Figure 95.

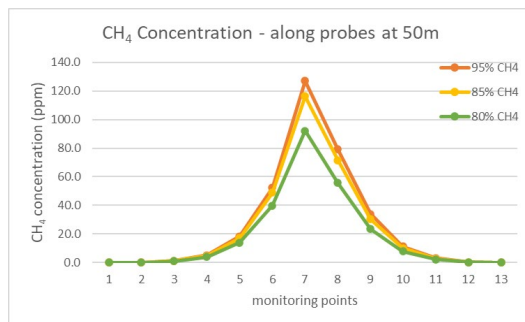


Figure 91: CH<sub>4</sub> concentration comparison along probes at 50m

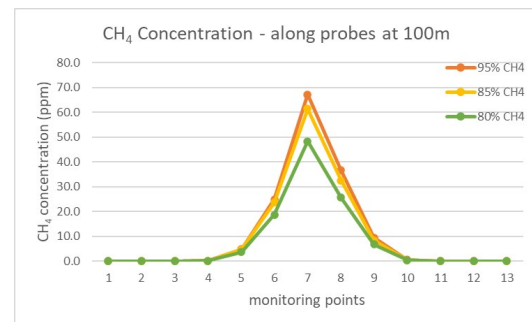


Figure 92: CH<sub>4</sub> concentration comparison along probes at 100m

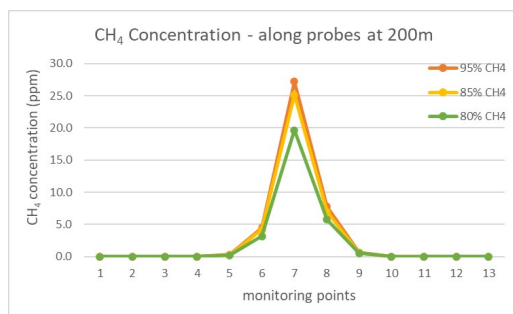


Figure 93: CH<sub>4</sub> concentration comparison along probes at 200m

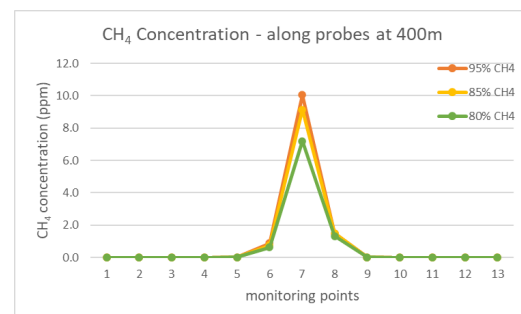


Figure 94: CH<sub>4</sub> concentration comparison along probes at 400m

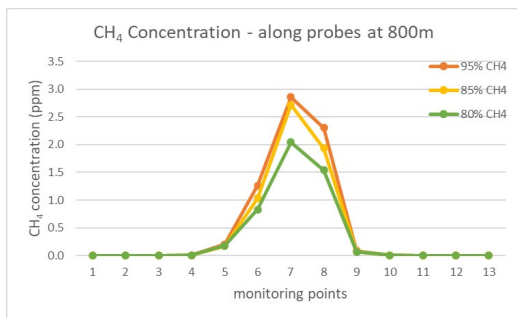


Figure 95: CH<sub>4</sub> concentration comparison along probes at 800m

The maximum cloud width and cloud length for all the cases is comparable, which indicates the cloud spread crosswind and downwind increases with the increase in the composition of CH<sub>4</sub> composition in the natural gas. No significant difference in the concentrations recorded for the range of CH<sub>4</sub> concentration in the natural gas. Methane flammability concentrations of process trip level (25% LFL) nor the alarm level for personnel response (10% LFL) were not predicted at any of the monitoring points for any of the three natural gas compositions evaluated. The results imply that the flammability hazard from this release is not of any significant concern.

## 6.7. Discussion

The main purpose is to study the dispersion behaviour with the change in composition of hydrogen sulphide containing natural gas. OpenFOAM based numerical model is built, and several simulations by varying the compositions of hydrogen sulphide in natural gas are conducted. The main conclusions are as follows:

- (i) Gas composition affects the dispersion behaviour of the toxic cloud. The calculated toxicity impact distance may be very sensitive to the natural gas with H<sub>2</sub>S composition exceeding 15 mol%. Detailed composition of the natural gas (especially the hydrogen sulphide composition) should be considered.
- (ii) Overall, the results indicate that in terms of hazards, the toxic impact over-rides the impact from flammability. This implies, the emergency response, site selection and other decisions on the sour natural gas pipeline routing should consider the toxicity as the criteria.

Based on the potential exposure level concentrations, the area surrounding the potential releases could be divided into the safety zone, warning area and dangerous area for land use planning and minimising exposure in the event of accidental release.

## 7. Conclusion

This research study led to the development of a methodology for the selection of the consequence modelling for hydrogen sulphide (H<sub>2</sub>S) containing natural gas leaks from pipelines. The study also identified the key modelling parameters to be subjected to the sensitivity analysis. This research followed the technical guidance for the vulnerability (hazard impact) analysis of extremely hazardous substances by United States Environmental Protection Agency (US EPA) and the safety report assessment guidance by the United Kingdom Health and Safety Executive (UK HSE). This consequence assessment methodology is mainly applicable for the land use planning and emergency response planning associated to the risk management of the hazardous chemical substance releases.

The study focused on the potential loss of containment (leak, continuous) from pipelines transferring untreated natural gas at high pressure. There are several tools and methodologies available to determine the release and dispersion characteristics of the loss of containment and the hazardous level distances. The study was performed in phases and used multiple tools for evaluating the modelling inputs and parameters. The first part of the research established that the depending on the gaseous mixture properties, and ambient conditions, the sour natural gas (hydrogen sulphide containing natural gas) cloud from a release could be (i) dense (gravity slump), (ii) buoyant (rises over time), or (iii) neutrally buoyant (neither rises nor drops but disperses over time). The second part of the research determined the compositions of natural gas with shifts in buoyancy behaviours and identified the list of modelling parameters to be subjected to sensitivity analysis. The third part of the research developed a higher order Computational Fluid Dynamics (CFD) model for sour natural gas dispersion modelling and determined the appropriate solver and the modifications required on the model to take account of the effect of turbulence and the compositions.

Whichever approach is adopted, it should be used with an understanding of its range of validity, its limitations, the input data required, the sensitivity to the different input data, and how the results can be verified. The findings in this research:

- (i) Enables the risk analysts, project specialists, and local planners on hazardous substance transfer route selection,
- (ii) Minimises the inconsistency in risk assessments, and



- (iii) Overcome the uncertainty in dispersion modelling whereby the right sized risk management can be deployed.

### 7.1. Release, dispersion and modelling

The dispersion process includes different phases (i) near source, (ii) interim and (iii) far-field. The near source dispersion is seriously affected by the release (leakage) conditions like the release hole size, shape, and the orientation of release. For the release and discharge calculations, 100% vaporisation is not critical for dispersion calculations, due to high turbulence mixing in release region. The interim phase dispersion is affected by the surrounding conditions like obstructions, wind speed and atmospheric stability. The far-field dispersion is significantly affected by the thermodynamic properties of the dispersed substance and the turbulence along dispersion path (e.g., due to the topography, terrain). The physical process of the dispersion is through the transport by wind and heat convection, and by turbulent diffusion (random mixing of air mass). Depending on the buoyancy, turbulence and the terrain, dispersion can decrease or increase mass in a vapour cloud (e.g., heavy gas accumulation in valleys as witnessed in the 2003 Kaixian blowout incident).

The research has evaluated the modelling tools and approaches for the three phases (a) discharge, (b) expansion and (c) dispersion following an accidental release. There are essentially three steps in the modelling:

- (i) The release rate from the containment (pipeline),
- (ii) The expansion from pressurised source (with momentum) to the substance reaching atmospheric pressure (called as pseudo source for dispersion), and
- (iii) Then the dispersion (by wind, heat convection and turbulent diffusion).

### 7.2. Modelling tools and methodology

The first part of the study used US EPA software ALOHA (CAMEO Suite by US EPA), the second part used commercially available and validated software packages commonly used in the Oil & Gas Industry – Aspen HYSYS and CANARY by Quest. The third part of the research used higher fidelity model OpenFOAM, an open-source CFD software.

The Gaussian modelling tools are quite suitable for emissions of pollutants whose density remains similar to that of air provided that the cloud does not move too far away from the ground and that there is no obstacle, no extreme meteorological conditions prevail, and there is a certain

horizontal homogeneity. If parameters move away from these discharge conditions, it is essential to consider sophisticated models like of the integral type or even the three-dimensional type.

It was clear that few CFD codes can model complex thermodynamics processes during expansion of H<sub>2</sub>S rich hydrocarbons; the combination of expansion process and selection of Equation of State (EoS) can lead to widely different input to dispersion in terms of temperature and composition, which subsequently affect the dispersion and the impact distance. In the integrated software tools like CANARY and ALOHA, these three steps are all sequentially carried out by the tool itself without requiring modeller intervention. It was observed that the computer tools can give substantially different results with respect to dispersion distances for the same accident scenario. The variations seem to be larger when the stagnant conditions are liquid or 2-phase. The default selections for the modelling approach and the simplifications in the modelling input have often proven to over-estimate or at times under-estimate the hazard impact distances.

This study highlights the crucial importance of the scientific assessment of models for its applicability. Only if the model is shown to be scientifically sound, can one have any confidence that a successful validation in one situation may lead to valid predictions in another. An important part of any model assessment is the comparison of model predictions against high quality data over the full range of application of the model and at a range of scales. Experimental data for H<sub>2</sub>S rich fluid release and dispersion is scarce and hence the model validations were carried out using Prairie Grass field trials for continuous releases of sulphur dioxide from a release closer to the ground in open well-ventilated area with cut grass terrain.

### 7.3. Parameter screening and model selection

The study has determined that the selection of the appropriate dispersion model is a key decision. It was noted that the selection of the buoyancy-based model (dense vs passive) in the integral tools and in some cases a switching from passive to dense for impact distance estimation formula is adopted when the gravity slump reaching ground level. The selection of the formula for calculations are selected based on the thermo-dynamic properties of the pure substance (the major component); in some tools a pseudo-substance is created to represent the multiple substances in the release fluid.

The key physical parameters that significantly impacts the far-field dispersion of natural gas releases are weather stability, wind speed and surface roughness (terrain effects). Natural gas dispersion is less sensitive to the humidity and ambient temperature changes. In addition to the

density of the cloud in relation to the air (under normal temperature and pressure conditions), the following also matters for the dispersion calculations:

- (i) Density at emission temperature (decrease in buoyancy through cold and increase in buoyancy through heat).
- (ii) Emission temperature, which may affect the temperature of the gas emitted at the source at the time of the thermodynamic flash.
- (iii) Possibility of mist formation, depending on the humidity of the air and the temperature
- (iv) Source elevation (ground level or elevated) and dimensions of the source (pseudo source in the event of accidental natural gas leak occur in pipeline transfer).

#### 7.4. Sourness screening and parametric sensitivity

The release density which impacts the cloud behaviour depends on the composition. This study covering a set of eight sour natural gas compositions from across the world revealed that the fluid phase could vary (liquid, 2-phase, or vapour) which a change in the natural gas composition, temperature, and pressure. The natural gas compositions evaluated had hydrogen sulphide composition ranging from 2.6% to 29%. ASPEN HYSYS with Peng-Robinson EoS was used to develop and evaluate the Pressure-Temperature phase equilibrium curves. CANARY was used for the dispersion modelling. Natural gas with greater than 15 mol% Hydrogen sulphide has shown to the dispersion behaviour closer to neutral or negatively buoyant.

The parametric sensitivity analysis for a release event from a natural gas transfer pipeline at ground level using eight different compositions revealed that the downwind dispersion of toxic cloud is dependent on the release hole size, release rate, and orientation of release; especially, the failure mechanism and related hole dimensions (size and shape) for larger hole releases need to appropriately be determined. It was observed that the downwind distances to hazard level ranges from 15 m to 1500 m and the toxic impact distance (from hydrogen sulphide exposure) outweighs the impact distance from flammability. Dispersion from small hole releases is not sensitive to the composition of the natural gas. Release rates and downwind dispersion are sensitive to low temperature releases of compositions with molar mass greater than 30 g/mol. The analysis concludes that the release and dispersion of toxic natural gas is significantly impacted by the natural gas composition with molar mass greater than 30 g/mol and the H<sub>2</sub>S content greater than 15 mol%. In such cases, the properties for the multi-component substance should be determined for the release conditions and software with multi-component modelling

capability should be utilized for the dispersion modelling. The analysis of the results suggest that water saturation of natural gas is not a significant parameter in downwind dispersion to hydrogen sulphide hazard levels.

As per the study by Derundi et. al. for heavy gas dispersion modelling study in the presence of large obstacles using  $k-\epsilon$  model, with the standard Jones and Launder values for the constants (ANSYS's FLUENT software) concluded that the impact of obstacles in dispersion of dense gas can be disregarded if the ratio of the obstacle and the cloud is less than 0.25. However, when the ratio is greater than 1, the presence of the obstacle cannot be disregarded. This means, the effects of the obstacle shall be represented in the computational domain to estimate the effects.

### 7.5. CFD simulations and analysis

CFD based codes and simulation software tools can model the thermodynamic processes during the dispersion of multi-component natural gas. The next part of the research used OpenFOAM, an open source CFD code, to evaluate the hydrogen sulphide diffusion process and its sensitivity to the composition. The study developed a two-step approach to generate the turbulence and evaluated the significance on the far-field dispersion behaviour for a steady state continuous release of sour natural gas. The composition considered is limited to sour natural gas with the principal component methane ( $\text{CH}_4$ ) and the component of toxic concern, hydrogen sulphide ( $\text{H}_2\text{S}$ ). Natural gas ( $\text{CH}_4$ ) with three  $\text{H}_2\text{S}$  compositions (5%, 15% and 20%) were evaluated for downwind dispersion concentrations.

A computational grid was created with a length ( $x$  direction) of 1100 m to reflect the five monitoring point arcs as in the Prairie Grass field trials in order to evaluate the far-field dispersion effects. Though the release point was closer to the ground, the computational grid was extended to 40 m vertically ( $z$  direction) to take account of the vertical velocity and temperature profile. The transport downwind follows a serpentine path, being influenced by both random and periodic wind oscillations, composed of both large- and small-scale eddies in the wind field. To take account of this, the computational grid was set up of 240 m in horizontal ( $y$ ) direction. A number of solvers were subjected to screening based on the applicability and modelling capability. Then simulations were carried out for the screened-in solvers - *fireFoam*, *simpleFoam*, *rhoSimpleFoam*, *rhoPimpleFoam*, *rhoReactingFoam* and *rhoReactingBuoyantFoam*. The estimated results were compared against the field trial observed (field trial) results. Based on the simulation results and comparison with the field trial result, the fully compressible combustion

solver, *rhoReactingBuoyantFoam* (with modifications) was identified as the best suited solver for sour natural gas dispersion modelling.

A two-step approach was used and proved to be useful where at first the model is run in steady-state mode and the velocity profile for the domain is established. This velocity profile is then used as the initial condition in the transient state simulations. OpenFOAM's boundary condition *atmBoundaryLayerInletVelocity* was used to generate the vertical velocity profile in the solution domain. For the top plane *fixedShearStress* boundary condition and for transient with fluctuation *inlet* boundary condition was used to match the velocity profile. From the different types of transient turbulence model in OpenFOAM, Unsteady RANS with Realizable k- $\epsilon$  model preserves the velocity profile much better as compared to SST k- $\omega$ . To represent the atmospheric turbulence that effects the local velocity field, a hypothetical inlet turbulence is generated using *turbulentInlet* boundary condition. Hydrostatic pressure contribution is significant for buoyant gas and was accounted in the simulations. Mesh independence was established for 2M cells and maintaining the skewness, orthogonality, aspect ratio, minimum face area and growth rate low. The selected turbulence model with a steady state velocity, temperature, Kinetic energy, and dissipation rate (Epsilon) values along the vertical profile at the monitoring points matched against the experimental values. This approach helped to mimic the real field prior to the release of the species. Validations were carried out using scatter plot representation and to satisfy Factor of two criteria. This research study points that methane flammability concentrations (hazard levels) were not predicted for any of the compositions at far-field implying that the flammability hazard is not of significant concern in comparison to the toxicity hazard (for far-field receptors of interest). However, it shall be noted that flammability hazard could be significant to the receptors of interest closer to the release source. Gas composition affects the buoyancy behaviour of toxic cloud, and the calculated toxicity impact distance is sensitive to the natural gas with H<sub>2</sub>S composition exceeding 15 mol%.

## 7.6. Discussion and future work

Numerical simulation of the release and dispersion of natural gas provides an enhanced information on the potential impact zone which forms an essential part for risk-based decision making, especially the multi-billion dollar worth engineering projects and emergency response planning. Incorrect selection of the modelling approach, input and environmental parameters could lead to an inaccurate consequence impact zone estimation which could result in disproportionate risk management efforts. This challenge can be addressed by selection of

software models appropriate for the release scenarios and through sensitivity analysis of the modelling inputs and parameters.

As part of the process risk assessments of H<sub>2</sub>S containing natural gas, consequence modelling sensitivity analysis should be carried out for the modelling tool, inputs and assumptions. Simpler tools can be used for initial screening or site selection and for emergency response planning applications. For natural gas compositions with higher molar mass and with higher compositions of H<sub>2</sub>S, tool capable of multi-component thermodynamics should be utilized. CFD or similar approach to be used where turbulence impact on far-field diffusion drives risk management efforts.

This research study points that gas composition affects the dispersion behaviour of the toxic cloud and the calculated toxicity impact distance is sensitive to the natural gas with H<sub>2</sub>S composition exceeding 15 mol%. Detailed composition of the natural gas (especially the hydrogen sulphide composition) should be considered. Overall, the results indicate that in terms of hazards, the toxic impact over-rules the impact from flammability. This implies, the emergency response, site selection and other decisions on the sour natural gas pipeline routing should consider the toxicity as the criteria.

Based on the literature review and the simulations carried out for this study, opportunities for further research were also identified:

- (i) Field trials on dispersion of sour natural gas: Develop experiment data for H<sub>2</sub>S containing natural gas dispersion, which can be used for better understanding of dispersion and also can be utilized for model validation.
- (ii) Toxic dose effect: The hazard impact from exposure to H<sub>2</sub>S is driven by two parameters, the toxic concentration, and the exposure time (also called as the toxic dose-load). The current study has demonstrated that the concentration at a receptor point far-field fluctuates for the duration of exposure due to the cloud meandering. With further research, numerical model can be developed to estimate the toxic dose from the concentration and duration estimations using CFD simulations.
- (iii) Natural gas composition: The CFD modelling simulations for natural gas considered two components CH<sub>4</sub> and H<sub>2</sub>S. Further research with natural gas with more than two components and its impact on H<sub>2</sub>S diffusion.

## Reference

1. AIHA (2011) *Emergency Response Planning Guidelines (ERPGs)*, American Industrial Hygiene Association.
2. Airliquide (2016) Gas encyclopedia [link](#) accessed on 07 Nov 2016;
3. Aloqaily, Arafat (2018) *Cross country pipeline risk assessments and mitigation strategies*, Gulf Professional Publishing ISBN: 78-0-12-816007-7.
4. Anderson, John David (1995) *Computational Fluid Dynamics: The basics with application*, McGraw-Hill.
5. API RP 49 (2010) *Recommended Practice for Drilling and Well Servicing Operations Involving Hydrogen Sulfide*, American Petroleum Institute.
6. Ashrafi, Khosro & Hoshyaripour, Gholamali (2010) 'A model to determine atmospheric stability and its correlation with CO concentration.' *International Journal of Civil and Environmental Engineering*. 2:83-88. <https://www.researchgate.net/publication/281611548>
7. AspenTech (2018) HYSYS user manual [link](#) accessed on 1 Sep 2018
8. AspenTech, (2013) *Aspen Physical Property System: Physical Property Methods*. Technology, Inc, Aspen. pp. 1–117
9. Atkinson, Graham (2017) 'Development of heavy vapour clouds in very low wind speeds.' *Journal of Loss Prevention in the Process Industries* 48 (1):162-172. DOI: [10.1016/j.jlp.2017.04.011](https://doi.org/10.1016/j.jlp.2017.04.011)
10. ATSDR (2006) [Agency for Toxic Substances and Disease Registry \(cdc.gov\)](https://www.cdc.gov/atsdr)
11. Baokui, G., Xuanzho, H., Hongqiang, Z., (2012) 'Study on H<sub>2</sub>S monitoring technique for high risk well site.' *International Symposium on safety science and technology, Procedia Engineer.* 45: 898-903
12. Barad, M.L. (Editor) (1958a): Project Prairie Grass, A Field Program In Diffusion. Geophysical Research Paper, No. 59, Vol I , Report AFCRC-TR-58-235(I), *Air Force Cambridge Research Center*. [PGrassVolume1](#)

13. Barad, M.L. (Editor) (1958b): Project Prairie Grass, A Field Program In Diffusion. Geophysical Research Paper, No. 59, Vol II, Report AFCRC-TR-58-235(II), *Air Force Cambridge Research Center*. [PGrassVolumell](#)
14. Bariha, Nilambar & Mishra, Indra & Srivastava, Vimal. (2016) 'Hazard analysis of failure of natural gas and petroleum gas pipelines.' *Journal of Loss Prevention in the Process Industries* 40 (1):217-226. DOI:[10.1016/j.jlp.2015.12.025](#)
15. Bauwens, C.R. & Dorofeev, S.B. (2014) 'CFD modelling and consequence analysis of an accidental hydrogen release in large scale facility.' *International Journal of Hydrogen Energy*. 39 (35):20447-20454. DOI: [10.1016/j.ijhydene.2014.04.142](#)
16. Beggs, D.H., 2002, Book: *Gas production operations*, Oil & Gas Consultants International (OGCI Publications)
17. Bhargava, Akshey (2016) 'Effect of wind speed and stack height on plume rise using different equations'. *International Journal of Engineering Science and Computing*. DOI:[10.4010/2016.748](#)
18. Bhaskaran, Rajesh & Collins, Lance (2018) Introduction to CFD Basics. Cornell [link](#) accessed on Sep 2018
19. Bogaers, Alfred E. J. & Jansen van Rensburg & Gerhardus J. (2018) A comparison of different CFD and Gaussian dispersion models, *Eleventh South African Conference on Computational and Applied Mechanics*. [link \(Academia.edu\)](#)
20. Briggs, Gary A. 1973. Diffusion estimation for small emissions : preliminary draft. Oak Ridge, TN: Atmospheric Turbulence and Diffusion Laboratory.
21. BSEE Safety Alerts. <https://www.bsee.gov/guidance-and-regulations/guidance/safetyalerts-program>, link accessed on August 2020.
22. CCOHS, The Candian Centre for Occupational Health and Safety, [link](#) accessed on 20 Sep 2016
23. CFD Online [https://www.cfd-online.com/Wiki/SST\\_k-omega\\_model](https://www.cfd-online.com/Wiki/SST_k-omega_model)
24. Chambers, T. & Johnson, J. A. (2009) Environmental mitigation monitoring: Hydrogen Sulfide (H<sub>2</sub>S) gas dispersion potentials & release scenarios of pacific OCS region's Oil & Gas platforms & pipelines located in the Santa Barbara channel and Santa Maria basin,



- California, OCS Study *MMS Report 2009-021, US Department of the Interior – Minerals Management Service*. [2009-021-H2S-Dispersion-Study.pdf \(boem.gov\)](#)
25. Chang, Joseph C. and Hanna, Steven R. (2005) 'Technical Descriptions and User's Guide for the BOOT Statistical Model Evaluation Software Package, Version 2.0'. [BOOT Tech & User Guide V2.01.doc \(harmo.org\)](#)
26. Chang, Joseph C. and Hanna, Steven R. (2010) 'Modelers' Data Archive—a collection of atmospheric transport and dispersion data sets.' *16th Conference on Air Pollution Meteorology*, American Meteorological Society. Paper 162348 [link \(icams-portal.gov\)](#)
27. Chou, Selene J. (2003) 'Hydrogen Sulfide: Human health aspect.' *Concise International Chemical Assessment Document 53 – Agency for Toxic Substances and Disease Registry*, World Health Organization
28. Cleaver, P. & Johnson, M. & Ho, B. (2007) 'A summary of some experimental data on LNG safety.' *Journal of Hazardous Materials*. 140 (3):429–438.
29. Coldrick, Simon (2017) 'How do we demonstrate that a consequence model is fit-for-purpose.' *IChemE Symposium Series No 162 HAZARDS*, [link \(icheme.org\)](#)
30. Colenbrander, G. W. (1980) 'A Mathematical Model for the Transient Behavior of Dense Vapor Clouds'. In *3rd International Symposium on Loss Prevention and Safety Promotion in the Process Industries*. Basel, Switzerland
31. Cornwell, John B. & Marx, Jeffrey D. (1996) 'The Significance of Hazard End Points in Quantitative Risk Analysis, Presented at the 1996 Process Plant Safety Symposium - Houston, Texas, AIChE.
32. Dahle, I.B., & Dybvig, G., & vErsdal, G., Guldbrandsen, & Hanson, B.A., & Tharaldsen, J.E., & Wig, A.S. (2012) 'Major accident and their consequences for risk regulation.' *Advances in Safety, Reliability and Risk Management*.
33. Daish, N.C., Britter, R.E., Linden, P.F., Jagger, S.F., Carissimo, B., (2000) 'Smedis: scientific model evaluation of dense gas dispersion models.' *International Journal of Environment and Pollution*. 14 (1–6), 39–51.
34. Danielsson, F., Fendler R., Hailwood M., Shrives J., (2009) 'Analysis of H<sub>2</sub>S – incidents in geothermal and other industries.' *OECD WGCA Steering Group of Analysis of H<sub>2</sub>S incidents*. [link \(silo.tips\)](#)

35. Deng Y., Hu H., Sun D., Hou L., Liang Y., (2018) 'A method for simulating the release of natural gas from the rupture of high-pressure pipelines in any terrain.' *Journal of Hazardous Materials*. 342:418-428
36. Derundi, Marco & Bovolenta, Daniele & Busini, Valentina & Rota, Renato, (2014) 'Heavy gas dispersion in presence of large obstacles; Selection of modeling tools.' *Industrial & Engineering Chemistry Research*. American Chemical Society. 53: 9303-9310 DOI: [10.1021/ie4034895](https://doi.org/10.1021/ie4034895)
37. Dincer, Ibrahim & Erdemir, Dogan (2021) 'Artificial Intelligence in Heat Storage Applications' *Heat Storage Systems for Buildings*.
38. Doolan C., (2012) 'Flow and noise simulation of the NASA tandem cylinder experiment using OpenFOAM.' *15th AIAA/CEAS Aeroacoustics Conference*, Florida. DOI: [/10.2514/6.2009-3157](https://doi.org/10.2514/6.2009-3157)
39. Egeberg, T., Venkatraman, M.M., Davidsen, T., Nassiri, S. (2012) 'Comparative study on gas dispersion.' *Report of a study performed by The Directorate for Civil Protection and Emergency Planning (DSB) and Scandpower Risk Management*.
40. El-Harbawi, M., Mustapha, S., Thomas S. Y. C., Abdul Rashid, Z., Abdul Rashid, S., and Sherif A. A., (2010). 'SCIA: GIS-Based Software for Assessing the Impacts from Chemical Industrial Accidents', *Practice Periodical of Hazardous Toxic and Radioactive Waste Management*.
41. Elliot, Doug & Kuo, J.C. & Nasir, Pervaiz (2008) *Plant processing of natural gas 2<sup>nd</sup> Edition*, The University of Texas at Austin.
42. Elsharkawy, A.M., (2002) Predicting the properties of sour gases and condensates: Equations of State and Empirical Correlations, SPE 74369
43. Ely, A.C. (2004), 'Improved modelling of Sub-Grid Pipework within a CFD flow simulation', *A dissertation presented in part fulfilment of the degree of MSc in CFD, University of Leeds*
44. Emeis, Stefan (2013), *Wind Energy Meteorology: Atmospheric Physics for Wind Power Generation*. Springer-Verlag Berlin Heidelberg, [DOI:10.1007/978-3-642-30523-8](https://doi.org/10.1007/978-3-642-30523-8)
45. Enger, Leif & Koracin, Darko, (1995) 'Simulations of dispersion in complex terrain using a higher-order closure model.' *Atmospheric environment*. 20(18): 2449-2465. DOI: [10.1016/1352-2310\(95\)00160-Z](https://doi.org/10.1016/1352-2310(95)00160-Z)

46. Engineering ToolBox (2019) Thermophysical properties – Air [link](#), accessed on 20 Dec 2019
47. Engineering ToolBox (2020a) Thermophysical properties – Hydrogen sulfide [link](#), accessed on 20 Feb 2020
48. Engineering ToolBox (2020b) Thermophysical properties – Methane [link](#) accessed on 20 Feb 2020
49. EPSC, (1999), *Atmospheric Dispersion*, European Process Safety Centre, Institution of Chemical Engineers
50. Ermak, D L. (1991) 'Gravity spreading in the dispersion of dense gas plumes.' *International conference and workshop on modeling and mitigating the consequences of accidental releases of hazardous materials*, Office of Science United States Dept. of Energy.
51. ESI (2020) 'atmBoundaryLayer Class Reference.' *OpenFOAM: API Guide, The open source CFD toolbox*. [link1](#) & [link 2](#) accessed on 10 June 2020
52. European Gas Pipeline Incident Data Group (1999) Gas Pipeline Incidents Fourth Report 1970–1998 [Google Scholar](#)
53. Ewan, Bruce C.R., and Moodie, K., (1986), 'Structure and velocity measurements in underexpanded jets', *Combustion Science and Technology*. 45 (5-6), 275-288
54. Fairhurst, S. & Turner, R.M. (1993) 'Toxicological assessments in relation to major hazards.' *Journal of Hazardous Materials*. 33:215-227
55. Fearnley, Jo & Nair, SreeRaj (2009) 'Using Predictive Risk Assessment to develop user friendly tools for on and off-site emergency planning', *ICHEME Symposium Series NO. 155, Hazards XXI*, Paper 73 [link \(icheme.org\)](#)
56. Fiates, Juliane & Santos, Raphael Ribeiro Cruz & Neto, Fernando Fernandes & Francesconi, Artur Zaghini & Simoes, Vinicius & Vianna, Sávio S.V. (2016) 'An alternative CFD tool for gas dispersion modelling of heavy gas', *Journal of Loss Prevention in the Process Industries*. 44:583-593,
57. Fiorucci, A. & Pontiggia, M. & Alba, M. & Scaioni, M. & Pendino, R. & Ugucioni, G. & Rota, R., (2008) 'Risk assessment of dangerous products release and dispersion: a

- comparison between CFD and integral models', *Chemical Engineering Transactions*, Simberto Senni Buratti Ed. 13:195-202
58. Flores F. & Garreaud R. & Muñoz R. C., (2014) 'OpenFOAM applied to the CFD simulation of turbulent buoyant atmospheric flows and pollutant dispersion inside large open pit mines under intense isolation', *Computers and Fluids*. 90:72-87.
  59. Fontaine, D.J. & Hall, M.E. Jr., (1991) 'Dispersion modelling of gas releases on Offshore platforms', *Safety and Environment in Oil and Gas Exploration and Production Conference* SPE 23288-MS [doi.org/10.2118/23288-MS](https://doi.org/10.2118/23288-MS)
  60. Frana, Karel & Honzejk, Vit. (2010). 'A comparison between classical DES and DDES using the in-house computational code'. *International conference on System Science and Simulation in Engineering - Proceedings*. 84-89.
  61. Franklin, Gabriel & Barros, Wagner & Marcos, Ceciliano & Cunha, Jeferson & Aquiles, da Rocha & Fagundes, Diego & Margotto, Romulo (2020) 'Computational Fluid Dynamic Modeling for Hazardous Gas Dispersion Analysis in Deepwater, Brazil. *Abu Dhabi International Petroleum Exhibition & Conference*, Paper Number: SPE-202709-MS. [doi.org/10.2118/202709-MS](https://doi.org/10.2118/202709-MS)
  62. Franks A.P. & Harper, P.J. and Bilo, M. (1996) 'The relationship between risk of death and risk of dangerous dose for toxic substances'. *Journal of Hazardous Materials*. 51, 11-34
  63. Fransen, R. & Collado Morata, E. & Duchaine, F. & Gourdain, N. & Gicquel, L.Y.M. & Vial, L. & Bonneau, G. (2012) 'Comparison of RANS and LES in high pressure turbines'. 3rd INCA Colloquim Toulouse: Safran Turbomeca, CERFACS [TR\\_CFD\\_11\\_144.pdf \(cerfacs.fr\)](https://cerfacs.fr/TR_CFD_11_144.pdf)
  64. Fuller, D.C. & Suruda, A.J. (2000) 'Occupationally related hydrogen sulfide deaths in the United States from 1984 to 1994.' *Journal of Occupational and Environmental Medicine*. 42(9):939-942. PMID: 10998771. [doi.org/10.1097/00043764-200009000-00019](https://doi.org/10.1097/00043764-200009000-00019)
  65. Gant, S.E. & Narasimhamurthy, V.D. & Skjold, T. & Jamois, D. & Proust, C. (2014) 'Evaluation of multi-phase atmospheric dispersion models for application to Carbon Capture and Storage.' *Journal of Loss Prevention in the Process Industries*. 32:286-298. [doi.org/10.1016/j.jlp.2014.09.014](https://doi.org/10.1016/j.jlp.2014.09.014)

66. GAO, (2012) *Pipeline Safety - Collecting Data and Sharing Information on Federally Unregulated Gathering Pipelines Could Help Enhance Safety*. GAO-12-388.
67. Guerra, M. J. (2006), *Aspen HYSYS Property Packages: Overview and Best Practices for Optimum Simulations*, AspenTech 1–36.
68. Guo, Boyun & Ghalambor, Ali (2005) 'Chapter 11 – Transportation.' *Natural Gas Engineering Handbook (Second Edition)*. Gulf Publishing Company. 219-262
69. Hanna, S.R., Briggs, G.A., and Hosker, R.P. Jr., (1982) *Handbook on atmospheric diffusion*. United States. [doi.org/10.2172/5591108](https://doi.org/10.2172/5591108).
70. Hanna, S.R., Chang, J.C., Strimaitis, D.G., (1993a). Hazardous gas model evaluation with field observations. *Atmospheric Environment*. 32:3619–3628.
71. Hanna, Steven & Chang, Joseph C. (1993b) 'Hazard response modeling uncertainty (a quantitative method) – Volume 1, Users guide for software for evaluating hazardous gas dispersion models'
72. Hanna, Steven & Chang, Joseph C. (1993c) 'Hazard response modeling uncertainty (a quantitative method) – Volume 2, Evaluation of commonly used hazardous gas dispersion models'
73. Hargreaves, D. M., & Wright, N. G. (2007), 'On the use of the k-ε model in commercial CFD software to model the neutral atmospheric boundary layer', *Journal of wind engineering and industrial aerodynamics*. 95(5):355-369. [doi.org/10.1016/j.jweia.2006.08.002](https://doi.org/10.1016/j.jweia.2006.08.002)
74. Harrison K.L., Bogard D. (2008), Comparison of RANS Turbulence Models for Prediction of Film Cooling Performance. [doi.org/10.1115/GT2008-51423](https://doi.org/10.1115/GT2008-51423) .
75. Haugen, D.A. (Editor) (1959) Project Prairie Grass, A Field Program In Diffusion, Geophysical Research Papers, No. 59, Vol III, AFCRC-TR-58-235(III), *Air Force Cambridge Research Center*. [PGrassVolumelll](#)
76. Havens, Jerry (1992), 'Review of dense gas dispersion field experiments', *Journal of Loss Prevention in the Process Industries*. 5(1):28-41 [//doi.org/10.1016/0950-4230\(92\)80062-D](https://doi.org/10.1016/0950-4230(92)80062-D).

77. Havens, Jerry A., and Thomas O. Spicer. (1985) 'Development of an Atmospheric Dispersion Model for Heavier-Than-Air Gas Mixtures'. Volume 1. Ft. Belvoir: Defense Technical Information Center.
78. Heinz, Stefan (2020) 'A review of hybrid RANS-LES methods for turbulent flows: Concepts and applications.' *Progress in Aerospace Sciences*. 114-100597, ISSN 0376-0421, <https://doi.org/10.1016/j.paerosci.2019.100597>
79. Huertas, J.I. & Martinez, D.S. & Prato, D.F. (2021) 'Numerical approximation to the effects of the atmospheric stability conditions on the dispersion of pollutants over flat areas.' *Scientific Reports* 11:11566. DOI:[/10.1038/s41598-021-89200-9](https://doi.org/10.1038/s41598-021-89200-9)
80. IChemE (2007) 'LNG fire protection and emergency response'. *BP Process Safety Series*, ISBN-13: 978 0 85295 515 4, Institute of Chemical Engineers
81. IOGP (2010) *Risk Assessment Data Directory - Consequence Modelling, Report No. 434-7*, IOGP
82. Jain, Ravi K. & Cui, Zengdi "Cindy" & Domen, Jeremy K. (2016) 'Chapter 4 - Environmental Impacts of Mining', *Environmental Impact of Mining and Mineral Processing*. Butterworth-Heinemann. 53-157, ISBN 9780128040409, DOI: [10.1016/B978-0-12-804040-9.00004-8](https://doi.org/10.1016/B978-0-12-804040-9.00004-8)
83. Jarrin, N., & Prosser, R. & Uribe, J.-C. & Benhamadouche, S. & Laurence, D. (2009). 'Reconstruction of turbulent fluctuations for hybrid RANS/LES simulations using a synthetic-eddy method'. *International Journal of Heat and Fluid Flow* 30(3), 435–442
84. Jie, Ji & Xiaoxia, Chen & Xuefeng, Han (2014), 'Rapid simulation and visualization analysis of liquid ammonia tank leakage risk', *International symposium on Safety science and technology*. [doi.org/10.1016/j.proeng.2014.10.486](https://doi.org/10.1016/j.proeng.2014.10.486)
85. Johnson, D.W., Marx, J.D., (2003) 'The importance of multiphase and multi-component modelling in consequence and risk analysis.' *Journal of Hazardous Materials*. 104(1-3): 51-64.
86. Kelley, B.T. & Valencia, J.A. & Northrop, P.S. & Mart, C.J., (2011), 'Controlled free zone for developing sour gas reserves', *Energy Podia* 4: 824-829
87. Khan, Faisal I. & Abbasi S. A., (1998a), 'Techniques and methodologies for risk analysis in chemical process industries', *Journal of Loss Prevention in the Process Industries*. 11(4):261-277. [https://doi.org/10.1016/S0950-4230\(97\)00051-X](https://doi.org/10.1016/S0950-4230(97)00051-X)

88. Khan, Faisal I. & Abbasi S. A., (1998b), *Risk assessment in chemical process industries*. Discovery publishing house.
89. Koopman, R.P. & Ermak, D.L. and Chan, S.T. (1989) 'A review of recent field tests and mathematical modelling of atmospheric dispersion of large spills of denser-than-air gases.' *Atmospheric Environment*. 23(4):731-745
90. Kulfan, Brenda M. (2012) 'CFD Validation Using Data from a Classic Experimental Test Program for a Highly Contoured Body of Revolution Having Regions of Convergent /Divergent Flows With Adverse/Favorable Pressure Gradients.' *49<sup>th</sup> AIAA Aerospace Sciences Meetings including the New Horizons Forum and Aerospace Exposition AIAA 2011-1235*. DOI:[10.2514/6.2011-1235](https://doi.org/10.2514/6.2011-1235)
91. Launder, B.E. & Spalding, D.B. (1972) *Mathematical Models of Turbulence*. Academic Press, Waltham.
92. Lawson, S.J. & Woodgate, M. & Steijl, R. & Barakos, G.N. (2012) 'High performance computing for challenging problems in computational fluid dynamics.' *Progress in Aerospace Sciences*. 52:19-29
93. Lee, M. & Moser, R.D. (2015) 'Direct numerical simulation of turbulent channel flow up to  $Re_{\tau} \approx 5200$ .' *Journal of Fluid Mechanics*. 774:395–415.
94. Lenntech (2020) 'Parts Per Million (ppm) Converter for Gases.' Available from: <https://www.lenntech.com/calculators/ppm/converter-ppm.htm> (Accessed 15 July 2020)
95. Li, Q. & Guo, T.M. (1991) 'A study on the super-compressibility and compressibility factors of natural gas mixtures.' *Journal of Petroleum, Science & Engineering*. 6:235-247
96. Libre, J. & Tripathi, A. & Guellec, M.L. & Mailliard, T. & Guerin, S. & Souprayen, C. & Castellari, A. (2010) 'Dispersion of accidental release of H<sub>2</sub>S on a gas production site followed in real-time by 3D modelling', *FABIG newsletter issue 55*:16–20
97. Libre, J. & Guerin, S. & Konate, B. & Castellari, A. & Mames, C. & Guellec, M.L., Mailliard, T. & Tripathi, A. & Souprayen, C. & Connan, O. & Leroy, C. & Laguioni, P. & Defenouillere, P. & Letellier, B. & Hebert, D. & Maro, Denis, (2011) 'Validation campaign of a CFD tool on a petrochemical site with wind fluctuations integration', *14th Conference on harmonisation within atmospheric dispersion modelling for regulatory purposes*. H14-175.

98. Linstrom, P.J. & Mallard W.G. (2017) NIST Chemistry WebBook; *NIST Standard Reference Database Number 69*. DOI: 10.18434/T4D303, accessed on 15 June 2017
99. Liu, Qiong & Gómez,F. & Pérez, J.M. & Theofilis, V. (2016) 'Instability and sensitivity analysis of flows using OpenFOAM', *Chinese Journal of Aeronautics*. 29(2): 316-325, ISSN 1000-9361. <https://doi.org/10.1016/j.cja.2016.02.012>.
100. Lysenko D. A., Ertesvåg I. S., Rian K. E., (2010) 'Modeling of turbulent separated flows using OpenFOAM.' *Computers and Fluids*. 80:408-422
101. Macchi, Marco & Wen, Jennifer X. & Volkov, Konstantin & Heidari, Ali & Chung, Yongmann M. (2016) 'Modeling liquid fuel cascades with OpenFOAM.' *Process Safety Progress*. 35(2):179-184.
102. Macdonald, R., (2003) *Theory and objectives of air dispersion modelling*, Course notes MME 474A Wind Engineering, Modelling air emissions for compliance, University of Waterloo.
103. Mack, A., & Spruijt, M.P.N., (2013) 'Validation of OpenFoam for heavy gas dispersion applications.' *Journal of Hazardous Materials* 262: 504– 516.
104. Mack, A., & Spruijt, M.P.N., (2014) 'CFD dispersion investigation of CO2 worst case scenarios including terrain and release effects.' *Energy Procedia* 51:363-372 .
105. Mannan, Sam (2014), *Lees' Loss Prevention in Process Industries*, AIChE (edited book)
106. Matha, M., Morsbach C.and Bergmann M. (2018) *A comparison of methods for introducing synthetic turbulence*. Conference: 7th ECCOMAS European Conference on Computational Fluid Dynamics, Volume: Proceedings of the 6th European Conference on Computational Mechanics: Solids, Structures and Coupled Problems, ECCM 2018 and 7th European Conference on Computational Fluid Dynamics, ECFD 2018
107. McQuaid, J. (1985), 'Heavy gas dispersion trials at Thorney Island', *Proceedings of Symposium held at the University of Sheffield - 1984, Chemical Engineering Monographs*. Elsevier Science.
108. Menter, F. R. (1994), 'Two-Equation Eddy-Viscosity Turbulence Models for Engineering Applications', *AIAA Journal*. 32(8):1598-1605.



109. Mohan, Manju & Panwar T. S. & Singh M.P. (1995) 'Development of dense gas dispersion model for emergency preparedness.' *Atmospheric Environment*. 29(16):2075-2087 DOI: [10.1016/1352-2310\(94\)00244-F](https://doi.org/10.1016/1352-2310(94)00244-F)
110. Mohsen-Nia, M. & Moddares, H. & Manoori, G. (1994) 'Sour natural gas and liquid equation of state.' *Journal of Petroleum Science and Engineering*, 12(2): 127-36.
111. Morio, Jerome & Balesdent, Mathieu (2015) *Estimation of Rare Event Probabilities in Complex Aerospace and Other Systems – A practical approach*. Woodhead Publishing in Mechanical Engineering
112. Morton, B., Taylor, G., & J.S., T., (1956) Turbulent gravitational convection flow from maintained and instantaneous sources – Proceedings from Royal Society, Series A, 234, 1
113. Moukalled, Fadi & Mangani, Luca & Darwesh, Marwa. (2015) *The Finite Volume Method in Computational Fluid Dynamics: An advanced introduction with OpenFOAM and Matlab*. DOI:[10.1007/978-3-319-16874-6](https://doi.org/10.1007/978-3-319-16874-6)
114. Muhlbauer W.K. (2004) *Pipeline risk management manual ideas, techniques and resources*, 3rd Edition, ISBN: 0-7506-7579-9, 14/327 – 328
115. NACE MR 0175 (2021) 'Petroleum and natural gas industries— Materials for use in H<sub>2</sub>S-containing Environments in oil and gas production— Part 1: General principles for selection of cracking-resistant materials', NACE MR0175/ISO 15156-1:2001(E) National Association of Corrosion Engineers.
116. Nair, Sreeraj & Ogbeifun, Noma O. & Wen, Jennifer (2022) 'Consequence assessment considerations for toxic natural gas dispersion modeling.' *Journal of Loss Prevention in the Process Industries*. 78:104792. <https://doi.org/10.1016/j.jlp.2022.104792>
117. Nair, Sreeraj & Salter, Jim (2019), 'Layout - A Cost Effective and Powerful Design Step in Risk Management', *Chemical Engineering Transactions*. 77:13-18 [//doi.org/10.3303/CET1977003](https://doi.org/10.3303/CET1977003)
118. Nair, Sreeraj R. & Wen, Jennifer (2019) 'Uncertainties in Sour Natural Gas Dispersion Modelling.' *Chemical Engineering Transactions*. 77:355-360. [//doi.org/10.3303/CET1977060](https://doi.org/10.3303/CET1977060)

119. Nasrifar, Kh. & Bolland, O. (2005) 'Thermodynamic Properties of Natural Gas Mixtures Using Equations of State', ECTP Paper 30, *Department of Energy and Process Engineering*, Norwegian University of Science and Technology (NTNU).
120. NFPA (2010) Standard System for the Identification of the Hazards of Materials for Emergency Response - H<sub>2</sub>S diamond, National Fire Protection Association.
121. Nilsen, S. & Hoiset, S. & Salaun, N. (2014) 'Improving safety risk tools for accidental fluid releases with high H<sub>2</sub>S concentrations', *Abu Dhabi International Petroleum Exhibition and Conference*, SPE-171809-MS.
122. NIOSH (2005) *Pocket Guide to Chemical Hazards: Hydrogen Sulphide*, Centers for Disease Control and Prevention, National Institute for Occupational Safety and Health (NIOSH), U.S. Department of Health and Human Services. [link](#) accessed on 21 Apr 2016.
123. NOAA (2013) ALOHA<sup>®</sup> (AREAL LOCATIONS OF HAZARDOUS ATMOSPHERES) 5.4.4, Technical Memorandum NOS OR&R 43, Technical documentation, National Ocean Service.
124. NOAA (2016) [HYDROGEN SULFIDE | CAMEO Chemicals | NOAA](#) accessed in December 2016
125. NOAA (2017) ALOHA fact sheet [ALOHA Fact Sheet \(noaa.gov\)](#) accessed in December 2017
126. NOAA (2018) Pasquill Stability Classes, Air Resources Laboratory, National Oceanic and Atmospheric Administration-USA [link](#) accessed in Feb 2018
127. NOAA (2020), Data Archive of Tracer Experiments and Meteorology – DATEM, Air Resources Laboratory, National Oceanic and Atmospheric Administration (<http://www.arl.noaa.gov/DATEM.php>) ; accessed on November 2020
128. NOAA (2022) Emergency preparedness (public exposure) [Emergency Response Planning Guidelines \(ERPGs\) | response.restoration.noaa.gov](#) accessed in January 2022
129. NORSOK (2001) 'Risk and emergency preparedness analysis.' *NORSOK Standard Z-013*. Rev2.

130. O'Shaughnessy, P.T. & Altmaier, R. (2011) 'Use of AERMOD to determine a hydrogen sulfide emission factor for swine operations by inverse modelling.' *Atmospheric Environment*. 45:4617-4625
131. Occupational Safety & Health Administration (OSHA), US Department of Labour, Hydrogen sulfide Health hazards <https://www.osha.gov/SLTC/>, accessed on Jan 2016.
132. OpenFOAM user manual <https://www.openfoam.com/documentation/> [OpenFOAM](#) (accessed on 20 Sep 2019)
133. Osman, K & Geniaut, B. & Herchin, N. & Blanchetiere, V. (2015 'A review of damages observed after catastrophic events experienced in the mid-stream gas industry compared to consequences modelling tools', *HAZARDS 25 IChemE Symposium Series No 160*.
134. Palazzi, E., M. Defaveri, G. Fumarola, and G. Ferraiolo. 1982. 'Diffusion from a Steady Source of Short Duration.' *Atmospheric Environment* no. 16 (12):2785-2790
135. Pandya, Nishant & Gabas, Nadine & Marsden, Eric (2012), 'Sensitivity analysis of Phast's atmospheric dispersion model for three toxic materials (nitric oxide, ammonia, chlorine).' *Journal of Loss Prevention in the Process Industries*. 25(1):20-32. DOI: [10.1016/j.ilp.2011.06.015](https://doi.org/10.1016/j.ilp.2011.06.015)
136. Pandya, Nishant & Gabas, Nadine & Marsden, Eric, (2013), 'Uncertainty Analysis of Phast's Atmospheric Dispersion Model for Two Industrial Use Cases.' *Chemical Engineering Transactions, AIDIC*. 31:97-102. <https://doi.org/10.3303/CET1331017>.
137. Papanikolaou, E. & Baraldi D. (2011) 'Comparison of modelling approaches for CFD simulations of high pressure hydrogen releases'. European Commission DG-JRC, *Institute for Energy*. [PapanikolaouBaraldi FinalSubmitted Efi V5.doc \(unipi.it\)](#)
138. Papanikolaou, E. & Baraldi, D. & Kuznetsov, M. & Venetsanos, A. (2012) 'Evaluation of notional nozzle approaches for CFD simulations of free-shear under-expanded hydrogen jets.' *International Journal of Hydrogen Energy*. 37(23):18563-18574
139. Parker, M., (2010) Method of removing H<sub>2</sub>S from sour gas & converting it to H<sub>2</sub> and H<sub>2</sub>SO<sub>4</sub>, Thesis, University of Standford.
140. Pasquill, F. (1961) 'The estimation of the dispersion of windborne material.' *Meteorol. Mag.* 90:33-49

141. Patterson, J. & Balin, R., & Jansen, K. (2021). 'Assessing and improving the accuracy of synthetic turbulence generation.' *Journal of Fluid Mechanics*. 906. doi:10.1017/jfm.2020.859
142. PennState (2020) [2.7: The Gibbs Phase Rule | PNG 301: Introduction to Petroleum and Natural Gas Engineering \(psu.edu\)](#) link assessed June 2020
143. Picknett, R.G. (1981) 'Dispersion of dense gas puffs released in the atmosphere at ground level', *Atmospheric Environment*. 15(4):509-525.
144. Poletto, R. & Craft, T. & Revell, A. (2013). A new divergence free synthetic eddy method for the reproduction of inlet flow conditions for LES. *Flow, Turbulence and Combustion* 91(3), 519–539.
145. Pontiggia M. & Busini, V. & Gattuso, M. & Uguccioni, G. & Rota R. (2012) 'Consequences Assessment of an Accidental Toxic Gas Release Through a CFD Tool: Effect of the Terrain and Major Obstacles', *Chemical Engineering Transaction*. 26:537-542 [//doi.org/10.1016/0004-6981\(81\)90181-5](https://doi.org/10.1016/0004-6981(81)90181-5)
146. Pope, Stephen B. (2002) *Turbulent flows*. Cambridge University Press
147. Qiao, Y. (2006) 'Quantitative transportation risk analysis based on available data/databases: decision support tools for hazardous materials transportation.' PhD Thesis, Chemical Engineering, Texas A&M University.
148. Qingchun, Ma & Laibin Zhang, (2011) 'CFD simulation study on gas dispersion for risk assessment: A case study of sour gas well blowout.' *Journal of Safety Science*. 49:1289–1295
149. Quest (2020) Canary by Quest <https://www.questconsult.com/software/canary/>, link accessed August 2020.
150. Reiffenstein, R. & Hulbert, W.C. & Roth, S.H. (1992) 'Toxicology of hydrogen sulfide.' *Annual Review of Pharmacology and Toxicology*. 32(1):109-134.
151. Reynolds, O. (1895). 'On the Dynamical Theory of Incompressible Viscous Fluids and the Determination of the Criterion.' *Philosophical Transactions of the Royal Society of London A*. 186: 123–164. DOI:[10.1098/rsta.1895.0004](https://doi.org/10.1098/rsta.1895.0004). [JSTOR 90643](https://www.jstor.org/stable/90643)
152. Richards, P. J. & Hoxey, R. P. (1993) 'Appropriate boundary conditions for computational wind engineering models using the k-ε turbulence model.' *Journal of Wind*

*Engineering and Industrial Aerodynamics*. 46-47: 145-153. DOI: [10.1016/0167-6105\(93\)90124-7](https://doi.org/10.1016/0167-6105(93)90124-7)

153. Ricou, F., & Spalding, D (1961), 'Measurement of entrainment by aximsymmetrical turbulent jets.' *Journal of Fluid Mechanics*. 11 (1):21-31.
154. Shaheed, R. & Mohammadian, A. & Kheirkhah Gildeh, H. (2019) 'A comparison of standard  $k-\epsilon$  and realizable  $k-\epsilon$  turbulence models in curved and confluent channels.' *Environmental Fluid Mechanics*. 19:543–568
155. Sharan, Maithili & Yadav, Anil & Singh, Manmeet (1996) 'Plume Dispersion Simulation in Low-Wind Conditions Using Coupled Plume Segment and Gaussian Puff Approaches', *Journal of Applied Meteorology*. 35: 1625-1631.
156. Shen, C. & Sun, F. & Xia, X. (2013) 'Analysis on capabilities of density-based solvers within OpenFOAM to distinguish aerothermal variables in diffusion boundary layer', *Chinese Journal of Aeronautics*. 26(6):1370-1379.
157. Shi, F. & Zhang, L. & Yang, J. & Lu, M. & Ding, J. & Li, H. (2015) 'Polymorphous FeS corrosion products of pipeline steel under highly sour conditions', *Journal Corrosion Science*. CS-6495
158. Simon, Coldrick (2017) 'Review of consequence model evaluation protocols for major hazards under the EU SAPHEDRA platform', HSE Research Report 1009. [www.hse.gov.uk/research/rrpdf/rr1099.pdf](http://www.hse.gov.uk/research/rrpdf/rr1099.pdf)
159. Simon, Gant & Weil, Jeffrey & Monache, Luca Delle & McKenna, Bryan & Garcia, Maria M. & Tickle, Graham & Tucker, Harvey & Stewart, James & Kelsey, Adrian & McGillivray, Alison & Batt, Rachel & Witlox, Henk & Wardman. Mike (2018) 'Dense gas dispersion model development and testing for the Jack Rabbit II phase 1 chlorine release experiments', *Atmospheric Environment*. 192:218-240. ISSN 1352-2310, DOI: [/10.1016/j.atmosenv.2018.08.009](https://doi.org/10.1016/j.atmosenv.2018.08.009).
160. Smagorinsky, J. (1963) 'General Circulation Experiments with the Primitive Equation I the Basic Experiment', *Monthly Weather Review*. 91, 99-164.
161. Soe, Thet Mon & Khaing, San Yu (2017) 'Comparison of Turbulence Models for Computational Fluid Dynamics Simulation of Wind Flow on Cluster of Buildings in Mandala', *International Journal of Scientific and Research Publications*. 7(8):337

162. Spalart, P.R. & Jou, W.H. & Strelets, M. & Allmaras, S.R. (1997) 'Comments on the Feasibility of LES for Wings, and on a Hybrid RANS/LES Approach', First AFOR Int. Conference on DNS/LES.
163. Spalart, P.R., Jou, W.H., Strelets, M., and Allmaras, S.R.: Comments on the Feasibility of LES for Wings, and on a Hybrid RANS/LES Approach, First AFOR Int. Conference on DNS/LES, edited by C.Liu and Z. Liu, Greyden, Columbus, OH, 1997
164. Spalart, P. R. & Deck, S. & Shur, M. & Squires, K. & Strelets, M. & Travin, A. (2006). 'A new version of detached-eddy simulation, resistant to ambiguous grid densities'. *Theoretical and Computational Fluid Dynamics* 20(3), 181–19
165. Speight, J. G. (2007) *Natural Gas – A basic handbook*. Gulf publishing company. ISBN 1-933762-14-4
166. Spicer, T., and J. Havens. 1989. User's Guide for the DEGADIS 2.1 Dense Gas Dispersion Model. Cincinnati: United States Environmental Protection Agency
167. Stephens, M. J. (2000) 'GRI-00/0189 - A model for sizing high consequence areas associated with natural gas pipelines', *Gas Research Institute*.
168. Stewart, James (2020) 'CFD modelling of underexpanded hydrogen jets exiting rectangular shaped openings', *Process Safety and Environmental Protection* 139:283-296, DOI: [10.1016/j.psep.2020.04.043](https://doi.org/10.1016/j.psep.2020.04.043).
169. Suzuki, Y. J. & Koyaguchi, T. (2013) '3D numerical simulation of volcanic eruption clouds using the 2011 Shinmoe-dake eruptions', *Earth Planets Space*. 65(10): 581-589.
170. Tapia, Xabier Pedruelo (2009) 'Modelling of wind flow over complex terrain using OpenFoam', *Department of Technology and Built Environment*, University of Gavle.
171. Tauseef, S. M. & Abbasi, T. & Abbasi, S. A. (2010) 'Risks of fire and explosion associated with the increasing use of liquefied petroleum gas (LPG)', *Journal of Failure Analysis and Prevention*. 10 (4): 322-333
172. Tauseef, S.M. & Abbasi, Tasneem & Saganya, R. & Abbasi, S.A. (2017) 'A critical assessment of available software for forecasting the impact of accidents in chemical process industry', *International Journal of Engineering, Science and Mathematics*. 6 (7): 269–P289. ISSN: 2330-0294 [4037 pdf.pdf \(ijesm.co.in\)](https://www.ijesm.co.in)

173. Taylor, D.W. (2007) 'The role of consequence modeling in LNG facility siting', *Journal of hazardous materials*. 142, 776-785.
174. Total esp. (2006) *Sour gas – A history of expertise, Exploration and Production*; [link](#), accessed on 10 Jan 2016
175. Uijt de Haag, P.A.M. & Ale B.J.M. (2005) 'CPR 18E Guideline for quantitative risk assessment (Purple book)', *Committee for the Prevention of Disasters. VROM - PGS 3. GEVAARLIJKE STOFFEN*
176. UK HSE (1993) *Oilfield reservoir souring*, OTH 92385, United Kingdom - Health & Safety Executive HMSO publication
177. UK HSE (2010) [RR789 - LNG source term models for hazard analysis \(hse.gov.uk\)](#)], [Link](#) accessed on 30 Nov 2021
178. UK HSE (2016), Toxicity levels of chemicals, Assessment of the Dangerous Toxic Load (DTL) for Specified Level of Toxicity (SLOT) and Significant Likelihood of Death (SLOD), United Kingdom - Health and Safety Executive. [link](#) accessed on 11 Jun 2016
179. UK HSE (2022) 'Safety Report Assessment Guidance - COMAH, *United Kingdom - Health and Safety Executive*. [link](#) assessed on 20 Nov 2022
180. US CSB (2021) 'Aghorn Operating Waterflood Station Hydrogen Sulfide release – Investigation details', US Chemical Safety and Hazard Investigation Board. [link \(CSB\)](#), accessed on 20 Nov 2021
181. US CSB, (2003) 'Investigation Report January 2003.: Hydrogen Sulfide Poisoning. Georgia-Pacific, Naheola Mill, Pennington, Alabama, January 16, 2002, Report No. 2002-01-I-AL.' Chemical Safety and Hazard Investigation Board. [link \(csb.gov\)](#)
182. US DoL (2022) United States Department of Labor, Occupational Health and Safety Administration (OSHA), 1910.119 App A - List of Highly Hazardous Chemicals, Toxics and Reactives (Mandatory) [link](#) accessed on 15 Aug 2022
183. US DoL, (2019), Occupational Safety (workforce exposure), Hydrogen Sulfide – Hazards, Occupational Health and Safety Administration (OSHA), United States Department of Labor. [link](#) accessed on 25 Jun 2019
184. US DoT (2018) 'Pipeline Risk Modeling Overview of Methods and Tools for Improved Implementation', *Pipeline and hazardous materials safety administration*, [link](#)

185. US EPA (1987) 'Technical Guidance for Hazards Analysis Emergency Planning for extremely hazardous substances' [Link \(epa.gov\)](#).
186. US EPA (2005), Appendix W to 40 CFR Part 51: Guideline on Air Quality Models, Alternate models recognized for specialized applications, [link](#) accessed on Jan 2016.
187. US EPA (2010) *Acute Exposure Guideline Levels for Selected Airborne Chemicals, Volume 9, Committee on Acute Exposure Guideline Levels*. Committee on Toxicology, National Research Council. ISBN: 0-309-15945-8. [link](#) accessed on Nov 2018
188. US EPA (2018) *ALOHA user manual*. United States – Environmental Protection Agency [link](#) accessed on 20 Sep 2018
189. Venetsanos, A.G., & Papanikolaou, E. and Bartzis, J.G., (2010), The ADREA-HF CFD code for consequence assessment of hydrogen applications, *International Journal of Hydrogen Energy*, 35, 3908-3918.
190. Versteeg, H.K., & Malalasekera, W. (1995) *An introduction to computational fluid dynamics, the finite volume method, Chapter 12*. 2<sup>nd</sup> Edition, Pearson, Prentice Hall.
191. Wang Lili & Wang Mengzhu &, Lv Yan & Qi Hanbing & Li Dong, (2016) Numerical Simulation of Gas Diffusion in Overhead Natural Gas Pipeline Leakage, *Scholars Journal of Engineering and Technology* (SJET) ISSN 2321-435X (Online). 4(3):142-147
192. Wen, J.X. & Heidari, A. & Xu, B. & Jie, H. (2013) 'Dispersion of carbon dioxide from vertical vent and horizontal releases - A numerical study', *Proceedings of IMechE Part E*. 227(2):125–139
193. Wen, Jennifer X. & Fur, Pierre Le & Jie, Hongen & Vendra, C. Madhav Rao (2016) 'Further development and validation of CO2FOAM for the atmospheric dispersion of accidental releases from carbon dioxide pipelines', *International Journal of Greenhouse Gas Control*. 293-304.
194. Wen, Jennifer X. & Vendra, C. Madhav Rao & Tam, Vincent H.Y. (2011) 'Numerical study of hydrogen explosion in refueling environment and in a model storage room', *International Journal of Hydrogen Energy*. 35(1) 385-394.
195. Wendt, John F (2009) *Computational Fluid Dynamics: An Introduction*, Von Karman Institute Book, Third Edition, Springer



196. Wilcox, D. C. (2008) 'Formulation of the  $k-\omega$  Turbulence Model Revisited.' *AIAA Journal*. 46:2823–2838. DOI:[10.2514/1.36541](https://doi.org/10.2514/1.36541)
197. Witlox, Henk W.M. & Harper, M. & Natarajan, S. & Williamson, A. (2015) 'Modelling of time-varying dispersion for elevated pressurised releases without rainout.' *Journal of loss prevention in the process industries*. 35:283-292
198. Woodward, J. L. (1998) *Estimating the flammable mass of a vapor cloud*. A CCPS concept book, AIChE
199. Wu, Y. & Carroll, J.J. & Zhu, W. (2012) 'Sour Gas and Related Technologies' *Proceedings of the Third International Acid Gas Injection Symposium (AGIS)*.
200. Xu, J. & Fan, Y. (2014) 'An individual risk assessment framework for high pressure natural gas wells with hydrogen sulfide, applied to a case study in China', *Journal Safety Science*. 68:14-23
201. Yang, D. & Chen, G. & Shi, J. & Xinhong, L. (2019) 'Effect of gas composition on dispersion characteristics of blowout gas on offshore platform.' *International Journal of Naval Architecture and Ocean Engineering*. 11:914e92 [link \(koreascience.kr\)](http://link.koreascience.kr)
202. Yang, Duoxing & Chen, Gangcai & Dai Z (2020) 'Accident modeling of toxic gas-containing flammable gas release and explosion on an offshore platform.' *Journal of Loss Prevention in the Process Industries*. 65:104118. DOI: [/10.1016/j.jlp.2020.104118](https://doi.org/10.1016/j.jlp.2020.104118)
203. Yang, Duoxing & Chen, Gangcai & Zhang, Renjian. (2006). 'Estimated Public Health Exposure to H<sub>2</sub>S Emissions from a Sour Gas Well Blowout in Kaixian County, China.' *Aerosol Air Qual. Res*. 6:430-443. DOI: [/10.4209/aaqr.2006.09.0018](https://doi.org/10.4209/aaqr.2006.09.0018)
204. Yang, Y., Gu, M., & Jin, X., (2009b), New inflow boundary conditions for modelling the neutral equilibrium atmospheric boundary layer in SST  $k-\omega$  model. In: *The Seventh Asia-Pacific Conference on Wind Engineering*, Taipei, Taiwan.
205. Yang, Y., Gu, M., Chen, S., & Jin, X. (2009a) 'New inflow boundary conditions for modelling the neutral equilibrium atmospheric boundary layer in computational wind engineering', *Journal of Wind Engineering and Industrial Aerodynamics*., 97(2), 88-95. DOI:[10.1016/j.jweia.2008.12.001](https://doi.org/10.1016/j.jweia.2008.12.001)
206. Ying Zhen Li, Chen Huang, Johan Anderson, Robert Svensson, Haukur Ingason, Bjarne Husted, Marcus Runefors, Jonathan Wahlqvist, (2017) Verification, validation and

- evaluation of FireFOAM as a tool for performance design, Report 3208 BRANDFORSK 2017:2 ISSN: 1402-3504 [FireFOAM validation link \(diva-portal.org\)](#)
207. Yusuf, S. N. A. & Asako, Y., Che Sidik, N. A. & Mohamed, S. B. & Aziz Japar, W. M. A. (2020). 'A Short Review on RANS Turbulence Models.' *CFD Letters*. 12(11):83–96.
  208. Zang, B. & Vevek, U. S. & Lim, Haoxiang & Wei, Xiaofeng & New, T. H. (2018). An assessment of OpenFOAM solver on RANS simulations of round supersonic free jets. *Journal of Computational Science*. 28. 10.1016/j.jocs.2018.07.002.
  209. Zemba, S.G. & Saikaly, R.S. & Welch, J.E. & Maksoudian, T.L. & Hibbard, C.S. & Molloy, K.P., (2014), 'CFD simulations of H<sub>2</sub>S-rich plumes from oil/gas well blowouts.', Paper 33608, *A&WMA's 107<sup>th</sup> Annual conference & exhibition, Navigating Environmental Crossroads*. P2642-2653
  210. Zhang, B. & Chen, G., (2010) 'Quantitative risk analysis of toxic gas release caused poisoning—A CFD and dose–response model combined approach.' *ICHEME Journal, Process Safety and Environmental Protection*. 88 (4): 253-262
  211. Zhang, J. & Lei, D. & Feng, W., (2011) 'Analysis of chemical disasters caused by release of hydrogen-sulfide bearing natural gas', *Procedia Engineering*. 26:1878-1890 ISSN 1877-7058 [doi.org/10.1016/j.proeng.2011.11.2380](https://doi.org/10.1016/j.proeng.2011.11.2380)
  212. Zhang, J. & Lei, D. & Feng, W. (2014) 'An approach for estimating toxic releases of H<sub>2</sub>S-containing natural gas,' *Journal of Hazardous Materials*. 264: 350-362. ISSN 0304-3894 <https://doi.org/10.1016/j.jhazmat.2013.09.070>.
  213. Zhang, Z. and Chen, Q. (2007). 'Comparison of the Eulerian and Lagrangian methods for predicting particle transport in enclosed spaces.' *Atmospheric Environment*. 41(25): 5236-5248. [link \(purdue.edu\)](#)
  214. Zhu, H. & Mao, Z. & Wang, Q. & Sun, J. (2013) 'The influences of key factors on the consequence following the natural gas leakage from pipeline.' *The 9th Asia-Oceania Symposium on Fire Science and Technology*. 592-601
  215. Zhu, Y. & Chen, G. & Deng, H. (2010) 'Analysis of Hydrogen Sulfide impact from sour gas well blowout in offshore platform', *Proceedings of the ASME 2010 29th International Conference on Ocean, Offshore and Arctic Engineering*. 29th International Conference on Ocean, Offshore and Arctic Engineering, China: 2:629-637. ASME. <https://doi.org/10.1115/OMAE2010-20874>



## Abbreviations

<b>ALOHA</b>	Areal Location of Hazardous Atmosphere (software tool)
<b>BIN</b>	Binary Interaction Numbers
<b>C<sub>2</sub>H<sub>6</sub></b>	Ethane
<b>C<sub>3</sub>H<sub>8</sub></b>	Propane
<b>CAMEO</b>	Computer Aided Management of Emergency Operations
<b>CFD</b>	Computational Fluid Dynamics
<b>CH<sub>4</sub></b>	Methane
<b>CO<sub>2</sub></b>	Carbon dioxide
<b>DDES</b>	Delayed Detached Eddy Simulation
<b>DFSEM</b>	Divergence Free Synthetic Eddy Method
<b>DNV</b>	Det Norske Veritas (a Software Company)
<b>DTL</b>	Dangerous Toxic Load
<b>EoS</b>	Equation of State
<b>EPA</b>	Environmental Protection Agency
<b>Fac2</b>	Fraction within a Factor of Two
<b>Fac5</b>	Fraction within a Factor of Five
<b>FB</b>	Fractional Bias
<b>GMB</b>	Geometric Mean Bias
<b>GV</b>	Geometric Variance
<b>H<sub>2</sub>S</b>	Hydrogen sulphide
<b>IDLH</b>	Immediately Dangerous to Life and Health
<b>LES</b>	Large Eddy Simulations
<b>MARPLOT</b>	Mapping Application for Response, Planning and Local Operational Tasks
<b>NACE</b>	National Association of Corrosion Engineers
<b>NOAA</b>	National Oceanic and Atmospheric Administration

<b>NMSE</b>	Normalized Mean Square Error
<b>OECD</b>	Organisation for Economic Cooperation and Development
<b>OGP</b>	Oil and Gas Producers Association
<b>OpenFOAM</b>	Open-source Field Operation and Manipulation
<b>OSHA</b>	Occupational Safety Health Administration
<b>PISO</b>	Pressure Implicit with Splitting of Operators
<b>PR</b>	Peng-Robinson EOS
<b>PT</b>	Patel-Teja EOS
<b>RANS</b>	Reynolds Averaged Navier-Stokes equations
<b>SPE</b>	Society of Petroleum Engineers
<b>SIMPLE</b>	Semi-Implicit Method for Pressure Linked Equations
<b>SRK</b>	Soave-Redlich-Kwong EOS
<b>SLOD</b>	Significant Likelihood of Death
<b>SLOT</b>	Specified Level of Toxicity
<b>STEL</b>	Short Term Exposure Limit
<b>TLV</b>	Threshold Limit Value
<b>TOPSIS</b>	The Technique for Order of Preference by Similarity to Ideal Solution
<b>US CSB</b>	United States Chemical Safety and Hazard Investigation Board
<b>US DoL</b>	United States Department of Labor
<b>US DoT</b>	United States Department of Transport
<b>US EPA</b>	United States Environmental Protection Agency
<b>UK HSE</b>	United Kingdom Health and Safety Executive

## Definitions

<b>Advection</b>	Along the wind (downwind) spread, the horizontal movement of mass of fluid
<b>Atmospheric dispersion</b>	The low momentum mixing of a vapour / gas or aerosol with air. The mixing is the result of turbulent energy exchange, which is a function of wind (mechanical eddy formation) and atmospheric temperature profile (thermal eddy formation)
<b>Atmospheric stability</b>	A measure of the degree of atmospheric turbulence, particularly vertical mixing in the atmosphere.
<b>Buoyant (Positively buoyant) gas</b>	A gas with density less than that of air at ambient temperature
<b>Choked flow</b>	Choked flow occurs with compressible fluids and is defined as the pressure where the discharge velocity becomes sonic (reaches the speed of sound). Choked flow usually occurs when the ratio of downstream to upstream pressure is in the range of 0.5 to 0.9.
<b>Concentration</b>	The relative amount of a substance when combined or mixed with other substances. Concentration can be expressed as mole fraction, mass fraction, component mole density or mass density
<b>Continuous release</b>	Emission that are long in duration compared with the travel time (time for cloud to reach a location of interest)
<b>Cricondenbar</b>	the maximum pressure above which no gas can be formed regardless of the temperature. The corresponding temperature is called cricondenbar temperature.
<b>Cricodentherm</b>	the maximum temperature above which liquid cannot be formed regardless of the pressure. The corresponding pressure is called cricodentherm pressure.
<b>Critical flow</b>	the flow above choked flow (where difference in pressure does not increase the flow)
<b>Critical point</b>	At the critical point, there is no change of state when pressure is increased or if heat is added
<b>Dense gas</b>	A gas with density exceeding that of air at ambient temperature (also referred as heavy gas, negatively buoyant gas). The vapours tend to sink to low spots and to spread along the ground by 'gravity spreading'.
<b>Dispersion</b>	A term used by modellers to include advection (downwind movement) and diffusion (spreading horizontally and vertically) of pollutants in air
<b>Footprint</b>	Typically the estimated footprint represents the area within which the concentration of a pollutant gas exceeds the set level of concern

<b>Gaussian model</b>	A dispersion model based on the concept of that atmospheric diffusion is a random mixing process driven by turbulence in the atmosphere.
<b>Gravity slumping</b>	The decrease in cloud height of a flowing dense gas due to the effects of gravity (negative buoyancy), also referred as ground hugging
<b>Integral model</b>	A dispersion model which averages or “integrates” the concentration in a given dimension or time so that concentrations can be described by solving an ordinary differential equation instead of a partial differential equation
<b>Jet discharge</b>	A release of vapour or aerosol at sufficient pressure that the momentum of the release provides the dominating mechanism for air entrainment and for the centreline trajectory of the release
<b>Nose of vapour cloud</b>	The front surface of vapour cloud, that is, the surface farthest along in the along-wind direction.
<b>Passive dispersion</b>	Dispersion caused by the normal turbulence in the atmosphere
<b>Sour gas</b>	Natural gas with toxic hydrogen sulphide
<b>Triple point</b>	The temperature and pressure at which the three phases (gas, liquid, and solid) of that substance co-exist in thermodynamic equilibrium
<b>Verification</b>	To check that a computer code produces adequate solutions of the equations it purports to solve, a task typically done by the originators of the code or the software developer.
<b>Validation</b>	Comparison with experiment and other models to ensure the credibility of the model, results, and applicability.

## Appendix A: OpenFOAM solver selection and set up

This appendix includes the details of a simple proto-type case for the dispersion modelling of Natural gas (Methane) using OpenFOAM which was developed at the initial stages of the research. The input, and criteria for the model development were analysed and the outcome from the initial sensitivity screening for meshing was carried out using the initial set of simulations.

The model development and the simulations were for the dispersion of buoyancy driven flows in open field with complex terrain to determine the distance of pollutant / hazardous material travel in the event of loss of containment. The release scenario considered is a 100% methane (gas) release from a small bore at a velocity of 0.1 m/s. The atmospheric conditions considered for the turbulence include wind velocity at 1 m/s, neutral stability, and temperature of 25 °C. An OpenFOAM tutorial case for Combustion (3D pool) was used with new geometry and application case specific boundary conditions, and fireFoam solver with the combustion properties turned off.

The objective was to simulate appropriate meshing for the selected geometry with different types of obstructions along the dispersion field of a pollutant gas. The geometry considered is a long vertical box with inlet, outlet, base with obstructions representing channel and mountains and sides. The overall modelling steps included (1) Geometry, (2) mesh generation, (3) case setup and solution, (4) post-processing. Low release velocities were used such that the methane mixing with air to be dominated by buoyancy rather than momentum (pseudo source, which is considered as the worst-case scenario release where the unignited methane travels to the maximum downwind distance).

FireFOAM, has been mainly developed and maintained by FM Global based on the platform of OpenFOAM. FireFOAM is a compressible flow solver and can run simulations using Large Eddy Simulation (LES) turbulence model. FireFOAM is aimed at modelling problems relevant to thermo- and fluid-dynamics and multiphase flow. Although the solver was developed to simulate fires, it has robust numerical schemes for tracking the dispersion and mixing of different species. For the study, the combustion, radiation, and pyrolysis components of fireFoam not to be used (Off / false) and use the solver to model the dispersion and mixing of methane in air. FireFOAM solver was chosen due to the following reasons:

- stable solver, low Mach number
- solutions for pressure differences



- transport of multiple species

### Turbulence and thermophysical models

The general turbulence library, fireFoam solver, can be used to run simulations using both LES and RANS turbulence models. fireFoam is a compressible flow solver, the ideal gas law is invoked as follows

$$P = \rho R_{\text{spec}} T$$

Equation 49

where,  $P$  is the gas pressure;  $T$  is the gas temperature;  $\rho$  is the gas density and  $R_{\text{spec}} = R^0/W$  is the specific gas constant in unit of J/(K·kg).

In fireFoam solver, transport equation for sensible enthalpy  $h_s$  is solved, and the relation between sensible and total enthalpy  $h$  is as follows:

$$h = h_s + \sum_k h_{f,k}^0 Y_k$$

Equation 50

where  $h_{f,k}^0$  and  $Y_k$  are the heat of formation and mass fraction, respectively, of species  $k$ . By default, in fireFoam, temperature and sensible enthalpy are connected by the widely used temperature dependent JANAF thermodynamic polynomial from NIST as follows:

$$h_s = \frac{R^0}{W} \left( \sum_{k=1}^5 \frac{a_k}{k} T^k + a_6 \right)$$

Equation 51

The PIMPLE algorithm is one of the most used one if we have transient problems because it combines the PISO and SIMPLE (SIMPLEC) one. The advantage is, that we can use larger Courant numbers ( $C_o \gg 1$ ) and therefore, the time step can be increased drastically.

For cases that the hydrostatic pressure contribution  $\rho(g \cdot h)$  is important, e.g. for buoyant and multiphase cases, it is numerically convenient to solve for an alternative pressure defined by  $p' = p - \rho(g \cdot h)$ . In OpenFOAM solver applications the  $p'$  pressure term is named  $p\_rgh$ , hydrostatic contribution [Pa].

The physical models include:

turbulence: constant/turbulenceProperties

heat transfer: constant/thermophysicalModels

chemistry: constant/chemistryProperties

combustion: constant/combustionProperties

The folder information and the model settings (On / Off) are given in the table.

Table 64: fireFoam model set up folders and files

O Folder	Constant Folder	system Folder
CH <sub>4</sub> - Methane k – turbulent kinetic energy N <sub>2</sub> – Nitrogen in air nut – turbulent viscosity O <sub>2</sub> - Oxygen p - Pressure p_rgh – dynamic Pressure ph_rgh – Hydrostatic pressure T – Temperature U – Velocity	polymesh Folder – Mesh Information trisurface folder - .stl file (geometry) chemistryProperties - OFF combustionProperties – OFF g – gravity hRef – reference height for hydrostatic pressure pRef – Reference pressure pyrolysisZones – OFF radiationProperties – OFF reactingCloud1Properties – OFF reactions – match each side of the reaction equation surfaceFilmProperties – OFF thermo.compressibleGas – species info thermophysicalProperties – thermal&chemical info turbulenceProperties – LES model inputs	controlDict – case controls decomposeParDict – parallelProcessing fvSchemes – transform cell-centre quantities to face-centre fvSolution – setting solvers to solve the matrix system topoSet – identify the region to patch createPatchDict – patch the topoSet region to value

thermodynamics package

```
{
  type          hePsiThermo;
  mixture       singleStepReactingMixture;
  transport     sutherland;
  thermo        janaf;
  energy        sensibleEnthalpy;
  equationOfState perfectGas;
  specie        specie;
}
```

combustion model                    noCombustion<psiThermoCombustion>

Fuel heat of combustion            : -1.35401e-10

stoichiometric air-fuel ratio        : 17.0854

stoichiometric oxygen-fuel ratio : 3.98918

Three species to represent 5% methane (CH<sub>4</sub>) in air was chosen and the respective mass concentrations are Oxygen (O<sub>2</sub>) 22.05%, Nitrogen (N<sub>2</sub>) 72.413% and CH<sub>4</sub> 5.5293%.

The geometry used for the simulations is box with length 75m, width 50 m and height 30 m. The geometry includes three obstructions as shown in figure.

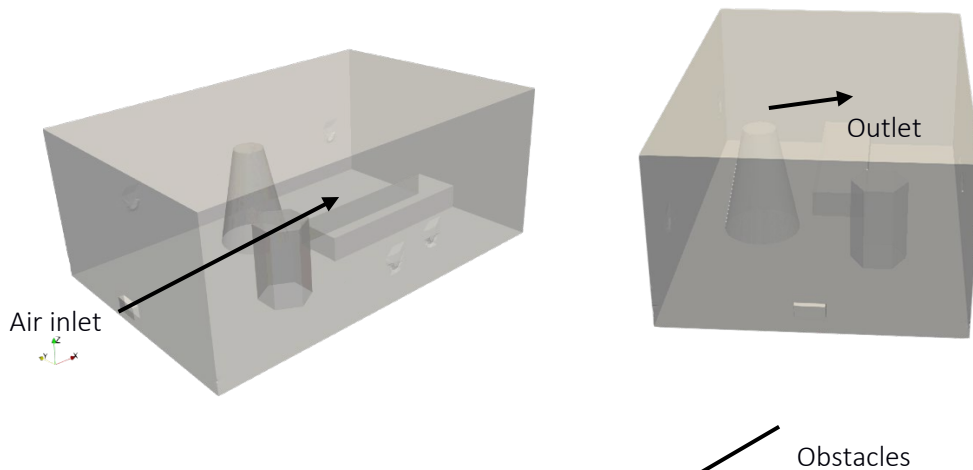


Figure 96: fireFOAM Geometry with obstructions 75 m box

Table 65: Initial and boundary conditions

Parameter	Initial value	Boundary type
k [m <sup>2</sup> /s <sup>2</sup> ]	1.0e-4	Outlet, sides type    inletOutlet; inletValue    \$internalField; value    \$internalField; base, inlet, inlet1 type    fixedValue; value    \$internalField;
p [Pa]	101325	type    calculated; value    \$internalField;
T [K]	293.15	Outlet, sides type    inletOutlet;

Parameter	Initial value	Boundary type
		inletValue    \$internalField; value        \$internalField; base type        zeroGradient; inlet, inlet1 type        fixedValue; value       uniform 300;
u  [m/s]	0	Outlet, sides type        pressureInletOutletVelocity; value       uniform (0 0 0); base type        noSlip; inlet type        fixedValue; value       uniform (1.0 0 0); inlet1 type        fixedValue; value       uniform (0.1 0 0);

### Meshing:

The creation of a mesh by *snappyHexMesh* is following a two-step approach:

Step 1: The background mesh is created by *blockMesh* consisting of all-hex cells with an aspect ratio of 1, i.e. cube-shaped cells with many intersections of the background mesh's cell edges with the tri-surface.

Step 2: *snappyHexMesh* then performs three basic sub-steps:

(a) Castellating: The tri-surface is approximated by splitting and removing cells outside the tri-surface.

Cell splitting: The cells of the background mesh near the objects surface are refined.

Cell removal: Cells of the background mesh inside the object are removed.

(b) Snapping: The remaining background mesh is modified in order to reconstruct the surface of the object.

(c) Layer addition: Additional hexahedral cells are introduced on the boundary surface of the object to ensure a good mesh quality.

The run commands for meshing are as follows:

```
$ surfaceFeatureExtract      # import feature edges from geometry
$ blockMesh                  # background meshing within boundary box
$ topoSet
$ createPatch -overwrite
$ snappyHexMesh -overwrite
```

Meshing was carried on the geometry with the base case mesh of 0.2 M hexahedral elements

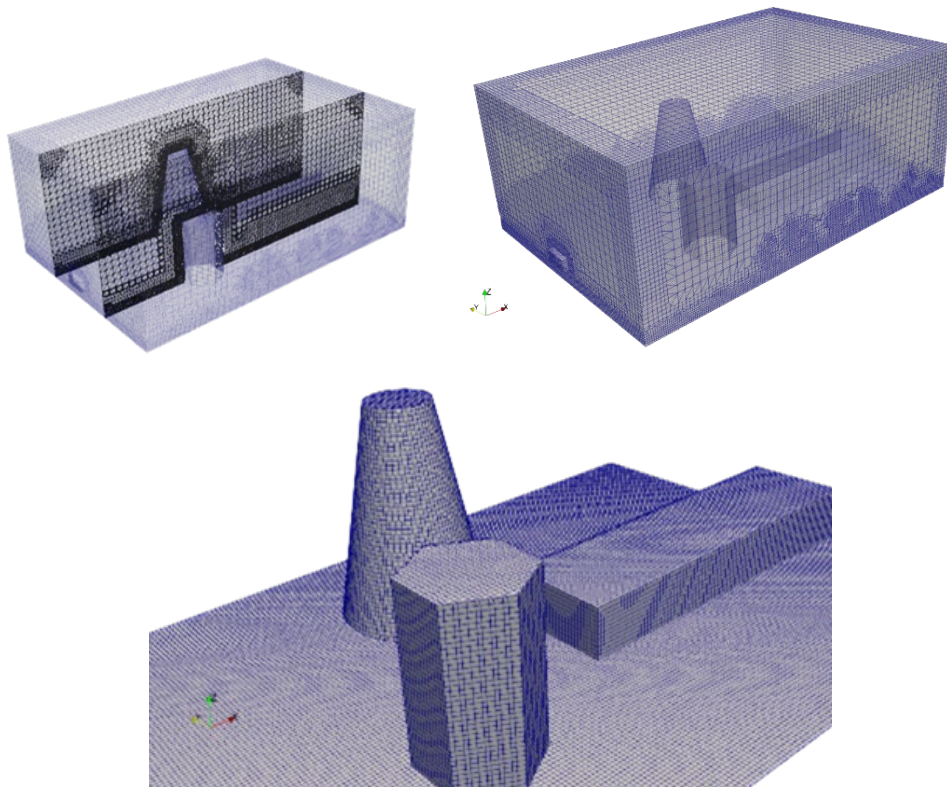


Figure 97: fireFOAM geometry and meshing

### Discretization schemes – Diffusive terms

The method highly depends on the quality of the mesh.

For meshes with low non-orthogonality use the corrected scheme or the limited 1 scheme.

For meshes with high non-orthogonality use the limited  $\Psi$  scheme. The higher the non-orthogonality the lower the value of the blending factor  $\Psi$ .

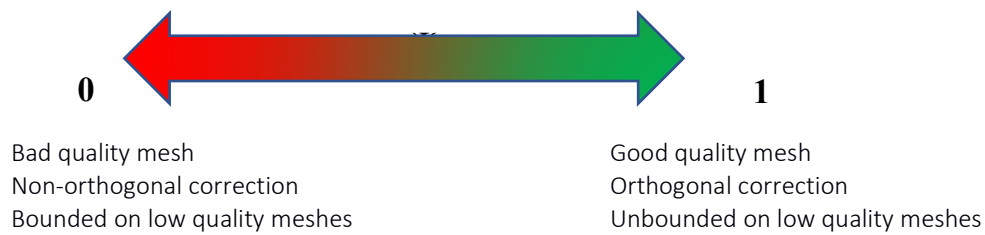


Figure 98: Meshing quality - non-orthogonality

### Mesh quality concerns

A good mesh is a mesh that serves the project objectives such that the results are physically realistic, reliable, and accurate. The final mesh will depend on the physics involved and the ability to generate an appropriate mesh able to resolve that physics, without over-doing. This is achieved by mesh quality reviews and meshing sensitivity. The key mesh quality parameters are given here:

#### 1. Non-orthogonality

The value of non-orthogonality is defined as the angle between the line connecting two cell centers and the normal of their common face. A non-orthogonality of 0.0 means the mesh is perfectly orthogonal (the best). If the non-orthogonality is higher than 80; then redo the mesh and improve the quality. Error is not reduced by mesh refinement and the stability affected by worst face. For LES simulations, better to have non-orthogonality less than 70.

#### 2. Skewness

Measure the distance between the intersection of the line connecting two cell centres with their common face and the centre of that face - smaller is better. High skewness is usually associated with small faces.

High skewness = high aspect ratio.

#### 3. Aspect ratio

A measure of the 'squareness' of cells, Aspect ratio 1.0 is best. Also, it was noted that high aspect ratio cells can make the matrix harder to solve

#### 4. Face aspect ratio:

The ratio between the longest and the shortest length.

#### 5. Cell aspect ratio:

If the mesh is pseudo-2D, then it's just the ratio between the biggest and the smallest areas of the cell's bounding box. If 3D, then it's the largest between ratio between the biggest and the smallest areas of the cell's bounding box.

#### 6. Cell volumes

The difference between min and max should be as small as possible (or the evolution should be as smooth as possible).

Meshing was carried on the geometry with the base case mesh of 0.2 M hexahedral elements. Geometry and meshing details are given in Figure 99.

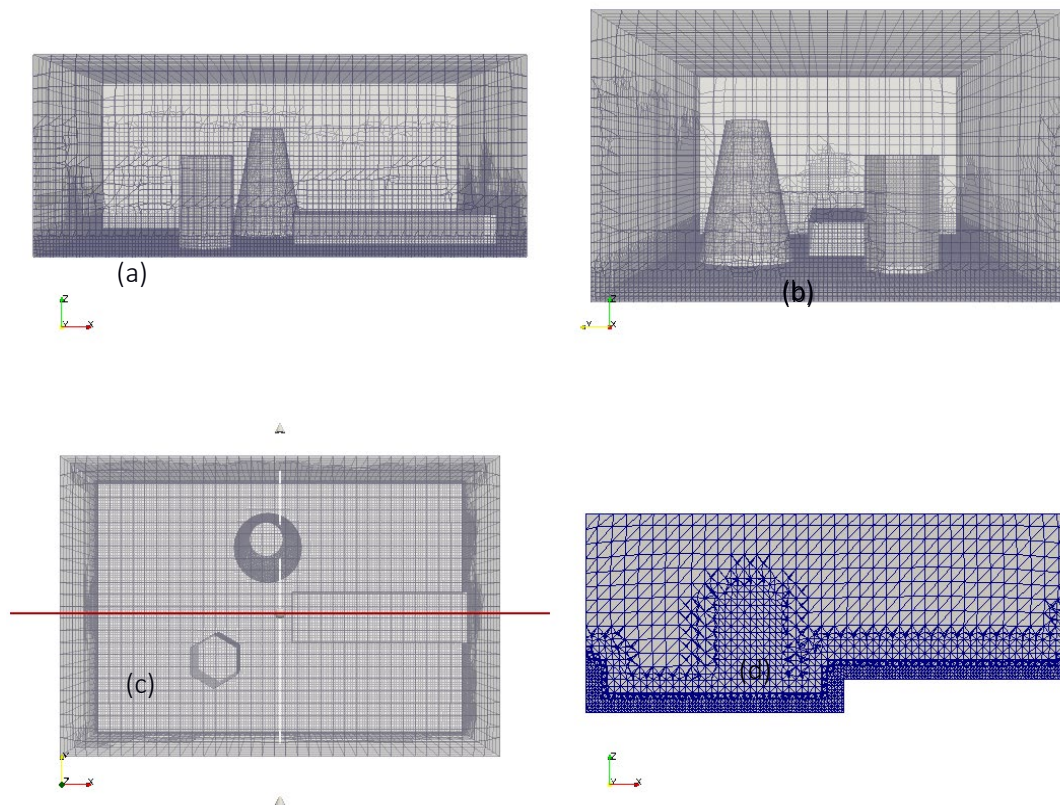


Figure 99: Geometry and with meshing details (base case)

(a) elevation – looking from side; (b) elevation – looking from inlet; (c) plan – looking from base; (d) elevation slice through middle (red line in (c)) with meshing details for pollutant inlet, and obstructions

#### Meshing sensitivity

Mesh sensitivity analysis is to be carried out to derive the optimum meshing for results and run time (Liu Q. et. al 2016). Good geometry (unique clean, watertight, without share angles) is

needed for good mesh, and a good mesh require to keep the skewness, orthogonality, aspect ratio, minimum face area and growth rate low. *checkMesh* help in checking for topological errors and mesh quality errors.

Sensitivity runs were completed for *snappyHexMesh* parameters and levels of refinements.

### Sensitivity 1: *resolveFeatureAngle*

*snappyHexMesh resolveFeatureAngle*: Applies maximum level of refinement to cells that can see intersections whose angle exceeds this. Base case with *resolveFeatureAngle* 30 and sensitivity run for 50. Sensitivity comparison results are given in Table 66 and Figure 100.

Table 66: *resolveFeatureAngle* sensitivity comparison

Case 1 with <i>resolveFeatureAngle</i> 30	Case 1 sensitivity <i>resolveFeatureAngle</i> 50																																
Mesh stats points: 148197 faces: 390293 internal faces: 361924 cells: 121449 faces per cell: 6.19369 boundary patches: 5 point zones: 0 face zones: 0 cell zones: 0	Mesh stats points: 148197 faces: 390293 internal faces: 361924 cells: 121449 faces per cell: 6.19369 boundary patches: 5 point zones: 0 face zones: 0 cell zones: 0																																
Overall number of cells of each type: hexahedra: 110868 prisms: 1100 wedges: 0 pyramids: 0 tet wedges: 82 tetrahedra: 0 polyhedra: 9399 Breakdown of polyhedra by number of faces: <table border="1" data-bbox="303 1680 574 1993"> <thead> <tr> <th>faces</th> <th>number of cells</th> </tr> </thead> <tbody> <tr><td>4</td><td>360</td></tr> <tr><td>5</td><td>560</td></tr> <tr><td>6</td><td>1692</td></tr> <tr><td>9</td><td>5202</td></tr> <tr><td>12</td><td>1285</td></tr> <tr><td>15</td><td>283</td></tr> <tr><td>18</td><td>17</td></tr> </tbody> </table>	faces	number of cells	4	360	5	560	6	1692	9	5202	12	1285	15	283	18	17	Overall number of cells of each type: hexahedra: 110868 prisms: 1100 wedges: 0 pyramids: 0 tet wedges: 82 tetrahedra: 0 polyhedra: 9399 Breakdown of polyhedra by number of faces: <table border="1" data-bbox="861 1680 1133 1993"> <thead> <tr> <th>faces</th> <th>number of cells</th> </tr> </thead> <tbody> <tr><td>4</td><td>360</td></tr> <tr><td>5</td><td>560</td></tr> <tr><td>6</td><td>1692</td></tr> <tr><td>9</td><td>5202</td></tr> <tr><td>12</td><td>1285</td></tr> <tr><td>15</td><td>283</td></tr> <tr><td>18</td><td>17</td></tr> </tbody> </table>	faces	number of cells	4	360	5	560	6	1692	9	5202	12	1285	15	283	18	17
faces	number of cells																																
4	360																																
5	560																																
6	1692																																
9	5202																																
12	1285																																
15	283																																
18	17																																
faces	number of cells																																
4	360																																
5	560																																
6	1692																																
9	5202																																
12	1285																																
15	283																																
18	17																																



Case 1 with <i>resolveFeatureAngle</i> 30	Case 1 sensitivity <i>resolveFeatureAngle</i> 50																																																
<p>Checking topology...</p> <p>Boundary definition OK.</p> <p>Cell to face addressing OK.</p> <p>Point usage OK.</p> <p>Upper triangular ordering OK.</p> <p>Face vertices OK.</p> <p>Number of regions: 1 (OK).</p> <p>Checking patch topology for multiply connected surfaces...</p> <table border="1" data-bbox="272 689 831 1093"> <thead> <tr> <th>Patch</th> <th>Faces</th> <th>Points</th> <th>Surface topology</th> </tr> </thead> <tbody> <tr> <td>inlet</td> <td>1249</td> <td>1419</td> <td>ok (non-closed singly connected)</td> </tr> <tr> <td>outlet</td> <td>1859</td> <td>2071</td> <td>ok (non-closed singly connected)</td> </tr> <tr> <td>base</td> <td>20124</td> <td>20777</td> <td>ok (non-closed singly connected)</td> </tr> <tr> <td>inlet1</td> <td>50</td> <td>66</td> <td>ok (non-closed singly connected)</td> </tr> <tr> <td>sides</td> <td>5087</td> <td>5496</td> <td>ok (non-closed singly connected)</td> </tr> </tbody> </table> <p>Checking geometry...</p> <p>Overall domain bounding box (0 0-1.78967e-10) (75 50 30)</p> <p>Mesh has 3 geometric (non-empty/wedge) directions (1 1 1)</p> <p>Mesh has 3 solution (non-empty) directions (1 1 1)</p> <p><b>Boundary openness</b> (-2.98365e-17-1.96801e-17-1.3414e-16) <b>OK.</b></p> <p><b>Max cell openness</b> = 3.34136e-16 <b>OK.</b></p> <p><u>Max aspect ratio</u> = 9.24581 <b>OK.</b></p> <p>Minimum face area = 0.0568635.</p> <p>Maximum face area = 8.79413.</p> <p>Face area magnitudes OK.</p> <p>Min volume = 0.0178995. Max volume = 17.1542. Total volume = 108124. Cell volumes OK.</p> <p>Mesh non-orthogonality Max: 53.1093; average: 4.58255</p> <p>Non-orthogonality check OK.</p> <p>Face pyramids OK.</p> <p><u>Max skewness</u> = 0.614635 <b>OK.</b></p> <p>Coupled point location match (average 0) OK.</p>	Patch	Faces	Points	Surface topology	inlet	1249	1419	ok (non-closed singly connected)	outlet	1859	2071	ok (non-closed singly connected)	base	20124	20777	ok (non-closed singly connected)	inlet1	50	66	ok (non-closed singly connected)	sides	5087	5496	ok (non-closed singly connected)	<p>Checking topology...</p> <p>Boundary definition OK.</p> <p>Cell to face addressing OK.</p> <p>Point usage OK.</p> <p>Upper triangular ordering OK.</p> <p>Face vertices OK.</p> <p>Number of regions: 1 (OK).</p> <p>Checking patch topology for multiply connected surfaces...</p> <table border="1" data-bbox="831 689 1394 1093"> <thead> <tr> <th>Patch</th> <th>Faces</th> <th>Points</th> <th>Surface topology</th> </tr> </thead> <tbody> <tr> <td>inlet</td> <td>1249</td> <td>1419</td> <td>ok (non-closed singly connected)</td> </tr> <tr> <td>outlet</td> <td>1859</td> <td>2071</td> <td>ok (non-closed singly connected)</td> </tr> <tr> <td>sides</td> <td>5087</td> <td>5496</td> <td>ok (non-closed singly connected)</td> </tr> <tr> <td>base</td> <td>20124</td> <td>20777</td> <td>ok (non-closed singly connected)</td> </tr> <tr> <td>inlet1</td> <td>50</td> <td>66</td> <td>ok (non-closed singly connected)</td> </tr> </tbody> </table> <p>Checking geometry...</p> <p>Overall domain bounding box (0 0-1.78967e-10) (75 50 30)</p> <p>Mesh has 3 geometric (non-empty/wedge) directions (1 1 1)</p> <p>Mesh has 3 solution (non-empty) directions (1 1 1)</p> <p><b>Boundary openness</b> (-3.1252e-17-3.10785e-17-4.3565e-16) <b>OK.</b></p> <p><b>Max cell openness</b> = 3.56124e-16 <b>OK.</b></p> <p>Max aspect ratio = 9.24581 <b>OK.</b></p> <p>Minimum face area = 0.0568635.</p> <p>Maximum face area = 8.79413.</p> <p>Face area magnitudes OK.</p> <p>Min volume = 0.0178995. Max volume = 17.1542. Total volume = 108124. Cell volumes OK.</p> <p>Mesh non-orthogonality Max: 53.1093; average: 4.58255</p> <p>Non-orthogonality check OK.</p> <p>Face pyramids OK.</p> <p>Max skewness = 0.614635 <b>OK.</b></p> <p>Coupled point location match (average 0) OK.</p>	Patch	Faces	Points	Surface topology	inlet	1249	1419	ok (non-closed singly connected)	outlet	1859	2071	ok (non-closed singly connected)	sides	5087	5496	ok (non-closed singly connected)	base	20124	20777	ok (non-closed singly connected)	inlet1	50	66	ok (non-closed singly connected)
Patch	Faces	Points	Surface topology																																														
inlet	1249	1419	ok (non-closed singly connected)																																														
outlet	1859	2071	ok (non-closed singly connected)																																														
base	20124	20777	ok (non-closed singly connected)																																														
inlet1	50	66	ok (non-closed singly connected)																																														
sides	5087	5496	ok (non-closed singly connected)																																														
Patch	Faces	Points	Surface topology																																														
inlet	1249	1419	ok (non-closed singly connected)																																														
outlet	1859	2071	ok (non-closed singly connected)																																														
sides	5087	5496	ok (non-closed singly connected)																																														
base	20124	20777	ok (non-closed singly connected)																																														
inlet1	50	66	ok (non-closed singly connected)																																														

Case 1 with <i>resolveFeatureAngle</i> 30	Case 1 sensitivity <i>resolveFeatureAngle</i> 50
ExecutionTime = 5545.22	ExecutionTime = 5363.7 s

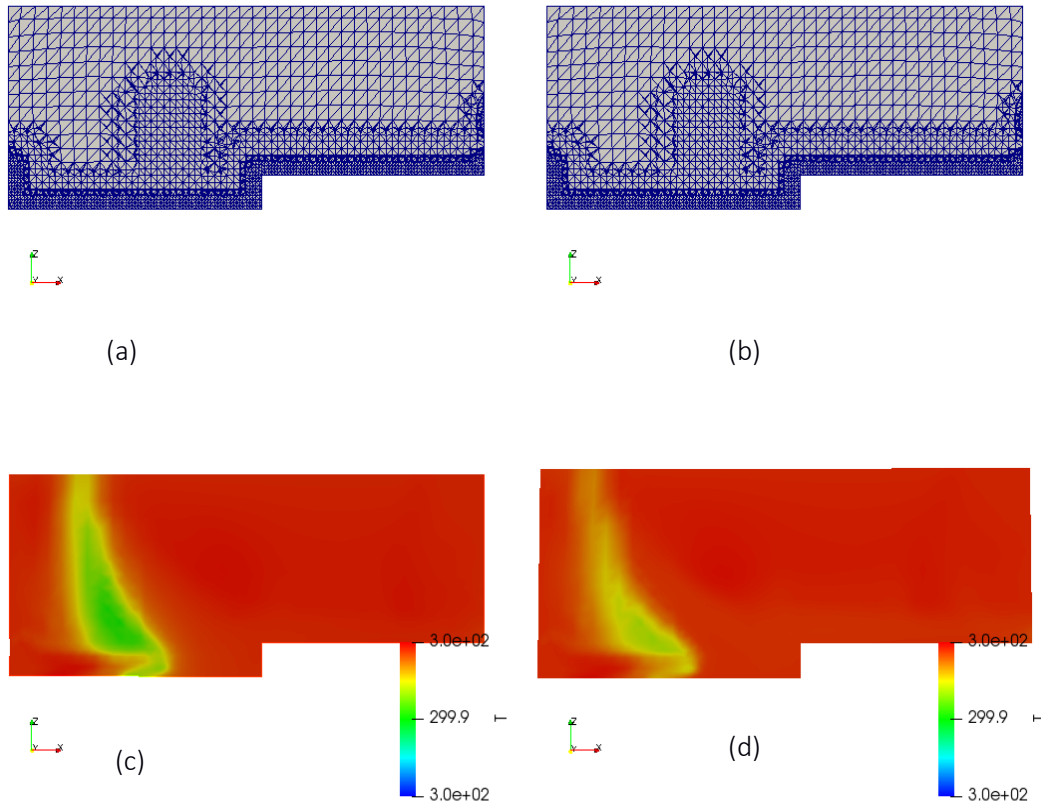


Figure 100: Meshing sensitivity - *resolveFeatureAngle*

(a) elevation slice with *resolveFeatureAngle* 30; (b) elevation slice with *resolveFeatureAngle* 50;  
(c) Temperature profile at 14 sec (for angle 30); (d) Temperature profile at 14 sec (for angle 50)

**Analysis notes:**

No change in skewness, and the aspect ratio, the non-orthogonality returned okay on *checkMesh*. Max cell openness changed from 3.34136e-16 to 3.56124e-16. No significant difference in the results, okay to proceed with *resolveFeatureAngle* 30.

**Sensitivity 2: *nCellsBetweenLevels***

snappyHexMesh *nCellsBetweenLevels*: Number of buffer layers of cells between different levels of refinement; Must be equal or greater than 1, integer values only. The sensitivity analysis was carried for *nCellsBetweenLevels* 4 and 2, results are given in Table 67 and Figure 101.

Table 67: *nCellsBetweenLevels* sensitivity comparison

Case02 with <i>nCellsBetweenLevels</i> 4	Case02 sensitivity <i>nCellsBetweenLevels</i> 2																																
<p>Mesh stats</p> <p>points: 148197</p> <p>faces: 390293</p> <p>internal faces: 361924</p> <p>cells: 121449</p> <p>faces per cell: 6.19369</p> <p>boundary patches: 5</p> <p>point zones: 0</p> <p>face zones: 0</p> <p>cell zones: 0</p> <p>Overall number of cells of each type:</p> <p>hexahedra: 110868</p> <p>prisms: 1100</p> <p>wedges: 0</p> <p>pyramids: 0</p> <p>tet wedges: 82</p> <p>tetrahedra: 0</p> <p>polyhedra: 9399</p> <p>Breakdown of polyhedra by number of faces:</p> <table> <thead> <tr> <th>faces</th> <th>number of cells</th> </tr> </thead> <tbody> <tr><td>4</td><td>360</td></tr> <tr><td>5</td><td>560</td></tr> <tr><td>6</td><td>1692</td></tr> <tr><td>9</td><td>5202</td></tr> <tr><td>12</td><td>1285</td></tr> <tr><td>15</td><td>283</td></tr> <tr><td>18</td><td>17</td></tr> </tbody> </table> <p>Checking topology...</p> <p>Boundary definition OK.</p> <p>Cell to face addressing OK.</p> <p>Point usage OK.</p> <p>Upper triangular ordering OK.</p> <p>Face vertices OK.</p>	faces	number of cells	4	360	5	560	6	1692	9	5202	12	1285	15	283	18	17	<p>Mesh stats</p> <p>points: 98405</p> <p>faces: 242108</p> <p>internal faces: 214485</p> <p>cells: 72269</p> <p>faces per cell: 6.31796</p> <p>boundary patches: 5</p> <p>point zones: 0</p> <p>face zones: 0</p> <p>cell zones: 0</p> <p>Overall number of cells of each type:</p> <p>hexahedra: 61711</p> <p>prisms: 1129</p> <p>wedges: 0</p> <p>pyramids: 0</p> <p>tet wedges: 85</p> <p>tetrahedra: 0</p> <p>polyhedra: 9344</p> <p>Breakdown of polyhedra by number of faces:</p> <table> <thead> <tr> <th>faces</th> <th>number of cells</th> </tr> </thead> <tbody> <tr><td>4</td><td>360</td></tr> <tr><td>5</td><td>574</td></tr> <tr><td>6</td><td>1584</td></tr> <tr><td>9</td><td>5393</td></tr> <tr><td>12</td><td>1184</td></tr> <tr><td>15</td><td>233</td></tr> <tr><td>18</td><td>16</td></tr> </tbody> </table> <p>Checking topology...</p> <p>Boundary definition OK.</p> <p>Cell to face addressing OK.</p> <p>Point usage OK.</p> <p>Upper triangular ordering OK.</p> <p>Face vertices OK.</p>	faces	number of cells	4	360	5	574	6	1584	9	5393	12	1184	15	233	18	16
faces	number of cells																																
4	360																																
5	560																																
6	1692																																
9	5202																																
12	1285																																
15	283																																
18	17																																
faces	number of cells																																
4	360																																
5	574																																
6	1584																																
9	5393																																
12	1184																																
15	233																																
18	16																																

Case02 with <i>nCellsBetweenLevels</i> 4	Case02 sensitivity <i>nCellsBetweenLevels</i> 2																																																
<p>Number of regions: 1 (OK).</p> <p>Checking patch topology for multiply connected surfaces...</p> <table border="1"> <thead> <tr> <th>Patch</th> <th>Faces</th> <th>Points</th> <th>Surface topology</th> </tr> </thead> <tbody> <tr> <td>inlet</td> <td>1249</td> <td>1419</td> <td>ok (non-closed singly connected)</td> </tr> <tr> <td>outlet</td> <td>1859</td> <td>2071</td> <td>ok (non-closed singly connected)</td> </tr> <tr> <td>base</td> <td>20124</td> <td>20777</td> <td>ok (non-closed singly connected)</td> </tr> <tr> <td>inlet1</td> <td>50</td> <td>66</td> <td>ok (non-closed singly connected)</td> </tr> <tr> <td>sides</td> <td>5087</td> <td>5496</td> <td>ok (non-closed singly connected)</td> </tr> </tbody> </table> <p>Checking geometry...</p> <p>Overall domain bounding box (0 0 -1.78967e-10) (75 50 30)</p> <p>Mesh has 3 geometric (non-empty/wedge) directions (1 1 1)</p> <p>Mesh has 3 solution (non-empty) directions (1 1 1)</p> <p><b>Boundary openness</b> (-2.98365e-17 -1.96801e-17 -1.3414e-16) <b>OK</b>.</p> <p><b>Max cell openness</b> = 3.34136e-16 <b>OK</b>.</p> <p><u>Max aspect ratio</u> = 9.24581 <b>OK</b>.</p> <p>Minimum face area = 0.0568635.</p> <p>Maximum face area = 8.79413.</p> <p>Face area magnitudes OK.</p> <p>Min volume = 0.0178995. Max volume = 17.1542. Total volume = 108124. Cell volumes OK.</p> <p>Mesh non-orthogonality Max: 53.1093 average: 4.58255</p> <p>Non-orthogonality check OK.</p> <p>Face pyramids OK.</p> <p><u>Max skewness</u> = 0.614635 <b>OK</b>.</p> <p>Coupled point location match (average 0) OK.</p>	Patch	Faces	Points	Surface topology	inlet	1249	1419	ok (non-closed singly connected)	outlet	1859	2071	ok (non-closed singly connected)	base	20124	20777	ok (non-closed singly connected)	inlet1	50	66	ok (non-closed singly connected)	sides	5087	5496	ok (non-closed singly connected)	<p>Number of regions: 1 (OK).</p> <p>Checking patch topology for multiply connected surfaces...</p> <table border="1"> <thead> <tr> <th>Patch</th> <th>Faces</th> <th>Points</th> <th>Surface topology</th> </tr> </thead> <tbody> <tr> <td>inlet</td> <td>1056</td> <td>1229</td> <td>ok (non-closed singly connected)</td> </tr> <tr> <td>outlet</td> <td>1989</td> <td>2222</td> <td>ok (non-closed singly connected)</td> </tr> <tr> <td>base</td> <td>20124</td> <td>20777</td> <td>ok (non-closed singly connected)</td> </tr> <tr> <td>inlet1</td> <td>50</td> <td>66</td> <td>ok (non-closed singly connected)</td> </tr> <tr> <td>sides</td> <td>4404</td> <td>4808</td> <td>ok (non-closed singly connected)</td> </tr> </tbody> </table> <p>Checking geometry...</p> <p>Overall domain bounding box (0 0 -1.78962e-10) (75.0158 50.0027 30)</p> <p>Mesh has 3 geometric (non-empty/wedge) directions (1 1 1)</p> <p>Mesh has 3 solution (non-empty) directions (1 1 1)</p> <p><b>Boundary openness</b> (-8.84406e-17 9.38974e-17 -8.41295e-17) <b>OK</b>.</p> <p>Max cell openness = <b>3.43583e-16</b> <b>OK</b>.</p> <p>Max aspect ratio = <b>9.9966</b> <b>OK</b>.</p> <p>Minimum face area = <b>0.0584073</b>.</p> <p>Maximum face area = 8.74941.</p> <p>Face area magnitudes OK.</p> <p>Min volume = 0.0175439. Max volume = 17.0323. Total volume = 108124. Cell volumes OK.</p> <p>Mesh non-orthogonality Max: <b>53.0934</b> <b>average: 5.92029</b></p> <p>Non-orthogonality check OK.</p> <p>Face pyramids OK.</p> <p><u>Max skewness</u> = <b>1.08267</b> <b>OK</b>.</p> <p>Coupled point location match (average 0) OK.</p>	Patch	Faces	Points	Surface topology	inlet	1056	1229	ok (non-closed singly connected)	outlet	1989	2222	ok (non-closed singly connected)	base	20124	20777	ok (non-closed singly connected)	inlet1	50	66	ok (non-closed singly connected)	sides	4404	4808	ok (non-closed singly connected)
Patch	Faces	Points	Surface topology																																														
inlet	1249	1419	ok (non-closed singly connected)																																														
outlet	1859	2071	ok (non-closed singly connected)																																														
base	20124	20777	ok (non-closed singly connected)																																														
inlet1	50	66	ok (non-closed singly connected)																																														
sides	5087	5496	ok (non-closed singly connected)																																														
Patch	Faces	Points	Surface topology																																														
inlet	1056	1229	ok (non-closed singly connected)																																														
outlet	1989	2222	ok (non-closed singly connected)																																														
base	20124	20777	ok (non-closed singly connected)																																														
inlet1	50	66	ok (non-closed singly connected)																																														
sides	4404	4808	ok (non-closed singly connected)																																														
ExecutionTime = 5545.22	ExecutionTime = 2828.68 s																																																

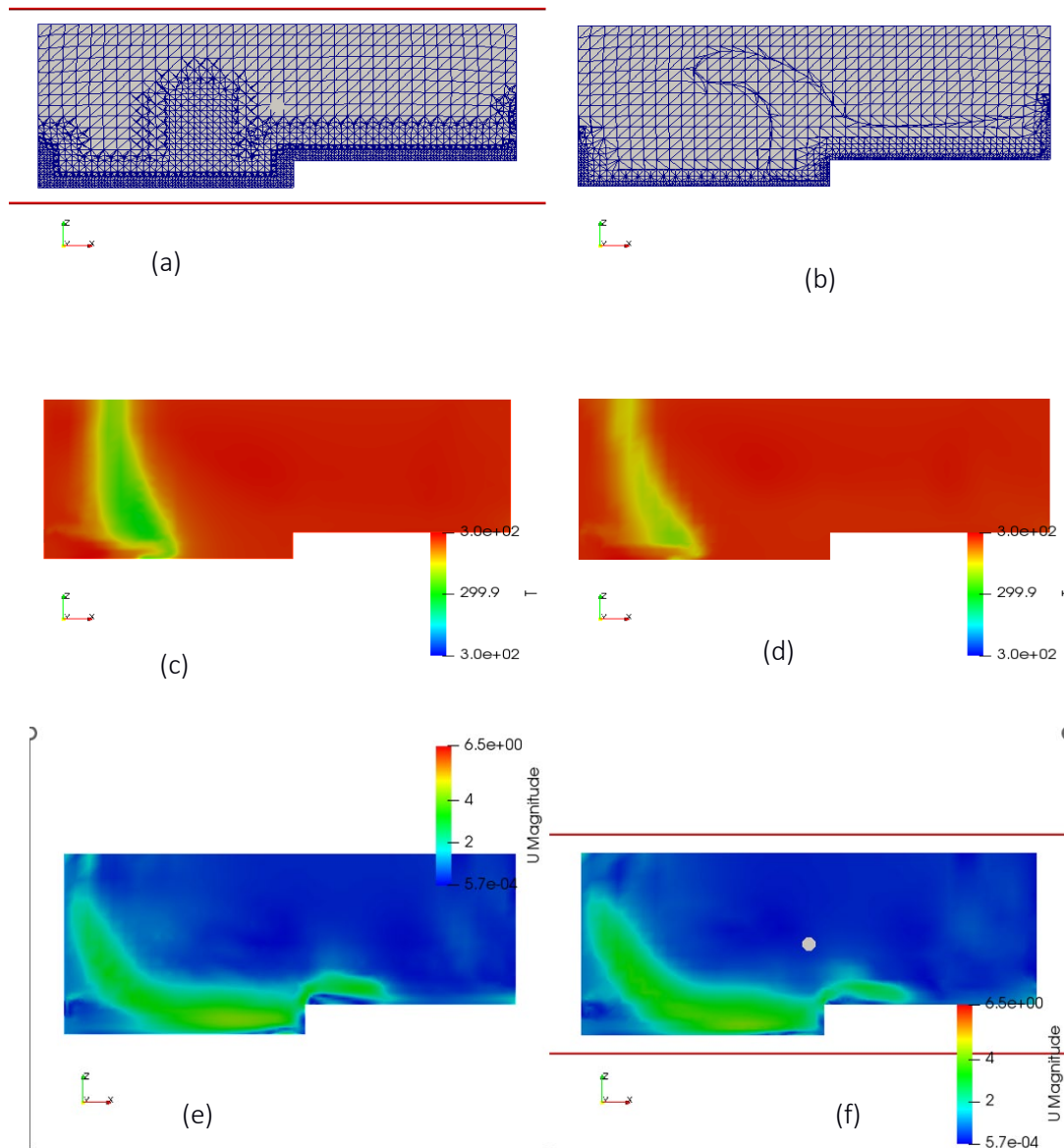


Figure 101: Meshing sensitivity – *nCellsBetweenLevels* – Temperature and Velocity

(a) elevation slice with *nCellsBetweenLevels* 4; (b) elevation with *nCellsBetweenLevels* 2;  
 (c) Temperature profile at 12 sec (Levels 4); (d) Temperature profile at 12 sec (Levels 2)  
 (e) Velocity (U) profile at 30 sec (Levels 4); (f) Velocity (U) profile at 30 sec (Levels 2)

#### Analysis notes:

In the comparison of base case *nCellsBetweenLevels* 4 and sensitivity case with value 2, it is okay to proceed with *nCellsBetweenLevels* 4.

- Max aspect ratio changed from 9.24581 to 9.9966
- Max cell openness changed from 3.34136e-16 to 3.43583e-16 OK.

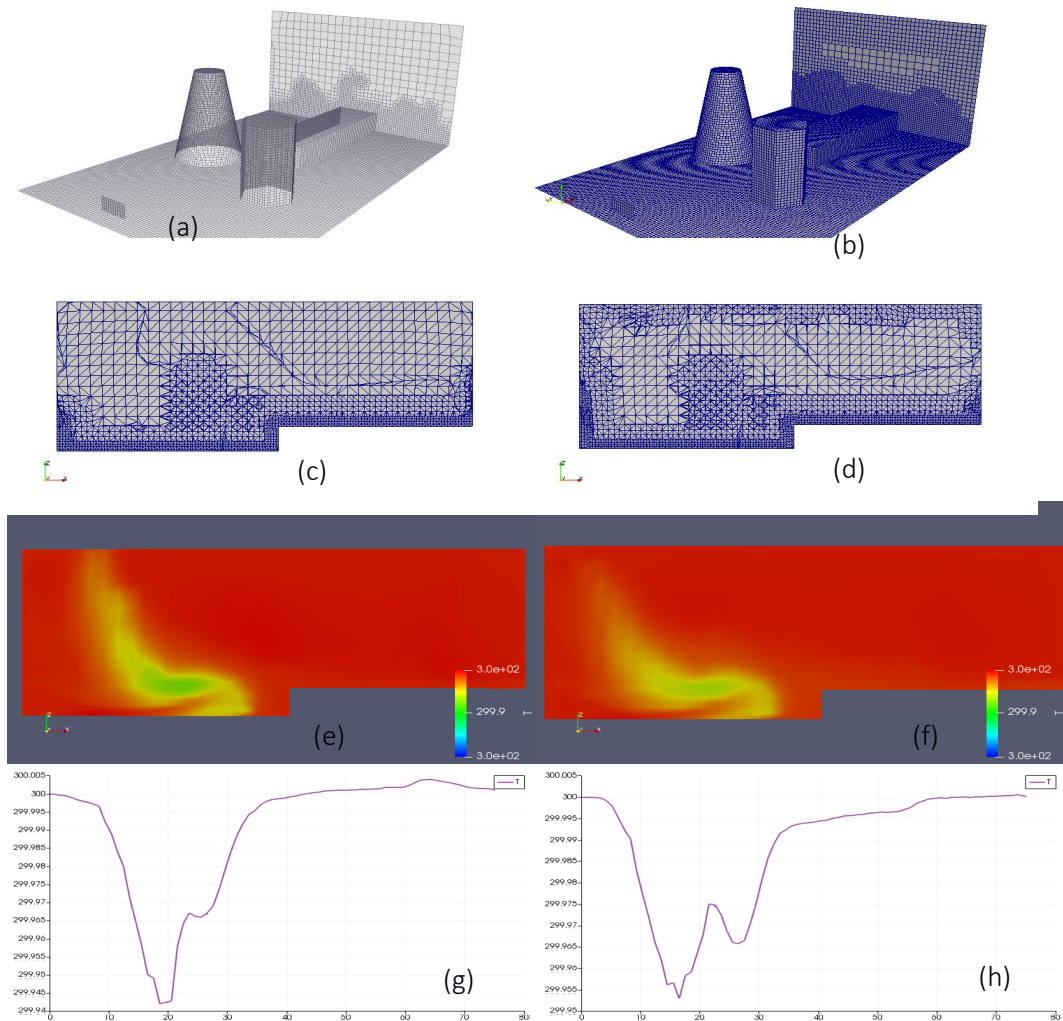
- Mesh non-orthogonality Max: 53.0934 average: 5.92029
- Non-orthogonality check OK.
- Max skewness changed from 0.614635 to 1.08267 (4 is better)

### Sensitivity 3: *snappyHexMesh* feature levels

Sensitivity runs were completed for *snappyHexMesh* levels of refinement. The summary is given in table below Table 68 and Figure 102.

Table 68: Meshing sensitivity for level of refinement

feature	level 0	level 1
Simulation duration (execution time)	5545 seconds (1.5 hours)	9196 seconds (2.5 hours)
Temperature at 20, 25, 8 (x,y,z) after 18 seconds	299.942 K (26.792 oC)	299.966 K (26.816 oC)
skewness (4 is better)	0.614635	0.558754
Max aspect ratio	9.24581	11.6517
non-orthogonality	Max.: 53.1093; Ave.: 4.58255	Max.: 51.3481; Ave.: 5.55088
Max cell openness	3.34136e-17	3.32816e-16



**Meshing sensitivity – featureLevel**

(a) base case elevation (level 0); (b) sensitivity elevation (level 1);

(c) elevation slice (level 0) (d) elevation slice (level 1)

(e) Temperature profile for level 0; (f) Temperature profile for level 1;

(g) Temperature plot over line ( $z = 8$ ) for level 0; (h) Temperature plot over line ( $z = 8$ ) for level 1

**Sensitivity 4: snappyHexMesh refinementSurfaces and features level**

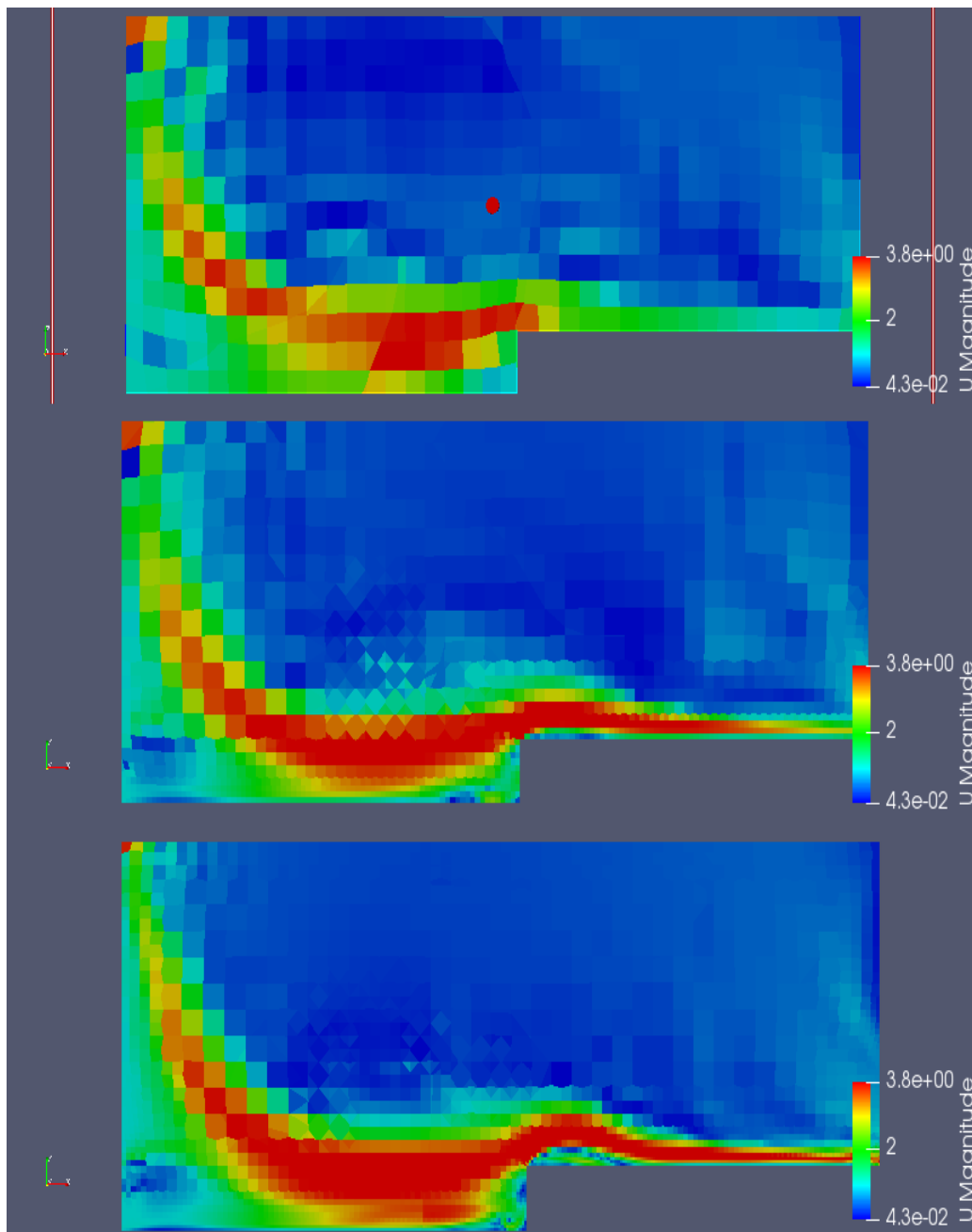
Sensitivity runs were completed for snappyHexMesh features level and refinementSurfaces. Three meshes (coarse, medium and fine) were generated and the set of input used for generating the mesh is given in Table 69. Simulations were carried out and the results are given in Figure 106 and Figure 104.

Table 69: Meshing sensitivity - refinementSurfaces

	Coarse Mesh	Medium Mesh	Fine Mesh
<b>features</b>	level 0	level 1	level 2
<b>refinementSurfaces</b>	All level (0 0)	Base level (2 2) and inlet1 (1 1)	Base level (3 3), inlet1 (2 2) and other surfaces (1 1)
<b>Meshing duration</b>	5.5 s	57 s	191 s
<b>Cells</b>	11942	120590	513633
<b>Faces</b>	37656	387546	1641164
<b>points</b>	13860	147156	616070
<b>Max. skewness</b>	3.06449	1.56859	0.753331
<b>Max. aspect ratio</b>	5.17393	9.24581	11.1045
<b>non-orthogonality</b>	Max: 42.4892 Ave: 4.56375	Max: 53.1093 Ave: 4.57138	Max.: 61.8604 Ave: 4.41225
<b>Simulation Duration</b>	95 s	5455s (1.5 hr)	36362 s (10.1 hr)



Figure 103:



refinementSurface sensitivity – velocity profile (U) at 43 seconds

(a) coarse mesh: for all level (0 0); (b) medium mesh: for base level (2 2), inlet1 (1 1); (c) fine mesh: base level (3 3), inlet1 (2 2), other surfaces (1 1)

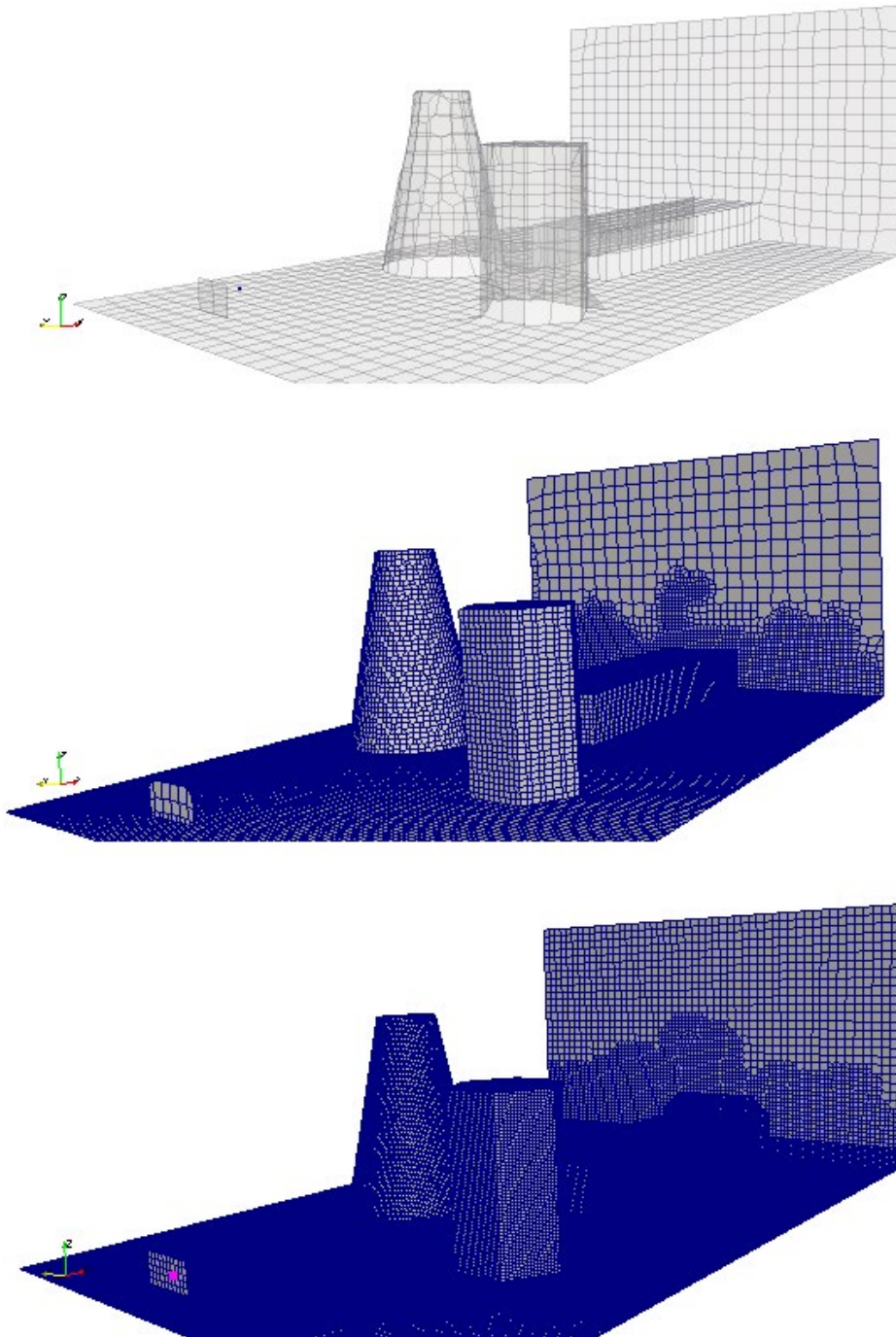


Figure 104: Meshing sensitivity – coarse, medium and fine mesh

- (a) coarse mesh: for all level (0 0)
- (b) medium mesh: for base level (2 2), inlet1 (1 1)
- (c) fine mesh: base level (3 3), inlet1 (2 2), other surfaces (1 1)

**Postprocessing:**

Pollutant / specie concentration and temperature readings were taken at three locations within the geometry. Probe functionality was utilised to get the results for Coarse and Medium meshes, while paraView's *ProbeLocation* feature was used to get results. A comparison of the species concentration and temperature at the Probe location 40 m, 18.2 m and 1.5m after 50 s is given in Table 70. The nitrogen concentration (mass %) estimations at the three probe locations for the duration of 80 s and for medium and coarse meshes are given in Figure 105 and Figure 106.

Table 70: Meshing sensitivity – species concentration comparison

	Coarse Mesh	Medium Mesh	Fine Mesh
CH4 (%)	0.19612	0.00431869	0.5813
N2 (%)	12.822	9.27	5.97
O2 (%)	86.98	90.298	93.44
Temperature (oC)	299.995	299.991	300

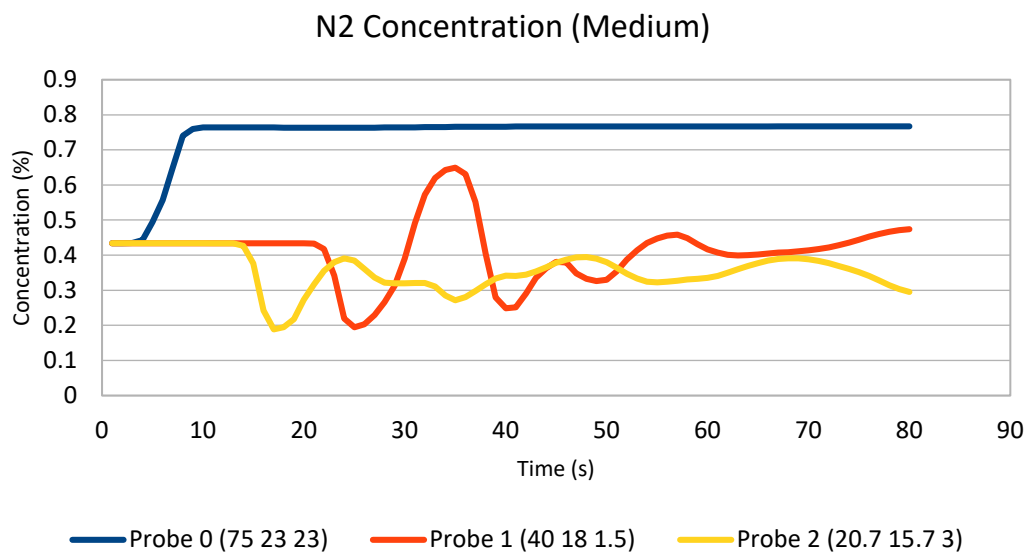


Figure 105: Nitrogen concentration at 3 probe locations for Medium mesh

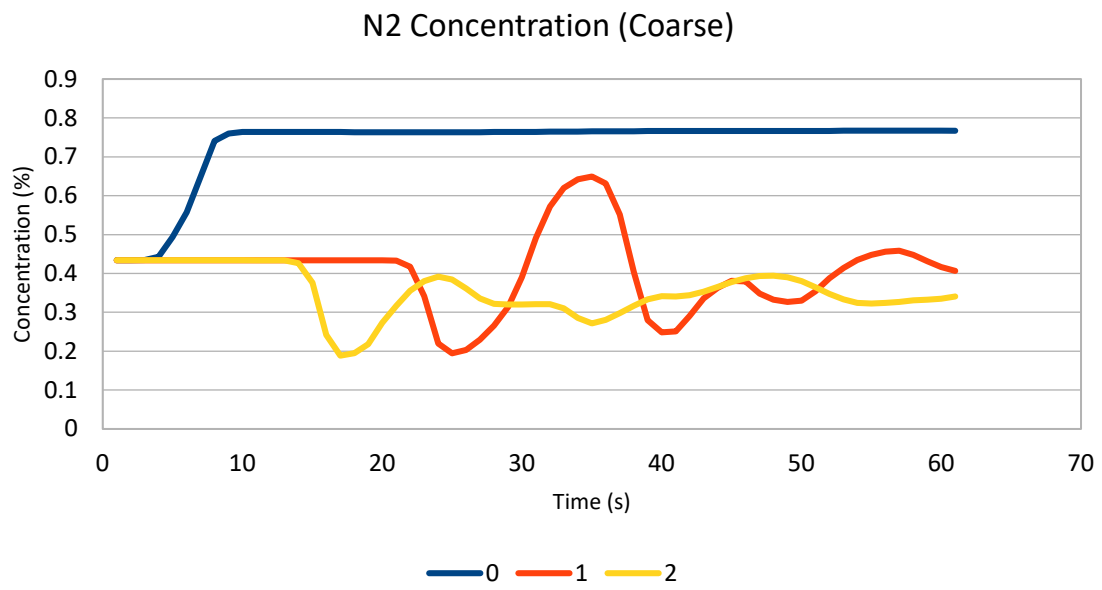


Figure 106: Nitrogen concentration at 3 probe locations for Coarse mesh

## Appendix B: *blockMesh, snappyHexMesh* – OpenFOAM system files

### **blockMesh**

```

FoamFile
{
  version 2.0;
  format ascii;
  class dictionary;
  object blockMeshDict;
}
// ***** //

scale 1;

convertToMeters 1;

vertices
(
/*
  (-148800 307200 38400)
  (1080000 307200 38400)
  (1080000 -307200 38400)
  (-148800 -307200 38400)
  (-148800 307200 0)
  (1080000 307200 0)
  (1080000 -307200 0)
  (-148800 -307200 0)
*/

  (-100000 120000 40000)
  (1000000 120000 40000)
  (1000000 -120000 40000)
  (-100000 -120000 40000)
  (-100000 120000 0)
  (1000000 120000 0)
  (1000000 -120000 0)
  (-100000 -120000 0)
);

blocks
(
  hex (0 1 2 3 4 5 6 7) (392 86 20) simpleGrading (1 1 0.5)
// hex (0 1 2 3 4 5 6 7) (359 79 20) simpleGrading (1 1 0.5)
// hex (0 1 2 3 4 5 6 7) (512 256 16) simpleGrading (1 1 1)
);

edges

```

```
(  
);  
  
boundary  
(  
  inlet  
  {  
    type      patch;  
    faces  
    (  
      ( 0 4 7 3 )  
    );  
  }  
  outlet  
  {  
    type      patch;  
    faces  
    (  
      ( 1 2 6 5 )  
    );  
  }  
  
  ymin  
  {  
    type      patch;  
    faces  
    (  
      ( 3 7 6 2 )  
    );  
  }  
  
  ymax  
  {  
    type      symmetry;  
    faces  
    (  
      ( 0 1 5 4 )  
    );  
  }  
  
  zmax  
  {  
    type      symmetry;  
    faces  
    (  
      ( 0 3 2 1 )  
    );  
  }  
}
```

```

ground
{
    type    wall;
    faces
    (
        ( 4 5 6 7 )
    );
}
);

```

```

mergePatchPairs
(
);

```

### snappyHexMesh

```

FoamFile
{
    version    2.3;
    format    ascii;
    class    dictionary;
    object    snappyHexMeshDict;
}
// ***** //

```

```

castellatedMesh    true;
snap                true;
addLayers           true;

```

```

geometry
{
    releaseTube.stl
    {
        type    triSurfaceMesh;
        name    tube;
        regions
        {
            releaseTube
            {
                name    releaseTube;
            }
            releasePoint
            {
                name    releasePoint;
            }
        }
    }
}

```

```

}
Box_0 { type searchableBox; min ( -762 -533 -50 ); max ( 635 533 728 );}
Box_1 { type searchableBox; min ( -5000 -1000 0 ); max ( 20000 1000 2000 );}
Box_2 { type searchableBox; min ( -124000 -1000 0 ); max ( 900000 1000 10 );}
Box_3 { type searchableBox; min ( -100000 -10000 0 ); max ( 20000 10000 4000 );}
Box_4 { type searchableBox; min ( -100000 -120000 0 ); max ( 1000000 120000 4000
);}
      cyl { type searchableCylinder; point1 ( -100 0 460 ); point2 ( 2000 0 460); radius
100;}
// density_50.stl      { type triSurfaceMesh; name density_50;}
// density_100.stl    { type triSurfaceMesh; name density_100;}
// density_200.stl    { type triSurfaceMesh; name density_200;}
// density_400.stl    { type triSurfaceMesh; name density_400;}
// density_800.stl    { type triSurfaceMesh; name density_800;}

};

castellatedMeshControls
{
    maxLocalCells 200000000;
    maxGlobalCells 300000000;
    minRefinementCells 20;
    nCellsBetweenLevels 3;
    maxLoadUnbalance 0.1;
    allowFreeStandingZoneFaces true;
    resolveFeatureAngle 30;
    features
    (
        {
            file "releaseTube.eMesh" ;
            level 10;
        }
    );

    refinementSurfaces
    {
        tube
        {
            level (9 9);
            regions
            {
                releaseTube          { level (10 10); }
                releasePoint         { level (10 10); }
            }
        }
    }

    refinementRegions
    {
        Box_0    { mode inside; levels ((0 2));}
    }

```



```

        Box_1    {    mode    inside; levels ((0 4));}
        Box_2    {    mode    inside; levels ((0 1));}
//      Box_3    {    mode    inside; levels ((0 3));}
        Box_4    {    mode    inside; levels ((0 1));}
        cyl      {    mode    inside; levels ((0 7));}
    }

    locationInMesh ( 10000 0 1000 ) ;
}

snapControls
{
    tolerance    4.0;
    implicitFeatureSnap false;
    explicitFeatureSnap true;
    multiRegionFeatureSnap true;
    detectNearSurfacesSnap true;
    nSmoothPatch 3;
    nSolverIter 30;
    nRelaxIter 5;
    nFeatureSnapIter 10;
    nSmoothInternal $nSmoothPatch;
}

addLayersControls
{
    layers
    {
//      releaseTube    {nSurfaceLayers 4;    firstLayerThickness 0.1;
        expansionRatio 1.2; }
//      releasePoint    {nSurfaceLayers 4;    firstLayerThickness 0.1;
        expansionRatio 1.2; }
        ground    {nSurfaceLayers 4;    firstLayerThickness 0.1;
        expansionRatio 1.3; }
    }
    relativeSizes true;
    expansionRatio 1.2;
    firstLayerThickness 0.1;
    minThickness 0.0001;
    nGrow 0;
    featureAngle 175;
    slipFeatureAngle 30;
    nMedialAxisIter 10;
    nRelaxIter 5;
    nSmoothSurfaceNormals 10;
    nSmoothNormals 10;
    nSmoothDisplacement 90;
    nSmoothThickness 10;
    maxFaceThicknessRatio 0.5;
    maxThicknessToMedialRatio 0.3;
}

```

```
minMedianAxisAngle 130;
nBufferCellsNoExtrude 0;
nLayerIter 50;
nRelaxedIter 0;

}

meshQualityControls
{
  maxNonOrtho 65;
  maxBoundarySkewness 20;
  maxInternalSkewness 4;
  maxConcave 80;
  minFlatness 0.5;
  minVol 1e-30;
  minTetQuality 1e-30;
  minArea 1e-30;
  minTwist 0.02;
  minDeterminant 0.001;
  minFaceWeight 0.05;
  minVolRatio 0.01;
  minTriangleTwist 0.001;
  nSmoothScale 4;
  errorReduction 0.75;
  relaxed
  {
    maxNonOrtho 75;
    maxInternalSkewness 8;
    minTetQuality -1e30;
    minTwist 1.0e-06;
    minDeterminant 1.0e-06;
    minFaceWeight 1.0e-06;
  }
}

mergeTolerance 1e-08;
debug 0;
```

**Boundary:**

```
FoamFile
{
  version 2.0;
  format binary;
  class polyBoundaryMesh;
  arch "LSB;label=32;scalar=64";
  location "constant/polyMesh";
  object boundary;
}
// ***** //
```

```
8
(
  inlet
  {
    type patch;
    nFaces 3182;
    startFace 6126065;
  }
  outlet
  {
    type patch;
    nFaces 3182;
    startFace 6129247;
  }
  ymin
  {
    type patch;
    nFaces 14504;
    startFace 6132429;
  }
  ymax
  {
    type symmetry;
    inGroups 1(symmetry);
    nFaces 14504;
    startFace 6146933;
  }
  zmax
  {
    type symmetry;
    inGroups 1(symmetry);
    nFaces 33712;
    startFace 6161437;
  }
  ground
  {
    type wall;
    inGroups 1(wall);
  }
}
```

```
    nFaces    137096;
    startFace 6195149;
  }
  releasePoint
  {
    type      wall;
    inGroups  1(wall);
    nFaces    503;
    startFace 6332245;
  }
  releaseTube
  {
    type      wall;
    inGroups  1(wall);
    nFaces    21122;
    startFace 6332748;
  }
)

// *****
//
```

## Appendix C: Turbulence at inlet using *fluctuationScale*

Series of simulations were run with different values of *fluctuationScale* and alpha values to get the following Standard Deviation ( $\sigma$ ) for velocity.

TABLE 17.2 Vector mean wind and standard deviation of eddy wind components and azimuth angle. Elevation angle,  $E^*$ , and azimuth angle,  $A^*$ , are given in degrees; mean wind speed,  $\bar{U}$ , and standard deviations,  $\sigma(u)$ ,  $\sigma(v)$ , and  $\sigma(w)$  in m/sec; standard deviation of azimuth angle is in degrees.

Run No.	Anemometer No.	$E^*$	$A^*$	$\bar{U}$	$\sigma(u)$	$\sigma(v)$	$\sigma(w)$	$\sigma(A)$
5	3	-6.5	169.9	5.557	1.17	1.23	0.433	13.2
	4	0.1	172.6	6.701	1.26	1.36	0.359	11.7
6	1	-5.6	174.7	7.256	1.11	1.09	0.611	8.7
	2	-10.7	176.4	6.441	1.04	1.04	0.545	9.4
	3	-6.2	175.8	5.421	0.953	0.882	0.421	9.5
	4	0.0	179.4	6.846	1.05	1.01	0.387	8.5
	5	-7.5	176.3	8.397	1.29	1.50	0.560	8.9
7	1	-2.7	201.7	5.158	1.79	1.90	0.583	21.7
	2	-5.4	202.9	4.354	1.41	1.61	0.417	22.3
	3	-7.4	203.8	3.342	1.14	1.28	0.352	23.5
	4	0.3	205.5	4.916	1.49	1.71	0.387	21.3
	5	-3.4	202.7	5.544	1.70	1.85	0.445	21.0
8	1	0.7	178.5	6.334	1.65	1.67	0.497	15.6
	2	-1.2	178.5	5.159	1.25	1.37	0.395	16.1
	3	-3.4	179.0	3.631	0.909	0.997	0.303	16.7
	4	4.6	183.0	5.617	1.44	1.66	0.372	17.4
	5	1.2	180.2	5.686	1.40	1.58	0.369	15.9
9	3	-3.6	184.0	5.720	1.05	1.17	0.444	11.0
10	1	-0.9	205.6	5.962	2.18	1.76	0.556	18.1
	2	-6.0	203.3	4.902	1.70	1.39	0.460	17.4
	3	-6.6	205.7	3.388	1.14	0.972	0.319	17.1
	4	1.9	212.8	5.706	1.93	1.51	0.358	16.2
	5	-0.5	207.9	5.432	1.63	1.57	0.403	17.6
13	1	-15.0	183.4	1.759	0.172	0.134	0.176, -1	4.1
	2	-28.6	188.0	1.767	0.174	0.104	0.702, -1	3.2
	3	-19.7	185.2	1.662	0.164	0.124	0.604, -1	4.2
	4	-2.3	191.7	1.873	0.202	0.126	0.112, -1	3.6
	5	-8.7	183.7	1.996	0.222	0.145	0.242, -1	4.5

For each set simulation were completed for steady-state and the boundary condition from end time of the simulation was manually.

After Steady-State simulation

```
(1.17316 2.53087e-07 -1.10448e-08)
(2.21335 2.59172e-07 3.03958e-06)
(1.17324 -1.30372e-07 2.81791e-05)
(1.17317 -1.76797e-07 -4.19296e-08)
(1.17323 1.61451e-07 2.88252e-05)
)
;

boundaryField
{
  inlet
  {
    type          atmBoundaryLayerInletVelocity;
    z0            constant 0.002;
    flowDir       constant (1 0 0);
    zDir          constant (0 0 1);
    kappa         0.41;
    Cmu           0.09;
    Uref          constant 6.88;
    Zref          constant 2;
    zGround       constant 0;
    value         nonuniform List<vector>
600
(
(9.81324 0 0)
(9.81324 0 0)
(9.81324 0 0)
(9.81324 0 0)
(9.81324 0 0)
(9.81324 0 0)
(9.81324 0 0)
(9.81324 0 0)
(9.81324 0 0)
(9.81324 0 0)
(9.71251 0 0)
(9.71251 0 0)
)
```

Before Transient simulation

```
(1.17316 2.53087e-07 -1.10448e-08)
(2.21335 2.59172e-07 3.03958e-06)
(1.17324 -1.30372e-07 2.81791e-05)
(1.17317 -1.76797e-07 -4.19296e-08)
(1.17323 1.61451e-07 2.88252e-05)
)
;

boundaryField
{
  inlet
  {
    type          turbulentInlet;
    fluctuationScale (0.6 0.6 0.6);
    alpha         0.5;
    referenceField nonuniform List<vector>
600
(
(9.81324 0 0)
(9.81324 0 0)
(9.81324 0 0)
(9.81324 0 0)
(9.81324 0 0)
(9.81324 0 0)
(9.81324 0 0)
(9.81324 0 0)
(9.81324 0 0)
(9.81324 0 0)
(9.71251 0 0)
(9.71251 0 0)
)
```

*turbulentInlet bc need these reference field from steady-state*

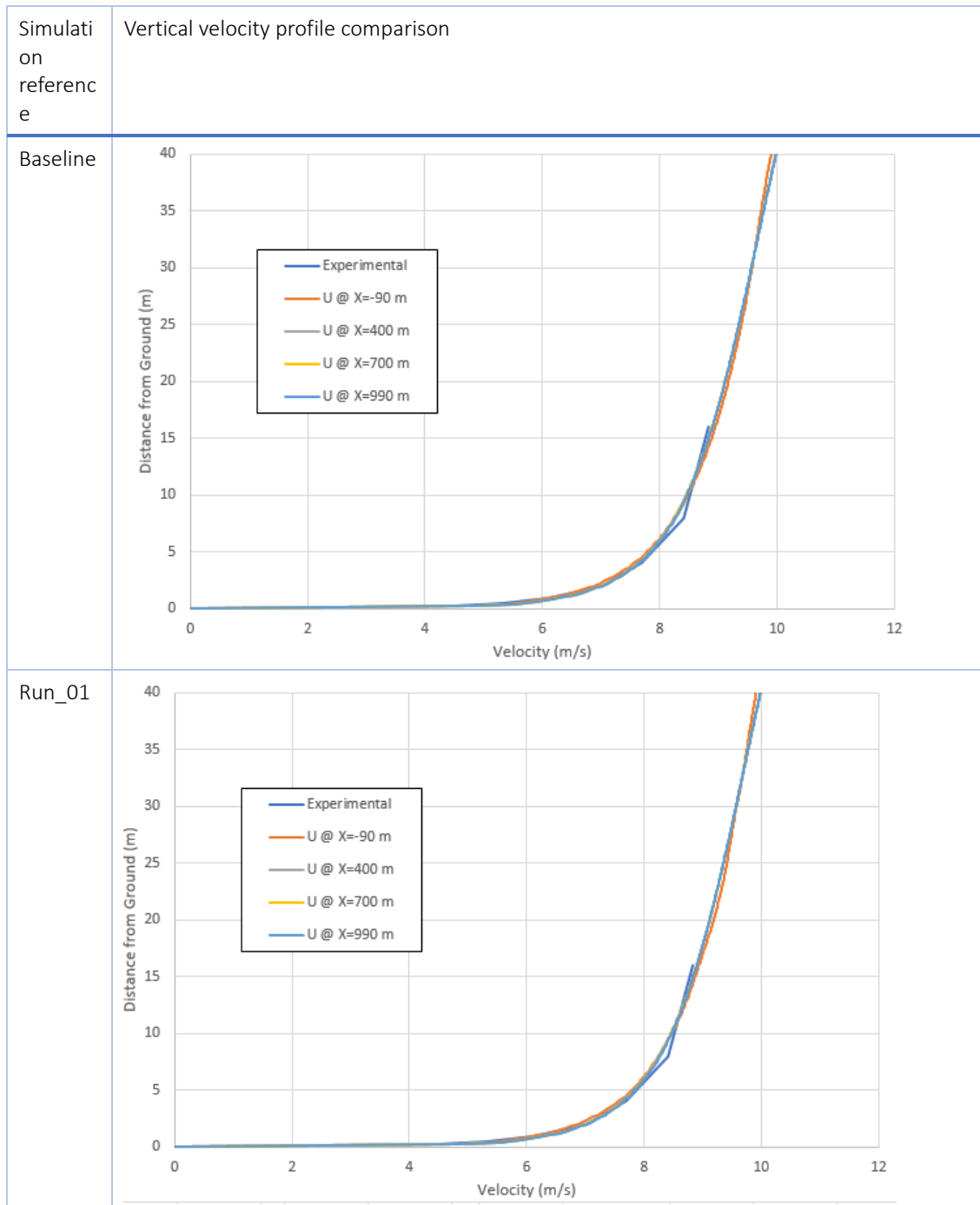
Following variation of *fluctuationScale* and *alpha* values were tried.

Table 71: *fluctuationScale* and *alpha* values used

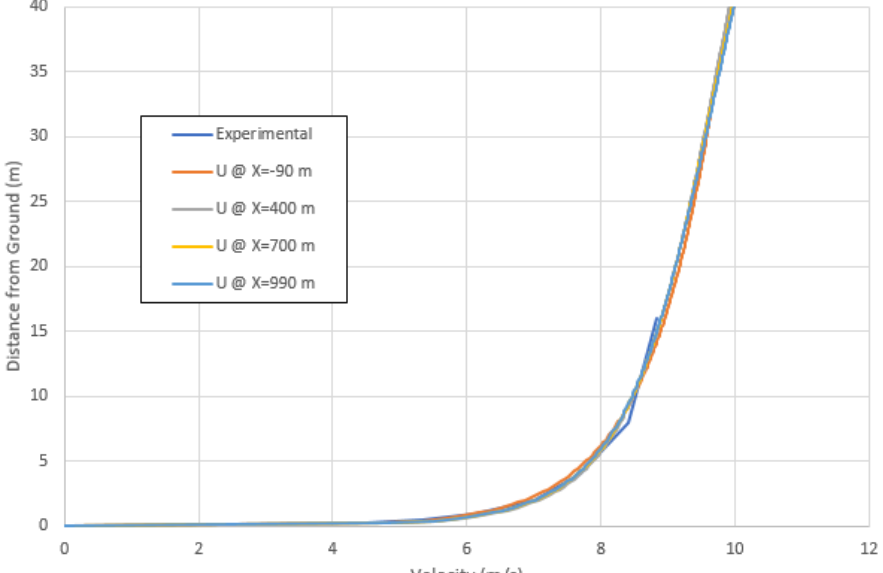
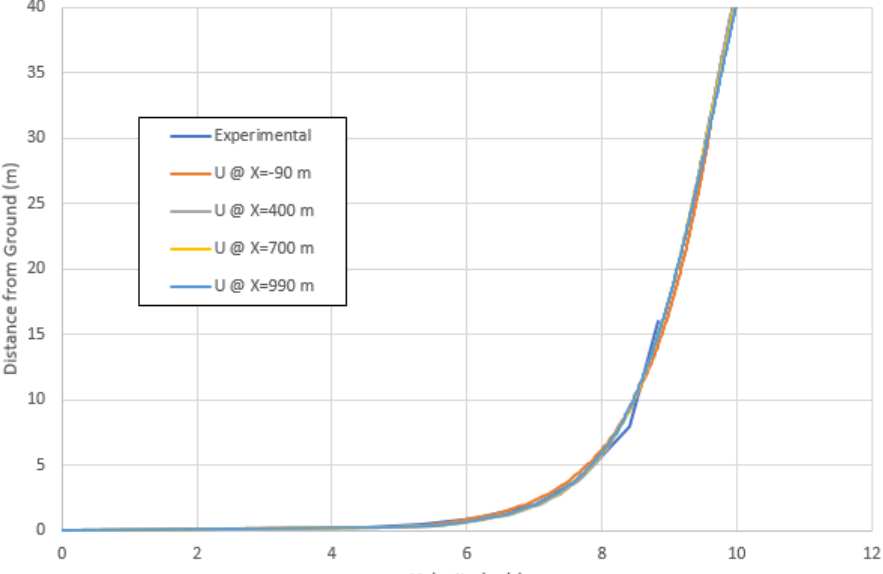
	<i>fluctuationScale</i>	<i>alpha</i>
Baseline	-	-
Run_01	(0.1 0.1 0.1)	1.0E-08
Run_02	(0.1 0.1 0.1)	0.5
Run_03	(0.1 0.1 0.1)	1
Run_04	(0.2 0.2 0.2)	1.0E-08
Run_05	(0.2 0.2 0.2)	0.5
Run_06	(0.2 0.2 0.2)	1
Run_07	(0.4 0.4 0.4)	1.0E-08
Run_08	(0.4 0.4 0.4)	0.5
Run_09	(0.4 0.4 0.4)	1
Run_10	(0.6 0.6 0.6)	1.0E-08
Run_11	(0.6 0.6 0.6)	0.5
Run_12	(0.6 0.6 0.6)	1

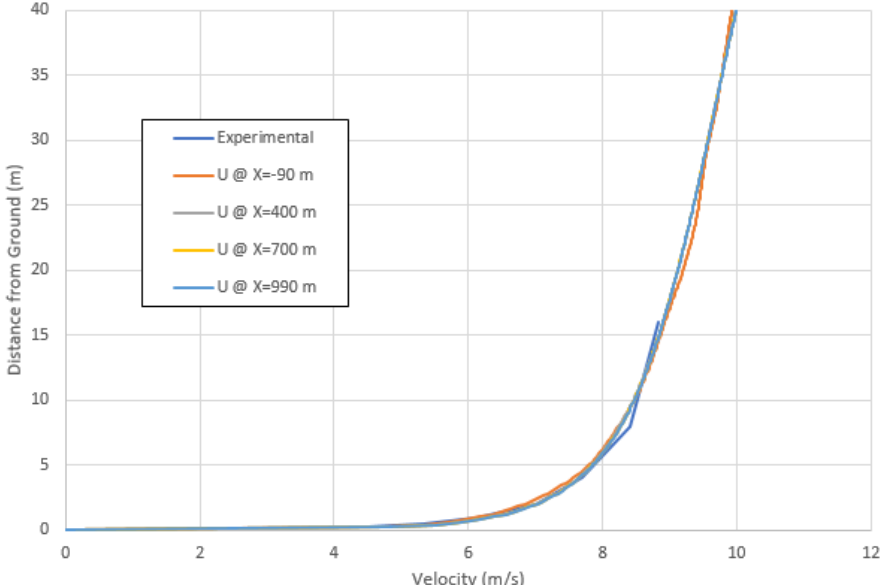
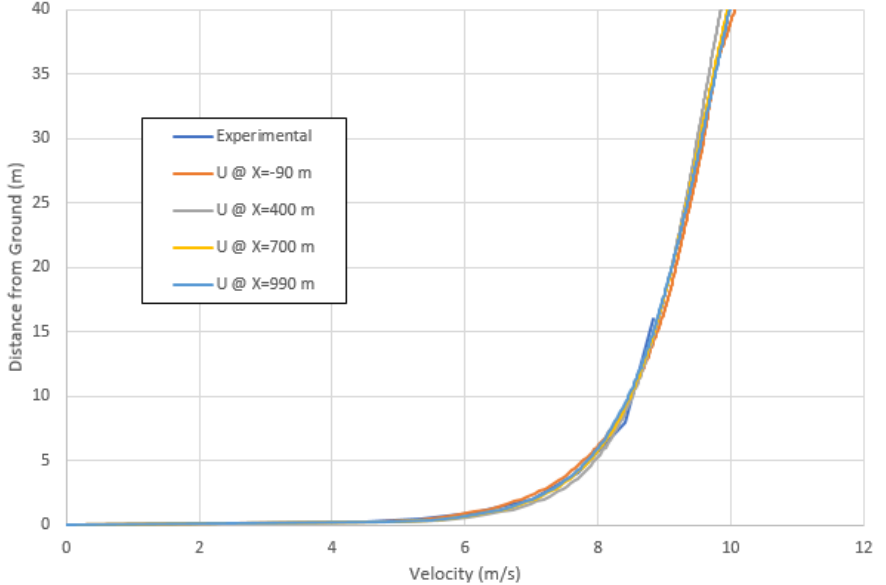
Simplified tunnel – transient – Vertical vlocity profile estimations for each set of *fluctuationScale* and *alpha* values compared with the field trial estimations are given in figures:

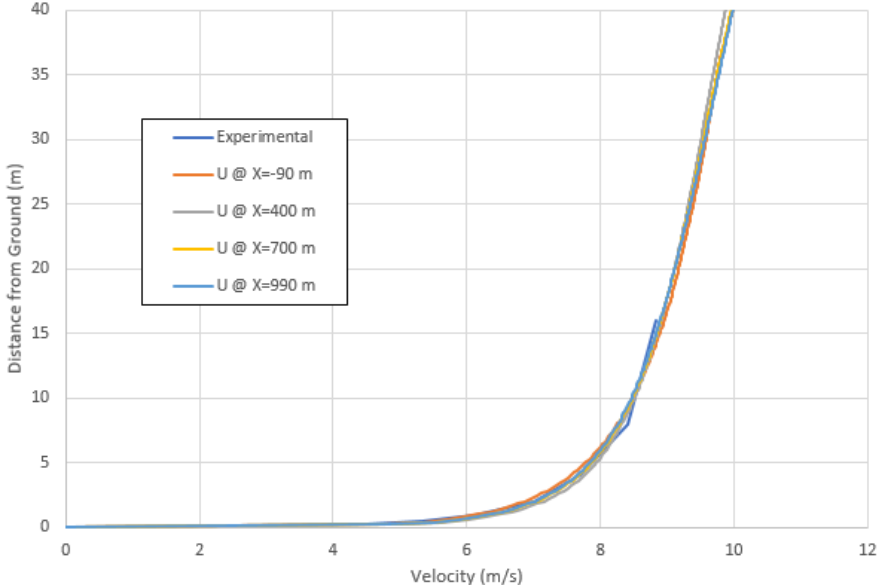
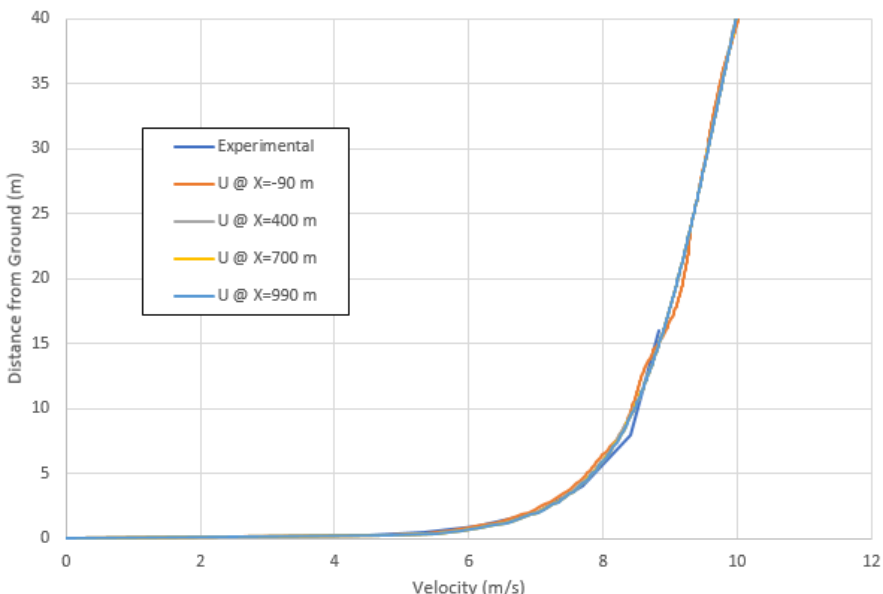
Table 72: Vertical velocity profile comparison

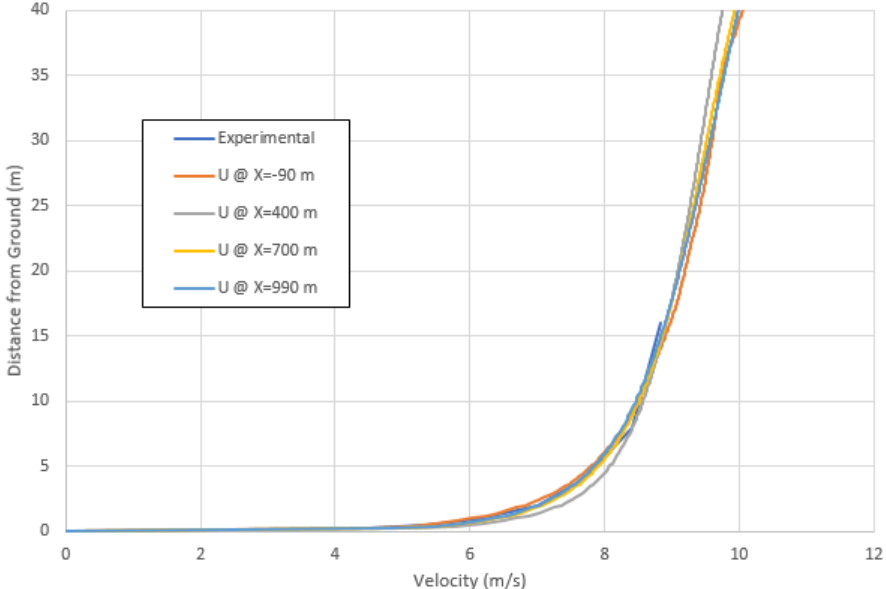
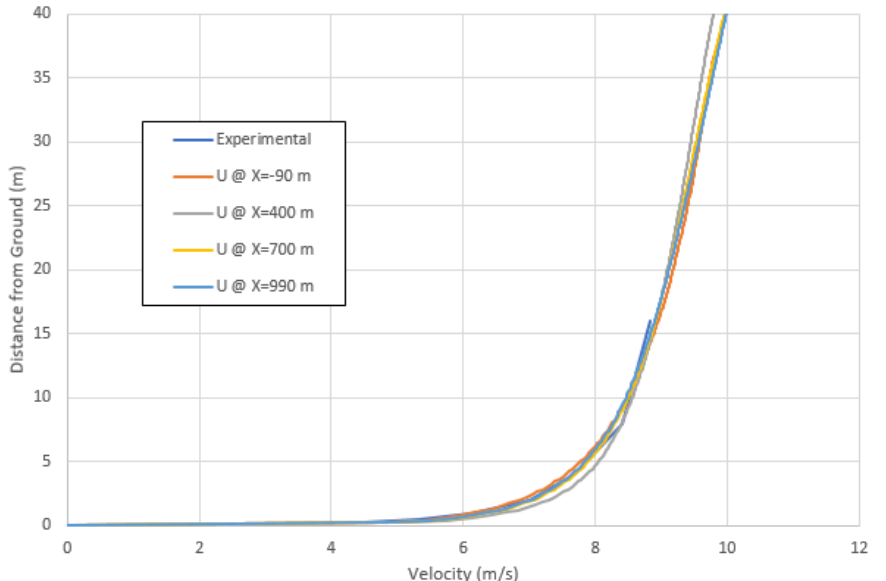


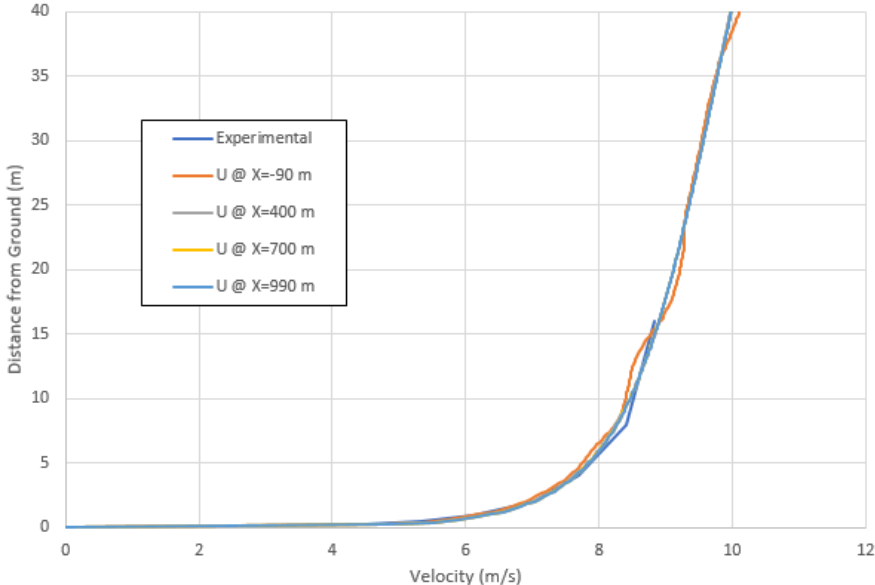
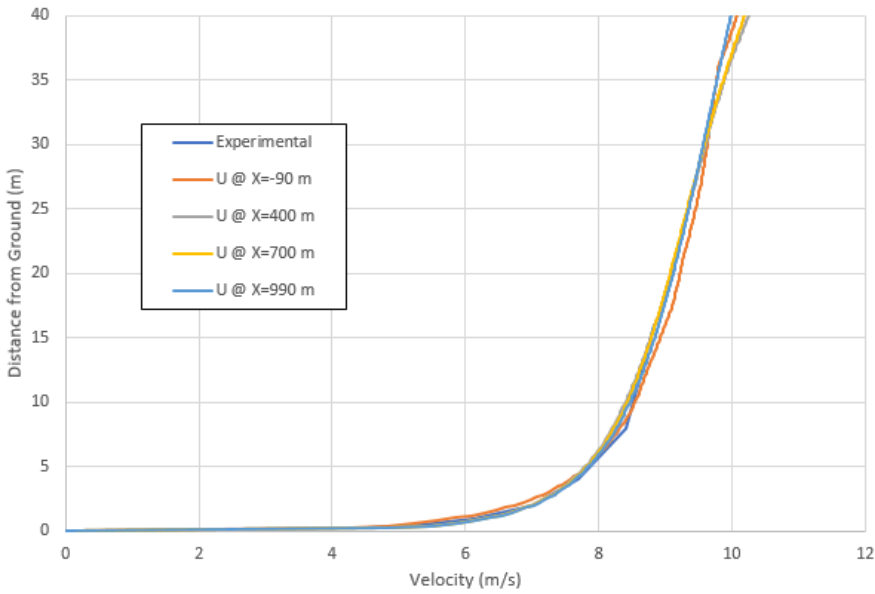


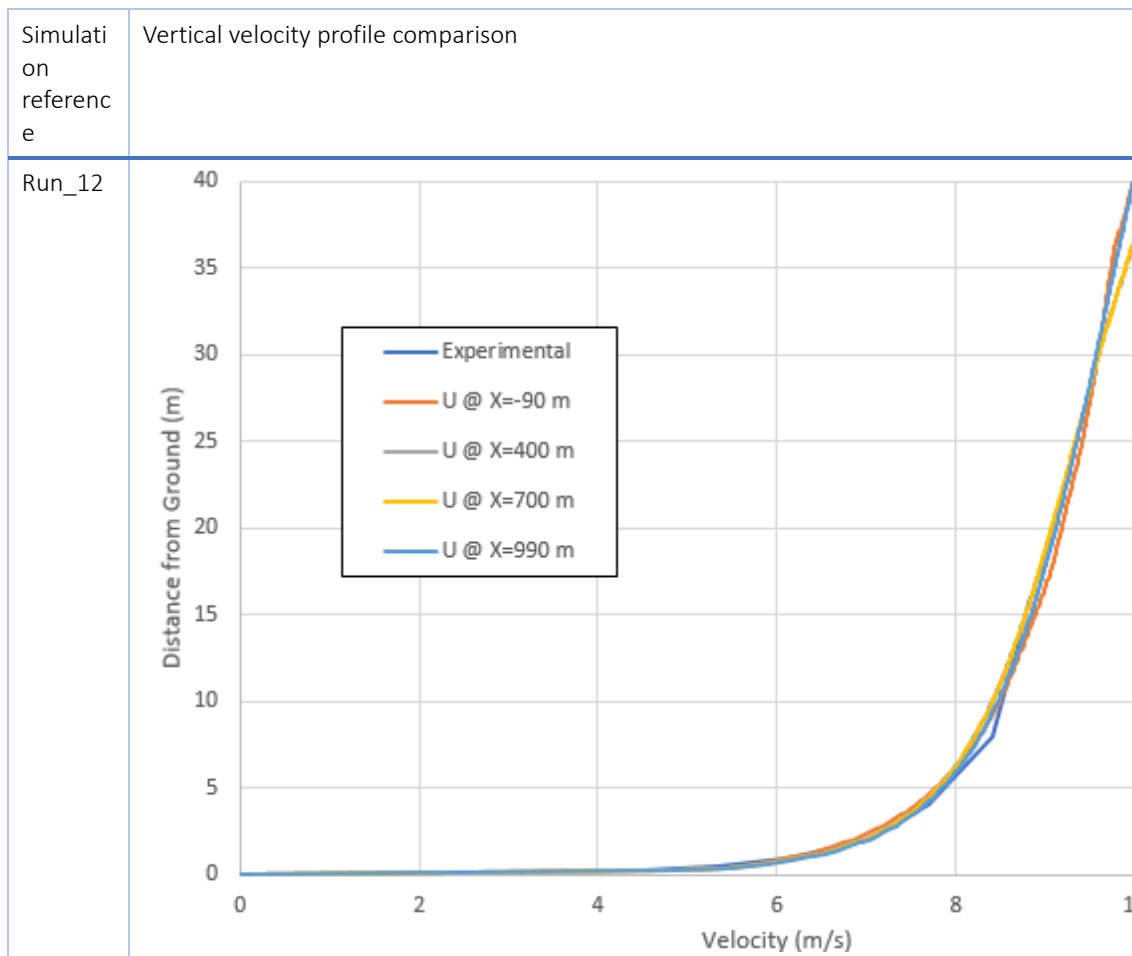
Simulati on referenc e	Vertical velocity profile comparison
Run_02	
Run_03	

Simulati on referenc e	Vertical velocity profile comparison
Run_04	
Run_05	

Simulati on referenc e	Vertical velocity profile comparison
Run_06	
Run_07	

Simulati on referenc e	Vertical velocity profile comparison
Run_08	
Run_09	

Simulati on referenc e	Vertical velocity profile comparison
Run_10	
Run_11	



Transient simulation velocity profile Standard deviation comparison vs observed values at field trials.

Table 73: fluctuationScale values

	<i>fluctuationScale</i>	<i>alpha</i>	$\sigma(U_x)$	$\sigma(U_y)$	$\sigma(U_z)$
Experimental	-	-	1.05	1.17	0.44
Baseline	-	-	2.94E-05	8.15E-07	7.6E-06
Run_01	(0.1 0.1 0.1)	1.0E-08	0.0059	0.00221	0.00182
Run_02	(0.1 0.1 0.1)	0.5	0.03758	0.05309	0.0289
Run_03	(0.1 0.1 0.1)	1	0.02036	0.02972	0.01738
Run_04	(0.2 0.2 0.2)	1.0E-08	0.00731	0.00207	0.00102

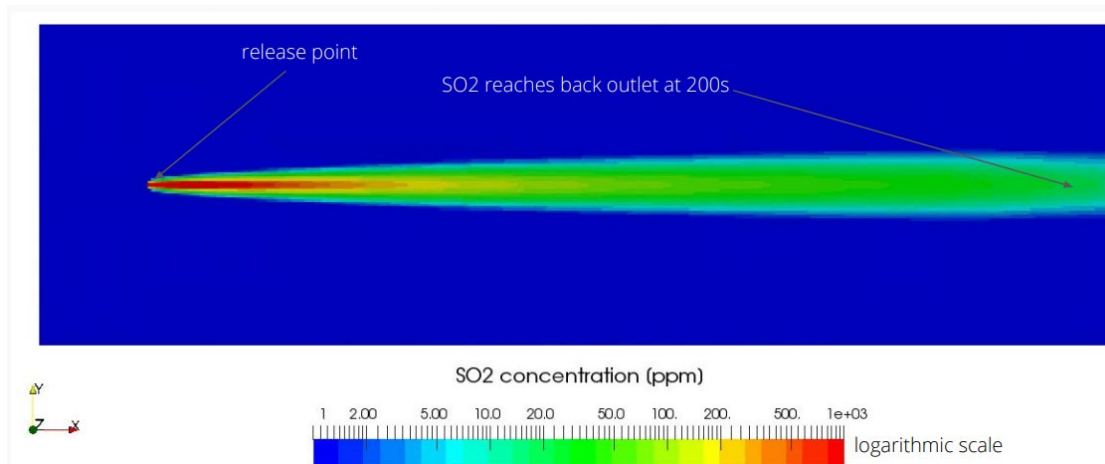
Run_05	(0.2 0.2 0.2)	0.5	0.07758	0.10061	0.05631
Run_06	(0.2 0.2 0.2)	1	0.04512	0.05853	0.0333
Run_07	(0.4 0.4 0.4)	1.0E-08	0.03118	0.00479	0.00549
Run_08	(0.4 0.4 0.4)	0.5	0.14936	0.2099	0.1137
Run_09	(0.4 0.4 0.4)	1	0.08712	0.12164	0.06654
Run_10	(0.6 0.6 0.6)	1.0E-08	0.04708	0.00714	0.00826
Run_11	(0.6 0.6 0.6)	0.5	0.22487	0.31539	0.16983
Run_12	(0.6 0.6 0.6)	1	0.12981	0.18236	0.09914

From the analysis of the different combination of parameters in *turbulentInlet* bc, it is evident that all of the combinations are able to maintain the intended velocity profile reasonably well. From the table above, it is clear that, for any fixed value of *fluctuationScale*, the standard deviation ( $\sigma$ ) increase first and then decreases and a for a fixed value of *alpha*,  $\sigma$  increases with *fluctuationScale*.

For the OpenFoam model validation, the *fluctuationScale* of (0.95 0.95 0.95) and *alpha* of 0.75 was used.

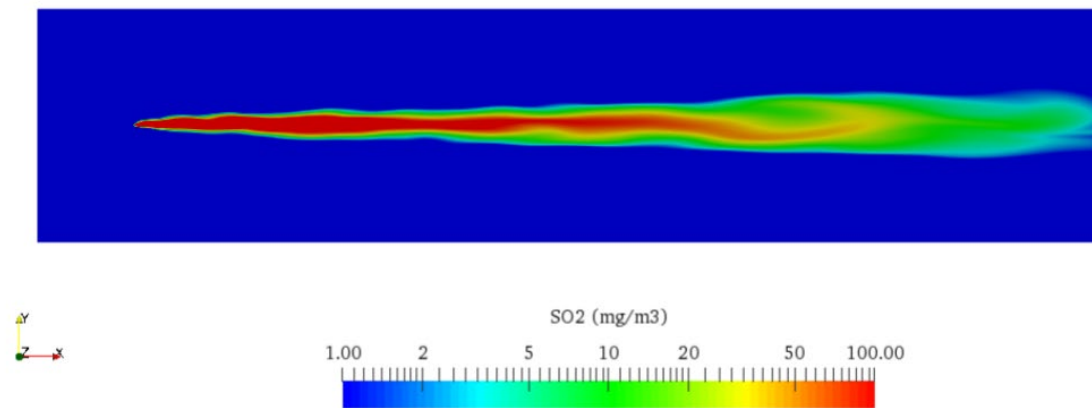
A comparison of the steady state dispersion of SO<sub>2</sub> and with fluctuating turbulence is given in the figures below.

**Steady state:**



**Transient**

Time: 155 sec

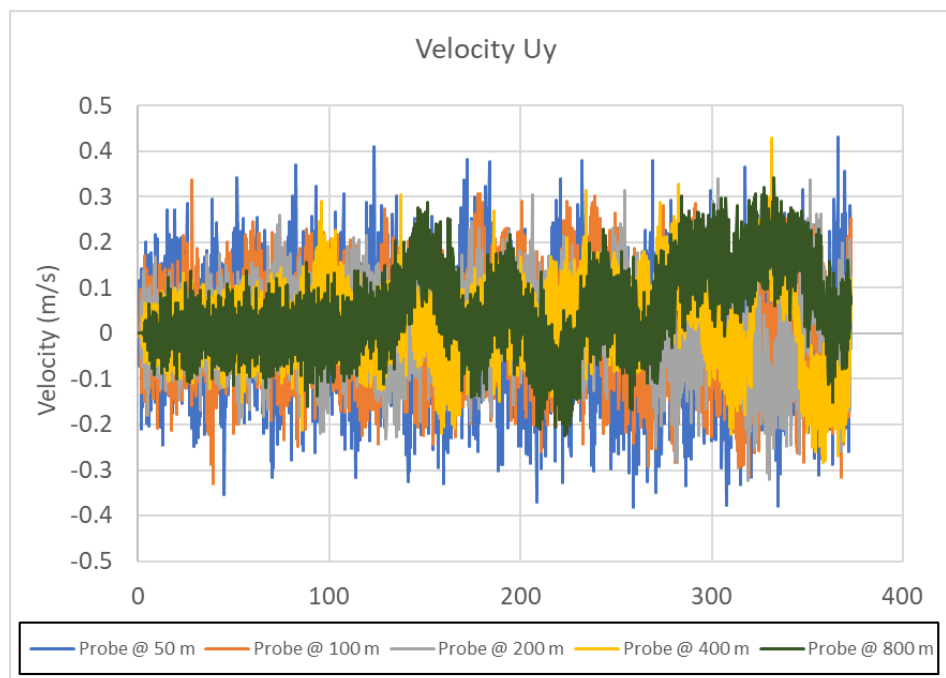
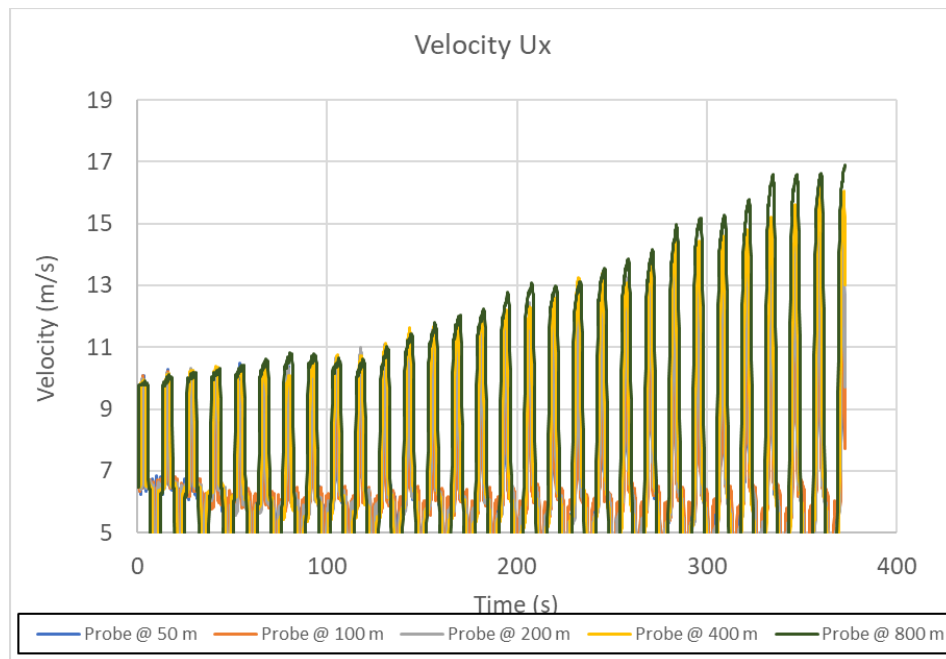


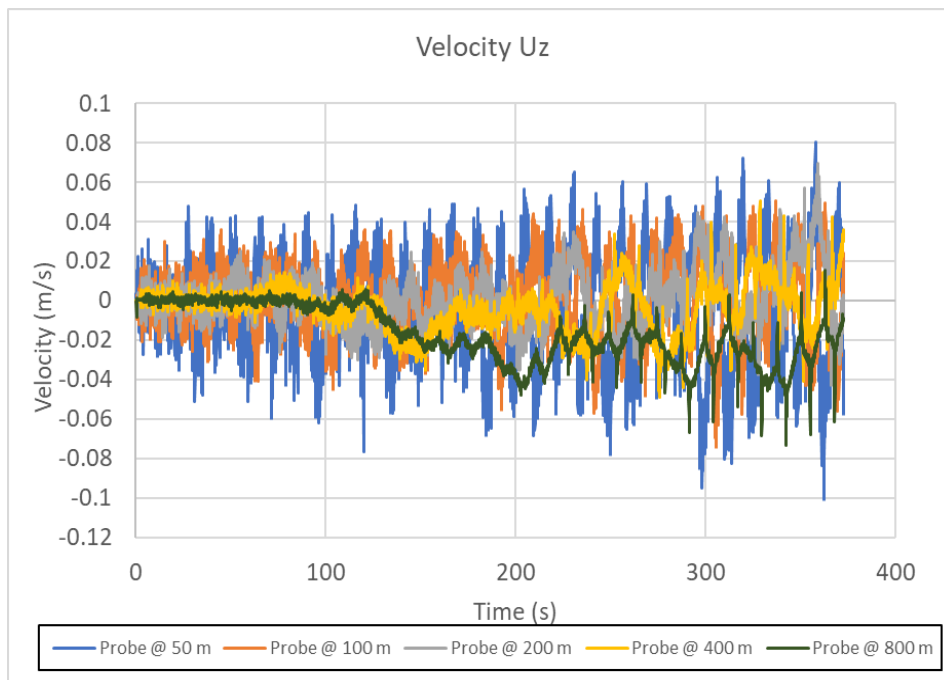


## Appendix D: OpenFOAM Velocity at the Probes

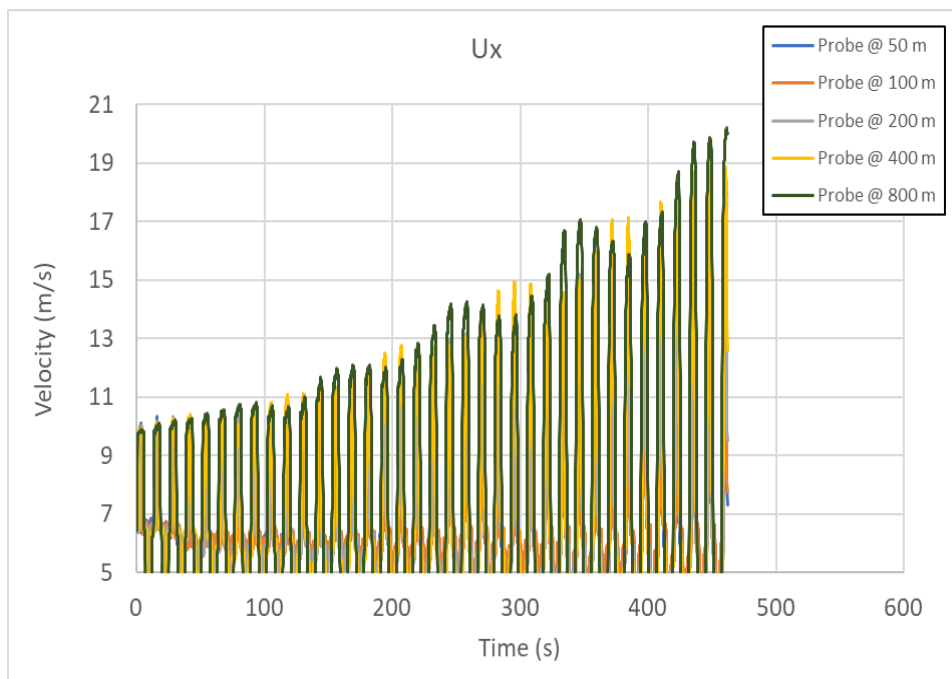
The velocity estimations for the OpenFOAM simulations for the sensitivity of H<sub>2</sub>S containing natural gas compositions is given in this section. The velocity (m/s) for the about 350 s estimated at the five probe locations along the central line of the monitoring arcs at downwind distances 50 m, 100 m, 200 m, 400 m, and 800 m.

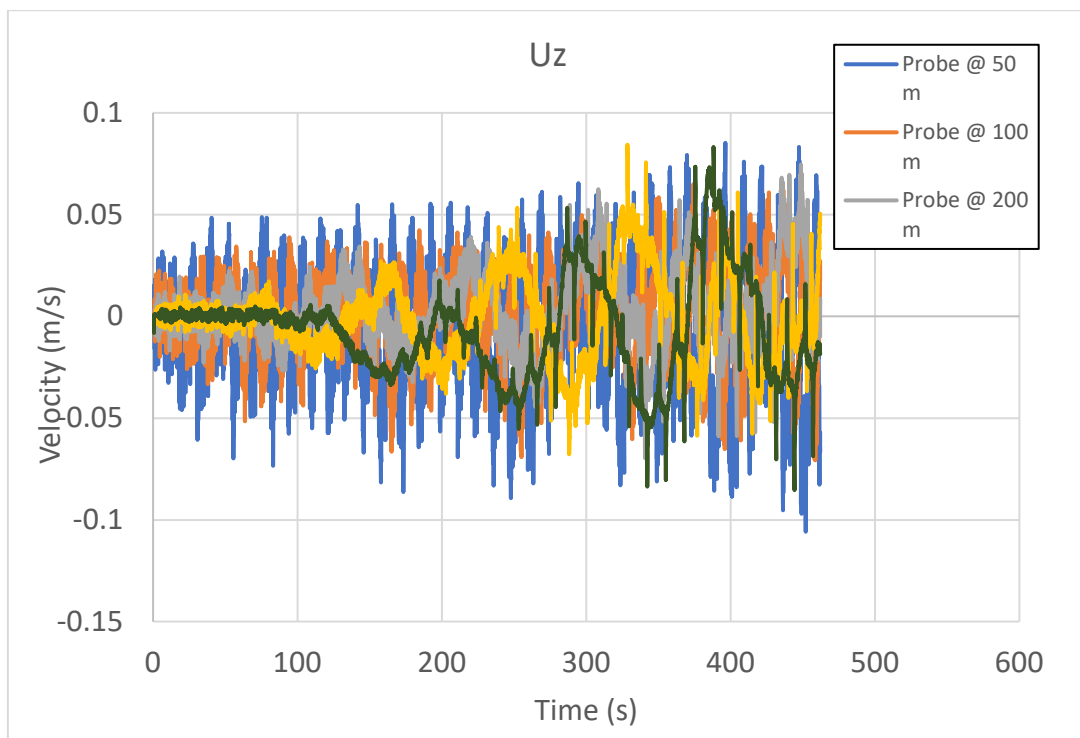
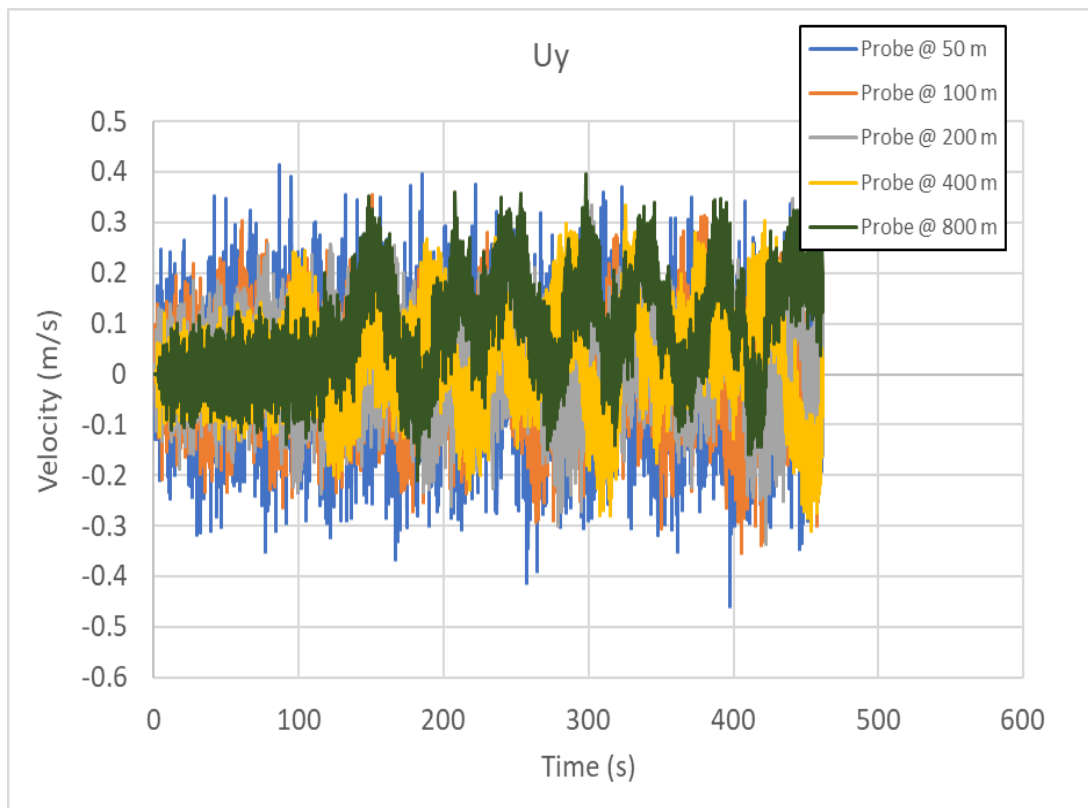
### Case 1: Velocity at the probes



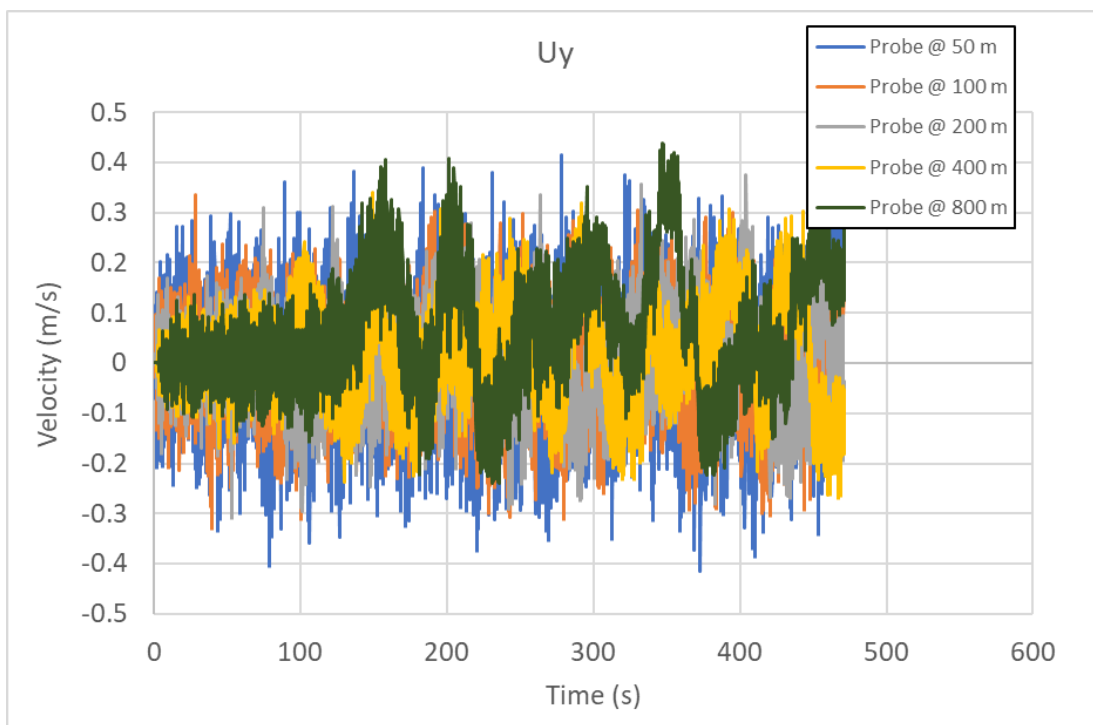
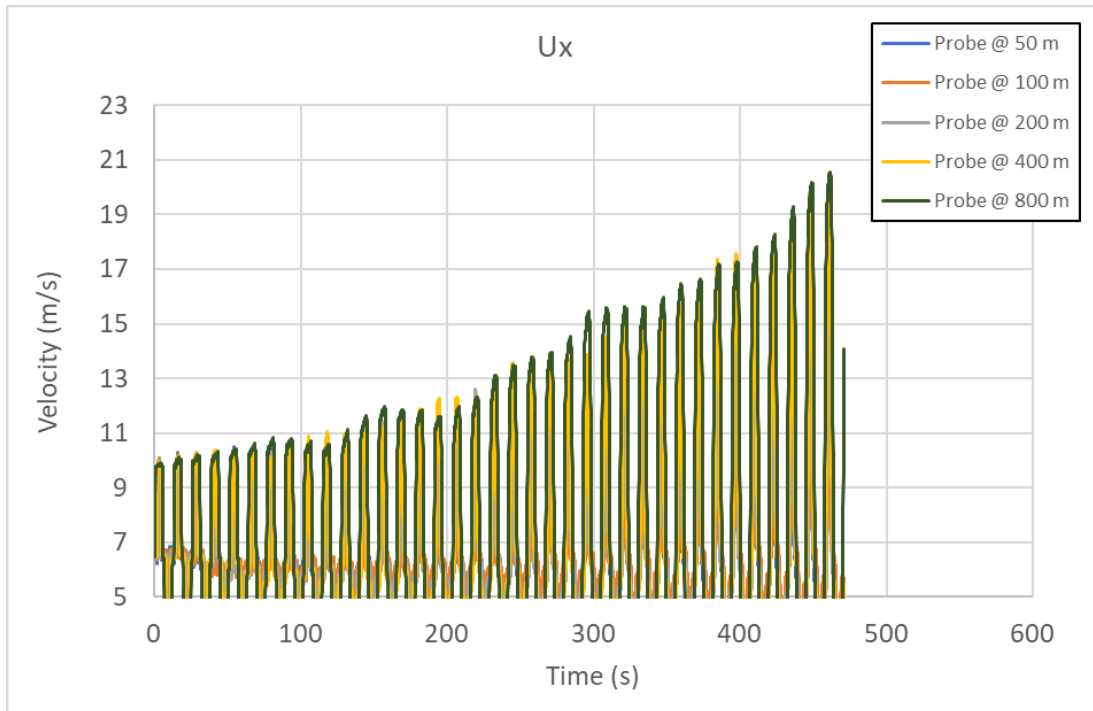


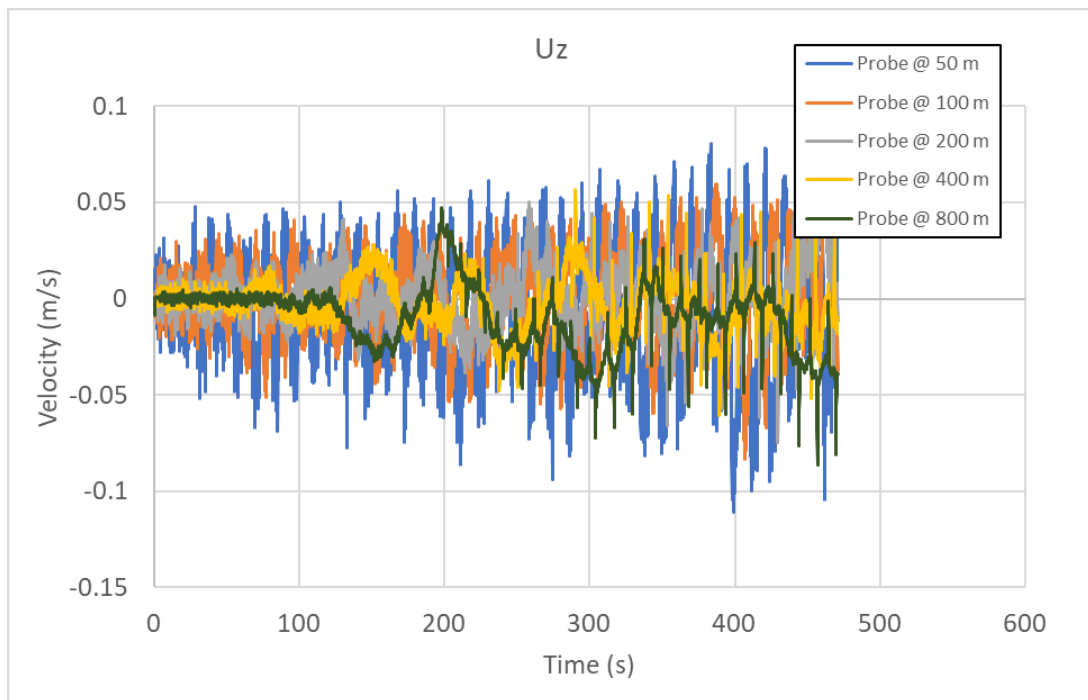
Case 2: Velocity at the probes





Case 3: Velocity at the probes





## Appendix E: Canary results for source term sensitivity

Sensitivity simulations were carried out for the release hole size, temperature, pressure, release orientation and the environmental parameters - stability class, wind speed, humidity, air temperature, soil temperature, and surface roughness. The list of cases with the corresponding input values for the source term sensitivity simulations carried out with Canary tool is given in this table.

Sensitivity	Canary Case reference	Natural gas (H <sub>2</sub> S%) ref.	Mol Wt.	Temperature (°C)	Pressure (bara)	Stability class	Wind (mph)	Humidity (%)	Air, Soil temp (°F)	Surf. Rough (m)	Line size (inch)	Hole size (inch)	Release rate (lb/s)
Orientation - horizontal	S1PLHO2	S1 (2.6%)	38.57	25	7.9	F	3.4	50	77	0.007	6	1	2.95
	S2PLHO2	S2 (8%)	26.75	25	7.9	F	3.4	50	77	0.007	6	1	1.42
	S3PLHO2	S3 (10%)	26.83	25	7.9	F	3.4	50	77	0.007	6	1	1.43
	S4PLHO2	S4 (14%)	19.95	25	7.9	F	3.4	50	77	0.007	6	1	1.27
	S5PLHO2	S5 (15%)	22.81	25	7.9	F	3.4	50	77	0.007	6	1	1.35
	S6PLHO2	S6 (16%)	24.48	25	7.9	F	3.4	50	77	0.007	6	1	1.4
	S7PLHO2	S7 (18%)	34.52	25	7.9	F	3.4	50	77	0.007	6	1	1.66
	S8PLHO2	S8 (29%)	29.05	25	7.9	F	3.4	50	77	0.007	6	1	1.54
Orientation - upwards	S1PLUO4	S1 (2.6%)	38.57	25	7.9	F	3.4	50	77	0.007	6	2	11.8
	S2PLUO4	S2 (8%)	27.65	25	7.9	F	3.4	50	77	0.007	6	2	5.7
	S3PLUO4	S3 (10%)	26.83	25	7.9	F	3.4	50	77	0.007	6	2	5.9
	S4PLUO4	S4 (14%)	19.95	25	7.9	F	3.4	50	77	0.007	6	2	5.1
	S5PLUO4	S5 (15%)	22.81	25	7.9	F	3.4	50	77	0.007	6	2	5.4
	S6PLUO4	S6 (16%)	24.48	25	7.9	F	3.4	50	77	0.007	6	2	5.6
	S7PLUO4	S7 (18%)	34.52	25	7.9	F	3.4	50	77	0.007	6	2	6.7
	S8PLUO4	S8 (29%)	29.05	25	7.9	F	3.4	50	77	0.007	6	2	6.1
Env. High wind, Unstable upwards	S1PHUO4	S1 (2.6%)	38.57	25	7.9	<b>C</b>	<b>20</b>	50	77	0.007	6	2	11.8
	S2PHUO4	S2 (8%)	27.65	25	7.9	C	20	50	77	0.007	6	2	5.7
	S3PHUO4	S3 (10%)	26.83	25	7.9	C	20	50	77	0.007	6	2	5.9

Sensitivity	Canary Case reference	Natural gas (H <sub>2</sub> S%) ref.	Mol Wt.	Temperature (°C)	Pressure (bara)	Stability class	Wind (mph)	Humidity (%)	Air, Soil temp (°F)	Surf. Rough (m)	Line size (inch)	Hole size (inch)	Release rate (lb/s)
	S4PHUO4	S4 (14%)	19.95	25	7.9	C	20	50	77	0.007	6	2	5.1
	S5PHUO4	S5 (15%)	22.81	25	7.9	C	20	50	77	0.007	6	2	5.4
	S6PHUO4	S6 (16%)	24.48	25	7.9	C	20	50	77	0.007	6	2	5.6
	S7PHUO4	S7 (18%)	34.52	25	7.9	C	20	50	77	0.007	6	2	6.7
	S8PMUO4	S8 (29%)	29.05	25	7.9	C	20	50	77	0.007	6	2	6.1
Base case	S1PLHO5	S1 (2.6%)	38.57	25	7.9	F	3.4	50	77	0.007	6	2	11.8
	S2PLHO5	S2 (8%)	27.65	25	7.9	F	3.4	50	77	0.007	6	2	5.7
	S3PLHO5	S3 (10%)	26.83	25	7.9	F	3.4	50	77	0.007	6	2	5.9
	S4PLHO5	S4 (14%)	19.95	25	7.9	F	3.4	50	77	0.007	6	2	5.1
	S5PLHO5	S5 (15%)	22.81	25	7.9	F	3.4	50	77	0.007	6	2	5.4
	S6PLHO5	S6 (16%)	24.48	25	7.9	F	3.4	50	77	0.007	6	2	5.6
	S7PLHO5	S7 (18%)	34.52	25	7.9	F	3.4	50	77	0.007	6	2	6.7
	S8PLHO5	S8 (29%)	29.05	25	7.9	F	3.4	50	77	0.007	6	2	6.1
	Env. Medium wind	S1PMH05	S1 (2.6%)	38.57	25	7.9	<b>D</b>	<b>13</b>	50	77	0.007	6	2
S2PMH05		S2 (8%)	27.65	25	7.9	D	13	50	77	0.007	6	2	5.7
S3PMH05		S3 (10%)	26.83	25	7.9	D	13	50	77	0.007	6	2	5.9
S4PMH05		S4 (14%)	19.95	25	7.9	D	13	50	77	0.007	6	2	5.1
S5PMH05		S5 (15%)	22.81	25	7.9	D	13	50	77	0.007	6	2	5.4
S6PMH05		S6 (16%)	24.48	25	7.9	D	13	50	77	0.007	6	2	5.6
S7PMH05		S7 (18%)	34.52	25	7.9	D	13	50	77	0.007	6	2	6.7
S8PMH05		S8	29.05	25	7.9	D	13	50	77	0.007	6	2	6.1
Env. High wind		S1PHHO5	S1 (2.6%)	38.57	25	7.9	<b>C</b>	<b>20</b>	50	77	0.007	6	2
	S2PHHO5	S2 (8%)	27.65	25	7.9	C	20	50	77	0.007	6	2	5.7

Sensitivity	Canary Case reference	Natural gas (H <sub>2</sub> S%) ref.	Mol Wt.	Temperature (°C)	Pressure (bara)	Stability class	Wind (mph)	Humidity (%)	Air, Soil temp (°F)	Surf. Rough (m)	Line size (inch)	Hole size (inch)	Release rate (lb/s)
	S3PHHO5	S3 (10%)	26.83	25	7.9	C	20	50	77	0.007	6	2	5.9
	S4PHHO5	S4 (14%)	19.95	25	7.9	C	20	50	77	0.007	6	2	5.1
	S5PHHO5	S5 (15%)	22.81	25	7.9	C	20	50	77	0.007	6	2	5.4
	S6PHHO5	S6 (16%)	24.48	25	7.9	C	20	50	77	0.007	6	2	5.6
	S7PHHO5	S7 (18%)	34.52	25	7.9	C	20	50	77	0.007	6	2	6.7
	S8PHHO5	S8 (29%)	29.05	25	7.9	C	20	50	77	0.007	6	2	6.1
Env. Humidity Low	S1PLHO6	S1 (2.6%)	38.57	25	7.9	F	3.4	<b>20</b>	77	0.007	6	2	11.8
	S2PLHO6	S2 (8%)	27.65	25	7.9	F	3.4	20	77	0.007	6	2	5.7
	S3PLHO6	S3 (10%)	26.83	25	7.9	F	3.4	20	77	0.007	6	2	5.9
	S4PLHO6	S4 (14%)	19.95	25	7.9	F	3.4	20	77	0.007	6	2	5.1
	S5PLHO6	S5 (15%)	22.81	25	7.9	F	3.4	20	77	0.007	6	2	5.4
	S6PLHO6	S6 (16%)	24.48	25	7.9	F	3.4	20	77	0.007	6	2	5.6
	S7PLHO6	S7 (18%)	34.52	25	7.9	F	3.4	20	77	0.007	6	2	6.7
	S8PLHO6	S8 (29%)	29.05	25	7.9	F	3.4	20	77	0.007	6	2	6.1
Env. Humidity High	S1PLHO7	S1 (2.6%)	38.57	25	7.9	F	3.4	<b>80</b>	77	0.007	6	2	11.8
	S2PLHO7	S2 (8%)	27.65	25	7.9	F	3.4	80	77	0.007	6	2	5.7
	S3PLHO7	S3 (10%)	26.83	25	7.9	F	3.4	80	77	0.007	6	2	5.9
	S4PLHO7	S4 (14%)	19.95	25	7.9	F	3.4	80	77	0.007	6	2	5.1
	S5PLHO7	S5 (15%)	22.81	25	7.9	F	3.4	80	77	0.007	6	2	5.4
	S6PLHO7	S6 (16%)	24.48	25	7.9	F	3.4	80	77	0.007	6	2	5.6
	S7PLHO7	S7 (18%)	34.52	25	7.9	F	3.4	80	77	0.007	6	2	6.7
	S8PLHO7	S8 (29%)	29.05	25	7.9	F	3.4	80	77	0.007	6	2	6.1
Temperature	S1PLHO8	S1 (2.6%)	38.57	48.89	7.9	F	3.4	50	120	0.007	6	2	50



Sensitivity	Canary Case reference	Natural gas (H <sub>2</sub> S%) ref.	Mol Wt.	Temperature (°C)	Pressure (bara)	Stability class	Wind (mph)	Humidity (%)	Air, Soil temp (°F)	Surf. Rough (m)	Line size (inch)	Hole size (inch)	Release rate (lb/s)
Sensitivity	S2PLH08	S2 (8%)	27.65	48.89	7.9	F	3.4	50	120	0.007	6	2	5.7
	S3PLH08	S3 (10%)	26.83	48.89	7.9	F	3.4	50	120	0.007	6	2	5.9
	S4PLH08	S4 (14%)	19.95	48.89	7.9	F	3.4	50	120	0.007	6	2	5.1
	S5PLH08	S5 (15%)	22.81	48.89	7.9	F	3.4	50	120	0.007	6	2	5.4
	S6PLH08	S6 (16%)	24.48	48.89	7.9	F	3.4	50	120	0.007	6	2	5.6
	S7PLH08	S7 (18%)	34.52	48.89	7.9	F	3.4	50	120	0.007	6	2	6.7
	S8PLH08	S8 (29%)	29.05	48.89	7.9	F	3.4	50	120	0.007	6	2	6.1
Temperature Low	S1PLH09	S1 (2.6%)	38.57	-6.67	7.9	F	3.4	50	20	0.007	6	2	<b>16.2</b>
	S2PLH09	S2 (8%)	27.65	-6.67	7.9	F	3.4	50	20	0.007	6	2	6.25
	S3PLH09	S3 (10%)	26.83	-6.67	7.9	F	3.4	50	20	0.007	6	2	6.25
	S4PLH09	S4 (14%)	19.95	-6.67	7.9	F	3.4	50	20	0.007	6	2	5.45
	S5PLH09	S5 (15%)	22.81	-6.67	7.9	F	3.4	50	20	0.007	6	2	5.8
	S6PLH09	S6 (16%)	24.48	-6.67	7.9	F	3.4	50	20	0.007	6	2	6.05
	S7PLH09	S7 (18%)	34.52	-6.67	7.9	F	3.4	50	20	0.007	6	2	<b>12.3</b>
	S8PLH09	S8 (29%)	29.05	-6.67	7.9	F	3.4	50	20	0.007	6	2	6.6
Surface Roughness Low	S1PLH10	S1 (2.6%)	38.57	25	7.9	F	3.4	50	77	0.00001	6	2	11.8
	S2PLH10	S2 (8%)	27.65	25	7.9	F	3.4	50	77	0.00001	6	2	5.7
	S3PLH10	S3 (10%)	26.83	25	7.9	F	3.4	50	77	0.00001	6	2	5.9
	S4PLH10	S4 (14%)	19.95	25	7.9	F	3.4	50	77	0.00001	6	2	5.1
	S5PLH10	S5 (15%)	22.81	25	7.9	F	3.4	50	77	0.00001	6	2	5.4
	S6PLH10	S6 (16%)	24.48	25	7.9	F	3.4	50	77	0.00001	6	2	5.6
	S7PLH10	S7 (18%)	34.52	25	7.9	F	3.4	50	77	0.00001	6	2	6.7
	S8PLH10	S8 (29%)	29.05	25	7.9	F	3.4	50	77	0.1	6	2	6.1

Sensitivity	Canary Case reference	Natural gas (H <sub>2</sub> S%) ref.	Mol Wt.	Temperature (°C)	Pressure (bara)	Stability class	Wind (mph)	Humidity (%)	Air, Soil temp (°F)	Surf. Rough (m)	Line size (inch)	Hole size (inch)	Release rate (lb/s)
Surface Roughness High	S1PLH11	S1 (2.6%)	38.57	25	7.9	F	3.4	50	77	0.1	6	2	11.8
	S2PLH11	S2 (8%)	27.65	25	7.9	F	3.4	50	77	0.1	6	2	5.7
	S3PLH11	S3 (10%)	26.83	25	7.9	F	3.4	50	77	0.1	6	2	5.9
	S4PLH11	S4 (14%)	19.95	25	7.9	F	3.4	50	77	0.1	6	2	5.1
	S5PLH11	S5 (15%)	22.81	25	7.9	F	3.4	50	77	0.1	6	2	5.4
	S6PLH11	S6 (16%)	24.48	25	7.9	F	3.4	50	77	0.1	6	2	5.6
	S7PLH11	S7 (18%)	34.52	25	7.9	F	3.4	50	77	0.1	6	2	6.7
	S8PLH11	S8 (29%)	29.05	25	7.9	F	3.4	50	77	0.1	6	2	6.1
Hole size - 3 in	S1PLH12	S1 (2.6%)	38.57	25	7.9	F	3.4	50	77	0.007	6	3	21.5
	S2PLH12	S2 (8%)	27.65	25	7.9	F	3.4	50	77	0.007	6	3	12.7
	S3PLH12	S3 (10%)	26.83	25	7.9	F	3.4	50	77	0.007	6	3	12.7
	S4PLH12	S4 (14%)	19.95	25	7.9	F	3.4	50	77	0.007	6	3	11.5
	S5PLH12	S5 (15%)	22.81	25	7.9	F	3.4	50	77	0.007	6	3	12.2
	S6PLH12	S6 (16%)	24.48	25	7.9	F	3.4	50	77	0.007	6	3	12.6
	S7PLH12	S7 (18%)	34.52	25	7.9	F	3.4	50	77	0.007	6	3	15
	S8PLH12	S8 (29%)	29.05	25	7.9	F	3.4	50	77	0.007	6	3	13.7
Pressure - High	S1PLH14	S1 (2.6%)	38.57	25	34.5	F	3.4	50	77	0.007	6	2	50
	S2PLH14	S2 (8%)	27.65	25	34.5	F	3.4	50	77	0.007	6	2	28
	S3PLH14	S3 (10%)	26.83	25	34.5	F	3.4	50	77	0.007	6	2	28
	S4PLH14	S4 (14%)	19.95	25	34.5	F	3.4	50	77	0.007	6	2	23
	S5PLH14	S5 (15%)	22.81	25	34.5	F	3.4	50	77	0.007	6	2	25
	S6PLH14	S6 (16%)	24.48	25	34.5	F	3.4	50	77	0.007	6	2	26.5
	S7PLH14	S7 (18%)	34.52	25	34.5	F	3.4	50	77	0.007	6	2	50

Sensitivity	Canary Case reference	Natural gas (H <sub>2</sub> S%) ref.	Mol Wt.	Temperature (°C)	Pressure (bara)	Stability class	Wind (mph)	Humidity (%)	Air, Soil temp (°F)	Surf. Rough (m)	Line size (inch)	Hole size (inch)	Release rate (lb/s)
	S8PLH14	S8 (29%)	29.05	25	34.5	F	3.4	50	77	0.007	6	2	50
Pressure - Low	S1PLH15	S1 (2.6%)	38.57	25	3.45	F	3.4	50	77	0.007	6	2	3
	S2PLH15	S2 (8%)	27.65	25	3.45	F	3.4	50	77	0.007	6	2	2.5
	S3PLH15	S3 (10%)	26.83	25	3.45	F	3.4	50	77	0.007	6	2	2.5
	S4PLH15	S4 (14%)	19.95	25	3.45	F	3.4	50	77	0.007	6	2	2.2
	S5PLH15	S5 (15%)	22.81	25	3.45	F	3.4	50	77	0.007	6	2	2.3
	S6PLH15	S6 (16%)	24.48	25	3.45	F	3.4	50	77	0.007	6	2	2.4
	S7PLH15	S7 (18%)	34.52	25	3.45	F	3.4	50	77	0.007	6	2	2.8
	S8PLH15	S8 (29%)	29.05	25	3.45	F	3.4	50	77	0.007	6	2	2.6

The results for the simulations, the release rate estimated for the cases and the downwind distances (m) to the H<sub>2</sub>S toxicity concentrations of concern are given the next table.

Sensitivity	Canary Case reference	Natural gas (H <sub>2</sub> S%)	Mol Wt.	Phase	Surf. Rough.	Hole size (inch)	Orientation (degree)	Release rate (g/s)	HG model couple (m)	H <sub>2</sub> S 500 ppm (m)	H <sub>2</sub> S 100 ppm (m)	H <sub>2</sub> S 75 ppm (m)
Orientation - horizontal	S1PLH02	S1 (2.6%)	38.57	2-Ph	0.007	1	1	1.34	62	5.2	170.7	170.7
	S2PLH02	S2 (8%)	26.75	Vapor	0.007	1	1	0.64	-	21.9	79.2	79.2
	S3PLH02	S3 (10%)	26.83	Vapor	0.007	1	1	0.65	-	48.8	147.8	147.8
	S4PLH02	S4 (14%)	19.95	Vapor	0.007	1	1	0.58	-	63.7	190.5	190.5
	S5PLH02	S5 (15%)	22.81	Vapor	0.007	1	1	0.61	-	64.0	187.5	187.5
	S6PLH02	S6 (16%)	24.48	Vapor	0.007	1	1	0.64	-	68.6	199.6	199.6
	S7PLH02	S7 (18%)	34.52	Vapor	0.007	1	1	0.75	-	71.9	201.2	201.2
	S8PLH02	S8 (29%)	29.05	Vapor	0.007	1	1	0.70	-	102.1	274.3	274.3
Orientation - upwards	S1PLU04	S1 (2.6%)	38.57	2-Ph	0.007	2	45	5.35	-	23.8	88.4	88.4
	S2PLU04	S2 (8%)	27.65	Vapor	0.007	2	45	2.59	-	43.3	151.5	151.5
	S3PLU04	S3 (10%)	26.83	Vapor	0.007	2	45	2.68	-	53.3	182.0	182.0
	S4PLU04	S4 (14%)	19.95	Vapor	0.007	2	45	2.31	-	70.1	234.1	234.1
	S5PLU04	S5 (15%)	22.81	Vapor	0.007	2	45	2.45	-	70.1	232.0	232.0
	S6PLU04	S6 (16%)	24.48	Vapor	0.007	2	45	2.54	-	76.8	250.2	250.2
	S7PLU04	S7 (18%)	34.52	Vapor	0.007	2	45	3.04	-	82.9	259.1	259.1
	S8PLU04	S8 (29%)	29.05	Vapor	0.007	2	45	2.77	-	120.7	359.7	359.7

Sensitivity	Canary Case reference	Natural gas (H <sub>2</sub> S%) reference	Mol Wt.	Phase	Surf. Rough	Hole size (inch)	Orientation (degree)	Release rate (g/s)	HG model couple (m)	H <sub>2</sub> S 500 ppm (m)	H <sub>2</sub> S 100 ppm (m)	H <sub>2</sub> S 75 ppm (m)
Env. High wind, Unstable, upwards	S1PHU04	S1 (2.6%)	38.57	2-Ph	0.007	2	45	5.35	-	6.1	14.6	14.6
	S2PHU04	S2 (8%)	27.65	Vapor	0.007	2	45	2.59	-	9.1	21.6	21.6
	S3PHU04	S3 (10%)	26.83	Vapor	0.007	2	45	2.68	-	10.7	25.0	25.0
	S4PHU04	S4 (14%)	19.95	Vapor	0.007	2	45	2.31	-	13.4	31.4	31.4
	S5PHU04	S5 (15%)	22.81	Vapor	0.007	2	45	2.45	-	13.1	30.5	30.5
	S6PHU04	S6 (16%)	24.48	Vapor	0.007	2	45	2.54	-	13.7	32.0	32.0
	S7PHU04	S7 (18%)	34.52	Vapor	0.007	2	45	3.04	-	13.7	31.4	31.4
	S8PMU04	S8 (29%)	29.05	Vapor	0.007	2	45	2.77	-	18.3	42.7	42.7
Base case	S1PLH05	S1 (2.6%)	38.57	2-Ph	0.007	2	1	5.35	-	112.8	338.3	338.3
	S2PLH05	S2 (8%)	27.65	Vapor	0.007	2	1	2.59	-	79.6	249.9	249.9
	S3PLH05	S3 (10%)	26.83	Vapor	0.007	2	1	2.68	-	97.5	294.1	294.1
	S4PLH05	S4 (14%)	19.95	Vapor	0.007	2	1	2.31	-	124.4	361.2	361.2
	S5PLH05	S5 (15%)	22.81	Vapor	0.007	2	1	2.45	-	125.3	362.7	362.7
	S6PLH05	S6 (16%)	24.48	Vapor	0.007	2	1	2.54	-	137.2	391.7	391.7
	S7PLH05	S7 (18%)	34.52	Vapor	0.007	2	1	3.04	-	146.3	404.5	404.5
	S8PLH05	S8 (29%)	29.05	Vapor	0.007	2	1	2.77	-	203.6	541.0	541.0
Env. Medium wind	S1PMH05	S1 (2.6%)	38.57	2-Ph	0.007	2	1	5.35	-	18.9	150.9	150.9
	S2PMH05	S2 (8%)	27.65	Vapor	0.007	2	1	2.59	-	28.3	64.0	64.0
	S3PMH05	S3 (10%)	26.83	Vapor	0.007	2	1	2.68	-	32.3	73.2	73.2
	S4PMH05	S4 (14%)	19.95	Vapor	0.007	2	1	2.31	-	41.1	91.4	91.4
	S5PMH05	S5 (15%)	22.81	Vapor	0.007	2	1	2.45	-	39.6	89.0	89.0
	S6PMH05	S6 (16%)	24.48	Vapor	0.007	2	1	2.54	-	41.8	93.0	93.0
	S7PMH05	S7 (18%)	34.52	Vapor	0.007	2	1	3.04	124	56.4	327.7	327.7
	S8PMH05	S8	29.05	Vapor	0.007	2	1	2.77	-	54.9	118.9	118.9
Env.	S1PHH05	S1 (2.6%)	38.57	2-Ph	0.007	2	1	5.35	70	18.3	150.9	150.9

Sensitivity	Canary Case reference	Natural gas (H <sub>2</sub> S%) reference	Mol Wt.	Phase	Surf. Rough	Hole size (inch)	Orientation (degree)	Release rate (g/s)	HG model couple (m)	H <sub>2</sub> S 500 ppm (m)	H <sub>2</sub> S 100 ppm (m)	H <sub>2</sub> S 75 ppm (m)
	S2PHH05	S2 (8%)	27.65	Vapor	0.007	2	1	2.59	58	13.1	94.5	94.5
	S3PHH05	S3 (10%)	26.83	Vapor	0.007	2	1	2.68	58	14.6	128.0	128.0
	S4PHH05	S4 (14%)	19.95	Vapor	0.007	2	1	2.31	70	18.6	161.5	161.5
	S5PHH05	S5 (15%)	22.81	Vapor	0.007	2	1	2.45	65	18.0	169.2	169.2
	S6PHH05	S6 (16%)	24.48	Vapor	0.007	2	1	2.54	61	18.6	190.5	190.5
	S7PHH05	S7 (18%)	34.52	Vapor	0.007	2	1	3.04	48	37.8	216.4	216.4
	S8PHH05	S8 (29%)	29.05	Vapor	0.007	2	1	2.77	55	67.1	301.8	301.8
	Env. Humidity Low	S1PLH06	S1 (2.6%)	38.57	2-Ph	0.007	2	1	5.35	87	112.8	338.3
S2PLH06		S2 (8%)	27.65	Vapor	0.007	2	1	2.59	-	79.6	249.9	249.9
S3PLH06		S3 (10%)	26.83	Vapor	0.007	2	1	2.68	-	97.5	294.1	294.1
S4PLH06		S4 (14%)	19.95	Vapor	0.007	2	1	2.31	-	125.0	359.7	359.7
S5PLH06		S5 (15%)	22.81	Vapor	0.007	2	1	2.45	-	125.3	362.7	362.7
S6PLH06		S6 (16%)	24.48	Vapor	0.007	2	1	2.54	-	137.2	390.1	390.1
S7PLH06		S7 (18%)	34.52	Vapor	0.007	2	1	3.04	-	145.7	403.9	403.9
S8PLH06		S8 (29%)	29.05	Vapor	0.007	2	1	2.77	-	204.2	541.0	541.0
Env. Humidity High	S1PLH07	S1 (2.6%)	38.57	2-Ph	0.007	2	1	5.35	-	113.7	338.6	338.6
	S2PLH07	S2 (8%)	27.65	Vapor	0.007	2	1	2.59	-	79.9	249.9	249.9
	S3PLH07	S3 (10%)	26.83	Vapor	0.007	2	1	2.68	-	97.5	294.1	294.1
	S4PLH07	S4 (14%)	19.95	Vapor	0.007	2	1	2.31	-	124.4	361.2	361.2
	S5PLH07	S5 (15%)	22.81	Vapor	0.007	2	1	2.45	-	125.0	362.7	362.7
	S6PLH07	S6 (16%)	24.48	Vapor	0.007	2	1	2.54	-	137.2	390.1	390.1
	S7PLH07	S7 (18%)	34.52	Vapor	0.007	2	1	3.04	-	146.3	405.4	405.4
	S8PLH07	S8 (29%)	29.05	Vapor	0.007	2	1	2.77	-	204.2	541.0	541.0
Temper	S1PLH08	S1 (2.6%)	38.57	2-Ph	0.007	2	1	22.68	-	82.3	260.6	260.6

Sensitivity	Canary Case reference	Natural gas (H <sub>2</sub> S%) reference	Mol Wt.	Phase	Surf. Rough	Hole size (inch)	Orientation (degree)	Release rate (g/s)	HG model couple (m)	H <sub>2</sub> S 500 ppm (m)	H <sub>2</sub> S 100 ppm (m)	H <sub>2</sub> S 75 ppm (m)
	S2PLH08	S2 (8%)	27.65	Vapor	0.007	2	1	2.59	-	79.6	251.5	251.5
	S3PLH08	S3 (10%)	26.83	Vapor	0.007	2	1	2.68	-	99.1	300.2	300.2
	S4PLH08	S4 (14%)	19.95	Vapor	0.007	2	1	2.31	-	126.5	370.3	370.3
	S5PLH08	S5 (15%)	22.81	Vapor	0.007	2	1	2.45	-	128.6	373.4	373.4
	S6PLH08	S6 (16%)	24.48	Vapor	0.007	2	1	2.54	-	140.2	400.8	400.8
	S7PLH08	S7 (18%)	34.52	Vapor	0.007	2	1	3.04	-	144.8	403.9	403.9
	S8PLH08	S8 (29%)	29.05	Vapor	0.007	2	1	2.77	-	204.2	542.5	542.5
	Temperature Low	S1PLH09	S1	38.57	2-Ph	0.007	2	1	7.35	69	151.8	392.3
S2PLH09		S2	27.65	Vapor	0.007	2	1	2.83	-	80.8	249.9	249.9
S3PLH09		S3	26.83	Vapor	0.007	2	1	2.83	-	97.5	293.2	293.2
S4PLH09		S4	19.95	Vapor	0.007	2	1	2.47	-	121.6	350.5	350.5
S5PLH09		S5	22.81	Vapor	0.007	2	1	2.63	-	125.6	360.6	360.6
S6PLH09		S6 (16%)	24.48	Vapor	0.007	2	1	2.74	-	137.2	388.6	388.6
S7PLH09		S7 (18%)	34.52	Vapor	0.007	2	1	5.58	77	436.8	1135.4	1135.4
S8PLH09		S8 (29%)	29.05	Vapor	0.007	2	1	2.99	-	203.3	537.1	537.1
Surface Roughness Low	S1PLH10	S1 (2.6%)	38.57	2-Ph	0.0001	2	1	5.35	-	158.5	472.7	472.7
	S2PLH10	S2 (8%)	27.65	Vapor	0.0001	2	1	2.59		79.6	249.9	249.9
	S3PLH10	S3 (10%)	26.83	Vapor	0.0001	2	1	2.68		97.5	294.1	294.1
	S4PLH10	S4 (14%)	19.95	Vapor	0.0001	2	1	2.31		124.7	361.2	361.2
	S5PLH10	S5 (15%)	22.81	Vapor	0.0001	2	1	2.45		125.3	363.0	363.0
	S6PLH10	S6 (16%)	24.48	Vapor	0.0001	2	1	2.54		137.2	391.7	391.7
	S7PLH10	S7 (18%)	34.52	Vapor	0.0001	2	1	3.04		146.3	404.5	404.5
	S8PLH10	S8 (29%)	29.05	Vapor	0.0001	2	1	2.77		203.6	541.0	541.0
Surf	S1PLH11	S1 (2.6%)	38.57	2-Ph	0.1	2	1	5.35		79.2	239.3	239.3

Sensitivity	Canary Case reference	Natural gas (H <sub>2</sub> S%) reference	Mol Wt.	Phase	Surf. Rough	Hole size (inch)	Orientation (degree)	Release rate (g/s)	HG model couple (m)	H <sub>2</sub> S 500 ppm (m)	H <sub>2</sub> S 100 ppm (m)	H <sub>2</sub> S 75 ppm (m)
	S2PLH11	S2 (8%)	27.65	Vapor	0.1	2	1	2.59		39.6	89.9	89.9
	S3PLH11	S3 (10%)	26.83	Vapor	0.1	2	1	2.68		45.7	101.8	101.8
	S4PLH11	S4 (14%)	19.95	Vapor	0.1	2	1	2.31		57.9	128.6	128.6
	S5PLH11	S5 (15%)	22.81	Vapor	0.1	2	1	2.45		56.4	125.0	125.0
	S6PLH11	S6 (16%)	24.48	Vapor	0.1	2	1	2.54		59.1	129.5	129.5
	S7PLH11	S7 (18%)	34.52	Vapor	0.1	2	1	3.04		57.9	125.0	125.0
	S8PLH11	S8 (29%)	29.05	Vapor	0.1	2	1	2.77		76.2	164.6	164.6
	Hole size - 3 in	S1PLH12	S1 (2.6%)	38.57	2-Ph	0.007	3	<b>1</b>	9.75		163.1	484.6
S2PLH12		S2 (8%)	27.65	Vapor	0.007	3	1	5.76		118.9	367.3	367.3
S3PLH12		S3 (10%)	26.83	Vapor	0.007	3	1	5.76		145.4	431.3	431.3
S4PLH12		S4 (14%)	19.95	Vapor	0.007	3	1	5.22		179.8	513.6	513.6
S5PLH12		S5 (15%)	22.81	Vapor	0.007	3	1	5.53		184.4	522.7	522.7
S6PLH12		S6 (16%)	24.48	Vapor	0.007	3	1	5.72		202.7	568.5	568.5
S7PLH12		S7 (18%)	34.52	Vapor	0.007	3	1	6.80		446.5	1107.9	1107.9
S8PLH12		S8 (29%)	29.05	Vapor	0.007	3	1	6.21		300.2	789.4	789.4
Pressure - High	S1PLH14	S1 (2.6%)	38.57	2-Ph	0.007	2	<b>1</b>	22.68	120	277.4	684.3	684.3
	S2PLH14	S2 (8%)	27.65	Vapor	0.007	2	1	12.70	-	181.4	539.5	539.5
	S3PLH14	S3 (10%)	26.83	Vapor	0.007	2	1	12.70	-	217.9	627.9	627.9
	S4PLH14	S4 (14%)	19.95	Vapor	0.007	2	1	10.43	-	253.9	711.1	711.1
	S5PLH14	S5 (15%)	22.81	Vapor	0.007	2	1	11.34	-	272.8	759.0	759.0
	S6PLH14	S6 (16%)	24.48	Vapor	0.007	2	1	12.02	-	300.2	823.0	823.0
	S7PLH14	S7 (18%)	34.52	2-Ph	0.007	2	1	22.68	135	839.7	1967.5	1967.5
	S8PLH14	S8 (29%)	29.05	2-Ph	0.007	2	1	22.68	287	1234.4	2907.8	2907.8
Pressure - Low	S1PLH15	S1 (2.6%)	38.57	Vapor	0.007	2	<b>1</b>	1.36	71	20.7	170.7	170.7
	S2PLH15	S2 (8%)	27.65	Vapor	0.007	2	1	1.13		51.8	164.6	164.6



Sensitivity	Canary Case reference	Natural gas (H <sub>2</sub> S%) reference	Mol Wt.	Phase	Surf. Rough	Hole size (inch)	Orientation (degree)	Release rate (g/s)	HG model couple (m)	H <sub>2</sub> S 500 ppm (m)	H <sub>2</sub> S 100 ppm (m)	H <sub>2</sub> S 75 ppm (m)
	S3PLH15	S3 (10%)	26.83	Vapor	0.007	2	1	1.13		64.0	194.5	194.5
	S4PLH15	S4 (14%)	19.95	Vapor	0.007	2	1	1.00		82.9	246.9	246.9
	S5PLH15	S5 (15%)	22.81	Vapor	0.007	2	1	1.04		82.9	245.4	245.4
	S6PLH15	S6 (16%)	24.48	Vapor	0.007	2	1	1.09		89.9	262.1	262.1
	S7PLH15	S7 (18%)	34.52	Vapor	0.007	2	1	1.27		93.0	259.7	259.7
	S8PLH15	S8 (29%)	29.05	Vapor	0.007	2	1	1.18		132.6	358.1	358.1

## Appendix F: Field trial wind data (for model Boundary condition)

In 1956 scientists have conducted experiment on dispersion of SO<sub>2</sub> near the town of O'Neil in Nebraska, USA. This program is known as **Prairie Grass** Project. They have conducted over 68 experiments over several days and with different flow rate and measured SO<sub>2</sub> concentration at 5 different distances, i.e, 50 m, 100 m, 200 m, 400 m and 800 m from the point of injections. Scientists also put the measuring points at different angle from the center line (-90° to 90° ). In the present study 3D Finite Volume CFD code OpenFOAM have been used to match data from one particular experiment, i.e, Run #9. Data are based on measurement made at a height of 2 m along base-line of SO<sub>2</sub> sampling network and at a distance of 450 m from the release point.

Table 8.1 (Continued)

HOURLY OBSERVATIONS							O'NEILL, NEBRASKA	
GAS RELEASE NO.	7	8	9	10	11	12		
JULY (1956)	10	10	11	11	14	14		
CST	1405	1705	1005	1205	0805	1005		
RADIATION (cal/cm <sup>2</sup> sec)								
Insolation	.0212	.0115	.0180	.0200	.0105	.0185		
Reflected	.0039	.0023	.0035	.0040	--	--		
Net Radiation	.0129	.0057	.0114	.0128	.0050	.0117		
AIR and SOIL TEMPERATURES (°C)								
Height (m)								
16.00	28.71	29.90	25.78	28.42	--	--		
8.00	29.04	30.15	20.25	28.98	24.16			
4.00	29.46	30.57	20.01	29.58	24.64			
2.00	30.27	31.10	27.39	30.45	25.01			
1.00	31.21	31.47	28.19	31.47	25.42			
.50	31.90	32.01	28.75	32.11	25.92	31.18		
.25	33.10	32.58	29.53	33.14	26.34	31.94		
.12	34.23	33.06	29.82	33.78	26.68	32.65		
-.03	34.90	33.74	26.64	31.79	24.23	28.88		
-.08	30.53	31.77	24.48	27.91	23.48	25.98		
-.12	24.23	26.77	23.14	23.93	24.25	24.16		
-.25	21.11	21.84	22.47	22.27	24.14	23.05		
-.50	20.03	19.99	20.42	20.34	21.49	21.34		
-1.00	18.22	18.22	18.28	18.20	18.75			
WIND SPEED (cm/sec)								
16.00	560	611	884	579	--			
8.00	508	540	842	530	944			
4.00	481	498	709	500	850			
2.00	444	452	700	468	781			
1.00	402	400	611	415	677			
.50	352	350	533	376	579			
.25	295	288	450	312	490			

Temperature

Vertical Wind profile

Gas release No.	8	9	10	11	12	13	14
Date	10 July	11 July		14 July		22 July	
Time (CST)	1655	0955	1155	0755	0955	1955	2155
Wind speed (m/sec)							
Source (10 min)	4.85	6.88	4.60	7.03	8.35	1.25	1.91
450 m (10 min)	4.75	7.13	4.65	7.74	8.25	1.81	1.81
Source (20 min)	4.70	6.83	4.52	7.61	8.07	1.37	1.75
450 m (20 min)	4.80	7.13	4.65	7.76	8.14	1.65	1.81
Wind direction (deg)							
Source (10 min)	184	204	225	184	194	190	170
450 m (10 min)	193	214	214	196	200	206	186
Source (20 min)	176	206	217	185	192	192	172
450 m (20 min)	181	214	217	196	199	206	186
Standard deviation of wind direction (deg)							
Source (10 min)	10.2	10.2	16.8	7.2	7.9	3.2	3.6
450 m (10 min)	9.6	10.2	14.1	6.8	5.1	2.4	3.1
Source (20 min)	16.3	9.5	18.3	6.9	9.9	5.0	4.3
450 m (20 min)	19.1	9.1	15.4	6.7	6.9	2.5	5.9

Vertical velocity and temperature profiles need to be established / maintained in the solution domain.

Wind data: Data are based on measurement made at a height of 2 m along base-line of SO<sub>2</sub> sampling network and at a distance of 450 m from the release point.

Table 6.1 (Continued)

Gas release No.	1	2	3	4	5	6	7
Date	3 July		5 July	6 July			10 July
Time (CST)	1055	1455	2155	0055	1355	1855	1355
Wind speed (m/sec)							
Source (10 min)	2.62*	2.01		1.40	6.47		4.19
450 m (10 min)		2.57		1.65	5.96	5.86	4.14
Source (20 min)	2.49*	2.14		1.58	6.57		4.19
450 m (20 min)		2.19		1.78	6.45	6.65	4.55
Wind direction (deg)							
Source (10 min)				216	176		188
450 m (10 min)				223	186	191	194
Source (20 min)				207	178		197
450 m (20 min)				226	184	190	200
Standard deviation of wind direction (deg)							
Source (10 min)				7.4	9.5		25.6
450 m (10 min)				7.6	9.1	7.1	27.1
Source (20 min)				9.7	11.1		31.7
450 m (20 min)				9.2	9.7	7.7	23.9
Gas release No.	8	9	10	11	12	13	14
Date	10 July	11 July		14 July		22 July	
Time (CST)	1655	0955	1155	0755	0955	1955	2155
Wind speed (m/sec)							
Source (10 min)	4.85	6.88	4.60	7.03	8.35	1.25	1.91
450 m (10 min)	4.75	7.13	4.65	7.74	8.25	1.81	1.81
Source (20 min)	4.70	6.83	4.52	7.61	8.07	1.37	1.75
450 m (20 min)	4.80	7.13	4.65	7.76	8.14	1.65	1.81
Wind direction (deg)							
Source (10 min)	184	204	225	184	194	190	170
450 m (10 min)	193	214	214	196	200	206	186
Source (20 min)	176	206	217	185	192	192	172
450 m (20 min)	181	214	217	196	199	206	186
Standard deviation of wind direction (deg)							
Source (10 min)	10.2	10.2	16.8	7.2	7.9	3.2	3.6
450 m (10 min)	9.6	10.2	14.1	6.8	5.1	2.4	3.1
Source (20 min)	16.3	9.5	18.3	6.9	9.9	5.0	4.3
450 m (20 min)	19.1	9.1	15.4	6.7	6.9	2.5	5.9

The SO tracer was transported in a 2-inch plastic pipe buried just beneath the surface of the ground and was released horizontally at a height of 46 centimeters. Source strength  $Q$  (g/sec) for PG Run No. #09 = 92 g/sec

**Table 5.1. Source strengths  $Q$  expressed in  $\text{g sec}^{-1}$  for individual Prairie Grass diffusion experiments**

Run No.	$Q$ ( $\text{g sec}^{-1}$ )	Run No.	$Q$ ( $\text{g sec}^{-1}$ )	Run No.	$Q$ ( $\text{g sec}^{-1}$ )
1	81.5	24	41.2	46	99.7
2	83.9	25	101.4	47	103.1
3	56.3	26	97.6	48S	104.0
4	50.5	27	98.8	48	104.1
5	77.8	28	41.7	49	102.0
6	89.5	29	41.5	50	102.8
7	89.9	30	98.4	51	102.4
8	91.1	31	96.0	52	104.0
9	92.0	32	41.4	53	45.2
10	92.1	33	94.7	54	43.4
11	95.9	34	97.4	55	45.3
12	99.1	35S	41.8	56	45.9
13	61.1	35	38.8	57	101.5
14	49.1	36	40.0	58	40.5
15	95.5	37	40.3	59	40.2
16	93.0	38	45.4	60	38.5
17	56.5	39	40.7	61	102.1
18	57.6	40	40.5	62	102.1
19	101.8	41	39.9	65	44.1
20	101.2	42	56.4	66	43.1
21	50.9	43	98.9	67	45.0
22	48.4	44	100.7	68	42.8
23	40.9	45	100.8		

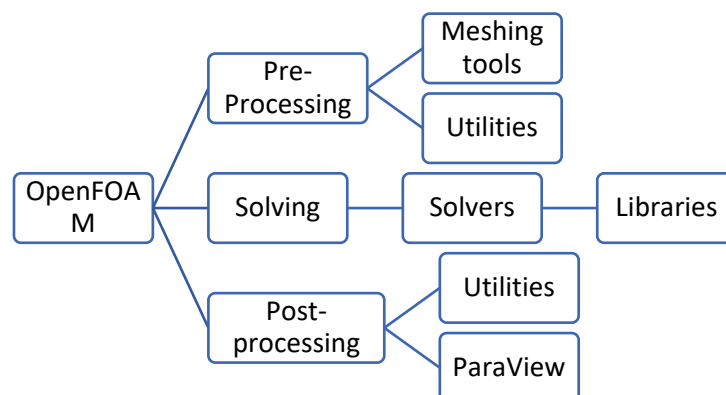
## Appendix G: OpenFOAM fundamentals

OpenFOAM's FVM uses a co-located methodology on an unstructured polyhedral grid with arbitrary grid elements. Fluid dynamic quantities are centred on the control volume centroids. A variety of available interpolation, discretization, and matrix solution schemes can be selected at runtime. OpenFOAM input dictionaries are designed to be human-readable ASCII text files, where the main basic entry types are given in table below.

Type	Description	Example
<b>boolean</b>	State	on, off, true, false
<b>label</b>	Integer	123
<b>scalar</b>	Float	123.456
<b>word</b>	a single word	value
<b>string</b>	quoted text	"this is a string value"
<b>list</b>	a list of entries bounded by () braces	(0 1 2 3 4 5)
<b>vector</b>	a list of 3 values, nominally (x y z) components	(0 0 0)
<b>sphericalTensor</b>	a spherical tensor	(0)
<b>symmTensor</b>	a symmetric tensor defined by (xx xy xz yy yz zz)	(0 0 0 0 0 0)
<b>tensor</b>	a nine-component tensor defined by (xx xy xz yx yy yz zx zy zz)	(0 0 0 0 0 0 0 0 0)
<b>dictionary</b>	collection of entries bounded by {} braces	labelType 1; wordType word; scalarType 1.0;

### OpenFoam workflow

OpenFOAM is in SI units. The workflow of using OpenFOAM is like conventional CFD programs, and it is categorized as pre-processing, solving and post-processing. Utilities helps the interface to the pre-processing and post-processing. The overall OpenFOAM structure is shown in Figure.



## OpenFOAM Structure

1. Pre-processing – sequence of steps
  - (i) Definition of the geometry of the region of interest: the computational domain.
  - (ii) Grid generation – the sub-division of the flow region into a number of smaller, non-overlapping sub-domains: a grid (or mesh) of cells (or control volumes or elements).
  - (iii) Selection of suitable models for the interesting physical and chemical phenomena.
  - (iv) Definition of fluid properties.
  - (v) Specification of the chemical and physical boundary conditions at cells which coincide with or touch the domain boundary.

The solution to a flow problem (velocity, pressure, temperature etc.) is defined at nodes or cell centers inside each cell. The accuracy of a CFD solution depends heavily on the number of cells in the grid. In general, the larger the number of cells, the better the solution accuracy. Optimal meshes are often non-uniform, finer in areas where large variations occur from point to point and coarser in regions with relatively little change.

### Computational grid – meshing

Mesh is generated using the OpenFOAM utilities like *blockMesh*, *snappyHexMesh* or by conversion using utilities like *fireToFoam*, *fluentMeshToFoam*, *gmshToFoam* etc.

*blockMesh* is a structured hexahedral mesh generator built using blocks and supports cell size grading and curved block edges. This is the simplest utility for converting geometry to mesh. The ordering of point is important and requires consistent block-to-block connectivity. The utility is controlled using a *blockMeshDict* dictionary, located in the case system directory, split into the following sections – points, edges, blocks and patches.

*snappyHexMesh* is a fully parallel, split hex, mesh generator that produces higher quality mesh. The utility is controlled using *snappyHexMesh* dictionary and is well suited to batch driven operation. Meshing process starts from any pure hex mesh (structured or unstructured), reads geometry in triangulated formats, e.g., in stl, obj, vtk. There is no limit on the number of input surfaces and can use simple analytically defined geometry, e.g., box, sphere, cone.

A boundary is a list of patches, each of which is associated with a boundary condition. A patch is a list of face labels which clearly must contain only boundary faces and no internal faces. A mesh with the general structure is known in OpenFOAM as a polyMesh. A boundary is generally broken

up into a set of patches. One patch may include one or more enclosed areas of the boundary surface which do not necessarily need to be physically connected. The patch types are specified in the mesh and field files of OpenFOAM case. The base type is specified under the type of keyword for each patch in the boundary file, located in the constant/polyMesh directory.

## 2. Solving

In OpenFOAM different applications are coded for simulations, like incompressible or compressible flow, heat transfer, multiphase flow, combustion, electro-magnetism, turbulence modelling and solid mechanics, e.g., icoFoam, simpleFoam. For this study, well established FVM will be used; FVM consists of the following steps:

- (i) Integration of the conservation of mass, energy and momentum equations over all the control volumes in the domain.
- (ii) Discretization – conversion of the resulting integral equations into a system of algebraic equations.
- (iii) Solution of the algebraic equations by an iterative method.

In the control volume integration, FVM ensures that a general flow variable, e.g. momentum or enthalpy, is conserved in each finite size cell.

Fluid property is the Input data to solver which includes density, dynamic viscosity, kinematic viscosity, specific heat, coefficient of thermal conductivity, thermal diffusivity. Flow property of the fluid is calculated by the solver in the domain and the properties include velocity, pressure, temperature, vorticity, turbulent viscosity, dissipation rate, mixture fraction, flame speed.

## 3. Post-processing

After simulation, CFD results are analysed using tools like paraView, paraFoam. The data is converted to other data files which can be used in other post-processing tools to analyse the results and visualize. Typical elements of post-processing are:

- (i) Definition of suitable cutting planes for visualization
- (ii) Contour plots of properties/flow variables
- (iii) Vector plots
- (iv) Streamlines
- (v) Line plots
- (vi) Balances

OpenFOAM installation include subdirectories like applications, source code (src), tutorials, dictionary files and other supporting installation and compilation file. Case structure: OpenFOAM cases are configured using several plain text input files located across the three directories (i) system, (ii) constant and (iii) time directory (0). Additional directories can be generated for the case specific results (field predictions as a function of iteration count or time), post Processing and data conversion.

- System directory includes controlDict, fvSchemes, fvSolution, fvOptions (optional) and other <system dictionaries>.
  - ControlDict includes files to control the simulation
  - decomposeParDict includes files for parallel simulation on High Performance Computing (HPC)
  - fvSchemes includes the discretisation schemes for both temporal and spatial
- Constant directory includes mesh files, transport properties and the selection of turbulence model. Mesh files includes files for boundary conditions, faces and nodes. polyMesh (geometry meshing information) and other <constant dictionaries>.
- Time *directory* include the field files for the initial time and subsequent result time directories. This includes files created for pressure (P), velocity (U), temperature (T), concentration (C), turbulent viscosity (nut). This directory is common for both steady and unsteady problems.

Post processing in OpenFOAM like other CFD tools is to derive the results in the form of customized values, field properties and images. OpenFOAM includes utility *paraFoam* for post-processing. A widely used alternative for post-processing is *paraView*, an open source, multi-platform data analysis and visualisation application. *paraView* is a cross platform application with Python scripting and batch processing capabilities.

As an alternative, the OpenFOAM data can also be converted into Visualization Tool Kit (VTK) format using the *foamToVTK* utility or during the simulation with the the *vtkWrite* function object that largely mirrors the functionality of the *foamToVTK* utility. The converted data can be post-processed in *paraView* or any other program supporting VTK format. OpenFOAM has the *probe* utility to define a location/s of interest within the domain for where the results can be extracted.



## Thermophysical models in OpenFOAM

Thermophysical models are used to describe cases where energy, mass transfer or compressibility is important. The *thermophysicalProperties* dictionary is read by any solver that uses the thermophysical model library which is constructed in OpenFOAM as a pressure-temperature ( $p - T$ ). There is one compulsory dictionary entry called *thermoType* which specifies the package of thermophysical modelling that is used in the simulation. The keyword entries in *thermoType* reflect the multiple layers of modelling and the underlying framework in which they combined. Additional layers include transport and mixture modelling. Below is an example entry for *thermoType*:

```
thermoType
{
  type          heRhoThermo;
  mixture       reactingMixture;
  transport     sutherland;
  thermo        janaf;
  equationOfState perfectGas;
  specie        specie;
}
```

## Turbulence modelling

OpenFOAM includes supports RAS, DES and LES turbulence modelling [Ref: OpenFOAM: User Guide: Turbulence]. Turbulence generation is driven by the velocity gradient. Errors arising from the gradient calculation, e.g., due to poor quality meshes, can lead to spurious turbulence predictions and solver instability. This effect can be partly compensated by the application of limited schemes. Turbulence models are specified in 'constant' folder. An example of specifying the turbulence for RAS  $k\omega$ - SST is given below.

```
simulationType  RAS;
RAS
{
  RASModel      kOmegaSST;    // On/off switch
  Turbulence     on;          // optionally write the model coefficients at
run-time
  printCoeffs   no;           // optionally override default model
coefficients
  kOmegaSSTCoeffs
  {
    ...
  }
}
```

Default coefficients are available for all models, based on their reference literature. Optionally users may override the default values by specifying a <model>Coeffs sub-dictionary. Coefficient names can be found by observing the solver output when setting the printCoeffs to yes.

Source code: \$FOAM\_SRC/TurbulenceModels, Source documentation

### Boundary conditions

Setting up of appropriate boundary conditions is vital for successful simulation, to minimize solver failure and optimize the computational time. OpenFOAM offers a wide range of boundary conditions which can be categorized to (OpenFOAM 2019):

- (i) basic like *fixedValue*, *fixedGradient*, *zeroGradient*,
- (ii) geometric constraints like *symmetry*, *wedge*, *empty*, *cyclic*, and
- (iii) derived like *slip*, *noSlip*, *fixedProfile*, *inletOutlet*.

The commonly used boundary conditions are Inflow (inlet) conditions, Wall, Outflow (outlet) conditions, symmetry condition, and periodic condition. Boundary conditions are assigned in the *boundaryField* section of the field files within each time directory for each mesh patch. The format follows:

```
boundaryField
{
  <patch 1>
  {
    type    <patch type>;
    ...
  }
  <patch 2>
  {
    type    <patch type>;
    ...
  }
  ...
  <patch N>
  {
    type    <patch type>;
    ...
  }
}
```

Each condition is set in a dictionary given by the name of the underlying mesh patch, according to the *type* keyword.